12-2005

The Development of Building Block Methodologies to Produce Nanostructured Heterogeneous Catalysts by Design

Jason Curtis Clark
University of Tennessee - Knoxville

To the Graduate Council:

I am submitting herewith a dissertation written by Jason Curtis Clark entitled "The Development of Building Block Methodologies to Produce Nanostructured Heterogeneous Catalysts by Design." I have examined the final electronic copy of this dissertation for form and content and recommend that it be accepted in partial fulfillment of the requirements for the degree of Doctor of Philosophy, with a major in Chemistry.

Craig E. Barnes, Major Professor

We have read this dissertation and recommend its acceptance:

Engin Serpersu, John F. C. Turner, Bin Zhao

Accepted for the Council:
Carolyn R. Hodges

Vice Provost and Dean of the Graduate School

(Original signatures are on file with official student records.)

To the Graduate Council:

I am submitting herewith a dissertation written by Jason Curtis Clark entitled “The Development of Building Block Methodologies to Produce Nanostructured Heterogeneous Catalysts by Design.” I have examined the final electronic copy of this dissertation for form and content and recommend that it be accepted in partial fulfillment of the requirements for the degree of Doctor of Philosophy, with a major in Chemistry.

Craig E. Barnes
Major Professor

We have read this dissertation
and recommend its acceptance:

Engin Serpersu

John F. C. Turner

Bin Zhao

Accepted for the Council:

Anne Mayhew
Vice Chancellor and Dean of the
Graduate School

(Original Signatures are on file with official student records)

The Development of Building Block Methodologies to Produce Nanostructured Heterogeneous Catalysts by Design

A Dissertation

Presented for the

Doctor of Philosophy Degree

University of Tennessee – Knoxville

Jason Curtis Clark

December 2005

Dedication

To my family, especially my mother, Marie C. Morrow,

and my brother Stephen Clark,

who support and love me unconditionally.

Acknowledgements

This dissertation would not have been possible without the assistance and efforts of many individuals. First and foremost I would like to thank my research advisor Dr. Craig E. Barnes for dedicating an immense amount of time, patience and effort in overseeing my graduate education. His adherence to high standards has driven me to become a better chemist and a better person. I would also like to thank my committee members, Prof. John F. C. Turner, Prof. Zhao, and Prof. Engin Serpersu for agreeing to commit time and effort to be on my committee. I would like to especially thank Dr. Turner who has provided many insightful discussions about chemistry and life. He has shown a great interest in my education throughout my entire graduate career and has been extremely supportive of me as a chemist and a person.

I would like to thank Dr. Hongjun Pan for his time, patience and efforts in teaching me so much about NMR spectroscopy. These lessons were invaluable and have helped me immensely in my research. I would like to thank Dr. James G. Goodwin, Jr. and Dora E. López at Clemson University. They performed all of the catalysts testing for samples that I synthesized. I would also like to thank current and former group members, Suree Saengkerdsub, Jeffrey Williams, Geoff Eldridge, Sasikumar Naidu, Narendra Ghosh, Richard Mayes, Ming-Yung Lee, and Dustin Collier for collaborative discussions, assistance in the lab, and for making life interesting during the past five years. Finally I would like to thank

Arthur Pratt in the glass blowing shop for making various apparatuses and for fixing my many, many mistakes.

I owe a great deal of thanks to the Joint Institute of Neutron Sciences for partially funding my graduate studies from 2003 until the present time. I would also like to thank those responsible for the Eugene Barber Fellowship in Chemistry for partial funding in 2003 and 2004. Finally I would like to thank the Neutron Science Consortium for funding travel expenses to Argonne National Lab for neutron scattering experiments.

Abstract

Building block methods were successfully developed to demonstrate the potential of this approach to synthesizing nanostructured heterogeneous catalysts by design. The octa(trimethyltin) cuboctameric spherosilicate, $Si_8O_{20}(SnMe_3)_8$, was used as the building block for the synthesis of these materials. The solid state structure of this building block was characterized and compared to other solid state structures of Si_8O_{12} containing compounds. These studies showed that this building block is composed of rigid tetrahedral units connect through a flexible siloxy bridge. The trimethyltin functionality present on this molecular precursor will react with metal chlorides to produce cross-linked metal oxide/silicate matrices where a distribution of different linking species is present.

Three different silylchlorides were used to cross-link spherosilicate building blocks. The resulting products consisted of a distribution of different types of silylchloride linking units present in the solid material. Silylchlorides were used to study this reaction because the resulting product can easily be probed using silicon-29 solid-state NMR. The effect of initial stoichiometry on the distribution of linking groups in the resulting matrix was investigated and it was found that as the initial concentration of silylchloride decreased relative to the initial concentration of building blocks, the distribution of linking groups in the final product favored a more cross-linked matrix. These findings led to the development of synthetic strategies to produce a cross-linked matrix where a

limiting amount of a silylchloride linking groups is present in the matrix having one type of environment throughout the entire material. These methods were then applied to reactions involving aluminum trichloride and titanium tetrachloride to produce solid acid catalysts. These catalysts were tested for the transesterification of triacetin with methanol. The catalysts were active for this reaction and triacetin conversion rates of 3 – 76% were observed after 8 hours. The titanosilicate catalysts were the most active and had reactive properties similar to commercially available catalysts.

TABLE OF CONTENTS

LIST OF TABLES

LIST OF FIGURES AND SCHEMES

Chapter 1: Introduction

1.1 Catalysis and the Economy

The impact of catalysts on the US and worldwide economy is indisputable. In 1989, the worldwide catalysis market based on catalyst sales was $5 billion. The market was $1.9 billion in the US and grew to nearly $3 billion in 1999.[1] However, the impact of catalysts goes well beyond sales. For example, the worldwide value of fuel and chemicals derived from catalysts in 1989 was nearly $3 trillion.[1] In the same year in the US, the value was estimated at $891 billion which represents approximately 17% of the country's GNP.[1] The total consumption of catalysts in the US in 1984 in dollars was $1330 billion of which $490 billion involved chemical processing, $390 billion involved petroleum refining, and $450 billion involved emission control.[2]

The impact of catalysts on our everyday lives may go unnoticed. For example, consider the extent of involvement that catalysis has on automotive transportation. Structural components and paints made up of polymeric materials were made from monomers which originated from a series of catalytic processes that were produced from raw materials such as crude oil and natural gas.[2] The fuels used to run the engine are catalytically refined from crude oils.[2] Finally, the by-products from combustion reactions that power the automotive engine must pass through catalysts for emissions control.[2] Catalysts are also becoming increasingly important in controlling pollution and other environmental uses.

1.2 Catalytic Activity

Due to the many important processes dependent upon catalysts and the worldwide economic reliance upon these materials, an interdisciplinary approach is being taken in the study of catalysis science with participants coming from the fields of chemistry, physics, chemical engineering, and materials science.[3] The investigation of catalysis from a broad array of scientists has resulted in a continually growing amount of publications which helps further our understanding of the subject.[3]

Understanding catalysts begins with relating some basic definitions to the challenges associated with catalysis. Catalysts are species that increase the rate of a reaction without being consumed in the reaction. The increased rate occurs because the catalyzed reaction has a lower activation energy when compared to that of the uncatalyzed reaction. However, the energy required or liberated in the reaction is not changed because it is governed by thermodynamics.[3]

The rate enhancement or reactive properties of catalysts can be expressed in terms of activity and selectivity. The activity of the catalysts describes the amount of reagent conversion per unit time and the selectivity can be defined as the ability to facilitate the formation of a desired reaction product when other products are possible.[3] The obvious question to understanding the reactive properties of catalysis is what exactly is responsible for the observed activity and selectivity induced by the catalyst.[4]

1.2.1 Active Sites

This question introduces the notion in catalysis of the active site. An active site consists of an atom or group of atoms where the reaction actually occurs.[3] These sites are the location within the catalyst where bond breaking happens and they are structurally different for different chemical reactions.[5] For example, in metal-oxide catalysts, a vacancy left by an oxygen atom that leaves the surface might be the active site.[5] C-H bond dissociation is often thought to occur at a single metal atom.[5] Dissociation of N≡N requires high coordination sites on Fe(111) and Fe(211) surfaces.[5]

The properties of the active site are extremely important and can include metal oxidation state, the local environment of the metal center (including coordination number and coordination geometry), the steric nature of the ligands surrounding the metal center, and the electronic interaction between the complex and the substrate.[4] All of the properties associated with the active site will influence the reactive properties of the catalyst. Characterization of the active site under real conditions is challenging and is one of the fundamental issues currently being addressed in catalysis sciences. This is a challenge because the preparation of a catalyst and the species that is actually active may not be the same. Catalytic precursors are prepared and used in the reactions. They often times must be activated to form the active species and this is difficult to characterize due to its dynamic nature. Catalytic sites undergo structural changes when reactants are adsorbed.[4,5] Thus techniques that elucidate the

structure of the sites must be applied under *in situ* conditions and be capable of probing the catalyst with time and spatial resolution.[5]

1.3 Categories in Catalysis Science

The field of catalysis science can be divided into two main categories: heterogeneous and homogeneous. Heterogeneous catalysts operate in a different phase than the substrate molecules that are part of the reaction being catalyzed. These catalysts are typically solid materials with the substrate molecules being in the liquid or gas phase. In homogeneous catalysts, the catalyst and the substrate molecules are all in the same phase. These catalysts are typically soluble organic or organometallic complexes which catalyze soluble or liquid substrate molecules.

One further category of catalysis is biological catalysts. These catalysts are typically enzymes and have observed selectivities that approach 100%. These catalysts exhibit higher activity and selectivity because the intricate tailoring of their active sites. These centers are surrounded by a flexible, protein based scaffold that is an ideal three-dimensional environment for substrates to "dock." This flexible backbone is dynamic in nature and readily encloses the adsorbed substrate creating an ideal reaction cavity whose shape is determined by the substrate. Because the backbone is flexible, it can change shapes to stabilize reaction intermediates and active complexes as the reaction proceeds. This process is called a "hand-in-glove" scheme and it dictates the activity and selectivity of the enzyme.[4] This type of engineering towards designing systems

having such specific sites is the ultimately goal in all of catalysis because it results in systems that approach 100% selectivity.

1.3.1 Comparing Homogeneous and Heterogeneous Catalysts

The nature of homogeneous catalysts when compared to heterogeneous catalysts leads to interesting advantages and disadvantages when considering fundamental and application viewpoints in catalysis sciences. Since the catalysts and the reaction products are all in the same phase for homogeneous systems, separation of these two components can be difficult. Thus costly separation steps must be put into place to recover and recycle the catalysts. Since the catalysts are often expensive metal complexes, this is a serious issue.[6] Heterogeneous catalysts do not suffer from the same problems associated with recovery and recycling as was just described because the catalysts are not in the same phase. Due to this advantage in post reaction processing, these types of catalysts are more attractive economically and are also more environmentally friendly.[6]

Despite the processing disadvantages associated with homogeneous catalysts, this area of research is extremely active because this class of catalysts are generally superior to heterogeneous analogous in terms of selectivity and activity.[7] A primary reason for this is that homogeneous catalysts can be more easily optimized. These catalysts are generally soluble organic or organometallic complexes. An array of characterization techniques is available to investigate the catalyst precursor structurally. These precursors are also structurally

identical. Since the entire reaction is in the same phase and the precursors are uniform, it is also easier to investigate reaction mechanisms associated with the catalysts. This has lead to optimization of these types of catalysts through tailoring the electronic properties and structural properties of the active site by changing the ligands around the site.[4] This tailoring of properties around an active site and determining a correlation between the structure of the catalyst with the activity and selectivity introduces a third major theme in catalysis science: the structure – reactivity relationship.[7]

In heterogeneous catalysis, an array of different sites may be present with each site having a different activity.[7] This array of sites is a result of the limits in the synthetic methods available for designing this class of catalysts. These methods which include precipitation, gelation, thermal decomposition of precursors, impregnation, ion exchange, and grafting do not offer the control necessary to produce uniform sites throughout the material.[8] Furthermore, the techniques available to probe the catalytic precursors are frequently more challenging than those used in with homogeneous situations because they require the use of surface techniques. This makes determining not only which sites are the most active, but also ascertaining the structure of these sites as challenging. This information is imperative if a structure – reactivity relationship is to be determined.[8]

Despite the shortcomings of heterogeneous catalysts in terms of synthesizing materials having uniform active sites throughout the material, examples exist where only heterogeneous versions are available. Many

examples of heterogeneous catalysts involve using various methods to grow microcrystalline metals or metal oxides on existing supports. These crystallites are active when they are prepared so that they maintain dimensions within a certain size range to maximize the number of surface atoms associated with the particles. This can only be achieved when these species are well separated so that they do not aggregate during the reaction and thus deactivate. Aggregation occurs frequently when such species are dispersed in solution. Therefore they can only be used in heterogeneous forms.

Supported gold nanoparticles are a primary example of a catalyst that is suitable for catalysis only in heterogeneous systems. Bulk gold is not active as a catalyst because it has a high ionization potential and thus a poor affinity towards substrate molecules.[9] Studies have indicated that dissociative adsorption of H_2 and O_2 will not occur on the smooth surfaces of gold at temperatures below 473K thus making it inactive for hydrogenation or oxidation reactions.[9] Contrary to these observations, nanoparticulates of gold are quite active in the selective oxidation of carbon monoxide. Two reasons are thought to be responsible for the activity of supported gold particles. The first of which is the size of the nanoparticle. Particles having a mean diameter between 2 to 10 nm are active as CO oxidation catalysts.[9] The second reason is the interaction of the gold particle with the support. Hemispherical particles of gold supported on metal oxide supports have activities that are several orders of magnitude greater than spherical particles on the same support for CO oxidation.[9]

1.3.2 Heterogenizing Organometallic Complexes

Due to aggregation problems mentioned earlier for homogeneous catalysis, efforts to "heterogenize" organometallic complexes that are useful homogeneous catalysts include anchoring the compounds onto a variety of different supports. This approach assumes that the structure of the complex does not change once it has been attached to a support and remains intact under reaction conditions. If these conditions are met, then structural information about the catalytic precursor is known and the catalysts would be easy to recover and recycle. However, it has been reported that these complexes can undergo changes during anchoring reactions and become less active which could be in part due to interactions with the support.[10,11] A second problem with this approach involves the loading of the complexes onto the support. If loadings exceed a certain concentration it has been shown that the metal centers can interact with each other and deactivate the catalyst.[11] A final issue that must be addressed involves the stability of the bonds that anchor the complex to the support under reaction conditions. Often times, the complexes will often "leach" from the support during the reaction and thus the observed activity is actually homogeneous in nature.[11]

One method that attempts to address the issues just mentioned for supported organic or organometallic complexes utilizes sol-gel processes to produce interphase catalysts.[11] In these type of systems, the catalytic centers are actually not grafted onto a pre-existing support, but rather are produced by the co-condensation of T-silyl-functionalized metal complexes or ligands with

various alkoxysilanes by the sol-gel process.[11] These methods can produce either mesoporous or micorporous materials depending upon the processing.[11] However some drawbacks have been observed using this method. Optimization of these interphase catalysts using the sol-gel process is challenging because of the number of parameters associates with the catalytic site and the support.[11] Examples of such parameters include the length of the chemical moiety that is used to anchor the catalytic center to the support, the density of active centers on the support, the surface properties of the support and the interaction of the catalytic site with the support.[11] Also, these catalysts in general have lower activities when compared to analogous homogeneous catalysts.[11] Reasons for the lowered activity are not known.

1.4 Characterization of the Active Species

As was previously described, active sites can be difficult to characterize because they are inherently unstable species and are not structurally the same as the synthesized precursors that are added to the reaction. Characterization of an active site can be more easily accomplished for homogeneous system because the catalytic precursor is typically well defined and known. By coupling this information with structural information that can be gain by *in situ* spectroscopic techniques, structures of this active site can be proposed. Use of this information has led to optimization of these catalysts which has resulted in systems where very high activity and selectivity are observed.[4]

Determination of the active site in heterogeneous catalysts can be more challenging. It consists of a surface atom or an ensemble of surface atoms that are responsible for the promotion of the surface reaction.[12] Characterization of these surface bound species can be extremely difficult. For example, nonporous metal oxides have had success in catalyzing many reactions including butane oxidation to maleic anhydride, water-gas shift, methanol oxidation, and ketene synthesis.[7] Some properties that are associated with metal oxide catalysis are redox properties; Bronsted and Lewis acidity; basic properties; lattice oxygen mobility; and the presence of defect sites.[13] Often times the activity is attributed to the surface morphology (different surface faces having different atomic structures) or to previously mentioned defect sites on the surface.[14] Thus, there is a need to characterize such sites so that the structure reactivity relationship can be defined is necessary.[7] One approach used to characterize such sites is to compare the activity of a pure phase with the density of defect sites.[14] Methods are then employed that maximize the number of defect sites. However, this strategy only determines that the defect sites are mostly responsible for the activity. It does not describe the structure of the site within the metal oxide. Knowledge of the chemical composition and electronic properties at this active site is essential to effectively optimize existing catalysts or to design new metal oxide catalysts.[15]

1.5 “Single site” Heterogeneous Catalysts

The optimization of catalysts based on the structure-reactivity relationship in heterogeneous catalysts requires that all sites be uniform. This uniformity of sites not only includes having the active species all be the same structurally, but the environment surrounding the sites should also be the same. This insures that the approach of the substrates to the site is also uniform. Such materials having these properties are termed “single-site” heterogeneous catalysts. Homogeneous catalysts are often single site in nature since the molecular precursors are pure compounds. However, in heterogeneous systems, where surface bound species are responsible for the catalysis, this is usually not the case. Several different species are usually present and they can have various different activities ranging from being very active to having little or no activity. Designing single-site heterogeneous catalysts which are very active and have selectivities that approach 100% is a major challenge currently facing catalysis scientists.[7]

1.6 Current Challenges in Catalysis

Several issues exist with catalysis that needs to be addressed in order to produce catalysts that display high activities and selectivities. High selectivity will improve the “atom economy” by catalysis and is of growing importance for technologies of the 21st century.[7] One of the issues that must be addressed is characterization of the active centers. The spectroscopic techniques needed to perform this task must have necessary time and spatial resolution ability because

these active centers are often dynamic in nature and inherently unstable.[5] Determining the nature of the active sites through spectroscopic techniques can lead to optimization of the catalyst by changing structural features of the catalyst to produce the desired species that promotes the reaction. This knowledge can then be used to design catalysts having optimal uniform active centers throughout.

The active centers should be identical in both their local environments such that substrate molecules can only approach and adsorb onto the site in one orientation. Well defined single-site catalysts will lead to a correlation of the structure and the activity and selectivity.

Understanding the structural properties of the active species and the mechanism of the reaction will lead to a more fundamental picture of the how the catalyst performs. This structure–reactivity relationship can then lead to the design and optimization of catalysts having enhanced activity and selectivity. Designing such highly active, single-site catalysts represents one of the ultimate goals in heterogeneous catalysis and, as was just discussed, can only be obtained through careful research from structural and reactivity studies of existing catalysts.

1.7 Synopsis of Current State in Heterogeneous Catalysis

Designing heterogeneous catalysts which display the activity and selectivity of high performance homogeneous catalysts is one goal in catalysis science. Progress toward this goal will reduce costs by simplifying post reaction

processing steps. Many industrial processes still relying on liquid catalysts face problems of high toxicity, corrosiveness, catalyst waste, use of large amounts of catalyst, and difficulties in separations and recovery.[16] Much of the research with these catalysts has been focused only on maximizing yields with little regard to the environmental impact associated with the production of inorganic waste and toxic by-products.[17] However, the increasing costs of waste disposal and public pressure to reduce toxic wastes is changing the viewpoint from focusing solely on yields of catalytic processes to increased consideration of replacing homogeneous acid catalysts with solid varieties.[17,18] Solid analogs will have several advantages including handling requirements, engineering processes related to recovery and recycling of the catalysts, regeneration of the catalysts, reactor corrosion problems, and environmental issues.[17,18]

1.8 Solid Acid Catalysis

One of the main subdivisions in heterogeneous catalysis is solid acids. Homogeneous acid catalysts are typically used more frequently in the fine, specialty, and pharmaceutical chemical industries with heterogeneous acid catalysts seeing widespread use mainly in the petrochemical industry.[17] Beginning in 1940, a push began to move from the use of liquid acid catalysts to utilizing solid acid catalysts for industrial processes because the solid versions would be more cost effective and less harmful to the environment.[18]

The following section will give an overview of some of the most important areas in solid acid catalysis research including several examples of solid acids as

well as porous materials which are often utilized to support acidic centers. These examples will include zeolites, acidic mesoporous molecular sieves, heteropolyacids, organic-inorganic composites, sulfated oxides, and aluminum trichloride supported on silica. Zeolites and mesoporous molecular sieves will be combined into one section entitled Porous Solids. The remaining sections include others prominent categories in solid acid catalysis research just mentioned.

1.8.1 Heteropolyacids

Heteropolyacids (HPA) are define as a condensate of a variety of oxoacids.[16] These compounds can be prepared having structures that can be categorized into such groups as Keggin and Wells-Dawson type heteropoly anions (Figure 1.1).[16,18] In the solid state, these compounds are ionic crystals made up of large polyanions, cations, waters of hydration, and other molecules.

The acidic properties of HPAs have been characterized and determined to be pure Bronsted acids.[19] In fact, it has been suggested that heteropolyacid $H_3PW_{12}O_{40}$ is a superacid and pyridine adsorption-desortpion experiments suggest that these species are more acidic than SiO_2-Al_2O_3.[19] The acid strength of this heteropolyacids has been determined in acetonitrile relative to other HPA's and the results were as follows: $H_3PW_{12}O_{40} > H_4SiW_{12}O_{40} > H_4GeW_{12}O_{40} > H_6P_2W_{18}O_{62} > H_5BW_{12}O_{40} > H_6CoW_{12}O_{40}$.[16] Due to the acid strength of the dodecatungstophosphoric acid because it has been studied more than any other HPA.[18] When compared to other inorganic acids in acetronitrile the following

Polyoxometallates (POMs)

Keggin, Dawson ions

$[X^{+n}M_{12}O_{40}]^{(8-n)-}$

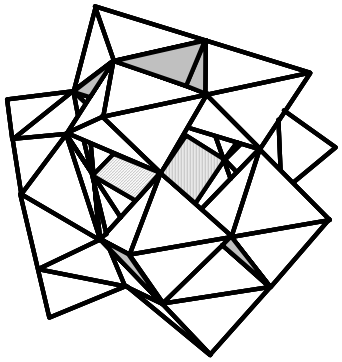

$Ti_{11}O_{13}(OR)_{13}$

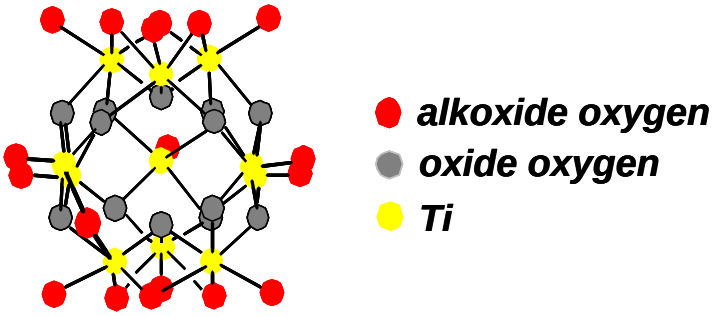

Figure 1. 1 Polyoxometallate having a structure typical of Keggin or Dawson type ion.

acid strengths were obtained: $H_3PW_{12}O_{40}$ > CF_3SO_3H > *p*-toluene-sufonic acid > H_2SO_4 > CF_3COOH > ClC_6H_4COOH.[16]

Despite the high acid strength of heteropolyacids, they are limited in their use in catalysis due to their low surface area. This problem has been addressed using two different methods: 1) preparing acid salts having large cations and 2) anchoring the heteropolyacids on high surface area supports.[18] However, both of these methods have limitations. In the case where H^+ is substituted with large cations, the acidity of the catalysts decreases as the concentration of the cation substitute increases.[18] Thus, a compromise must be made between the surface area and global acidity. Limitations in supported heteropolyacids arise from their size. These molecules potentially can plug pores when anchored on porous materials and thus loading and accessibility by the substrate can become an issue.[18] Leaching is a second problem frequently observed with supported HPAs during reactions.[16]

Examples of reactions catalyzed using supported heteropolyacids are the single pot synthesis of methyl-*tert*-butyl ether from *t*-butyl alcohol and methanol using clay as a support.[18] High loadings of heteropolyacids on ordered mesoporous silica were active and selective for isobutene/butane alkylation, aromatic alkylation with long chain alkyl groups, and C_4-C_9 isomerozation.[18] Heteropolyacid materials having both mesoporous and microporous surface properties simultaneously have been prepared by substituting large cations for H^+ and were used for the hydrolysis of ethyl acetate in excess water. Activities up to thirty-five times that of an aluminosilicate zeolites were observed for these

reactions.[16] These catalysts were also tested for reactions involving bulky substrates and showed activity for the hydrolysis of 2-methylphenyl acetate, hydrolysis of maltose, and the hydration of 2,3-dimethyl-2-butene.[16]

1.8.2 Inorganic-Organic Composites

Ion-exchange resins have been immobilized in silica matrices using sol-gel techniques to produce high surface area polymer resin-silica composite materials. One of the most studied of these materials is the perfluorosulfonic catalyst, Nafion entrapped in silica developed at DuPont.[16,18] These materials have surface area of 150-500 m^2/g and have been utilized as catalysts for reactions such as alcohol dehydration, Friedel-Crafts aromatic alkylation, and α-methyl-styrene dimerization.[18]

1.8.3 Sulfated Oxides

Sulfated metal oxides have an increased surface acidity and enhanced catalytic activity when compared to untreated versions.[18] These materials have the ability to catalyze reactions that required homogeneous "superacids."[18] Examples of reactions that are catalyzed using these materials are isomerization, alkylation, acylation, and esterification.[20] Despite the observed activity for these reactions, questions remain about the acid strength of these materials. Conflicting interpretations about the nature of the acid sites have been presented. Pyridine adsorption studies suggests that only Lewis acid sites are present, while other reports suggests that the activity is due to Bronsted acid

sites.[21] Other researchers claim that both types of acid sites are present and that the ratio of these sites depends upon preparation and handling of the material.[21]

1.8.4 Aluminum Trichloride on Silica

The surface of silica-gels can be functionalized with $AlCl_3$ to produce solid acid materials capable of catalyzing alkylation, isomerization, and hydrocarbon cracking reactions. All of these reactions are important and have specific uses in the petrochemical industry.[22-24] These catalysts are prepared by refluxing aluminum trichloride in carbon tetrachloride in the presence of dehydrated silica. The solvent appears to have an affect on the acidity because using hydrogen containing solvents such as methylene chloride or chloroform and donor solvents (benzene) resulted in less acidic materials.[23]

1.8.5 Porous Solids

Probably the most selective family of heterogeneous acid catalysts is zeolites. These materials are micorporous, crystalline silicates and metallosilicates typically made up of four or five ring siloxy groups with metal atoms substituted for silicon atoms throughout the three-dimensional framework (Figure 1.2). Due to the crystalline nature of zeolites, the active sites can be probed using a number of spectroscopic techniques which help identify and elucidate these active sites.[8] These studies have provided a wealth of information regarding the relationship between the structure of the active sites within the zeolites and the activity and selectivity.[8,25]

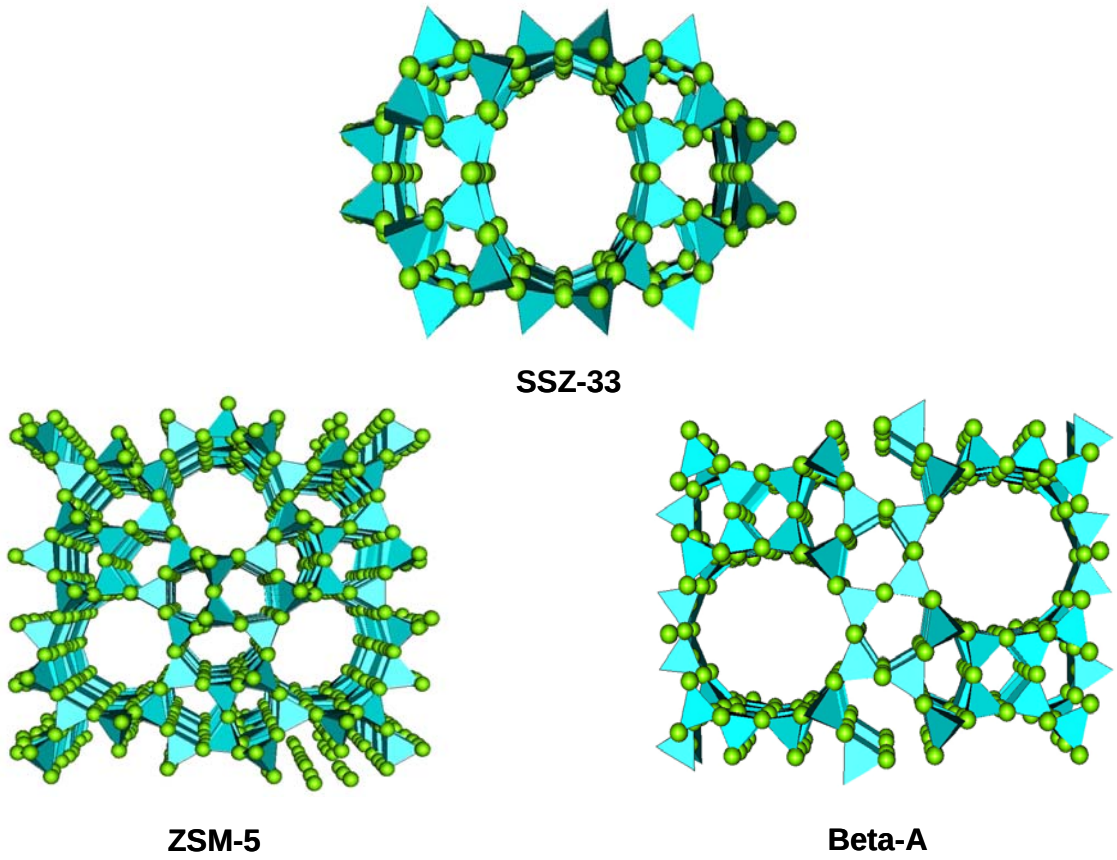

Figure 1. 2 Structure of three common zeolites showing well defined pores.

Zeolites perform extremely well in terms of reactivity and selectivity.[8,25] Their selectivity has been attributed to the regular pore structure which form well defined channels that act as microscopic reaction cavities. The size of the pore networks vary for different zeolites, and the variable sizes of the channels determine the selectivity of the reaction being catalyzed by size discrimination of the substrates and the reaction products. This shape selectivity by mass transport discrimination occurs when the diffusion coefficients of the molecules within the pores are different by at least one order of magnitude.[25]

The reactive properties just described has had an enormous impact in the petrochemical industry where they are utilized in fluid catalytic cracking (FCC) reactions.[25] For example, ZSM-5 was used in a process to selectively crack linear olefins versus branched olefins in the gasoline range to produce higher octane fuels.[25] Zeolites having small and medium pores have been used industrially for catalytic dewaxing processes.[25] The selective hydroisomerization of long chain *n*-parafins to monobranched isomers versus multibranched isomers also illustrates the selectivity of these materials.[25]

Using the structural information known for zeolites, systematic modifications and optimizations have been made so that improvements in performance were observed.[8] These solids are acidic in nature and contain both Bronsted and Lewis type acid sites. The strength and density of these acid sites can be controlled through synthesis or post synthesis methods.[25] The hydrophobic-hydrophilic nature of the material can also be tuned by adjusting the

Si/Al ratio.[25] Finally, the pore sizes in zeolites can also be varied by changing the organic templates used during synthesis.[26]

Despite the great utility of zeolites and the extensive amount of research conducted on them, they are not useful catalysts for reactions involving larger molecules that can not diffuse into the micropores of these materials.[26] Thus, the need to produce heterogeneous catalysts that can catalyze reactions involving larger molecules is necessary. However, normal techniques used to produce zeolites typically can not be employed to produce zeolites having mesoporous properties.[26]

The need for mesoporous solids resulted in the development of new approaches to porous solid synthesis. A large variety of mesoporous materials have been synthesized through the use of micelle templating techniques and used as inorganic supports for heterogeneous catalysts. Such materials include the following: the M41S family which utilizes long chain alkylammonium templates, the HMS family which utilizes long aliphatic amines as templates, and the MSU family which utilizes poly(ethylene oxide) surfactants and block copolymers as templates and are categorized by the type of template utilized in their synthetic processes.[27]

The pore properties of these materials can be tuned by varying the synthetic method. For example, the M41S family of mesoporous materials has large ordered channels that range from 1.5 – 10 nm.[26] They can be synthesized so that they have hexaganol (MCM-41), cubic (MCM-48), or laminar (MCM-50) ordered arrays of channels.[26] Of these, MCM-41 is the most important. It can be

synthesized such that various metal-oxide domains are present in the walls of these silicate materials.[26] Materials made having additional metals incorporated into the wall composition of MCM-41 exhibit interesting catalytic properties including redox and acidic properties.[26]

Despite the great utility of these materials as supports for catalysts, some problems still exist. It was found by UV-vis and EXAFS that domains of Ti-O-Ti were present in the walls along with isolated metal centers.[26] Attempts to isomorphously substitute chromium atoms for silicon atoms into the structure resulted in a material having only a small amount of Cr^{3+} ions in the walls of the material.[26] Substitution of metals into the framework of these materials can also result in leaching of metal ions during the reaction. This was observed when manganese is introduced into the walls of the material. It appeared that the manganese migrated to the pores of the material during calcinations.[26]

An obvious extension of the technology employed to make mesoporous silicate materials is the synthesis of mesostructured metal oxides. These materials would be interesting not only as supports, but as catalysts themselves. Some progress has been made in this area with aluminia and zirconia, but more work needs to be done to further advance this area.[26]

1.9 Fundamental Issues and Challenges Addressed in this Thesis

Several issues exist in designing heterogeneous catalysts which can lead to enhanced understanding of how these species perform. One important item is the design of catalysts that have sites uniformly dispersed throughout the

material. Furthermore, all sites should have one unique environment throughout the material so that a correlation between structure and reactivity can be determined.

Elucidation of this relationship dictates that the solid materials be well characterized from both a structural and reactivity viewpoint. The following section will describe building block techniques that have been developed to synthesize materials that can be used to produce next generation heterogeneous catalysts. These methods provided a means to obtain metal centers having uniform environments dispersed in silicate based materials. This discussion will then be followed by an overview of the methods used to characterize these materials.

1.9.1 Building Block Solids

Building block solids are materials that are synthesized by linking together preformed, molecular precursors to form a three dimensional matrix of connected building units. In this thesis, the molecular precursor $Si_8O_{20}(SnMe_3)_8$ is utilized as a building block because it is a chemically robust, thermally stable moiety that is reactive towards many metal chlorides via a metathesis reaction first described by Feher and Weller in 1994.[28] A detailed structural description of the $Si_8O_{20}(SnMe_3)_8$ building block precursor will be given in chapter 2 of this thesis and a detailed description of the metathesis reaction utilized will be given in chapter 3.

The thermal and chemical stability of Si_8O_{20} is essential to this method and introduces one key tenant in building block synthesis: the building unit must maintain structural integrity under the reaction conditions utilized to synthesize building block materials. If the conditions used for producing the catalyst cause disruption of the building block, then all control over the reaction and ultimate structure of the product will be lost. This control is essential if this method is to be applied to developing next generation heterogeneous catalysts because these materials will require catalytic centers that are uniform throughout so that a correlation between structure and reactivity can be established.[7]

A second requirement for this method to be successful in addressing current issues in heterogeneous catalysis is the size of the building unit. It should be large enough so that the metal species used to link the building units are separated in space such that they do not interact with each other during synthesis or during catalysis. Chapter 2 of this thesis gives structural description of the building blocks used herein and confirms that the size of the Si_8O_{20} building unit is large enough to prevent metal centers from interacting in the structural studies of the molecular species $Si_8O_{20}(Cp_2TiCl)_8$.

The final tenant of building block synthesis requires that the functional units on the building block and the functional groups on the linking units are not reactive towards each other. This is important because it prevents domains of linking units and domains of building blocks from forming within the material. This type of complementary functionality will be described in detail in chapter

three. Previous investigations where vanadyl trichloride was used as a linking unit show that the reactions utilized herein meet this tenant.[29]

The three requirements of stability of the building block, complementary functionality, and adequately sized building units are met using the octafunctional spherosilicate $Si_8O_{20}(SnMe_3)_8$ in reactions with various metal chlorides. Therefore this reaction can be utilized to produce building block materials. In addition, it was shown that in the investigation mentioned above involving vanadyl trichloride with $Si_8O_{20}(SnMe_3)_8$ that the use various addition sequences resulted in producing materials where control over the immediate environment of the vanadyl groups was achieved.[29]

These methods involve simple concepts and were carried out in this thesis using silylchlorides for proof of concept studies. In these studies, “deeply embedded” centers were made by adding a limiting amount of metal chloride to an excess of $Si_8O_{20}(SnMe_3)_8$ (Figure 1.3). Deeply embedded, in this context, refers to complete or near complete substitution around a linking group. For example, a deeply embedded linking group forms when three or four building blocks are linked together with tetrachlorosilane. Due to the excess of the functional groups present on the building blocks in these reactions, all metal chloride groups react and form oligomeric species consisting of a few linked building blocks. These oligomeric species are then cross-linked using a robust linking unit. This method can easily be applied to designing deeply embedded catalytic centers by using potentially active centers as the initial metal chloride to produce solids have uniform embedded sites throughout the material.

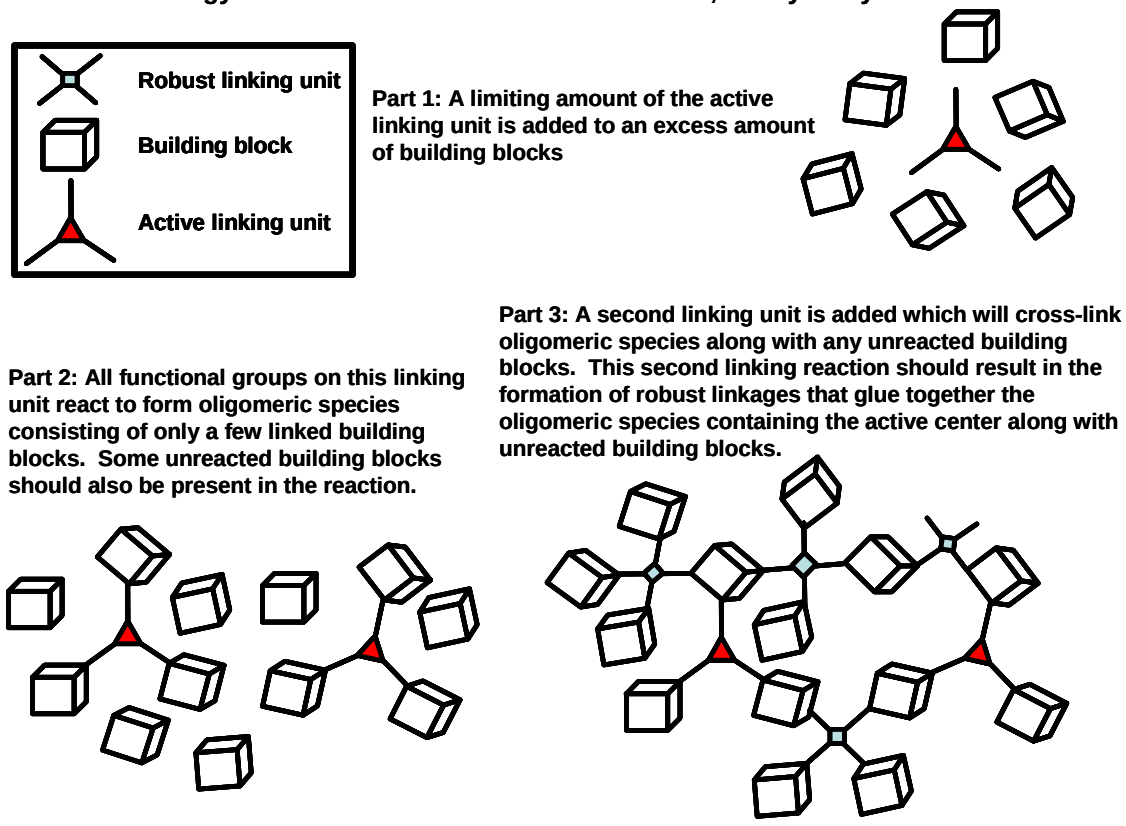

Figure 1. 3 Synthetic strategy to produce embedded catalytic centers.

Furthermore, these embedded sites could prevent the active species from leaching during catalytic reactions.

Surface bound species can also be prepared by using a different addition sequence (Figure 1.4). In this procedure, building blocks are first cross-linked with a robust chemically inert linking unit such that an extended solid is produced but residual functional groups are present on the building block. These groups should be dispersed throughout the solid matrix. This material can then be exposed to an active metal so that all of the functional groups on the building block solid are replaced by the active species. Since the support produced by the cross-linking reaction should be rigid in nature and the functional groups spatially isolated, the active species should be prevented from further cross-linking and thus will only be attached to the support through one bond and remain on the surface of the material.

1.9.2 Amorphous Solids

The building block materials described herein are amorphous in nature due primarily to two factors. First, the metal oxide bonds that link together spherosilicate building blocks are irreversibly formed under the reaction conditions utilized. Second, the building block has eight functional groups present for reaction with linking units. The linking units utilized in the reactions described herein have between two to four functional groups. Thus the degrees of freedom associated with this high number of functional groups results in a random distribution of units linking varying amounts of building blocks. A more

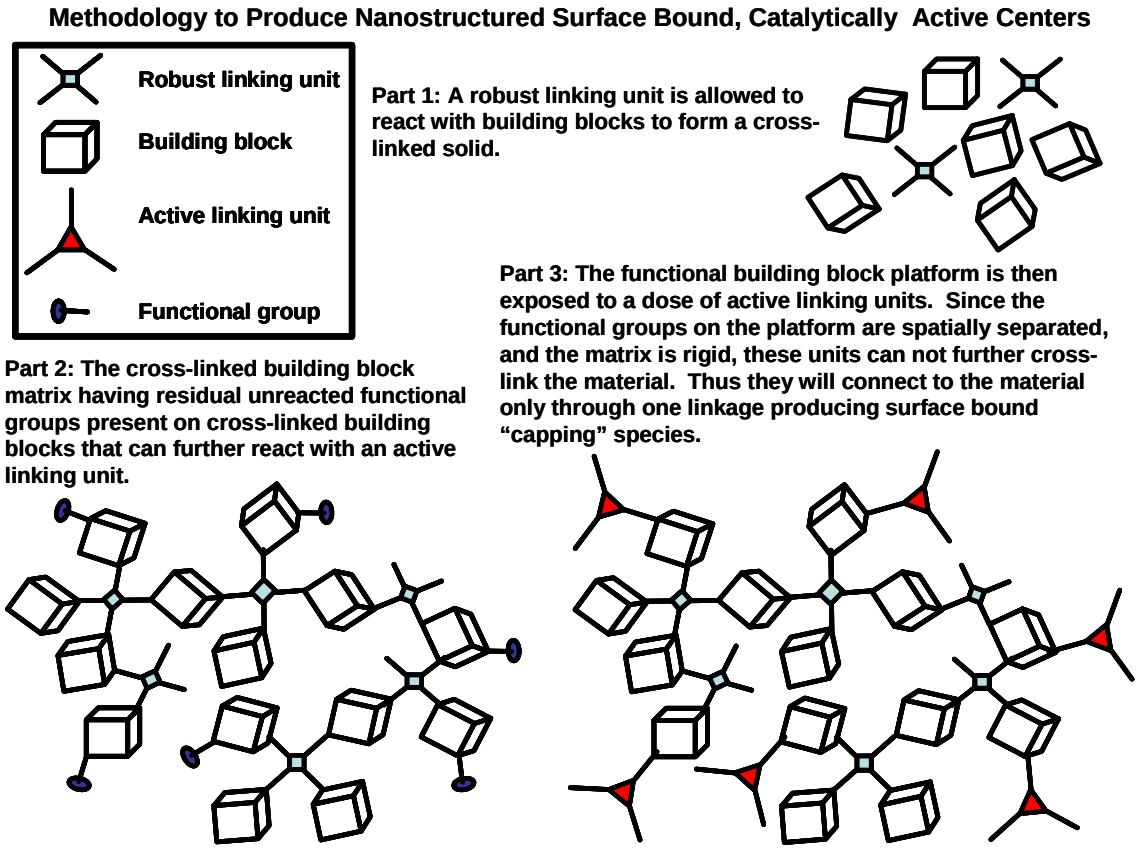

Figure 1.4 Synthetic strategy to produce surface bound, "capping" catalytic sites.

detailed discussion of the amorphous nature of these materials is given in chapter 3 of this thesis.

1.9.3 Characterization of Solid Materials

The amorphous nature of these materials makes their characterization challenging. Due to the lack of long range ordered in these materials, routine diffraction techniques can not be employed to gain insight into their structure. Thus, several techniques must be used to determine their structural features. The following section will introduce the methods used to characterize the spherosilicate based building block materials described in this thesis.

1.9.3.1 Infrared (IR) Spectroscopy

Infrared spectroscopy provides information about the vibrations of bound atoms in molecules and solids. This technique is widely used in catalysis providing a wealth of information about structural features, surface properties, sorbate-sorbent interactions, and reaction intermediates.[3] Vibrational data can also be used to identify specific functional groups present in a compound or materials. IR was used in the studies described in this thesis to characterize reaction products and to follow changes to materials after various treatments were applied using signals in the spectra that were assigned to specific functional groups. Examples of functional groups within the solids probed using IR spectroscopy were metal-oxygen-silicon bonds, alkyl groups, and hydroxyl groups.

1.9.3.2 Surface Area and Pore Property Determination

Physisorption of condensable gasses onto the internal and external surface of solid materials is a commonly used method to determine the surface area and porosity of heterogeneous catalysts. Physisorption involves the non-covalent attraction of a gas with an outgassed solid.[30,31] The gas in this context is termed the adsorptive and the solid is called the adsorbent.[30] By dosing a solid material with an adsorptive at constant temperature, adsorptive isotherms are measured.

Adsorption-desorption methods have been used extensively to investigate porous materials.[32] Such materials have been classified by the IUPAC and fall into one of three categories: microporous (pore diameters not exceeding 20 Å), mesoporous (pore diameters in the 20 – 500 Å range), and macroporous (pore diameters exceeding 500 Å).[30] Information about the porosity of a material can be determined by examining isotherms obtained from gas adsorption experiments. Descriptions of these isotherms and the types of materials that produce such results can be found in the literature.[30,33]

The instrument used to characterize the surface area and pore properties of the materials described in this thesis was limited to the mesoporous range. It does not measure pore properties below 20 Å and thus any microporous properties could not be determined for these materials.

1.9.3.2.1 Determining Specific Surface Area

The physisorption isotherms yield information about the surface area as well as the properties of the pores of a material. The specific surface area of materials can be determined from the isotherms by either the Brunauer-Emmett-Teller (BET) method or the comparative method.[33] The BET method is based on determination of the monolayer capacity of the surface of a sample by fitting gas adsorption data to the BET equation.[33] The monolayer capacity is then multiplied by the cross-sectional area of the adsorptive molecule on the adsorbant.[33] The comparative method compares adsorption data from a porous material to that of a suitable reference material having a known surface area. The BET method is the more widely used of these methods and is a standard method for determining surface area.[30,33] This method was used in all surface area studies described in this thesis.

1.9.3.2.2 Determining Pore Diameter

The average pore diameter of materials having an ordered pore structure can be determined because of geometrical relations that exist due to the ordering of the pores. For example, in calculations of pore diameter based on materials having uniform cylindrical pores, the diameter of the ordered pores is directly related to the pore volume and indirectly related to the geometrical surface area.[33] The pore volume and the geometrical surface area can be obtained from the adsorption data.[33] However, uncertainties exit in the methods for determining

the geometrical surface area.[33] Therefore other methods should be used if accurately pore diameter measurements need to be made.

The average pore diameter was taken for samples described in this thesis. In all cases, the average pore diameter was determined to be in the microporous range. However, since the instrument used does not probe this region and uncertainties exist in the methods used to calculate this parameter, we are not confident in these values. However, they will be presented to compare synthesized samples.

1.9.3.2.3 Determining Pore Volume

The total pore volume can be calculated using the total amount of adsorbed gas at a relative pressure close to the saturation vapor pressure.[33] This is achieved by converting the amount of adsorbed gas to the corresponding liquid volume adsorbate at the appropriate temperature.[33] This method works for mesoporous materials and assumes that the density of the condensed adsorbate in the pores is equal to the density of the bulk liquid adsorbate.[33]

1.9.3.2.4 Determining Pore Size Distribution

Pore size distributions can also be determined from the isotherm data obtained from adsorption-desorption measurements by many methods. The most notable being the Barrett, Joyner, and Halenda (BJH) method.[34] Details of this method can be found in the literature.[34] This theory can be applied to both the adsorption and the desorption isotherms. However, significant differences in

the pore size distribution can be obtained for these two isotherms in the hysteresis region.[33] It is recommended in the literature that the pore size distribution should be calculated using the adsorption isotherm to avoid artifacts and to get a more accurate determination.[33] These artifact occur due to the delay in desorption attributed to pore network effects.[33]

1.9.3.3 Nuclear Magnetic Resonance (NMR)

NMR provides useful information about the structure and electronic environments of a nucleus in a compound or material. This information can be obtained because a difference in the local magnetic field of a nucleus occurs due to many factors including the electrons in the compound or material. The local magnetic field differences is what makes this area of spectroscopy valuable because it results in the nuclear magnetic field having a different frequency than that of the applied filed. These different frequencies can be detected are the resonance signals observed are termed chemical shift values. These values in many cases can be used to identify chemical groups.

1.9.3.3.1 Solid State NMR

The NMR of solid materials presents a number of challenges mainly due to the lack of motion in the solid state. Lack of motion results in resonance signals being broad and convoluted making spectral interpretation extremely difficult. The broadening of individual signals in solid state NMR occurs for several reasons. The individual nuclei in the solid will each experience the fields

of neighboring nuclei which have random spin directions. The interaction of a nucleus with randomly oriented neighboring spins results in a range of frequencies that add to linewidth. A second contribution to linewidth concerns the relaxation of the nuclei. It is known that T_1 relaxation times are long in the solid state due to the lack of modulation of the dipole-dipole interaction. However, T_2 is shortened because the individual nuclei in the solid produce a oscillating magnetic field in the solid as they precess in the applied field. This can cause energy exchange between nuclei which shorten the spin state lifetime and thus shortens T_2 relaxation. The linewidth of NMR transitions and spin state lifetimes are inversely related to one another via the uncertainty principle. Short spin state lifetimes lead to uncertainty in the energies of the states and thus a range of energies for transitions between states. A third contribution to linewidth is the chemical shift anisotropy. The chemical shift is a tensor quantity which does not average to an isotropic value in the solid state due to restricted motion. These factors which all contribute to linewidth were overcome by the revolutionary technique of magic angle spinning (MAS) solid-state NMR.[35]

1.9.3.3.2 Magic Angle Spinning (MAS) NMR

Dipole-dipole interactions between nuclei in the solid-state significantly contribute to the linewidth of resonance signals. This interaction is inversely proportional to the third power of the distance between the two nuclei and directly proportional to the angle θ between the direction of the applied field (*z*

component B_z) and the line drawn between the two nuclei by the following equation:

$$B_z = \frac{K\mu}{r^3}(3\cos^2\theta - 1)$$

where K is a constant, μ is the magnetic moment, and r is the distance of a second nucleus. Fortunately, dipolar interactions disappear when the angle between the two nuclei satisfies $3\cos^2\theta$-1 = 0 or θ = 54°44'. Thus spinning the sample at high spin rates at this angle (termed the magic angle) will have dramatic effects on the linewidth of the resonance signals. At these high spin rates, all nuclei in the sample have an average angle of 54°44' with respect to the applied field and the dipolar interactions will disappear resulting in a narrowing of the linewidth. The technique which places the sample in the field at an angle if 54°44' is termed magic angle spinning (MAS) NMR .[35]

1.9.3.3.3 Cross-Polarization Magic Angle Spinning NMR

Nuclei with spin-½ and low magneticgyric ratios (γ) suffer from low inherent sensitivities which can lead to overly long instrumental collection times to achieve acceptable signal-to-noise ratios. When coupled with long relaxation properties the detection of NMR signals for such nuclei can become virtually impossible. One technique that can be used to enhance the signal and reduce relaxation time is call cross-polarization (CP) NMR (Figure 1.5). This double irradiation technique allows exchange of polarization between the ^{1}H and the

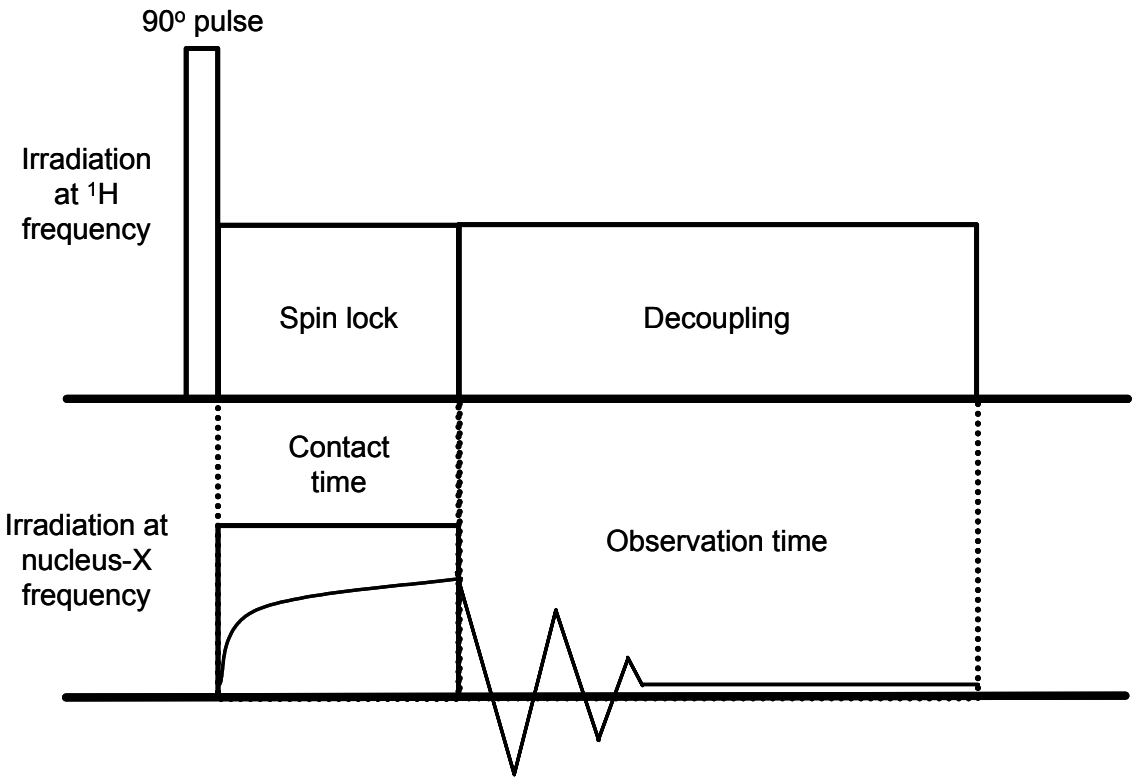

Figure 1. 5 Cross-Polarization (CP) NMR pulse sequence.

nuclei of interest. This is achieved by first preparing the ^{1}H nuclei for cross-polarization by applying a 90^{o} pulse which results in the ^{1}H magnetization being in the *xy* plane. The phase of the magnetization is then changed by 90^{o} and it remains in the *xy* plane. This technique is called "spin locking." The X nuclei are then excited by a long pulse of specific amplitude that allows the X nuclei to precess at the same rate as the ^{1}H nuclei. This is known as Hartmann Hahn matching. Energy is exchanged between the two nuclei until equilibrium is reached between the two spins which results in an enhancement of the population difference for the X nuclei. This pulse sequence can be repeated once the ^{1}H nuclei have reached equilibrium thus reducing the waiting times between experiments. The increased intensity of the signal from the X nuclei is due to the increased population difference that was just described by a factor of $\frac{\gamma_H}{\gamma_X}$.[35]

The CPMAS experiment requires the presence of ^{1}H nuclei. This can also be useful when assigning signals by comparing CPMAS spectra with simple magic angle spinning spectra for the same sample. X nuclei having ^{1}H nuclei in close proximity will experience greater enhancements than X nuclei that are separated from ^{1}H nuclei spatially by longer distances in the CPMAS experiment. This enhancement will be noticeable when compared to a MAS experiment.[36] This technique can also be extremely valuable when determining the presence of X-H nuclei having low concentrations in the solids since the sensitivity of the signal is enhanced.[35,36]

1.10 Thesis Overview

Addressing current challenges in heterogeneous catalysis will require novel approaches to synthesizing catalysts because traditional methods lack the necessary control to tailor the active sites in such a way as to optimize the activity and selectivity in a predictable manner.[7] In order for this to occur, materials need to be developed that have well defined, uniform sites throughout the entire material. A correlation between the structure and the reactivity can be achieved only through complete structural characterization of the active site. In this thesis, methods are described which show that by using building block methods to synthesize heterogeneous catalysts; control over the local environment of the active centers is realized. This control allows for the synthesis of building block materials where site isolated centers are placed into a silicate support having one unique local environment throughout the material. The remaining portion of this section describes the content of the following chapters of this thesis which outline the steps taken to produce such materials.

Chapter 2 contains structural studies of cubic and pentagonal prismatic, spherosilicate building blocks in the solid state. The cubic spherosilicate is the building block that is used for the synthesis of the nanostructured materials described in this thesis. Single crystal X-ray diffraction was used to study the structure of stannylated spherosilicates and a novel octatitanocene cubic sperosilicate. The X-ray data for these compounds are compared to structural data for analogous compounds found in the Cambridge Structural Database. This study highlights the flexibility of the siloxy bridge in the spherosilicates which

link together rigid SiO_4 tetrahedral subunits. These compounds are introduced as suitable molecular building block precursors to be used in the preparation of building block materials. The reaction of the octameric stannalyated spherosilicate with dichlorotitanocene is a molecular illustration of the utility of the reaction of the mixed tin-silicon ether functionality with metal chlorides to make metal oxide/silicate based materials. This reaction also provides some preliminary evidence that the Si_8O_{20} building block does not loose its structural integrity during the reaction of $Si_8O_{20}(SnMe_3)_8$ with metal chlorides in making molecular species.[37] The material presented in this chapter has been submitted to The Journal of Organometallic Chemistry for publication and is currently being revised.

Chapter 3 presents the results of our first attempts at preparing building block solids. These solids are insoluble, amorphous materials that result from the cross-linking the $Si_8O_{20}(SnMe_3)_8$ building block with various silanes. A simple method is described where the local environment of the silane linking units can be controlled to produce tailored solids. This was achieved using various silane linkers along with different addition sequences. These materials proved to be easily characterized using silicon-29 solid state NMR. The synthetic procedures outlined in this chapter form the basis for a major theme of this thesis: preparing metal oxide/silicate based materials in a controlled manner so that the local environment around specific metal sites is uniform throughout the material. This is important because these methods can be applied to many different linking units which could serve as catalysts. This approach to designing such catalysts

is an important step in creating next generation “catalysts by design.” Such catalysts are extremely important in establishing a correlation between structure and activity and selectivity.

Chapter 4 describes a study where the methods outlined in chapter 3 were utilized to prepare titanosilicates and aluminosilicates. These materials were then investigated for their activity as solid acid catalysts. The specific reaction that was probed was the transesterification of triacetin with methanol. This reaction is a model reaction for the production of biodiesel fuels.

Chapter 5 concludes the thesis and discusses possible future studies. The future work is related is related to each specific chapter.

Chapter 2: Synthesis and Structure of Functional Spherosilicate Building Block Molecules for Materials Synthesis

2.1 Introduction

Spherosilicates are molecular cage compounds of the general formula $(XSiO_{1.5})_n$ (X = inorganic or organic substituents, n = 6,8,10,12,14) comprised of Si—O—Si based rings which result from oxygen shared $XSiO_3$ tetrahedral units.[38-40] These compounds are interesting from both application and fundamental perspectives. They are useful in a broad range of areas including cosmetics, atom scavengers, cores for branched dendritic macromolecules, molecular composite materials, and optical fibers.[41-45] They are structurally important because the cubic Si_8O_{12} and the pentagonal prismatic $Si_{10}O_{15}$ contain double four ring (D4R) and double five ring (D5R) units respectively. Both D4R and D5R ring units are also found in many natural and synthetic zeolites and silicates.[46,47] Due to their occurrence in these important materials, spherosilicate based compounds have been used as models in structural and vibrational model studies.[46-50]

Materials scientists have has also employed spherosilicates as building blocks in developing new materials.[38] Several schemes have been developed to attach synthetically useful groups to the *exo*cage position.[38] Once accomplished, these silicate building blocks can be used as polyfunctional monomers that may be cross-linked together to produce 3-dimensional silicate polymers. For example, high surface area materials have been made from the sol-gel

polymerization of $(CH_3O)_8Si_8O_{12}$ while multicomponent, porous inorganic materials have been made by the reaction of $Si_8O_{20}[N(CH_3)_3(C_2H_4OH)]_8 \bullet nH_2O$ with $Zr(C_5H_7O_2)_4$.[51-53] Inorganic/organic hybrid porous materials have been made by linking together Si_8O_{12} units with organic groups of various lengths via a hydrosilylation reactions using Si-H containing cubane Si_8O_{12} cages and cubic spherosilicates containing vinyl groups.[54,55] These cross-linked Si_8O_{12} cores have also been studied theoretically.[56]

Cubic spherosilicates bearing *exo*cage trialkyltin functional groups are reactive towards many metal halides via a metathesis reaction whereby novel metallosilicate materials are produced.[28,57] It has recently been shown that the nanoscale size associated with Si_8O_{12} units allows for tailoring of the immediate chemical environment in such metallosilicates.[29] Herein we describe the synthesis and structures of several cubic and pentagonal prismatic stannylated spherosilicates $Si_8O_{20}(SnR_3)_8$ (R = Me and ^{n}Bu) and $Si_{10}O_{25}(SnMe_3)_{10}$. Furthermore, $Si_8O_{20}(SnMe_3)_8$ has been used to synthesize the octatitanocene derivative, $Si_8O_{20}(Cp_2TiCl)_8$. Structural comparisons of these compounds with related spherosilicates reveal new insights into their properties as potential building blocks in the preparation of nanostructured silicate materials.

2.2 Experimental

Solution nuclear magnetic resonance (NMR) spectra were recorded at 9.4 Tesla on a broadband Bruker Avance (400 MHz ^{1}H) instrument. Chemical shifts were referenced to the following: ^{1}H NMR $\delta(C_6D_5H)$ 7.15; ^{13}C NMR δ (C_6D_6)

128.39; ^{119}Sn δ (Me_4Sn) 0; and ^{29}Si δ (Me_4Si) 0. Solid state NMR spectra were recorded at 9.4 Tesla on a Varian Inova multinuclear instrument. Silicon-29 CPMAS NMR of crystalline anhydrous $Si_8O_{20}(SnMe_3)_8$ and amorphous $Si_8O_{20}(SnMe_3)_8$ was recorded at spin rates of 5.5 kHz and referenced externally to the trimethylsilyl signal at δ 11.72 ppm for $Si_8O_{20}(SiMe_3)_8$ on a broadband Varian Inova spectrometer in 5mm pencil rotors. At least six different signals were observed between -99 and -105 ppm for crystalline anhydrous $Si_8O_{20}(SnMe_3)_8$ (Figure 2.1 a). The tetrahydrate $Si_8O_{20}(SnMe_3)_8$•$4H_20$ was dehydrated and determined to be amorphous by powder X-ray diffraction. This silicon-29 CPMAS solid state NMR of the amorphous powder had at least five different signals between -99 and -104 ppm (Figure 2.1 b).

Elemental analyses were performed at Desert Analytics (Tucson, Az) unless otherwise noted.

Thermal Gravimetric Analysis (TGA) was performed on a TA Instrument Q50 TGA equipped with platinum pans.

Single crystal structures were determined using a Bruker model AXS Smart 1000 X-ray diffractometer equipped with a CCD area detector with a graphite monochromated Mo source (K_α radiation, v = 0.71073 Å). The instrument was fitted with an upgraded Nicolet model LT-2 low-temperature device. Crystals coated with paratone oil (Exxon) were mounted on a “hair loop” under a nitrogen stream at –100^{o}C. Global refinement of unit cell and orientation matrix data and data reductions were performed using SAINT 6.02.[58] All calculations were performed using the SHELXTL 5.1 proprietary software

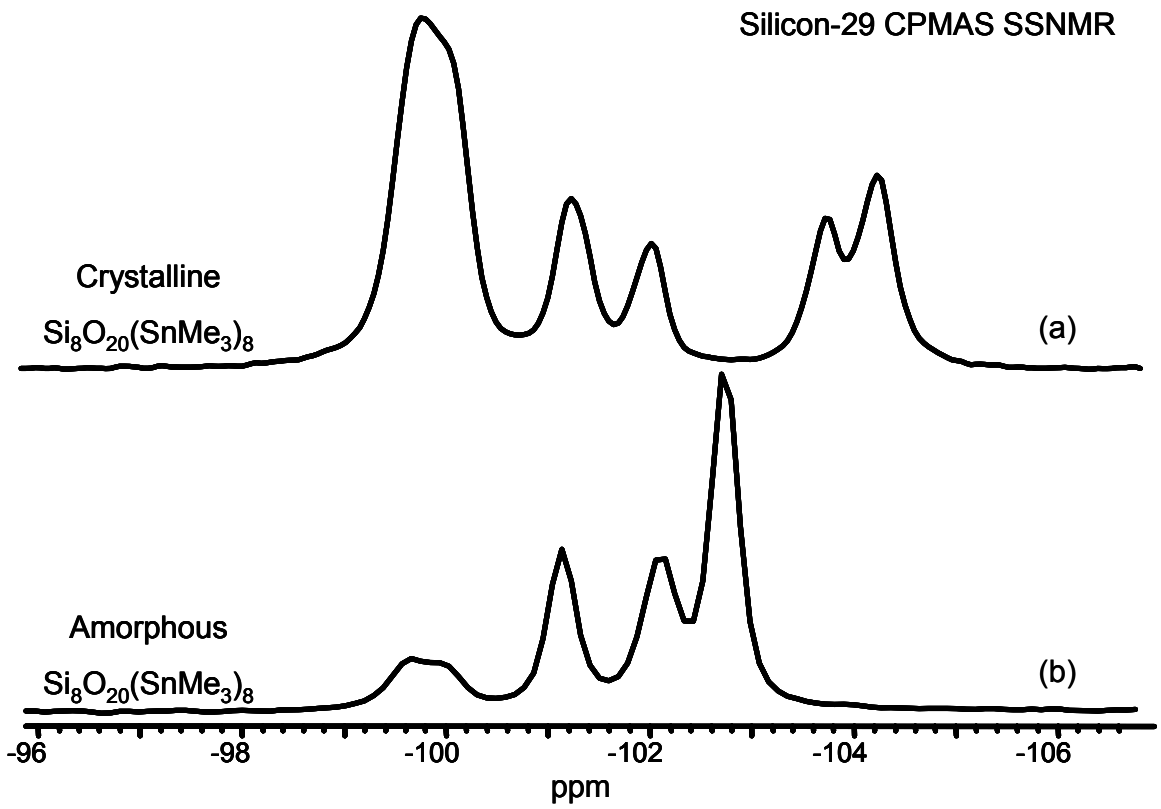

Figure 2. 1 Silicon-29 CPMAS solid-state NMR of anhydrous crystalline and amorphous $Si_8O_{20}(SnMe_3)_8$ showing the chemical shift range for the cage silicon nuclei.

package.[58] The SADABS program was used to make empirical adsorption corrections.[59] Complete structural and refinement tables along with tables of bond distances for the four compounds investigated in this study are given in the appendices of this thesis.

Structural parameters from single crystal X-ray data for compounds containing the cubic Si_8O_{12} and pentagonal prismatic $Si_{10}O_{15}$ spherosilicate fragments were obtained from the Cambridge Structural Database (CSD).[60] Seventy structures containing the Si_8O_{12} cubic spherosilicate were found in the CSD database. Structural information was available for thirty-six of the seventy structures (eighteen members of this group were molecules containing the Si_8O_{20} core).[41,61-92] Four compounds containing the $Si_{10}O_{15}$ core were found in the CSD database for which structural information was available.[41,85,93]

2.2.1 Synthesis of $Si_8O_{20}(SnMe_3)_8 \bullet 4H_2O$ (I•4H$_2$0)

$Si_8O_{20}(SnMe_3)_8 \bullet 4H_2O$ was synthesized according to the procedures of Feher and Waller with minor modifications.[57] Octahydridosilsesquioxane, $H_8Si_8O_{12}$ was added portion wise to a solution of bis(trimethyltin)oxide, $(Me_3Sn)_2O$ in toluene.[57,94,95] The amount of $H_8Si_8O_{12}$ needed was determined by monitoring the reaction via ^{1}H NMR. The reaction was stirred overnight under nitrogen. After the reaction was complete, all volatiles were removed and the resulting white powder was dissolved in boiling hexanes in air and small, white, needle shaped crystals formed upon cooling. The mixture was allowed to sit at 5^{o}C overnight. The crystals (6.77g, 3.65 mmol, 91% based on $H_8Si_8O_{12}$) were

collected by cannulating the mother liquor away and drying under vacuum overnight. Dissolving a small amount of the crystals in benzene and allowing the solvent to slowly evaporate in air yielded a crystal of the tetrahydrate $Si_8O_{20}(SnMe_3)8•4H_2O$ suitable for X-ray analysis. Analyses using multinuclear NMR was performed and the results were as follows: ^{1}H NMR δ 0.36 (s) $^2J(Sn^{117}H, Sn^{119}H)$ = 56.1, 59.4 Hz, $^1J(CH)$ = 130.9 Hz; ^{13}C NMR δ -2.92 (s) $^1J(Sn^{117}C, Sn^{119}C)$ = 387.5, 405.4 Hz; ^{119}Sn NMR δ 118.67 (s); and ^{29}Si NMR δ -101.144 (s) $^2J(SiSn)$ = 12.4 Hz.

The overall molecular structure was verified by its single crystal X-ray structure. Four H_2O molecules per $Si_8O_{20}(SnMe_3)_8$ were found in the crystal. TGA analysis of the crystals showed approximately a 4% weight loss at 100^{o}C in air, consistent with the loss of four water molecules (3.74 % theoretical weight loss).

$Si_8O_{20}(SnMe_3)_8•4H_2O$ was heated to 100^{o}C under vacuum overnight and recrystallized in dry hexanes at 5^{o}C under dry nitrogen. These crystal were found to be the anhydrous form of $Si_8O_{20}(SnMe_3)_8$ and were suitable for X-ray analysis.

2.2.2 Synthesis of $Si_{10}O_{25}(SnMe_3)_{10}•4H_2O$

The procedure for the preparation of $Si_{10}O_{25}(SnMe_3)_{10}$ was similar to that of $Si_8O_{20}(SnMe_3)_8$. To a solution of $(Me_3Sn)_2O$ in toluene, a mixture of (1:1) $H_8Si_8O_{12}$ and $H_{10}Si_{10}O_{15}$ was added stepwise until all $(Me_3Sn)_2O$ had reacted as indicated by ^{1}H NMR.[94] The resulting mixture of $Si_{10}O_{25}(SnMe_3)_{10}$ and

$Si_8O_{12}(SnMe_3)_8$ was separated by fractional crystallization from hexanes. The first crop of crystals grown at 5°C was pure $Si_8O_{12}(SnMe_3)_8$ according to ^1H NMR and the second crop was 93% $Si_{10}O_{25}(SnMe_3)_{10}$ and 3% $Si_8O_{20}(SnMe_3)_8$. The crystalline product was analyzed using multinuclear NMR as follows: ^1H NMR δ 0.42 (s) $^2J(Sn^{117}H, Sn^{119}H)$ = 56.7, 59.4 Hz, $^1J(CH)$ = 130.3 Hz; ^{13}C NMR δ -2.80 (s) $^1J(Sn^{117}C, Sn^{119}C)$ = 386.8, 404.6 Hz; ^{119}Sn NMR δ 116.21 (s); and ^{29}Si NMR δ -101.9 (s) $^2J(SiSn)$ = 12.5 Hz.

The overall molecular structure of the tetrahydrate $Si_{10}O_{25}(SnMe_3)_{10}\bullet 4H_2O$ was verified by single crystal X-ray analysis. Four H_2O molecules per $Si_{10}O_{25}(SnMe_3)_{10}$ were found in the crystal before heating under vacuum. TGA analysis of the crystals showed approximately a 3 % weight change between 35-90°C. This is consistent with the loss of four water molecules (3.01 % theoretical weight loss). Elemental analysis: found 15.08 % C and 4.26 % H, calculated for $Si_{10}Sn_{10}O_{25}C_{30}H_{90}{\cdot}4H_2O$ 15.07 % C and 4.13 % H.

2.2.3 Synthesis of $Si_8O_{20}(Cp_2TiCl)_8\bullet 3CH_2Cl_2$

The synthesis of $Si_8O_{20}(Cp_2TiCl)_8\bullet 3CH_2Cl_2$ has been described in the thesis of Suree Saengkerdsub entitled Group 4 Metallocene and Half-sandwich Derivatives of Spherosilicates: Preparation from $Si_8O_{20}(SnMe_3)_8$ and Their Olefin Polymerization Activity.[37]

2.3 Results and Discussion

The general approach to the synthesis of trialkyl tin substituted spherosilicates was first described by Feher and Weller.[57] Reaction of tin ethers R_3Sn-O-SnR_3 with Si-H functionalities to produce mixed silicon-tin ethers (≡Si-O-Sn≡) proceeds smoothly and in high yield. In the case of the decatin cage complex, $Si_{10}O_{25}(SnMe_3)_{10,}$ the silicon hydride precursor can only be isolated as an inseparable mixture with the octamer, $Si_8O_{12}H_8$. Titration of the mixture with the trimethyl tin ether gave the corresponding tin products cleanly. Fractional crystallization gave pure samples of the decatin compound, **II** for characterization.

The tin-substituted spherosilicates react with many high valent transition metal and main group chlorides (e. g. $AlCl_3$, $SiCl_4$, $TiCl_4$, $VOCl_3$) to cleanly metathesize the trialkyl tin group for the metal chloride.[96] The reaction of titanocene dichloride Cp_2TiCl_2, with **I** illustrates the utility of this reaction. At room temperature, Cp_2TiCl_2 reacts with $Si_8O_{20}(SnMe_3)_8$ in a variety of organic solvents to produce the titanocene substituted spherosilicate, $Si_8O_{20}(Cp_2TiCl)_8$ (**III**).

Under the conditions of the reaction, reaction of only one of the two chloride ligands on titanocene dichloride is observed. In the cases of this and other polychlorides, adjusting of the conditions of the reaction and stoichiometric ratios of spherosilicates-to-chloride complex leads to a general methodology for the designed preparation of tailored mixed metal-silicate building block materials.[28,29] Complete structural, elemental and spectroscopic characterization data for compounds **I** - **III** are given in the experimental section and following discussion.

2.3.1 Structural Characterization of $Si_8O_{20}(SnMe_3)_8 \cdot 4H_2O$ (I•$4H_2O$)

$Si_8O_{20}(SnMe_3)_8 \cdot 4H_2O$ crystallizes in the P-1 space group. Structure and refinement data are given in Table 2.1. The structure of the octakis trimethyltin silicate (I) tetrahydrate in the crystal may be described as distorted, cubic Si_8O_{12} cages surrounded by eight trimethyl tin groups bound to the eight oxygen atoms external to the silicate cage (Figure 2.2). Only one half of the molecule is unique by virtue of crystallographically imposed inversion symmetry at the center of the Si_8O_{12} cage. The crystal also contains four water molecules (two unique) present as Lewis base adducts coordinated to tin in two of the unique trimethyltin groups.

The Si_8O_{12} core exhibits a significant tetragonal distortion from ideal cubic symmetry. Two opposite Si_4O_4 faces of the cube are pulled away from each other thus distorting the equatorial ring of the four Si_4O_4 parallel to the distortion axis. The four Si—O—Si cage edges parallel to the distortion axis accommodate this elongation by opening up the Si—O—Si angle around oxygen until it is close to linear (average angle 172°). The Si—O bond lengths along these edges and along other Si_4O_4 faces of the cube are not lengthened appreciably over average Si—O bond distances observed in similar silicate cage structures (*vide infra*).

The oxygen atoms of the two water molecules in the crystal are within bonding distance (Sn(3)-O(12) 2.645 Å Sn(2)-O(11)2.799 Å) to two tin atoms of separate trimethyltin groups in the crystal (Figure 2.2).[97-105] The water oxygen atoms are positioned *trans* to the terminal oxygens of the cage. The three methyl groups are almost coplanar with the tin atoms forming the equatorial triangle of

Table 2.1 Structural and refinement data for single crystal X-ray data of all structures described in this thesis.

Identification code	I	I · $4H_2O$	II	III
Molecular formula	$Si_8O_{20}(SnMe_3)_8$	$Si_8O_{20}(SnMe_3)_8 \cdot 4H_20$	$Si_{10}O_{25}(SnMe_3)_{10} \cdot 4H_2O$	$Si_8O_{20}(TiClCp_2)_8 \cdot 2CH_3Cl$
Formula weight	1855.06	1927.12	2390.88	2507.74
Temperature	173(2) K	293(2) K	173(2) K	198(2) K
Wavelength	0.71073 Å	0.71073 Å	0.71073 Å	0.71073 A
Crystal system	Triclinic	Triclinic	Orthorhombic	Triclinic
Space group	P -1	P-1	P b c a	P-1
a	11.339(3) Å	11.2046(6) Å	21.834(5) Å	13.6919(5) Å
b	11.569(3) Å	12.0644(6) Å	26.567(7) Å	14.1160(5) Å
c	13.258(3) Å	12.3545(6) Å	28.037(7) Å	14.2380(5) Å
α	68.973(4)°	86.6650(10)°	90°.	101.9820(10)°
β	76.426(4)°	81.8930(10)°	90°.	99.8590(10)°
γ	71.264(4)°	85.4890(10)°	90°.	107.7540(10)°
Volume	1523.2(7) $Å^3$	1646.35(14) $Å^3$	16264(7) $Å^3$	2481.12(15) $Å^3$
Z	1	1	8	1
Density (calculated)	2.022 Mg/m^3	1.944 Mg/m^3	1.953 Mg/m^3	1.678 Mg/m^3
Absorption coefficient	3.436 mm^{-1}	3.187 mm^{-1}	3.224 mm^{-1}	1.149 mm^{-1}
F(000)	888	928	9200	1270
Crystal size	0.5x.05x0.5 mm^3	0.5 x 0.4 x 0.4 mm^3	0.20 x 0.15 x 0.10 mm^3	0.2 x 0.2 x 0.05
Theta range for data collection	1.91 to 23.32°	1.67 to 28.28°	1.41 to 23.27°.	1.51 to 27.65°
Index ranges	-12<=h<=12, -12<=k<=12, -14<=l<=14	-14<=h<=14, -15<=k<=16, -15<=l<=16	-23<=h<=24, -29<=k<=29, -31<=l<=31	-17<=h<=17, -18<=k<=18, -18<=l<=18
Reflections collected	11644	17832	120540	27306
Independent reflections	4387 [R(int) = 0.0182]	7705 [R(int) = 0.0240]	11673 [R(int) = 0.0641]	27306
Completeness to theta=	23.32°: 99.4 %	28.28°: 94.4 %	23.27°: 99.7 %	27.65°: 96.4 %
Absorption correction	Semi-empirical from equivalents	Semi-empirical from equivalents	Semi-empirical from equivalents	Semi-empirical from equivalents
Refinement method	Full-matrix least-squares on F^2	Full-matrix least-squares on F^2	Full-matrix least-squares on F^2	Full-matrix least-squares on F^2
Data / restraints / parameters	4387 / 0 / 283	7705 / 5 / 317	11673 / 16 / 806	27306 / 3718 / 1022
Goodness-of-fit on F^2	1.026	1.135	1.216	1.021
Final R indices [I>2sigma(I)]	R1 = 0.0261, wR2 = 0.00733	R1 = 0.0243, wR2 = 0.0634	R1 = 0.0323, wR2 = 0.0790	R1 = 0.0670, wR2 = 0.1694
R indices (all data)	R1 = 0.0292, wR2 = 0.0760	R1 = 0.0267, wR2 = 0.0647	R1 = 0.0637, wR2 = 0.1137	R1 = 0.0884, wR2 = 0.1860
Largest diff. peak and hole	2.059 and -0.411 $e.Å^{-3}$	0.363 and -1.802 $e.Å^{-3}$	2.547 and -0.888 $e.Å^{-3}$	0.876 and -0.948 e.A^-3

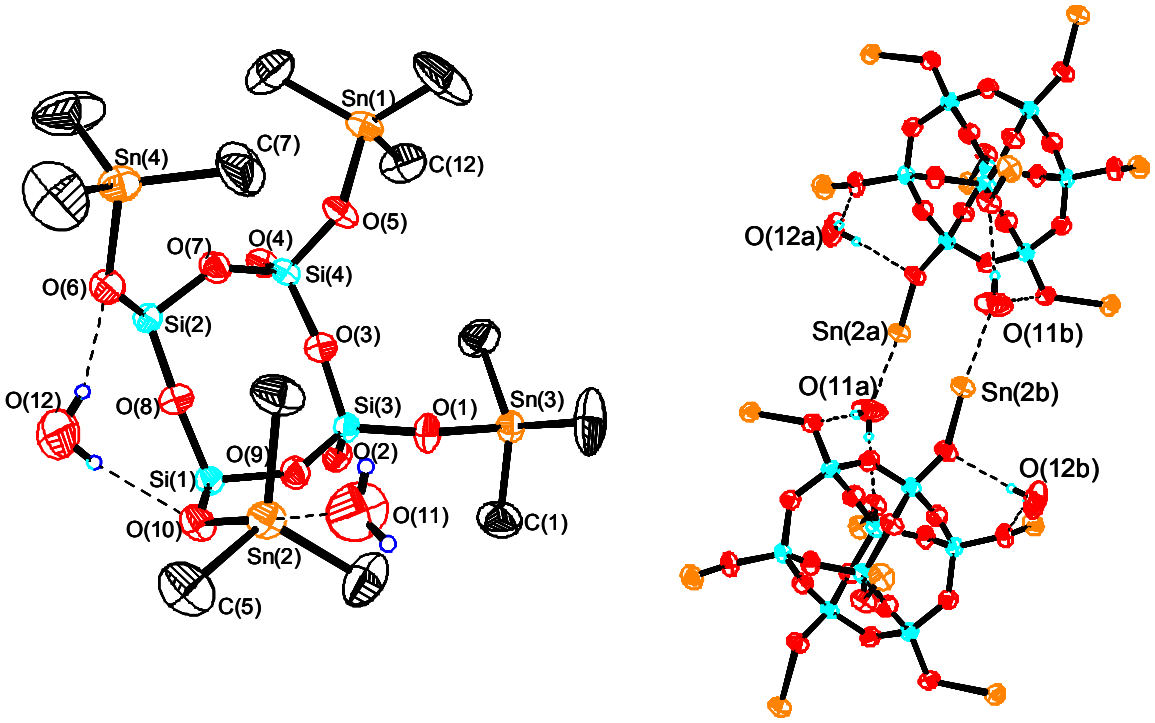

Figure 2. 2 Single crystal X-ray structure of $Si_8O_{20}(SnMe_3)_8 \cdot 4H_2O$.

an overall trigonal bipyramidal coordinate geometry around tin. The other two unique trimethyl tin groups in the structure have overall tetrahedral arrangements of the three methyl groups and terminal oxygen atom bond to tin.

The hydrogen atoms of the water molecules in the crystal are directed away from the trimethyltin group to which the oxygen is interacting and form hydrogen bonds to two *exo*cage oxygen atoms of a neighboring silicate cube in the lattice (Figure 2.2). It is interesting to note that in both cases two hydrogen bonds from one water molecule (O(12)) bracket the elongated edge of the Si_8O_{12} core.

The combination of Sn••••O_{water} Lewis base interactions and hydrogen bonding described above produces a 2-dimensional ordering of $Si_8O_{20}(SnMe_3)_8$ molecules in the solids state. Planes of $Si_8O_{20}(SnMe_3)_8$ molecules in the crystal, linked through water can clearly be seen in molecular packing diagrams (Figure 2.3). No unusual or strong intermolecular contacts are observed between planes in the lattice.

2.3.2 Structural Characterization of Anhydrous $Si_8O_{20}(SnMe_3)_8$ (I)

$Si_8O_{20}(SnMe_3)_8$ crystallizes in the P-1 space group. Structure and refinement data are given in Table 2.1. The structure of anhydrous $Si_8O_{20}(SnMe_3)_8$ (**I**) is similar to that of the tetrahydrated form in that it can be described as distorted, cubic Si_8O_{12} cages surrounded by eight trimethyltin groups bound to eight oxygen atoms external to the silicate cage (Figure 2.4). In contrast to the tetrahydrate structure, the substitutuent geometry around all tin

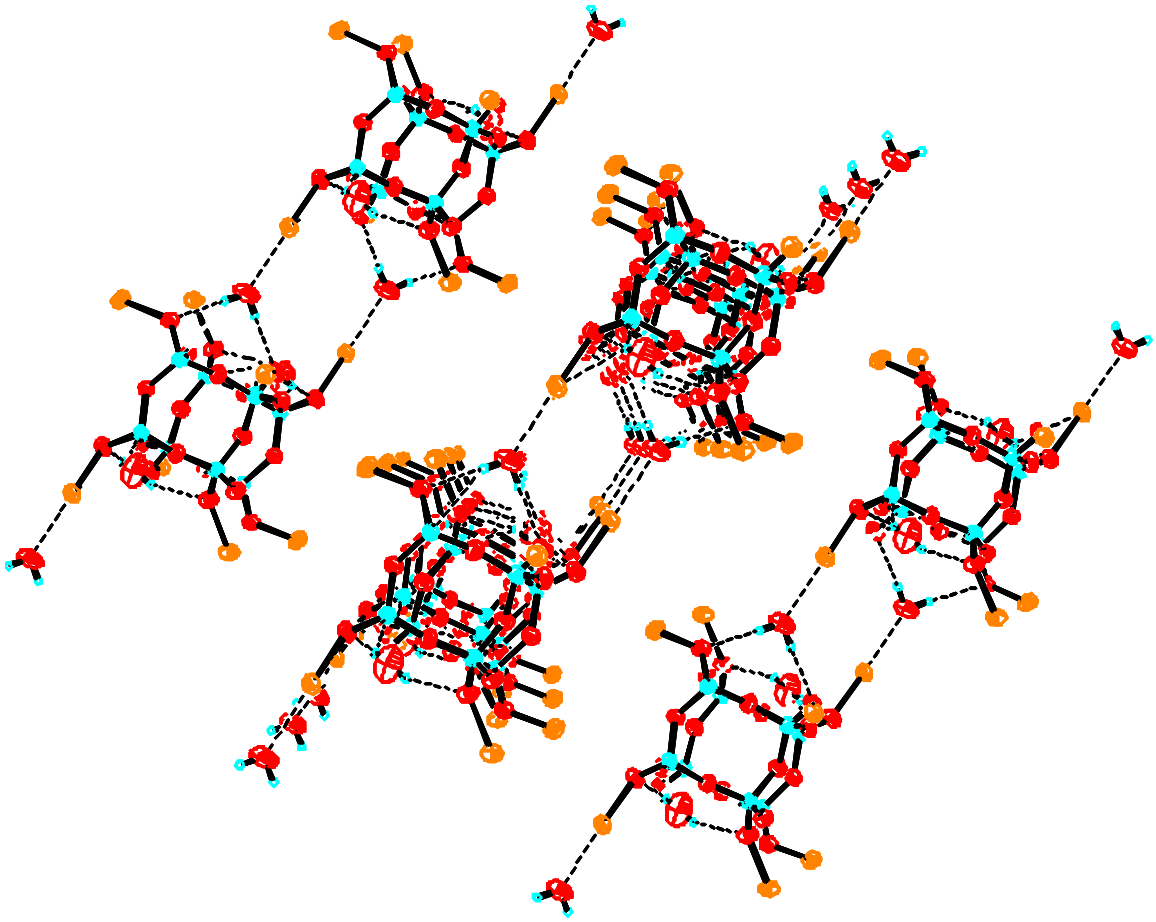

Figure 2. 3 Packing diagram of $Si_8O_{20}(SnMe_3)_8 \cdot 4H_2O$.

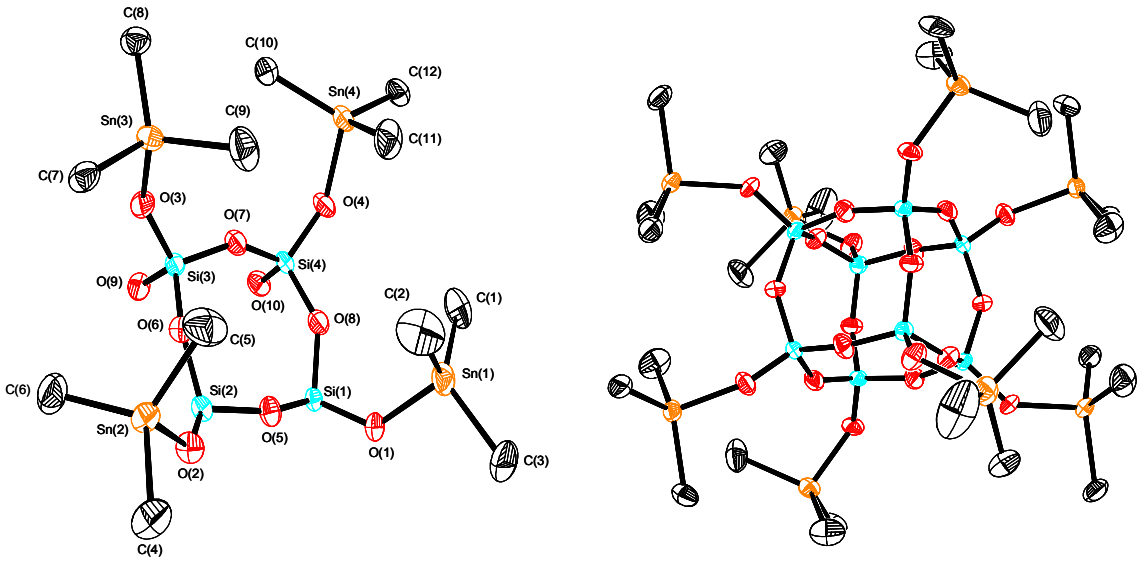

Figure 2. 4 Single crystal X-ray structure of $Si_8O_{20}(SnMe_3)_8$.

atoms is tetrahedral. Also, the distortion of the cubic silicate cage is not nearly as pronounced. The largest Si—O—Si cage angles in this structure are 160.0° and 161.4° which is approximately 11° less than what is observed in the hydrated structure.

The observed packing of $Si_8O_{20}(SnMe_3)_8$ in the crystal is also different. In this structure, no ordering of $Si_8O_{20}(SnMe_3)_8$ molecules into sheets is observed (Figure 2.5).

2.2.3 Structural Characterization of $Si_8O_{20}(Cp_2TiCl)_8 \cdot 3CH_2Cl_2$ (III)

Data were collected on a twinned crystal of $Si_8O_{20}(Cp_2TiCl)_8 \cdot 1.5CH_2Cl_2$ having two domains related by 180° rotation along the -110 axis in real space. The reflection file was sorted between the two twin components which are estimated to occur at a 20 : 80 split in the crystal. Reflections fell into three groups: completely resolved, partially overlapping and completely overlapping. Saint (version 6.02) successfully derived integrated intensities for all but a few reflections from both twin components in all categories using a single BASF scale factor of 0.20981. Both independent data sets from the two twin components were used in the refinement of the model. Structure and refinement data are given in Table 2.1.

The structural model developed for $Si_8O_{20}(Cp_2TiCl)_8 \cdot 3CH_2Cl_2$ involves a combination of crystallographically imposed symmetry and disorder. The disorder is found in the titanocene groups and in the methylene chloride solvate molecules. Because of the disorder in the titanocene fragments of the molecule,

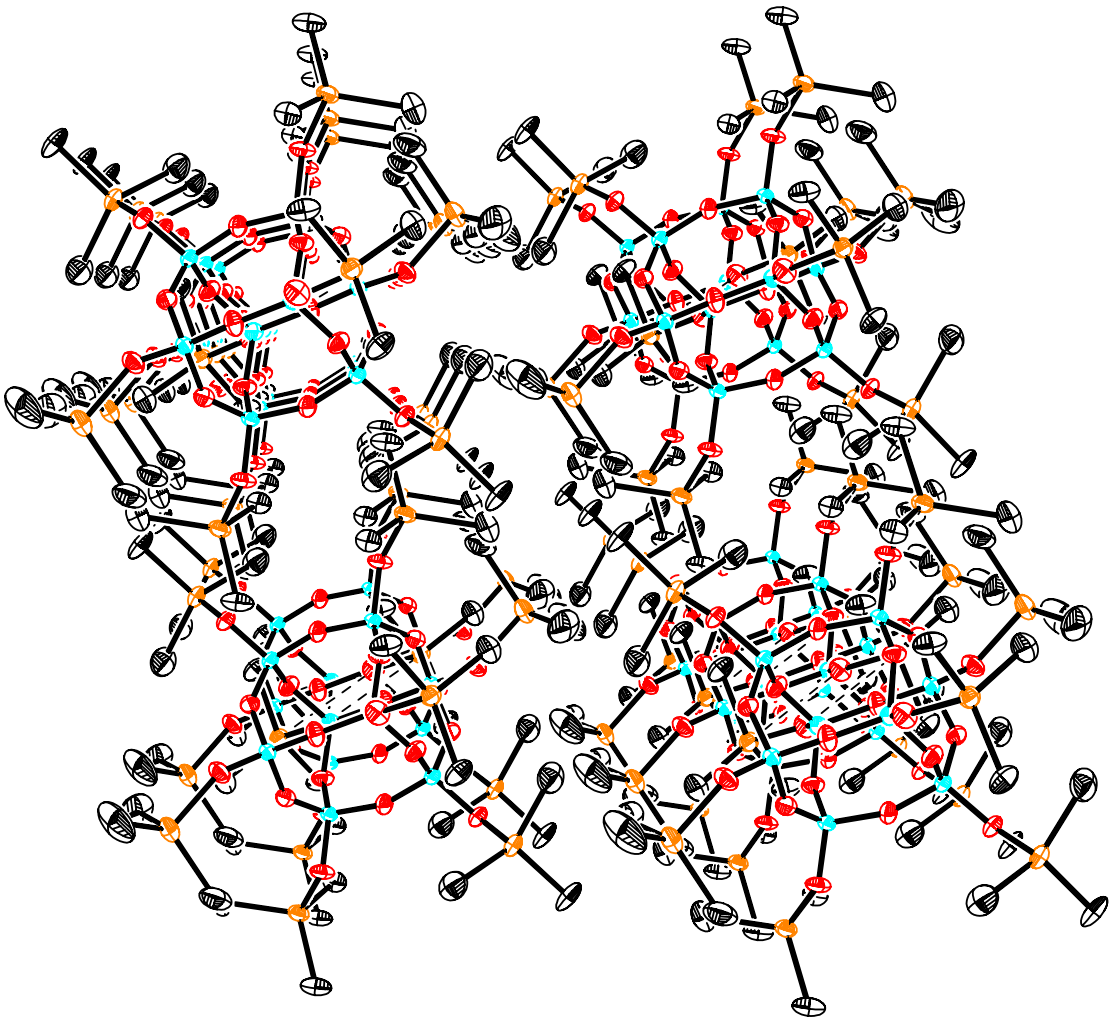

Figure 2. 5 Packing diagram of $Si_8O_{20}(SnMe_3)_8$.

all Cp rings were restrained to be planar and titanium atoms Ti(3) and Ti(4), along with their respective disorder partners (Ti(3'), Ti(4')) were modeled with equivalent atomic displacement parameters. Figure 2.6 shows the structure of $Si_8O_{20}(Cp_2TiCl)_8$ without the disordering in the titanocene groups.

Only half of the central Si_8O_{20} core and its Cp_2TiCl substituents are unique due to the presence of crystallographically imposed inversion symmetry at the center of the cube. There is no disorder in the central Si_8O_{20} core. However, all of the titanocene groups are disordered and two different types of disorder are observed (Figure 2.7). In two cases, only the Cp rings bound to Ti(1) and Ti(2) are disordered. In these cases, the Cp centroid positions are slightly shifted and the carbon atoms are rotated. Surprisingly, only one chlorine atom could be assigned. The thermal ellipsoid for this chlorine atom is larger than usual which could indicate the presence of two Cl atom positions that are close together and not resolved with the data in hand. Attempts to model this as two distinct atoms were not successful. The occupation of the two components in both cases was modeled by a standard floating occupancy free variable and was found to be approximately 1:1 for the case involving Ti(1) and approximately 3:1 for the case involving Ti(2).

The other two unique titanocene groups in the molecule (Ti(3) and Ti(4)) show similar disorder originating in the position of the titanium atoms. Ti(3) and Ti(4) constitute one set of adjacent titanium atoms across an edge of the Si_8O_{20} core (Part 1) while Ti(4´) and Ti(3´) represent the second set of titanium positions (Part 2). The titanocene units are unequally disordered between two different

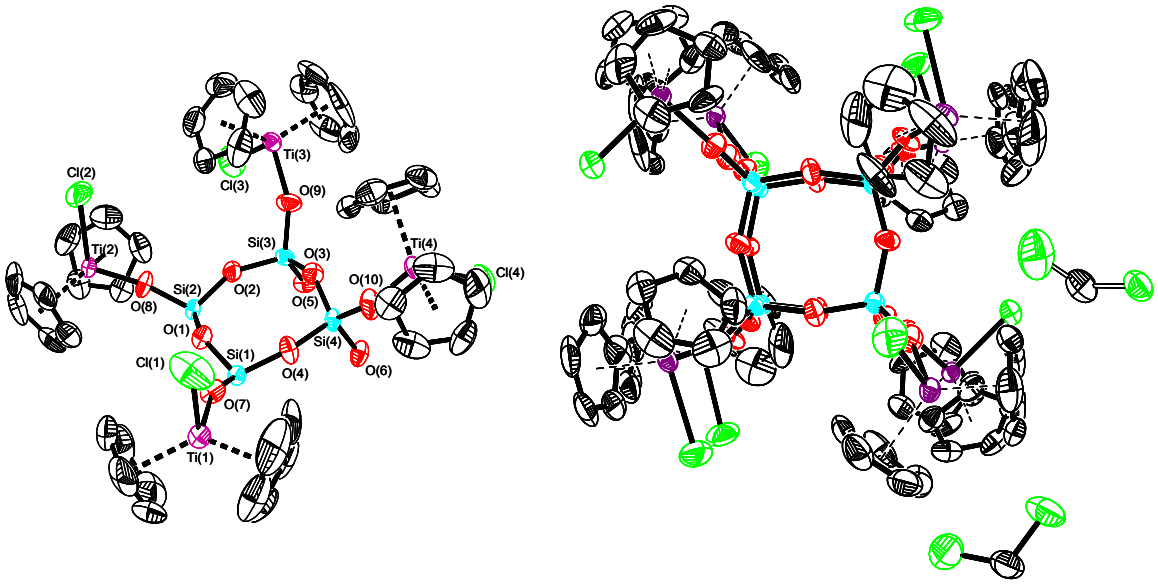

Figure 2. 6 Single crystal X-ray structure of $Si_8O_{20}(Cp_2TiCl)_8 \cdot 3CH_2Cl_2$.

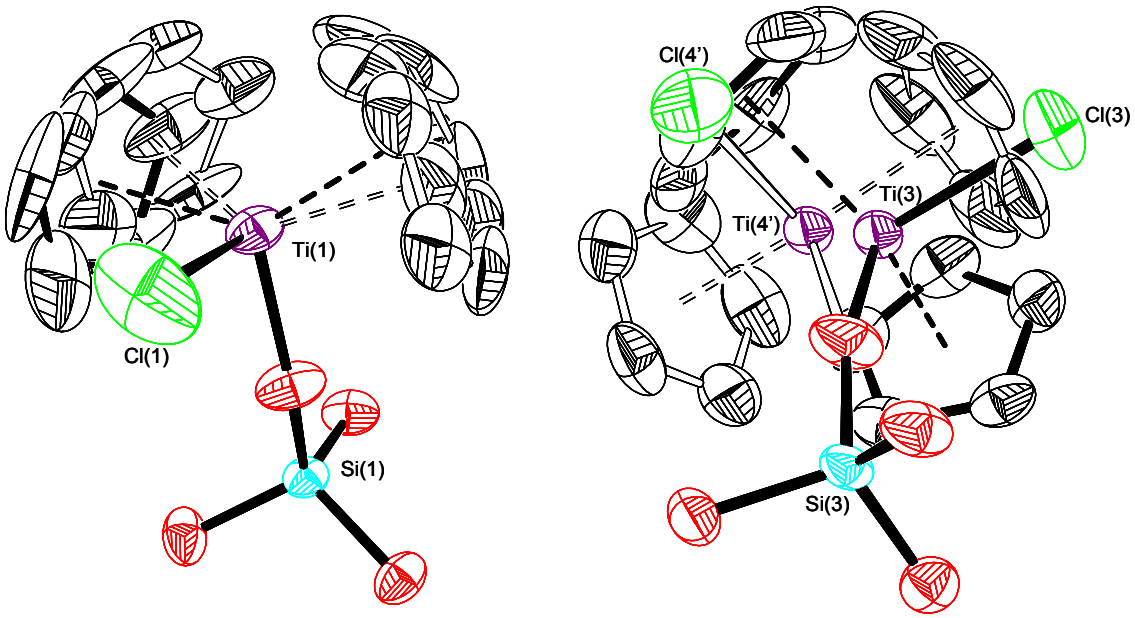

Cp Ring disorder Around Ti(1)

Ti disorder at Ti(3)

Figure 2. 7 Disordered Cp_2TiCl groups observed in the single crystal X-ray structure of $Si_8O_{20}(Cp_2TiCl)_8 \cdot 3CH_2Cl_2$.

locations of the titanium atoms (Ti(3) and Ti(3') vs. Ti(4) and Ti(4')), Cp centroid positions, as well as chlorine atoms. The titanocene groups are related by a change in position of the titanium atoms as well as rotation of the Cp_2TiCl unit by approximately 90^o around the Ti-O bond. The occupation of the two components was modeled by a standard floating occupancy free variable and was found to be approximately 1.5:1 for both titanocene groups (Ti(3)/TI(3') and Ti(4)/Ti(4').

One methylene chloride solvate molecule is nondisordered but only occurs as one half of an equivalent per cube in the crystal. The other solvate molecule occurs as a full equivalent but is disordered roughly equally between two orientations that share the same central carbon position. The two orientations are related to one another by rotation of the Cl-C-Cl plane around the C_2 axis of the molecule.

2.2.4 Structural Charaterization of $Si_{10}O_{25}(SnMe_3)_{10}•4H_2O$ (II)

$Si_{10}O_{25}(SnMe_3)_{10}•4H_2O$ crystallizes in the Pcba space group. Structural and refinement data are given in Table 2.1. The structure of the decakis trimethyltin silicate tetrahydrate in the crystal may be described as a highly distorted, pentagonal prism of five Si_4O_4 rings each sharing two edges. The ten trimethyltin groups are bound to ten oxygen atoms external to the silicate cage. Four water molecules are also present in the crystal. Three of the four molecules are Lewis base adducts with tin in trimethyltin groups and the fourth water is hydrogen bonded to an *exo*cage oxygen belonging to the silicate molecule. The two pentagonal faces making up the spherosilicate cage are not symmetrical due

to “puckering” of corresponding Si—O—Si edges of the two opposite faces that is observed in other $Si_{10}O_{15}$ containing structures (Figure 2.8).[41,85,93]

Three of the trimethyltin groups in $Si_{10}O_{25}(SnMe_3)_{10}$ are disordered. Two have tin atoms occupying two sites ((Sn10) and Sn(11)) with one of the methyl groups (C(25) occupying the same position and the other four methyls (C(30) and C(32) bound to Sn(10) and C(29) and C(31) bound to Sn(11)) disordered between two positions (Figure 2.9). In the third trimethyltin group, the tin in disordered between two sites with occupancies of 95% and 5%. The positions of all three methyl group carbons associated with the more prevalent tin position have been located. Since the other tin site has such a low occupancy factor, none of the methyl groups associated with this tin could be located. No disorder with the $Si_{10}O_{15}$ cage was observed.

The water molecules present in this structure are found as either Lewis base adducts, hydrogen bounded, or a combination of both as previously stated. The interactions observed for one are quite similar to that described in the tetrahydrate of $Si_8O_{12}(SnMe_3)_8$. For two of the water molecules, a similar type of interaction is observed where the oxygen from the water interacts with a tin group, but only one hydrogen of the water molecule interacts with a terminal oxygen bearing a trimethyltin group of a neighboring $Si_{10}O_{25}(SnMe_3)_{10}$ molecule. The last water does not show any specific interaction with tin. One of the hydrogen atoms of this water molecule is hydrogen bonded to an oxygen bearing a trimethyltin group.

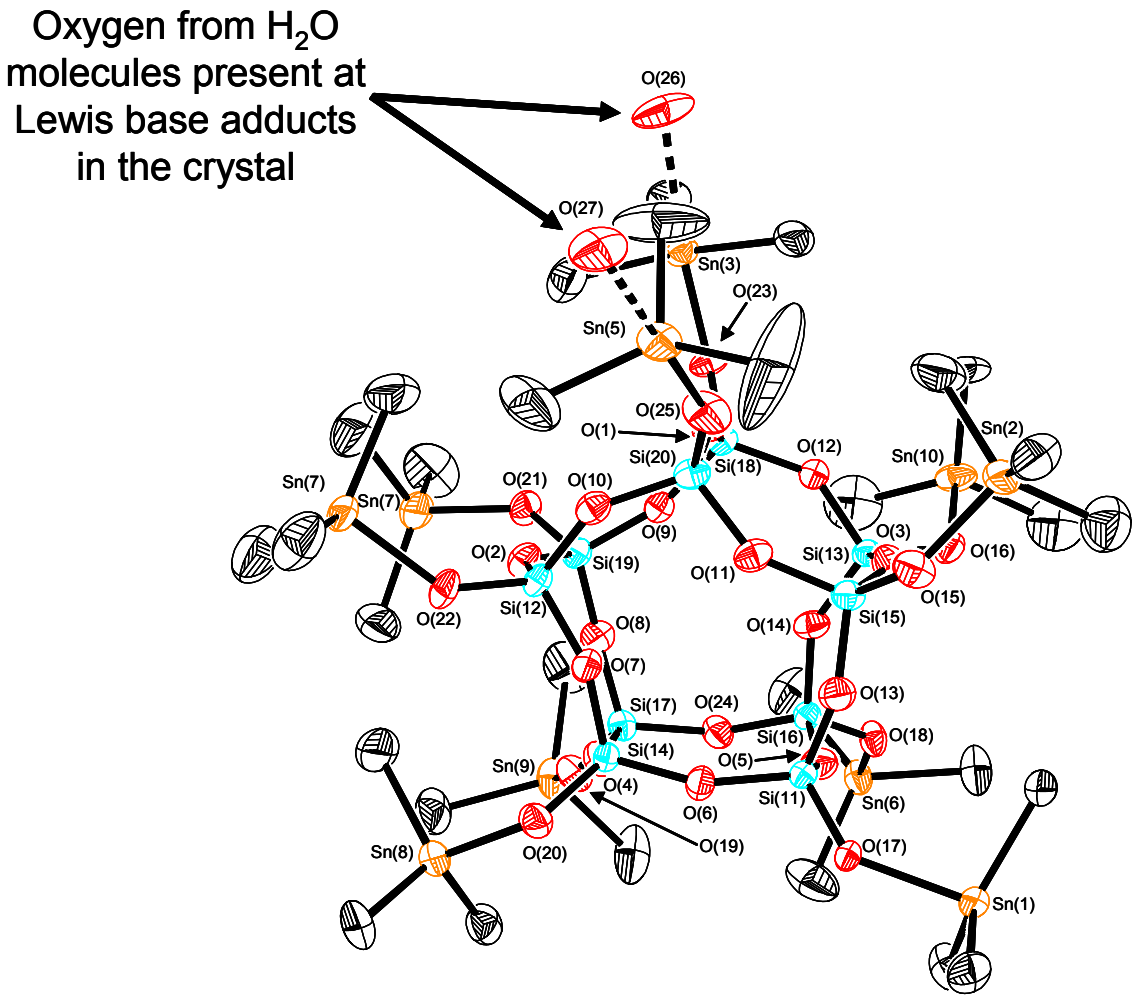

Figure 2. 8 Single crystal X-ray structure of $Si_{10}O_{25}(SnMe_3)_{10}•4H_2O$.

View of Disorder of trimethyltin groups in $Si_{10}O_{25}(SnMe_3)_8 \cdot 4H_2O$

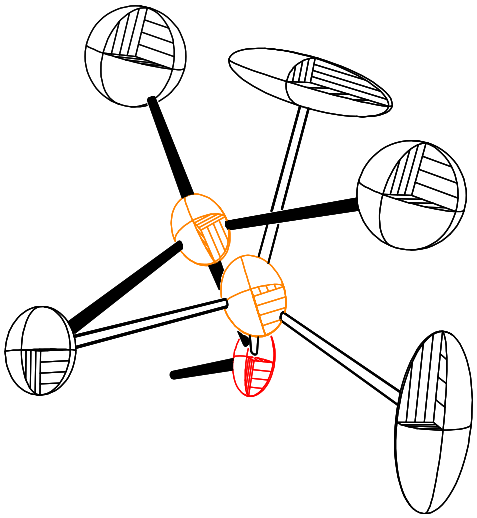

Structure of $Si_{10}O_{25}(SnMe_3)_8 \cdot 4H_2O$ showing disordered trimethyltin groups

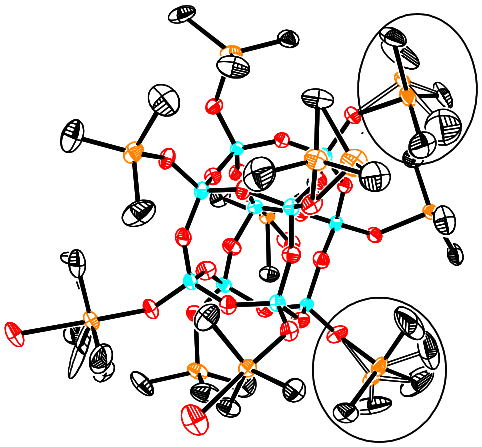

Figure 2. 9 Disordered Me_3Sn groups observed in the single crystal X-ray structure of $Si_{10}O_{25}(SnMe_3)_{10} \cdot 4H_2O$.

Much like in the $Si_8O_{20}(SnMe_3)_8 \cdot 4H_2O$ structure, a consequence of the combination of Sn••••O interactions and hydrogen bonding is the occurrence of two dimensional planes of $Si_{10}O_{25}(SnMe_3)_{10}$ molecules in the solid state (Figure 2.10). A second similarity between the two structures is that no strong intramolecular interactions are apparent between these planes of molecules.

2.2.5 Structural Comparisons of Si_8O_{20} Cage Unit in $Si_8O_{20}(Cp_2TiCl)_8$ and $Si_8O_{20}(SnMe_3)_8 \cdot 4H_2O$ with other Cubic Spherosilicates

The structure of $Si_8O_{20}(SnMe_3)_8 \cdot 4H_2O$ is unusual within the context of other cubic spherosilicates in that the Si_8O_{20} unit is considerably distorted. The cubic Si_8O_{12} core is elongated along an axis through opposite Si_4O_4 faces. This results in a small compression in the direction perpendicular to the elongation (Figure 2.11). This distortion is due to atypical Si—O—Si angles in the Si_8O_{12} unit when compared to other reported Si—O—Si angles in cubic Si_8O_{12} silasesquioxanes and spherosilicates. The average Si—O—Si angle in the structures reported in the CSD database is 149° with a maximum value of 163° and a minimum value of 140°. Bieniok and Bürgi compared *average* Si—O—Si and O—Si—O non-bonding distances for cubic Si_8O_{12} containing structures with zeolites and silicate minerals having D4R subunits.[46] In the study described herein, the individual non-bonding angles and distances were examined for both Si—O—Si and O—Si—O. This approach proved to be more informative in this instance because in $Si_8O_{20}(SnMe_3)_8 \cdot 4H_2O$ two Si—O—Si angles approach linearity having observed maximum angles of 172.13° and 171.10° and observed

One “Plane” Showing H-bonding between molecules

Two “Planes” Showing H-bonding between layers

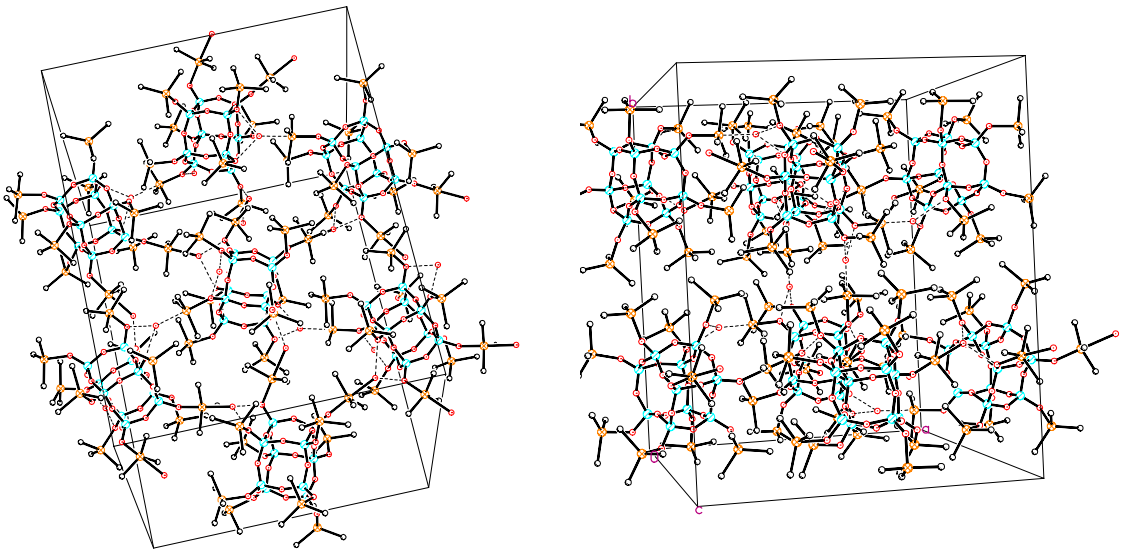

Figure 2. 10 Packing diagram for $Si_{10}O_{25}(SnMe_3)_{10}•4H_2O$.

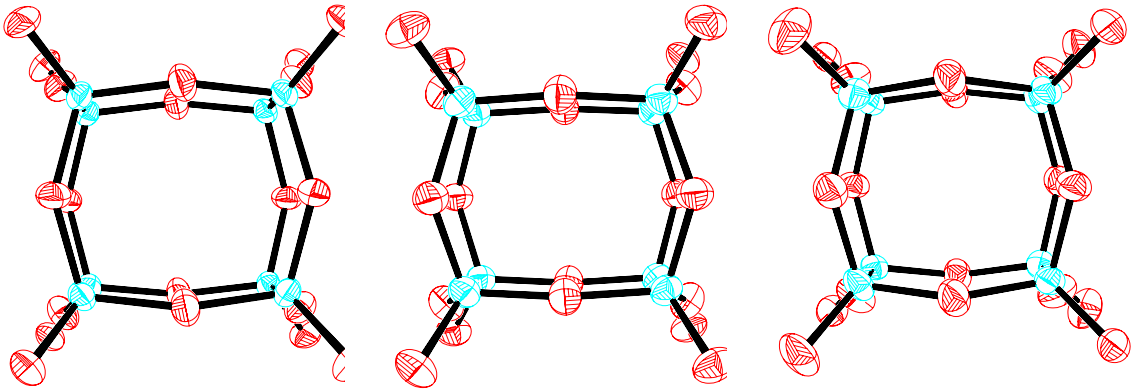

$Si_8O_{20}(SnMe_3)_8$ $Si_8O_{20}(SnMe_3)_8{\cdot}4H_2O$ $Si_8O_{20}(TiCp_2Cl)_8{\cdot}CH_2Cl_2$

Figure 2. 11 Si_8O_{20} cage structures for I, I•$4H_2O$, and III.

minimum angles of 136.35° and 137.21° (Figure 2.12). The average of 154° for these angles is not too far from the average of 149° previously stated for other Si_8O_{12} containing structures and is certainly well within the upper and lower values for these angles. However, the individual angles are the largest reported for any structure containing the D4R fragment. The SiO_4 tetrahedral units observed in this structure are not unusual when compared to other analogous structures (Figures 2.13 – 2.14). Thus, the prominent tetragonal distortion observed in the structure of $Si_8O_{20}(SnMe_3)8{\bullet}4H_2O$ results primarily from the opening up of the Si—O—Si angle around oxygen corresponding in the tilting of rigid SiO_4 tetrahedra. This is in agreement with the conclusions from Bieniok and Bürgi.[46] While it is tempting to correlate the distortion observed in the flexible Si—O—Si angle with the water molecule which is hydrogen bonded to the two *exo*cage oxygens along the elongated edge, we feel further structural studies are needed to support this claim before its generality can be ascertained.

In marked contrast to the structure of $Si_8O_{20}(SnMe_3)_8{\bullet}4H_2O$, the Si_8O_{12} core observed in the $Si_8O_{20}(Cp_2TiCl)_8$ structure does not exhibit any unusual structural characteristics (Figure 2.12 – 2.14).

2.2.6 Structural Comparisons of $Si_{10}O_{25}$ Cage Unit in $Si_{10}O_{25}(SnMe_3)_{10}$ with other Pentagonal Prismatic Spherosilicates

The structure of the $Si_{10}O_{15}$ cage within $Si_{10}O_{25}(SnMe_3)_8$ shows some unusual features when compared to the structures of other compounds containing $Si_{10}O_{15}$ cage units. The SiO_4 tetrahedral subunits that make up this

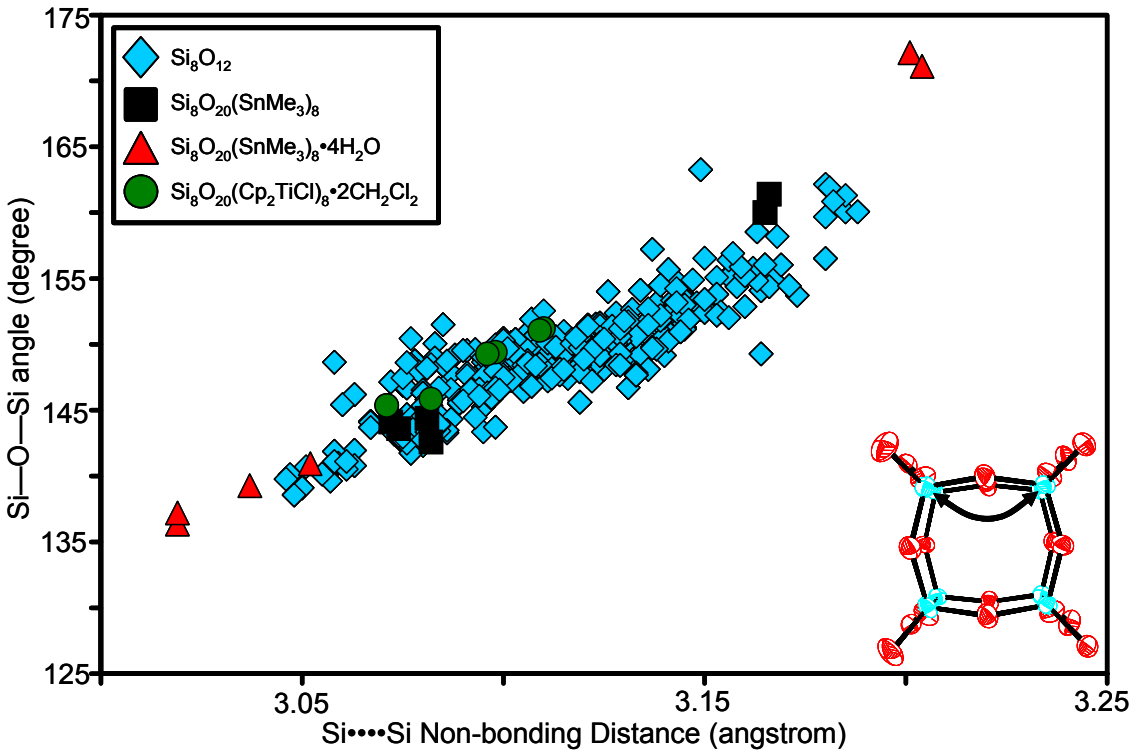

Figure 2. 12 Distribution in Si-O-Si angles and non-bonding distances observed in the solid structure of compounds containing a Si_8O_{12} cage.

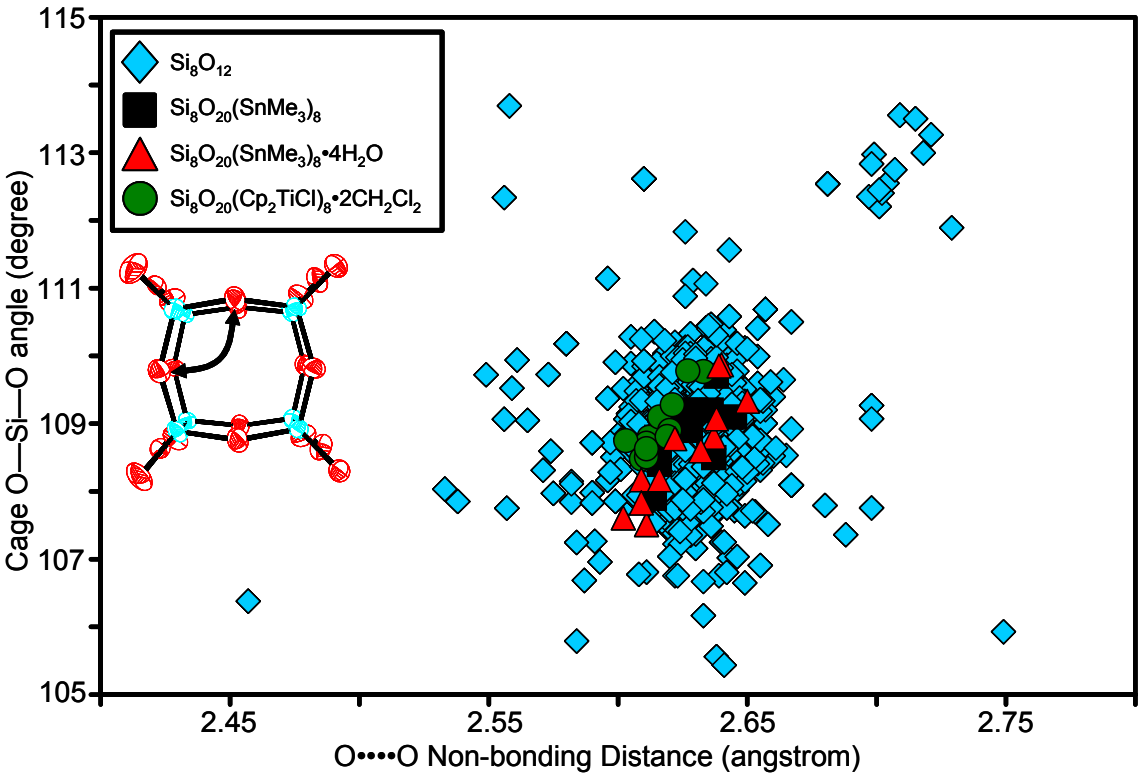

Figure 2. 13 Distribution of O-Si-O non-bonding distances and angles involving the cage oxygens of tetrahedral units observed in the solid structure for compounds containing Si_8O_{20} compounds.

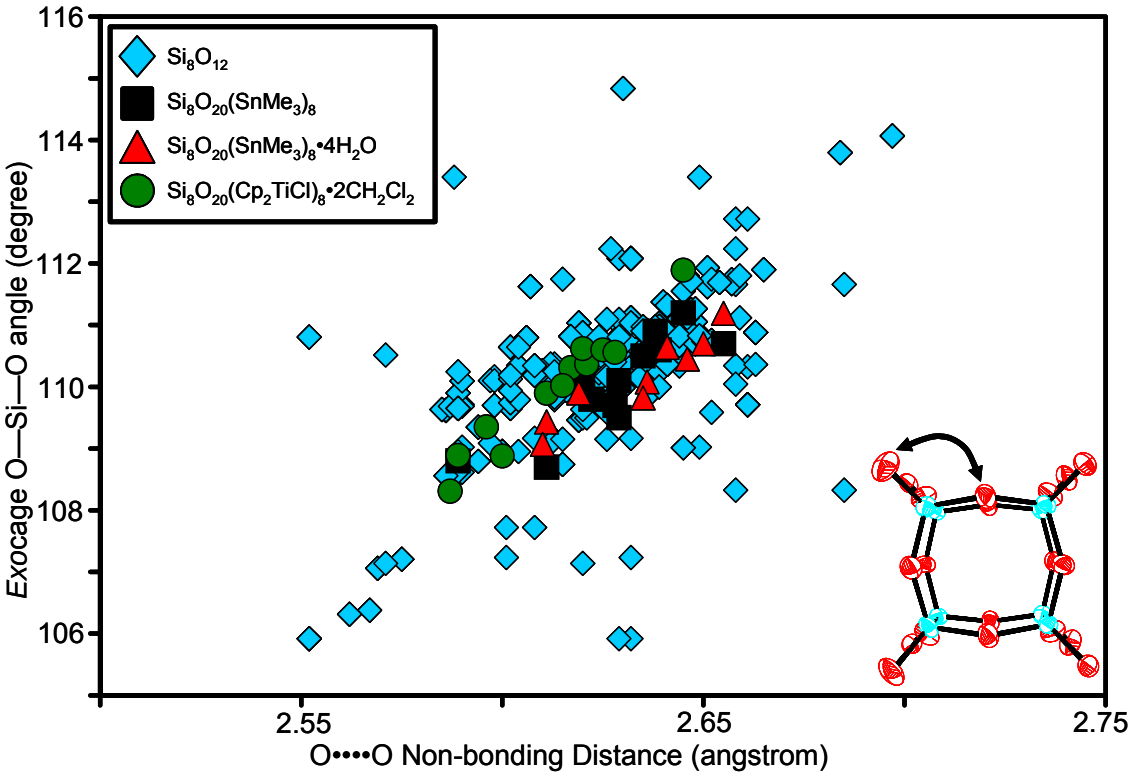

Figure 2. 14 Distribution of O-Si-O non-bonding distances and angles involving the *exo*cage oxygen of tetrahedral units observed in the solid structure for compounds containing Si_8O_{20} compounds.

cage have a larger distribution of observed non-bonding O••••O distances and O—Si—O angles around individual silicon atoms. This is evident in plots of this angle as a function of the non-bonding O••••O distance (Figures 2.15 – 2.16). In one case, a SiO_4 unit (Si(20)) in $Si_{10}O_{25}(SnMe_3)_{10}$ has an unusually small observed O—Si—O angle of 105.5(3)^o. In fact all of the cage O—Si—O angles associated with this silicon have observed values below the value associated with a perfect SiO_4 tetrahedron (109.5^o). As a consequence, the O—Si—O angles involving the *exo*cage oxygen have observed angles of 110.2(3)^o, 113.2(4)^o, and 112.2(3)^o. This is the largest perturbation from ideal tetrahedral symmetry observed in any $Si_{10}O_{15}$ containing structures found in the CSD. The trimethyltin group bound to this SiO_4 unit has a water molecule coordinated to the tin. However, another SiO_4 unit bound to a trimethyltin group in the molecule that also has a water molecule coordinated to tin does not exhibit the same type of distortion. We are not sure what the causes of distortions in the SiO_4 unit are at this time.

The observed Si—O—Si angles and non-bonding distances in $Si_{10}O_{25}(SnMe_3)_{10}$ also have a larger distribution of values than is observed in other structures containing $Si_{10}O_{15}$ units (Figures 2.17 – 2.18). This is observed in both the square faces and the pentagonal faces. The Si—O—Si angles and distances found in the pentagonal faces of $Si_{10}O_{25}(SnMe_3)_{10}$ have observed non-bonding Si•••Si distances that are all slightly longer than what is observed in other D5R containing structures. Reasons for the larger distributions are not known. The presence of the water molecules interacting both as Lewis bases

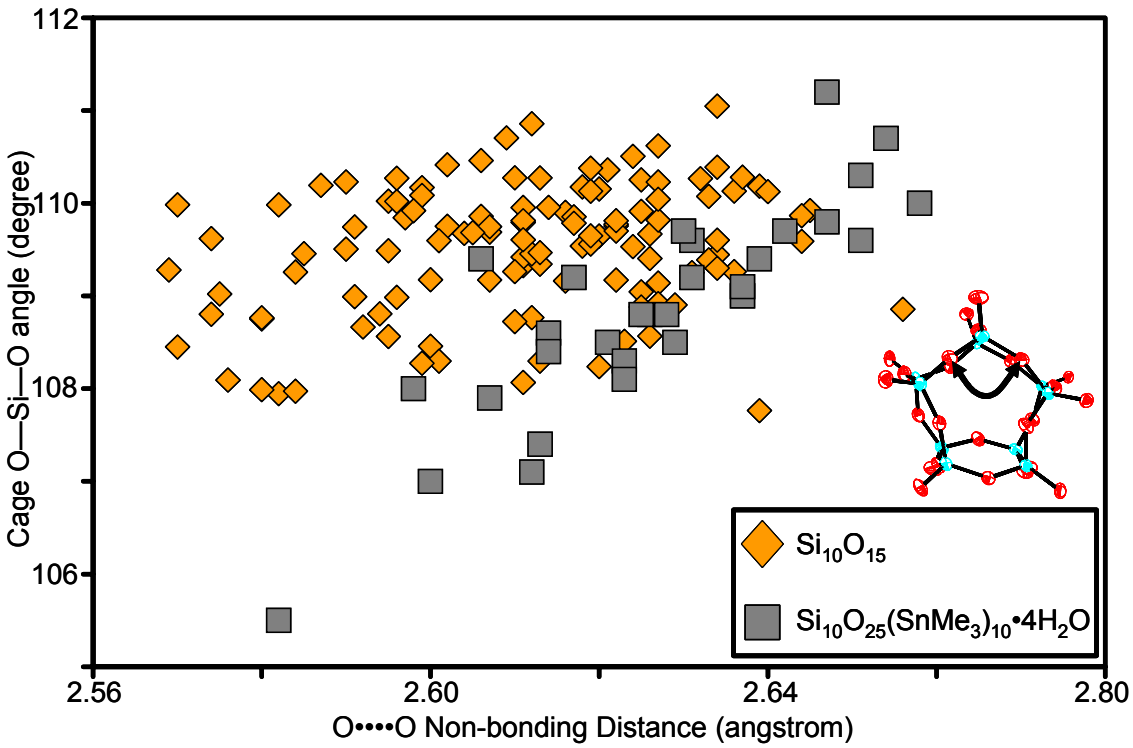

Figure 2. 15 Distribution of O-Si-O non-bonding distances and angles involving the cage oxygens of tetrahedral units observed in the solid structure for compounds containing $Si_{10}O_{15}$ compounds.

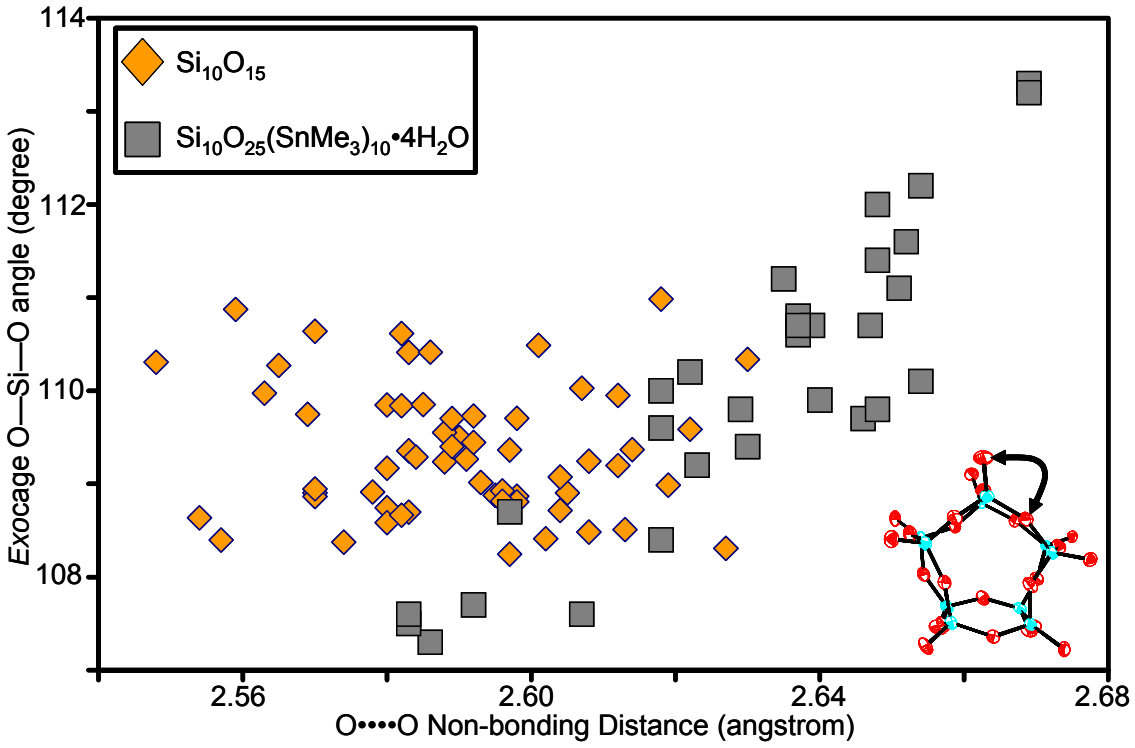

Figure 2. 16 Distribution of O-Si-O non-bonding distances and angles involving the *exo*cage oxygen of tetrahedral units observed in the solid structure for compounds containing $Si_{10}O_{25}$ compounds.

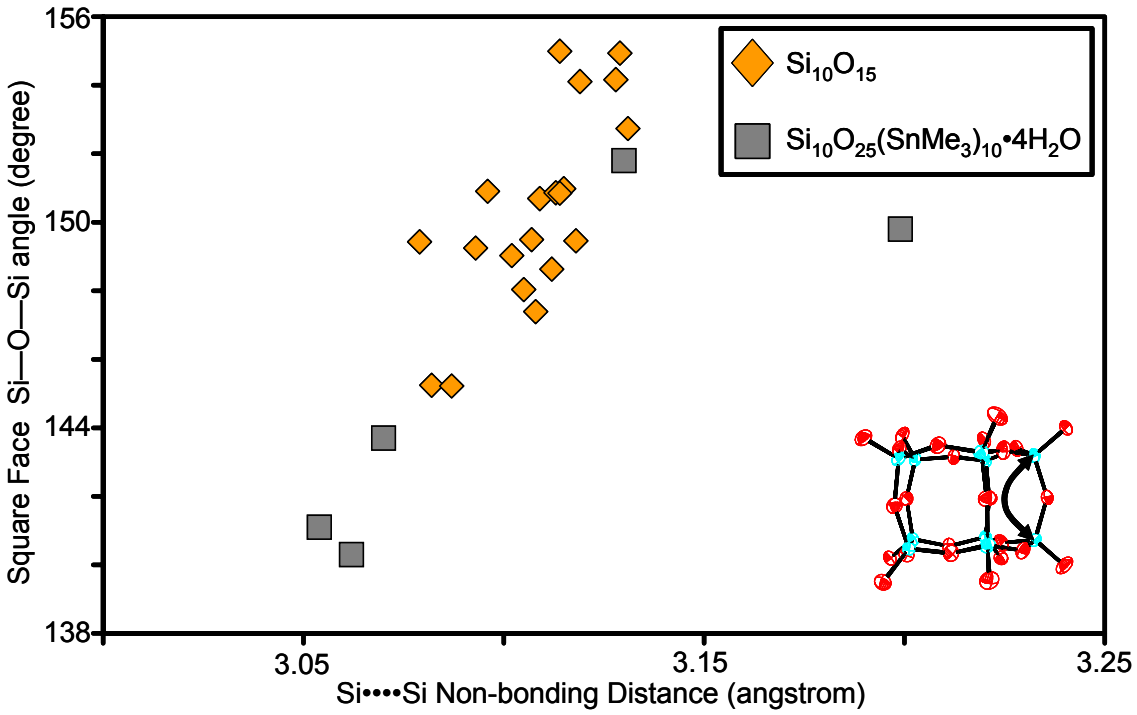

Figure 2. 17 Distribution in Si-O-Si angles and non-bonding distances of the square faces observed in the solid structure of compounds containing a $Si_{10}O_{15}$ cage.

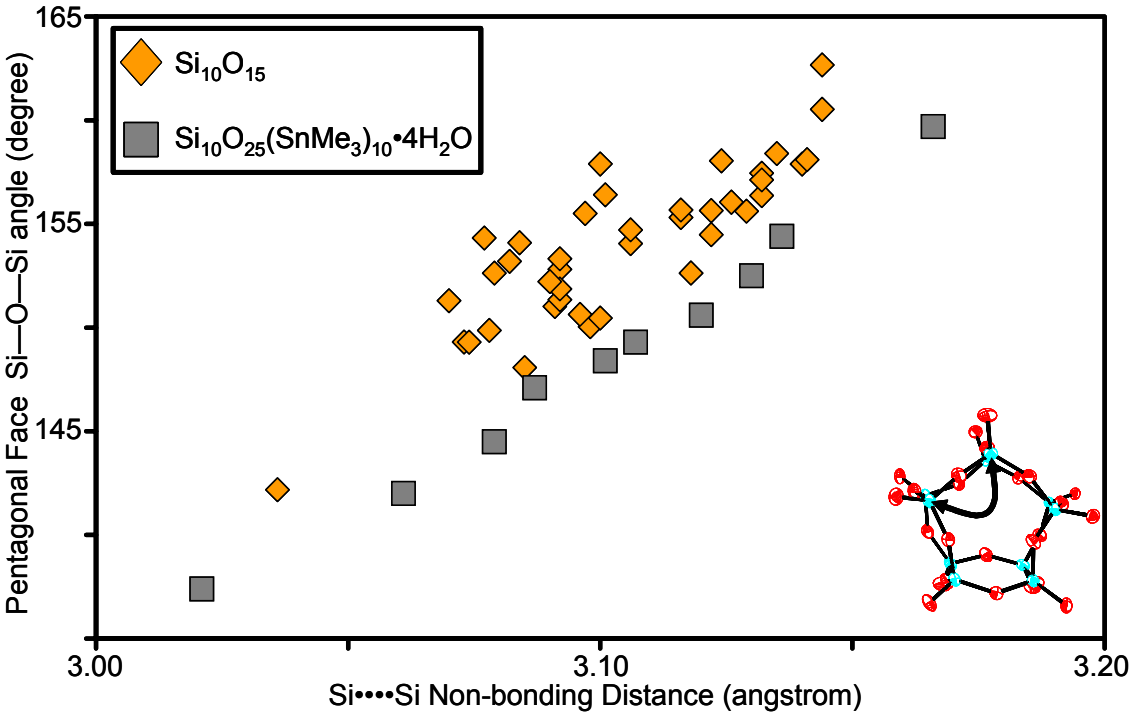

Figure 2. 18 Distributions in Si-O-Si angles and non-bonding distances of the pentagonal faces observed in the solid structure of compounds containing a $Si_{10}O_{15}$ cage.

with tin and hydrogen bonding to *exo*cage oxygen atoms may contribute to these structural features. However, given that only four structures containing $Si_{10}O_{15}$ cages have been reported in the CSD, it is difficult to identify all underlying factors influencing these structural features with great certainty. Stronger conclusions await descriptions of other structurally well characterized examples of $Si_{10}O_{15}$ containing compounds.

2.4 Summary and Conclusions

The synthesis and structure of several members of a family of trialkyltin derivatized spherosilicates has been described. The trialkyltin functionality allows for further reaction with metal chlorides as illustrated in the synthesis of $Si_8O_{20}(Cp_2TiCl)_8$. The solid-state structures of $Si_8O_{20}(SnMe_3)_8 \bullet 4H_2O$, $Si_8O_{20}(SnMe_3)_8$, $Si_8O_{20}(Cp_2TiCl)_8$, and $Si_{10}O_{25}(SnMe_3)_{10}$ have been described. Disorder was found for the functional groups covalently bonded to *exo*cage oxygen atoms in $Si_8O_{20}(Cp_2TiCl)_8$, and $Si_{10}O_{25}(SnMe_3)_{10}$. In all cases, no disorder was found for the spherosilicate core.

Comparisons with structural data for previous cubic and pentagonal prismatic containing spherosilicates indicate that the cage units in both Si_8O_{12} and $Si_{10}O_{15}$ spherosilicates are typically rigid and do not vary significantly from ideal values. Observed distortions are mostly caused by variations in the edge Si—O—Si angles connecting SiO_4 tetrahedral units. The large distribution of the observed angles seen in the spherosilicates bearing trimethyltin groups may be due to the presence of Lewis base and hydrogen-bonding interactions between

water in the crystal with tin groups of stannylated spherosilicates and *exo*cage oxygen atoms.

The structural variations observed for spherosilicate building units found in the compounds described herein are important because they are the basic building units present in many zeolites and silicates.[50] The molecular dimensions of these silicate cage units fall into the nanoscale size regime. Furthermore, they are both chemically and thermally robust. These properties make them attractive candidates as building blocks for the construction of mesoscopically designed solids.[29] Materials produced from such methods could have a wide applicability in the areas of catalysis and materials chemistry.

Chapter 3: The Reaction of $Si_8O_{20}(SnMe_3)_8$ Building Block with Silylchlorides: A New Synthetic Methodology for Preparing Building Block Solids

3.1 Introduction

Within technological settings, heterogeneous catalysis is generally found to be more practical than homogeneous catalysis. One significant advantage of heterogeneous catalysts is the ease of separation of the catalyst from the reaction products. For example, heterogeneous catalysts frequently can be removed from a reaction using simple filtration techniques.[106] Homogeneous catalysts often must be separated from the reaction products which is frequently achieved using costly techniques involving distillation or chromatography.[6,106-108] A second practical advantage of heterogeneous catalyst is that these materials commonly involve metals or metal oxides that are typically thermally robust. Homogeneous catalysts are commonly organometallic complexes which do not always display this type of stability. Since reaction rates often times increase with temperature, stability at higher temperatures is frequently advantageous.[106] Another example of a applied advantage is that heterogeneous catalysts may not be susceptible to moisture or oxygen which can cause many organometallic complexes used as homogeneous catalysts to decompose.[106]

Despite the practical advantages of heterogeneous catalysts, homogeneous catalysts typically are superior in terms of several criteria involving catalytic performance. The efficiency is generally better in this class of catalysts

because all molecules should be available for catalysis in homogenous phases.[106] In contrast, heterogeneous catalysts operate at surfaces and not all atoms are located on the surface. Thus heterogeneous catalysts tend not to exhibit the high "atomic" efficiencies observed in homogeneous catalysts. Furthermore, tailoring homogeneous catalysts to optimize the overall reactivity is more easily achieved by altering the ligands around a metal center to improve selectivity and activity.[106,107] Thus the important structure-reactivity relationship discussed in the introduction of this thesis is obtainable with homogeneous catalysts.

In heterogeneous formulations, an array of sites exists on the surface which vary from being very active to having little or no activity.[106] Characterizing the local environments of an array of sites and determining the structural features responsible for the reactivity can be quite challenging. Therefore establishing a correlation between the structure of the most active sites with catalytic performance is not as easy as in homogeneous catalysts.

Next generation catalysts should offer the advantages of both homogeneous and heterogeneous catalysts. Such "ideal" catalysts should be heterogeneous in nature so that post reaction processing is simplified. They should have a high density of active centers at the surface, and all centers should be identical and optimized in terms of selectivity and activity.[107] Very few methods have been developed which allow such catalysts to be designed due to the limited preparative methodologies available.

One approach to the design of heterogeneous catalysts having uniform catalytic sites involves grafting organometallic complexes that are active homogeneous catalysts onto surfaces of various supports.[6,27] However, this technique suffers from two major drawbacks. First, grafted metal complexes frequently "leach" from the support during reactions because the bonds which anchor the complexes are not completely stable under reaction conditions.[27] When this happens, the activity observed can be in part due to homogeneous complexes. Second, high loading of grafted complexes on surfaces frequently can not be achieved while maintaining site isolation. Aggregation occurs producing a variety of species having different activities or worse, the catalysts deactivates.[10,27]

Recently a promising method utilizing building block techniques for creating single-site, metal oxide based heterogeneous catalysts where control over the local environment is achieved was described.[29] In this method, preformed molecular precursors are cross-linked to form a three dimensional matrix of intact building blocks. Within this matrix, all of the metal centers have the same local environment.

This approach to developing new materials relies upon several conditions to be successful. First, the molecular precursors used as building blocks should be thermally and chemically robust so that they can withstand reaction conditions. Any breakdown of the building unit will result in total loss of control of the reaction. Second, the reaction that cross-links building blocks should not allow aggregation of either linking groups or building blocks to occur thus

avoiding the development of building block rich or linking group rich domains in the matrix.

To avoid the formation of such domains, proper sized building blocks should be used such that the metrics of the building unit prevents linking metal atoms from interacting and aggregating. The linking reaction should also involve distinct and complementary groups on the building block and the linking groups. These complementary functionalities insure that the building blocks will not react with other building blocks and linking groups will not react with other linking groups. Thus, linking units will only react with building blocks as illustrated in the following equations:

$$\text{BB-x + link-y} \rightarrow \text{BB-link + x-y}$$

$$\text{link-y + link-y} \rightarrow \text{no reaction}$$

$$\text{BB-x + BB-x} \rightarrow \text{no reaction}$$

where -x represents the reactive group on building block and -y represents the reactive group on linking unit.

The building block method differs from traditional grafting techniques for designing single-site heterogeneous catalysts. In this approach, the potential active centers *participate* in the formation of the support by linking together the building blocks. This participation of the active species in the development of the support offers several advantages in making novel heterogeneous catalysts. One is the degree of connectivity associated with the active centers and the support. The degree of connectivity refers to the number of bounds between the active species and the support, i.e. the number of building blocks that the linking

group connects. Active centers can be attached to the support through multiple metal oxide bonds (as opposed to being anchored via a tether) to produce highly embedded catalytic centers. Due to these multiple bonds, these centers should not be as susceptible to leaching under reaction conditions. By varying the conditions to control this degree of connectivity, active centers can be embedded into a cross-linked matrix of building blocks where the catalytic sites have mainly, if not exclusively, one unique environment throughout the material. Tailoring the local environment of the active sites through the degree of connectivity is analogous to changing the ligands around homogeneous catalysts which is performed to optimize the catalytic performance and establishes a structure-reactivity relationship. A final consequence of the active species involvement in the development of the support is that the building blocks should spatially isolate the active centers within the support. Since materials prepared from nanometer sized building blocks are expected to be porous in nature and exhibit a high surface area, a high density of sites per unit volume or mass can be achieved and the spatial isolation should prevent aggregation of these sites during catalytic processes.

The octa(trimethyltin) cuboctomeric spherosilicate, $Si_8O_{20}(SnMe_3)_8$, is a suitably sized molecular precursor that has been used previously in the synthesis of building block materials.[28,29] The Si_8O_{12} core of the cubic spherosilicate exhibits relatively high thermal stability.[50] The mixed tin-silicon ether functionality ($\equiv$Si-O-$SnMe_3$) present on all eight corners of this cubic building block is reactive towards many metal chlorides to form a new silanolate linkage ($\equiv$Si-O-Metal) and

free trimethyltin chloride in anhydrous organic solvents.[28,29] This metathesis reaction is quite general and encompasses a wide variety of main group and high valent transition metal chlorides as potential linking groups between building blocks.

Herein we describe the development of nanostructured solids utilizing the reaction of $Si_8O_{20}(SnMe_3)_8$ with multiple silylchloride linking groups in combination with variable addition strategies.[29] Nanostructuring in this context refers first to the linking units being separated in space by distances dictated by the size of the Si_8O_{20} spherosilicate. Silylchlorides can be employed in this reaction to covalently link Si_8O_{20} building blocks through robust siloxy bonds to produce a silicate platform. In the platform, the silyl linking groups are isolated due to the metrics of the spherosilicate building block. Nanostructuring also refers to the connectivity, i.e. local environment of the linking group, being identical throughout the platform. Silylchloride linking groups were used for this study because the immediate environment of these groups can easily be probe spectroscopically using silicon-29 solid-state NMR.

This study describes the synthesis and characterization of nanostructured building block materials where control over immediate environments of silylchloride linking groups is demonstrated. The methodologies described herein for designing tailored building block solids are directly applicable for use in designing novel single-site metal oxide based heterogeneous catalysts.

3.2 Experimental

Due to the moisture sensitive nature of these reactions, several steps were taken to rigorously exclude all sources of water. Because silyl chlorides will react with hydroxyl groups present on the surface of glassware, all Schlenk reaction vessels and glass transfer apparatuses used in these procedures were treated with chlorotrimethylsilane/triethylamine (Sigma-Aldrich 97+%) prior to use. Hexanes and toluene (Fisher Scientific) solvents were dried using sodium potassium allow and distilled. $Si_8O_{20}(SnMe_3)_8$, was heated overnight at 100^oC under vacuum to remove waters of hydration in the crystal. *Caution: Trimethyltin containing compounds are extremely toxic and volatile and should be handled properly to minimize if not exclude contact via while manipulating them.*

Figure 3.1 shows a picture of a standard setup used to introduce volatile silylchloride reagents and solvents into reactions. A N_2/vacuum manifold was used during the transferring of reaction components. A Schlenk containing solvent was fitted with a high vacuum stopcock and attached to this manifold through a flexible, metal high vacuum transfer hose. A glass transfer “T” which connects the reaction Schlenk with a thick wall capillary was also attached to the manifold. Isolation valves were located between the manifold and the glass transfer “T” as well as on this transfer “T” just above the reaction.

To transfer reaction components, the entire system was evacuated using a lab “roughing” vacuum pump and isolated so that the whole system remained under static vacuum. Under reduced pressure, solvent vapors passed through the main N_2/vacuum manifold, through the glass transfer “T” and condensed into

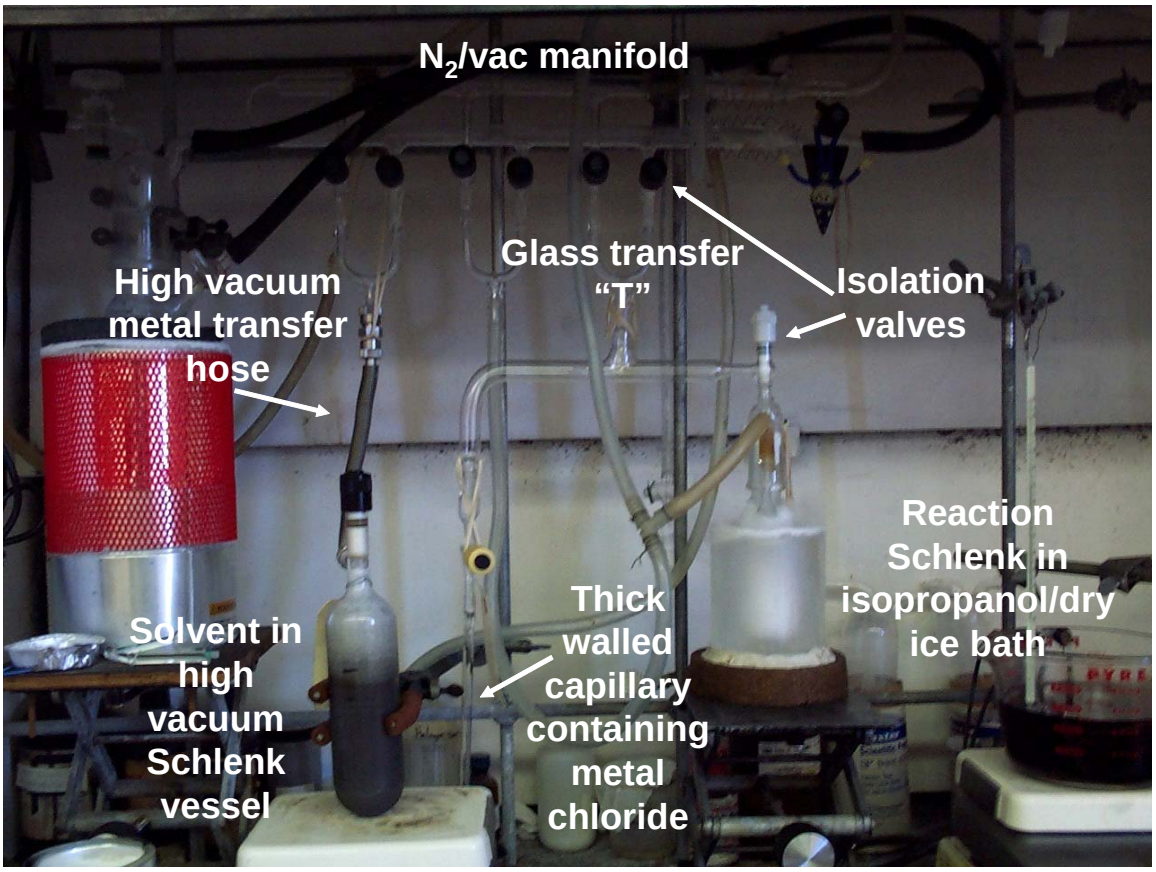

Figure 3. 1 Picture of reaction set up used to synthesize building block materials.

the Schlenk vessel submerged in an isopropanol/dry ice bath. The amount of solvent was estimated using the outer circumference of the Schlenk housing the solvent and the liquid levels in the Schlenk. After the appropriate amount of solvent was added to the reaction Schlenk, the glass transfer "T" which connected the thick wall capillary (Figure 3.2) and the reaction Schlenk was isolated using the appropriate isolation valvue and remained under static vacuum. The appropriate amount of silylchloride was then added to the reaction by vapor transfer methods (a more detailed description of this process for the addition of silylchlorides will be given in a later section of this chapter). Once all reactants were added to the reaction Schlenk, this vessel was isolated by closing the isolation valve and the reaction was allowed to run under vacuum at an appropriate temperature.

Frequently it was found that silyl chlorides from supply houses required distillation for purification. During distillation a large low boiling fraction of the silyl chlorides was discarded before collecting a constant boiling fraction. Only fractions that boiled within 2 ^{o}C of boiling points reported in the literature were collected and used in subsequent reactions. All silanes were distilled, degassed and stored under vacuum in Schlenk vessels equipped with high vacuum Teflon stock cocks. All solvents and silanes were delivered into reaction vessels using vapor transfer methods (*vida infra*).

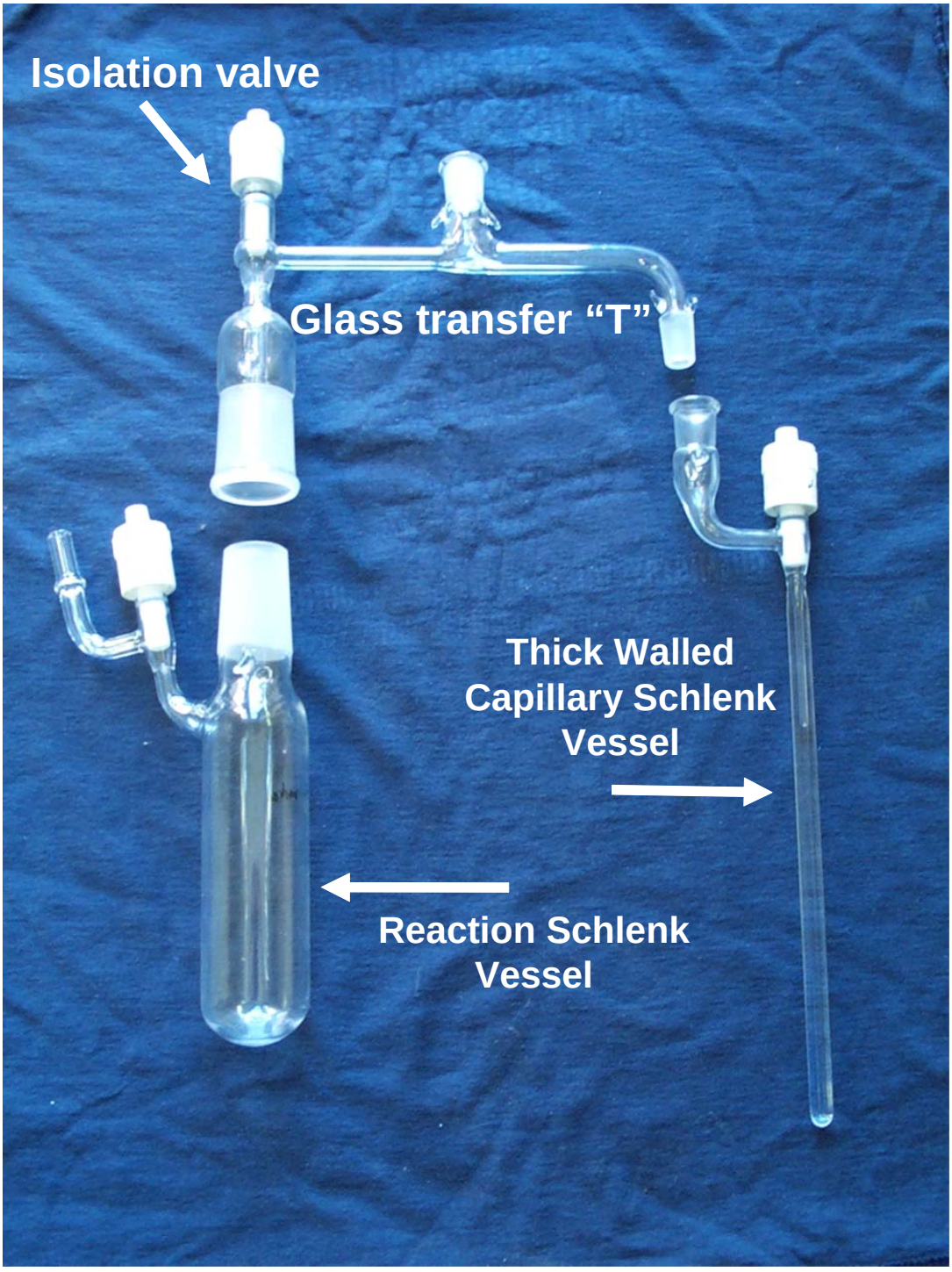

Figure 3. 2 Picture of thick walled capillary and glass trasfer "T" used to deliver silyl chlorides to the reaction.

3.2.1 Instrumentation

Silicon-29 solid state NMR experiments were acquired at 79.43 MHz at spin rates of 3.555 – 5.555 kHz on a Varian Inova spectrometer. Samples were placed in 5mm pencil rotors in a N_2 dry box and sealed using paraffin wax.[28]

BET nitrogen adsorption-desorption surface area analysis was performed using a Quanta Chrome Nova 1000 instrument.

Infrared spectra were obtained using a Bio-Rad FTS-60A spectrometer. Samples were prepared for IR analysis by mixing an appropriate amount in potassium bromide and making pellets.

3.2.2 General Procedure for the Preparation of Cross-linked Solids

In a typical reaction to make cross-linked Si_8O_{20} spherosilicate solids, approximately 1.00 g of $Si_8O_{20}(SnMe_3)_8$ was added to a Schlenk flask in a N_2 dry box. The flask was then attached to a glass T on a N_2/vacuum manifold and evacuated. Next, approximately 40 mL of solvent was vapor transferred through the manifold into the reaction Schlenk at -78^oC. The amount of solvent delivered from the Schlenk vessel was estimated from the diameter of the vessel and the height of the liquid column. While stirring, an appropriate amount of silylchloride was added to the reaction from a thick walled capillary style Schlenk tube (Figure 3.2). The silylchlorides used in this study were tetrachlorosilane ($SiCl_4$), trichlorosilane ($HSiCl_3$), and dichlorodimethylsilane (Me_2SiCl_2). The amount of silane delivered from the capillary was initially estimated from the diameter of the capillary and the change in height of the liquid column.

The actual amount delivered was more accurately determined by the weight difference of the capillary before and after delivery of the silane. It was found empirically that for the silanes discussed herein, a multiplicative correction factor of 1.2 was applied to the initial estimate based on volume measurements in order to deliver the desired amounts. Below is an example calculation showing how the corrected liquid column height (H_{corr}) difference needed to deliver 500 ml of $SiCl_4$ from a capillary having an inner diameter of 0.15 cm was determined:

$$V = \pi r^2 H$$
$$500\ ml = \pi (0.15 cm^2) H$$
$$H = 7.07\ cm$$
$$H_{corr} = (7.07 cm)(1.2)$$
$$H_{corr} = 8.48\ cm$$

Table 3.1 summarizes the reaction conditions and stoichiometries used for the samples described in this study. It also lists the error associated with the delivery method just described. In all instances, four chloride-to-tin ratios were used (4 : 1, 3 : 1, 2 : 1, 1 : 1) for each silyl chloride linker. The chlorine-to-tin ratio refers to the ratio of silylchloride groups on the linker to the trimethyltin group on the building block. For example $SiCl_4$ has four silylchloride groups and $Si_8O_{20}(SnMe_3)_8$ has eight mixed tin-silicon ether groups present. A chlorine-to-tin ratio of 4 : 1 requires an initial stoichiometry of eight $SiCl_4$ per $Si_8O_{20}(SnMe_3)_8$.

After the addition of the silane, the reactions were allowed to stir at either 50°C in hexanes overnight under a N_2 atmosphere or 80-90°C in toluene for 2

Table 3. 1 Table listing reaction conditions as well as initial stoichiometries used for the reactions described in this chapter.

Sample Identification	Silane Linker	Temperature (°C)	Solvent	Sn : Cl		Silane Mass (grams)			Observation After 1 (Hexanes) or 2 Days (Toluene)	Recovered Product Mass (grams)
				Target	Actual	Target	Actual	% Error		
40506	$SiCl_4$	50°C	Hexanes	1 : 4	1 : 3.95	0.728	0.720	1.099	clear gel, small amount of white precipitate	0.548
40504	$SiCl_4$	50°C	Hexanes	1 : 3	1 : 2.79	0.558	0.519	6.989	clear gel, small amount of white precipitate	0.646
40422	$SiCl_4$	50°C	Hexanes	1 : 2	1 : 1.89	0.407	0.384	5.651	clear gel, small amount of white precipitate	0.654
40421	$SiCl_4$	50°C	Hexanes	1 : 1	1 : 0.909	0.186	0.169	9.140	clear gel, small amount of white precipitate	0.829
41130	$SiCl_4$	80-90°C	Toluene	1 : 4	1: 3.99	0.689	0.688	0.145	clear gel, small amount of white precipitate	0.533
41117	$SiCl_4$	80-90°C	Toluene	1 : 3	1 : 3.24	0.560	0.606	-8.214	clear gel, small amount of white precipitate	0.651
41129	$SiCl_4$	80-90°C	Toluene	1 : 2	1 : 1.86	0.353	0.328	7.082	clear gel, small amount of white precipitate	0.503
41208	$SiCl_4$	80-90°C	Toluene	1 : 1	1 : 0.965	0.186	0.180	3.226	clear gel, small amount of white precipitate	0.412
40223	$HSiCl_3$	50°C	Hexanes	1 : 4	1 : 3.73	0.796	0.743	6.658	white powder	0.420
40218	$HSiCl_3$	50°C	Hexanes	1 : 3	1 : 2.76	0.597	0.549	8.040	white powder	0.281
40217	$HSiCl_3$	50°C	Hexanes	1 : 2	1 : 1.92	0.391	0.376	3.836	white powder	0.329
40216	$HSiCl_3$	50°C	Hexanes	1 : 1	1 : 0.842	0.178	0.167	6.180	white powder	0.378
41217	$HSiCl_3$	80-90°C	Toluene	1 : 4	1 : 3.83	0.794	0.760	4.282	white powder	0.400
41213	$HSiCl_3$	80-90°C	Toluene	1 : 3	1 : 2.75	0.562	0.518	7.829	clear gel, small amount of white precipitate	0.423
41212	$HSiCl_3$	80-90°C	Toluene	1 : 2	1 : 2.16	0.398	0.431	-8.291	clear gel, small amount of white precipitate	0.459
41209	$HSiCl_3$	80-90°C	Toluene	1 : 1	1 : 0.982	0.200	0.197	1.500	clear gel, small amount of white precipitate	0.504
40305	Me_2SiCl_2	50°C	Hexanes	1 : 4	1 : 3.91	1.138	1.112	2.285	white powder	0.430
40302	Me_2SiCl_2	50°C	Hexanes	1 : 3	1 : 2.92	0.871	0.847	2.755	white powder	0.392
40225	Me_2SiCl_2	50°C	Hexanes	1 : 2	1 : 1.97	0.570	0.562	1.404	white powder	0.453
40224	Me_2SiCl_2	50°C	Hexanes	1 : 1	1 : 0.931	0.294	0.274	6.803	white powder	0.236
50106	Me_2SiCl_2	80-90°C	Toluene	1 : 4	1 : 4.10	1.155	1.185	-2.597	clear solution	0.436
41221	Me_2SiCl_2	80-90°C	Toluene	1 : 3	1 : 2.98	0.912	0.907	0.548	clear solution	0.492
41220	Me_2SiCl_2	80-90°C	Toluene	1 : 2	1 : 1.94	0.540	0.524	2.963	clear gel	0.427
41218	Me_2SiCl_2	80-90°C	Toluene	1 : 1	1 : 0.917	0.258	0.237	8.140	clear gel	0.400

days sealed under vacuum. In most cases, a gel or white powder formed during this time. After stirring, all volatiles were removed and a white or off-white powder was observed in all cases. Table 3.1 summarizes observations of each sample recorded just prior to removing volatiles. The powder was then heated overnight at 100^{o}C under vacuum then analyzed using multinuclear NMR and N_2 adsorption-desorption measurements to determine total surface area and pore size distribution.

3.2.3 Tailoring the Matrix: The Method of Sequential Additions

A general three step procedure was used to produce building block solids having either hydridosilyl or dimethylsilyl linkers present where all silylchloride groups have reacted with building blocks. These samples are referred to as embedded, meaning these linking groups are 100% cross-linked in the matrix. First an initial, limiting dose of silane linker was added to a solution of $Si_8O_{20}(SnMe_3)_8$ to produce soluble oligomeric species consisting of the maximum number of building blocks bound to each linking center. A second dose of a different silylchloride was then added to cross-link these oligomeric species together along with any unreacted $Si_8O_{20}(SnMe_3)_8$ building blocks. A final dose of a silylchloride was added to react with any residual trimethyltin groups present in the matrix.

In a typical reaction, an initial, limiting amount of chlorosilane was added to approximately 1 g of $Si_8O_{20}(SnMe_3)_8$ dissolved in approximately 40 ml of toluene and allowed to stir for 2 days at 80-90^{o}C sealed under vacuum (Table

3.2). Next, a cross-linking dose of tetrachlorosilane was added to attain a target total chlorine-to-tin ratio of 2 : 1 (Table 3.2). This initial dose of cross-linking tetrachlorosilane must be large enough to cross-link unreacted building blocks and oligomeric species so that the product phase separates from the reaction but not be too large to avoid the formation of capping species that do not perform linking function in the matrix. Empirically it was found that the amount of cross-linking silylchloride needed when tetrachlorosilane is used is between 1.5 : 1 and 2 : 1 *total* silylchloride groups to mixed tin-silicon ether group. The total silyl chloride refers to the sum of Si-Cl groups form both doses.

After the appropriate amount of $SiCl_4$ was added, the reaction was allowed to stir at 80-90^oC for 2 additional days after which a clear gel was present. All volatiles were removed and an off-white powder was observed. This powder was then exposed to tetrachlorosilane vapor overnight to react with any residual trimethyltin groups remaining in the product (Table 3.2). All volatiles were removed and the resulting white powder was heated overnight at 100^oC under vacuum.

In order to obtain a building block platform having only capping dichlorohydridosilyl or chlorodimethylsilyl groups, a slightly different synthetic approach was utilized. A solid matrix was synthesized by cross-linking $Si_8O_{20}(SnMe_3)_8$ building blocks using $SiCl_4$ as a linking agent. The reaction conditions and workup procedures used to synthesize the platform were the same as those previously described involving $SiCl_4$ in toluene at temperatures of 80-90^oC. The chlorine-to-tin ratio used was 1.5 : 1. The amount of cross-linking

Table 3. 2 Table listing initial stoichiometries used in the synthesis of nanostructure building block solids.

Sample Id	Silane Linker	Link	Silane Sn : Cl		Mmoles Added		Observation After Reaction	Cross-linking Sn : Cl_{total}		Observation After Treatment	Vapor Phase Sn : Cl_{total}		Observation after treatment	Recovered mass (grams)
			Target	Actual	Sn	Cl		Target	Actual		Target	Actual		
050107	Me_2SiCl_2	Dilink	4 : 1	4.8 : 1	4.39	0.91	Clear Solution	1 : 3	1 : 2.8	Cloudy gel	1 : 4	1 : 4.2	White powder	0.499
050311	$HSiCl_3$	trilink	4 : 1	4.0 : 1	4.23	1.12	Clear Solution	1 : 3	1: 2.5	Cloudy gel	1 : 4	1 : 4.3	White powder	0.476

Sample 050311 and 050310 used sample 050305 as a platform for further reaction			Cross-linking Sn : Cl_{total}		Observation After Reaction	Silane Sn : Cl_{total}		Observation After Reaction	Vapor Phase Sn Cl_{4l}	Observation after treatment	Recovered mass (grams)
			Target	Actual		Target	Actual		Mass (grams)		
050311	Me_2SiCl_2	Capping	1 : 1.5	1 : 1.39	Cloudy gel	1 : 3	1 : 3.1	White powder	0.207	White powder	0.358
050310	$HSiCl_3$	Capping	1 : 1.5	1 : 1.39	Cloudy gel	1 : 3	1 : 3.3	White powder	0.244	White powder	0.358

silylchloride used in this step must be sufficient to cause the reaction product to phase separate while leaving residual unreacted trimethyltin groups on the developed solid platform. This building block platform was then exposed to trichlorosilane or dichlorodimethylsilane vapor overnight. All volatiles were removed and an off-white powder was observed. This powder was exposed to tetrachlorosilane in the gas phase to react with any trace mixed tin-silicon ether groups remaining (Table 3.2).

3.3 Results and Discussion

The synthesis and characterization of nanostructured building block materials where control over the immediate environment of silylchloride linking units was achieved by investigating a series of reactions involving $Si_8O_{20}(SnMe_3)_8$ with tetrachlorosilane ($SiCl_4$), trichlorosilane ($HSiCl_3$), and dichlorodimethylsilane (Me_2SiCl_2). In these reactions, Si_8O_{20} silicate building units are “linked” together via a metathesis reaction where silylchloride groups react with mixed tin-silicon ethers to form new siloxane linkages and trimethyltin chloride (Figure 3.3).

$$\equiv Si\text{-}O\text{-}SnMe_3 + Cl\text{-}Si\equiv \rightarrow \equiv Si\text{-}O\text{-}Si\equiv + ClSnMe_3$$

Under the non-aqueous conditions utilized for these reactions, the silylchloride linkers will only react with functional groups on the building block. Thus, the formation of domains of linking groups within the resulting solid matrix does not occur. This linking together of preformed molecular precursors is referred to as a “building block” approach to materials synthesis (Figure 3.4).

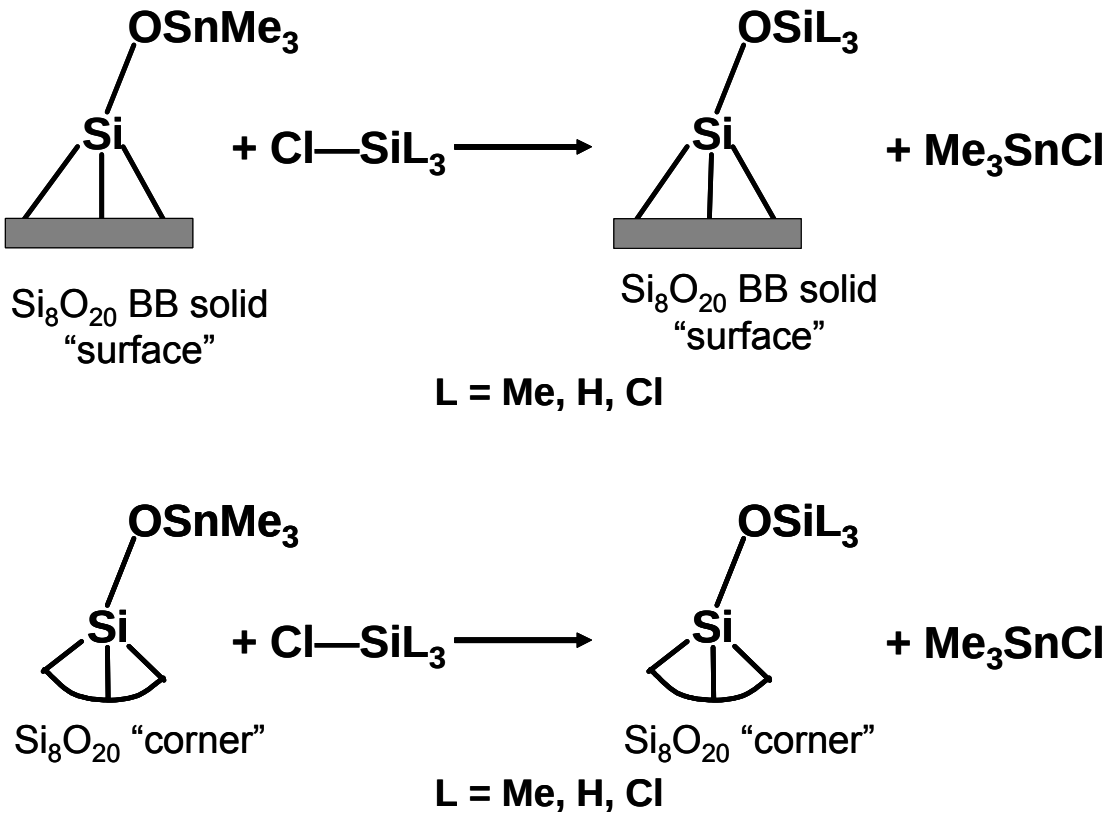

Figure 3. 3 Illustration of the reaction taking place between trimethyltin groups and silylchloride groups.

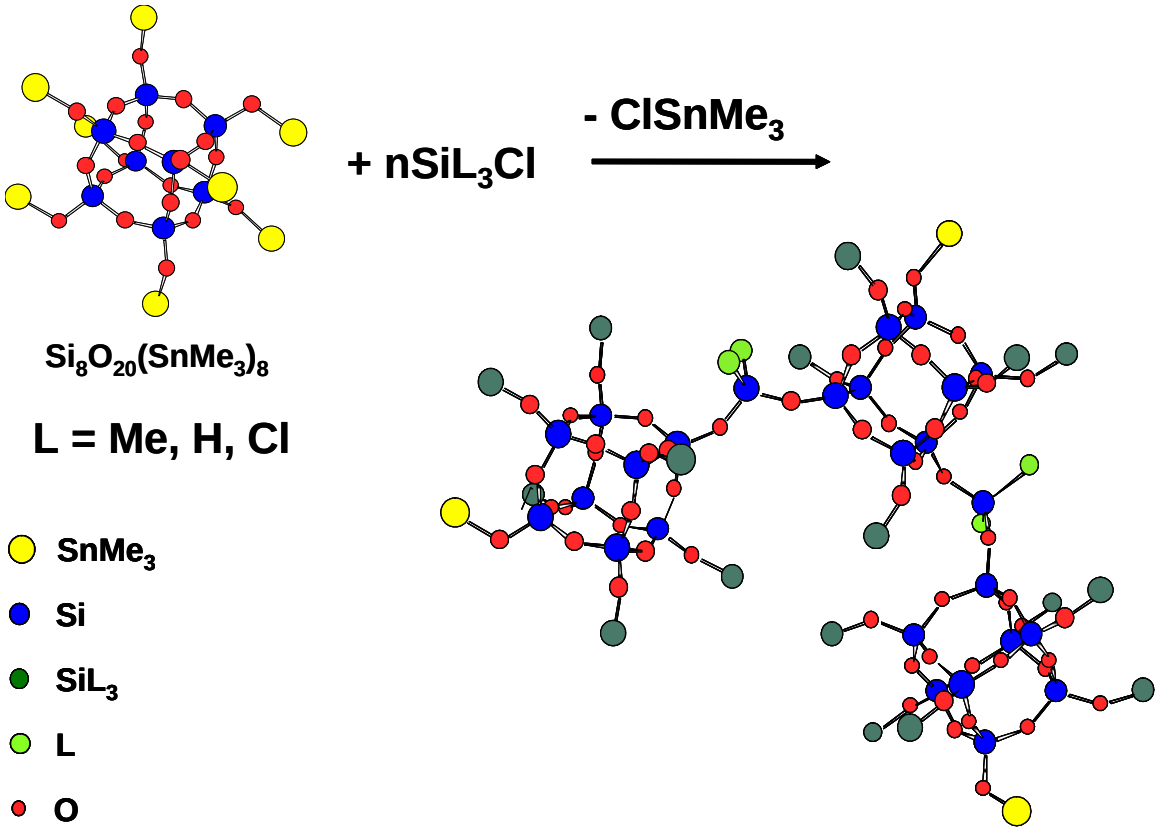

Figure 3. 4 Illustration of building block synthesis.

The irreversible linking of building blocks in these reactions produces a random substitution pattern of links around the eight positions on the cubic spherosilicate building block and a random distribution of linking groups in the matrix. Thus, these materials are expected to be amorphous and porous due to inexact fitting of building blocks in the matrix and irreversible linking.

By changing reaction conditions, initial stoichiometries, and using different silylchlorides, the degree of cross-linking (i.e. the types of linking units in the resulting product) can be influenced. This is a fundamental goal of my research: to develop a methodology by which nanostructured heterogeneous catalysts may be prepared by design. As was stated earlier, nanostructuring in this context refers to controlling the number and types of linking groups in the solid matrix. In addition, the linking units should remain separated in space as dictated by the size and rigidity of the spherosilicate cube and the distances between corners. As a result of this spatial separation, the linking groups remain isolated in the matrix.

3.3.1 Silicon-29 Solid-state NMR: A Spectroscopic Probe

Since these materials are amorphous in nature, traditional diffraction methods are not applicable for structural characterization. However, silicon-29 magic angle spinning (MAS) NMR provides a powerful tool to obtain information about the structure of these materials. This technique can supply valuable information about the types of silylchloride linkages present via chemical shift. Figure 3.5 summarizes the chemical shift ranges that have been reported in the

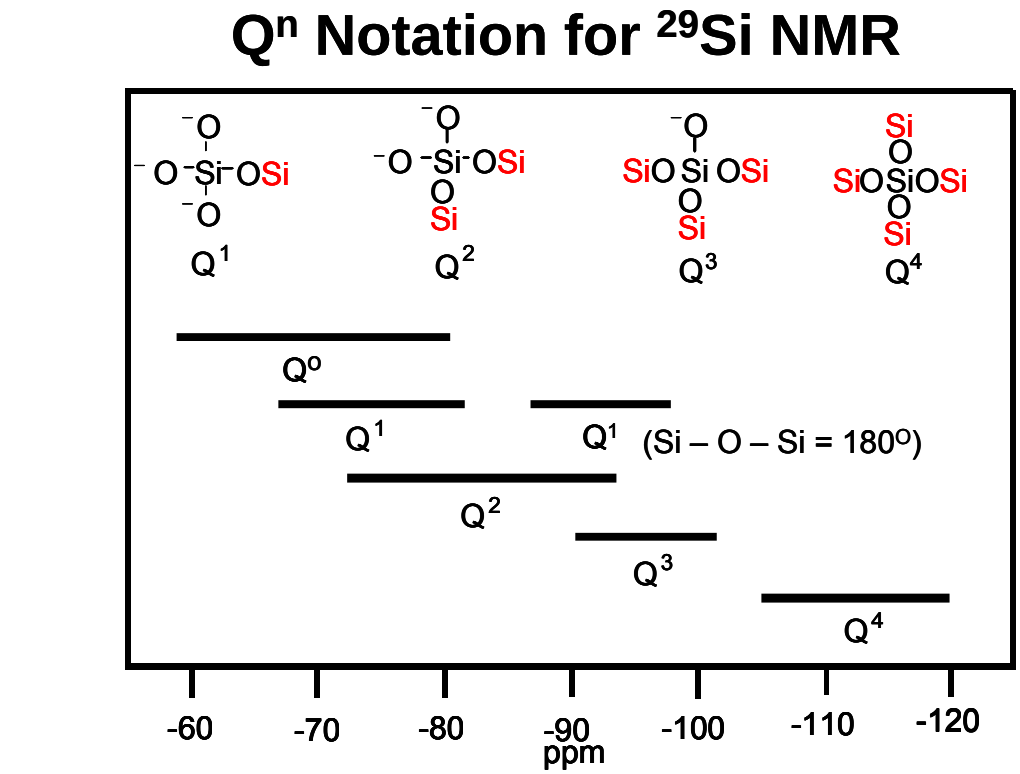

Modified from Günter Engelhardt, D.M., *High-resolution solid-state NMR of silicates and zeolites*. Vol. xiv. 1987, New York: Wiley. 485

Figure 3. 5 Q^n notation for silicon-29 NMR of silicates.

literature for silicon-29 nuclei in *silicates*. The Q^n notation has been developed to distinguish between SiO_4 tetrahedra in silicates based upon the number of hydroxyl groups versus the number of siloxy groups surrounding a probe silicon.[109] In this terminology, the superscript "n" refers to the number of silicon-oxygen-silicon units around a central SiO_4^{-4} tetrahedron. As can be seen in Figure 3.5, as $-O^-$ groups are replaced by –OSi substituents around a silicon-29 probe, its chemical shift becomes more negative.

In reactions involving silylchlorides with $Si_8O_{20}(SnMe_3)_8$, siloxane linkages are formed at the corners of the spherosilicate building block and a Q^4 silicon results for each corner of the Si_8O_{20} cage. Due to the presence of methyl, hydrido, or chloro groups bound to the *linking* silicon atoms in these building block materials, these tetrahedral silicon centers do not fall into the traditional Q^n type notation. We have however been able to derive useful correlations between the number of Si-Cl bonds to a linking silicon atom and the observed silicon-29 chemical shifts. As illustrated in Figure 3.6, different types of silylchloride linking groups can be clearly identified from their observed silicon-29 chemical shifts. In addition, these signals are more resolved than what is observed in pure silicates.

It should be noted that in the reactions involving $SiCl_4$, if all four silylchloride groups react with mixed tin-silicon ether groups, a Q^4 type *linking* silicon will result. The formation of a Q^4 type linking group is not possible in reactions involving the $HSiCl_3$ and Me_2SiCl_2. In all cases Q^4 silicon environments result for each silicon in the Si_8O_{20} building block when a new siloxy linkage is formed.

^{29}Si NMR Chemical Shift Ranges for Various Silyl Linking Units

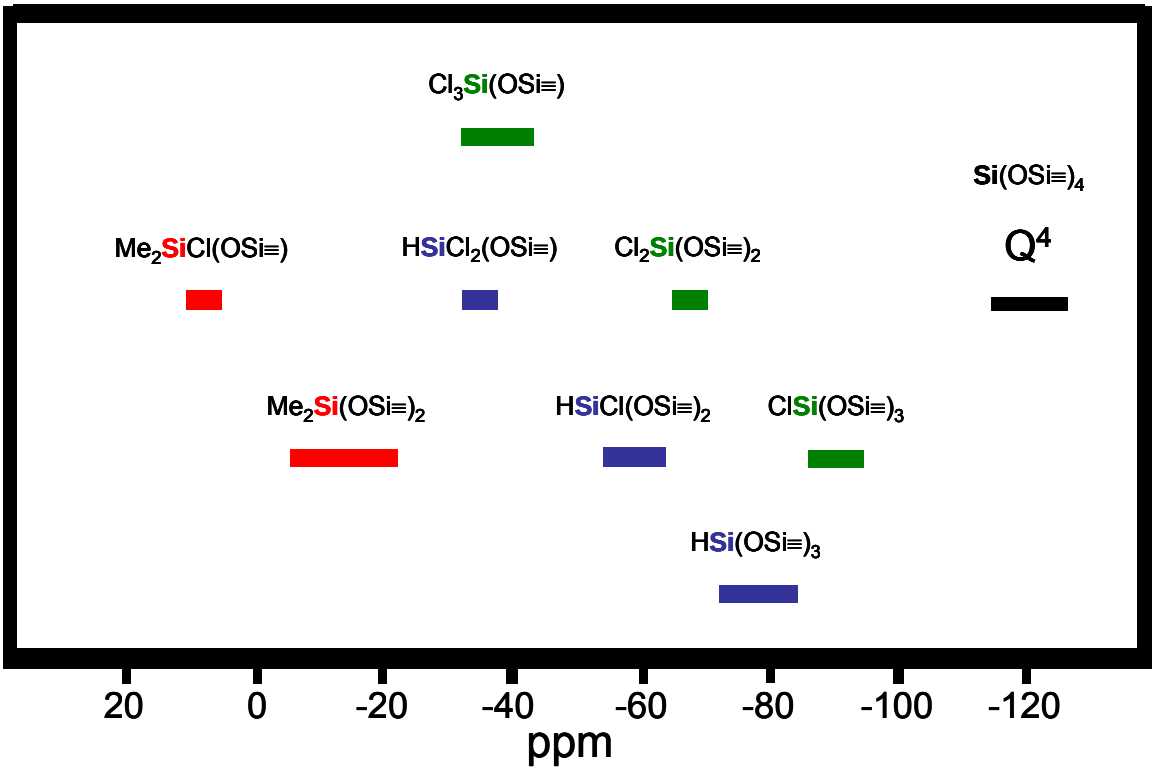

Figure 3. 6 Silicon-29 chemical shift for liking silylchloride groups.

Despite the chemical shift information gained from MAS NMR, there are some limitations to this technique. Deeply embedded **Si**$(OSi\equiv)_4$ Q^4 silicon nuclei have no effective spin-lattice relaxation mechanisms available to them. Thus, the times associated with relaxation of these types of silicon-29 nuclei can be extremely long. The ultimate consequence of this is that quantitative information obtained by integrating observed signals in silicon-29 spectra is not reliable due to expected saturation of NMR transitions. Furthermore, the experimental times required to acquire data with acceptable signal-to-noise ratios can be very long. These relaxation problems are most prominent in all the materials described herein and especially when tetrachlorosilane is used as a linker because there are no protons associated with this group (*vide infra*).

Surface bound trichlorosilyl groups, which may rotate freely on the surface, are capable of fast motion that provides an efficient relaxation mechanism.[35] This relaxation mechanism is possible with all capping moieties such as surface bound dichlorohydridosilyl and chlorodimethylsilyl groups. Dimethylsilyl and hydridosilyl linking groups posses a second important mechanism for relaxation. This mechanism involves dipolar interactions of silicon-29 nuclei with hydrogen atoms (^{1}H) present on the linkers. The dipolar (through-space) relaxation mechanism is proportional to the product of the gyromagnetic ratio squared (γ^2) for the two nuclei and is inversely proportional to the sixth power of the distance between the nuclei.[35] Since ^{1}H has a high γ value, its presence in the matrix provides an efficient means of allowing silicon-29 nuclei. However, due to the inverse distance dependence in dipolar

relaxation, not all of the silicon-29 nuclei present in the matrix may relax identically. Therefore integrated signal intensities generally do not accurately reflect relative numbers of nuclei and cannot be used to quantify different types of silicon atoms in the matrix.

Cross-polarization magic angle spinning NMR (CPMAS) provides an additional tool for determining structural information about the materials. The cross-polarization of silicon-29 from ^{1}H occurs through dipolar interactions between the two nuclei. Since ^{1}H has is 100% naturally abundant, significant enhancements in silicon-29 signals that have protons in close proximity can be observed. Furthermore, this enhancement can be very useful in making signal assignments when MAS and CPMAS spectra are compared. Cross-polarization experiments can also be used advantageously to observe signals from silicon-29 nuclei having hydrogen atoms in close proximity that are not prominent in MAS experiments because they are present in low concentrations. Examples of signals that are expected to show enhancements for linking species described in this study are the dimethylsilyl linking unit (=$SiMe_2$) and the hydridosilyl linking unit (≡SiH). The cage silicon bearing these linking groups as well as cage silicon bearing trimethyltin groups are also expected to show enhancement in CPMAS experiments (*vide infra*).

In contrast to the solid state silicon-29 MAS experiment, the CPMAS experiments do not require long experimental times if adequate concentrations of hydrogen atoms are present in the sample. In CPMAS experiments, delay times required for relaxation time correspond to the abundant nuclei (^{1}H) which relaxes

more efficiently than silicon-29 nuclei due to reasons previously discussed above. However, there are some disadvantages to using the cross-polarization technique with the samples discussed in this study. Silicon-29 nuclei in these samples will cross-polarize at different rates due to variations in the spatial separation between silicon and hydrogen atoms.[36] Thus, quantitative information again can not be obtained. Second, this technique can not be used to probe samples made by linking $Si_8O_{20}(SnMe_3)_8$ with tetrachlorosilane because there are no available protons for cross-polarization.

3.3.2 Justification for Using Silylchlorides as Linking Units

Chemical shift information, along with the cross-polarization properties of silicon-29 nuclei, make silylchlorides good candidates for model studies to develop the methods needed to produce building block solids by design. Few metals having potential catalytic properties can be as easily observed using solid-state NMR or other spectroscopic techniques. Since structural characterization is essential if a correlation between activity and selectivity, and structure is to be realized, then appropriate “proof of concept” model studies are extremely important. Furthermore, chemically robust linking groups will also be needed to prepare supported catalysts. In most cases metal loadings will be low (up to 5 wt%) due to the cost of the metals and to provide adequate heat transport properties.

3.3.3 Adjustable Parameters Effecting Cross-linking

A number of parameters were investigated to develop the methodology that allows for control over the cross-linking properties of the resulting materials. The first parameter that was investigated was the *initial reaction stoichiometry* of chlorosilane linkers to stannylated spherosilicate building blocks. The hypothesis here is that as the initial amount of linking silylchloride decreased, the degree of cross-linking will increase. Degree of cross-linking refers to the number of linkages formed around a chemical entity used to covalently bond silicate cubes together relative to the maximum number of bonds that can be formed around a linking atom. The second parameter studied was the properties of the *linking unit* itself. The use of silylchlorides having groups that are inert in reactions with $Si_8O_{20}(SnMe_3)_8$ will also influence the number of building blocks that can be linked together around a single silyl linking unit. For example, when tetrachlorosilane is used as the linking silylchloride, up to four Si_8O_{20} units can be connected by siloxane linkages (Figure 3.7). In the case of trichlorosilane and dichlorodimethylsilane only the silylchloride groups will react with the mixed tin-silicon ether group present on the building block. Thus, $HSiCl_3$ can form links with up to three building blocks while Me_2SiCl_2 can link a maximum of two Si_8O_{20} units (Figure 3.7). A linking group that has achieved the maximum degree of cross-linking is referred to as a “deeply embedded” linking group. In cases where linking groups are attached to the matrix by only one bond it is described as a “capping” group.

Controlling Cross-linking Using Blocking Groups

- **Me** and **H** groups are not reactive in this system
- **4** linkages possible with $SiCl_4$
- **3** linkages possible with $HSiCl_3$
- **2** linkages possible with Me_2SiCl_2

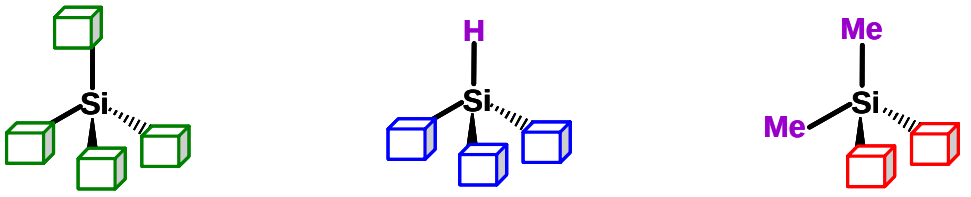

tetrasubstituted trisubstituted disubstituted

Figure 3. 7 Illustration of blocking groups on silylchloride linking groups.

3.3.4 Tailoring the Cross-linking Properties

Throughout this part of the study, a single silane linker was employed. Four ratios of silylchloride per mixed tin-silicon ether were used to investigate the effects on the degree of cross-linking. The ratios used in this series of reactions ranged from having an excess of four silylchloride units per mixed tin-silicon ether group to a stoichiometric equivalent of silylchloride group per tin functionality on the building block. As expected, as the initial concentration of silylchloride decreased, the degree of cross-linking increased (*vide infra*).

The first series of reaction studied involved $SiCl_4$ as the linking unit. In this reaction, a maximum of four building blocks can be connected through a single silyl linking unit. Figure 3.8 shows the silicon-29 MAS solid state NMR for the products of this series of reactions run in toluene at 80-90^{o}C. When an excess amount of tetrachlorosilane is used (chlorine-to-tin ratio of 4 : 1), mostly capping units (-45 ppm) and silyl linking units connecting only two building blocks (-65 ppm) are observed with possibly a trace amount of linking units connecting three Si_8O_{20} building blocks (-90 ppm) are observed in the NMR spectrum. Also, no observable signal was seen between -99 and -104 ppm in the silicon-29 MAS NMR. This is consistent with the complete reaction of all mixed tin-silicon ether groups. The absence of such groups in the final product was further verified by observing no signal in the tin-119 MAS NMR.

In the other spectra shown in Figure 3.8, as the initial amount of $SiCl_4$ is decreased, the distribution of linking units shifts towards a higher degree of cross-linking and an increase in the amount of residual trimethyltin groups on

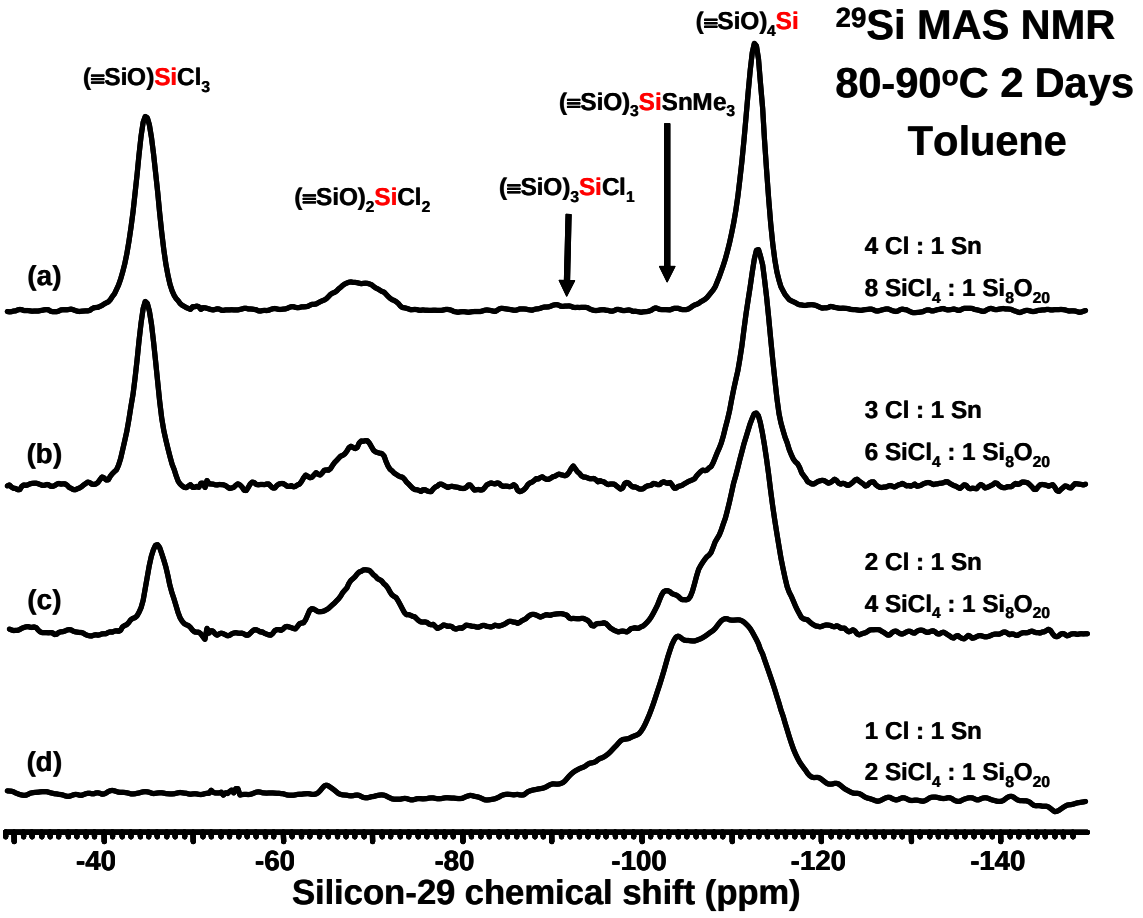

Figure 3. 8 Silicon-29 MAS NMR spectra of materials cross-linked at 80-90°C in toluene using tetrachlorosilane.

unreacted corners of linked Si_8O_{20} spherosilicates in the matrix. At the lowest initial concentrations of tetrachlorosilane, only silyl linkages connecting three and four building blocks are present along with a large amount of residual trimethyltin groups. The silicon-29 MAS NMR spectrum of this highly cross-linked material also shows a broadening of the Q^4 signal. This broadening is consistent with the development of an increasing number of local environments around *pseudo*tetrahedral Q^4 type silicon atoms in the sample. Despite evidence that molecular Si_8O_{20} cages can distort from octahedral symmetry in the solid state (depending upon the substituent attached), the individual SiO_4 tetrahedra that make up the cage generally exhibit very similar geometries. However, in a highly cross-linked material, Q^4 linking groups may deviate from idea T_d in symmetry due to slight perturbations in O-Si-O bond angles brought about by cross-linking. This distribution of local environments around SiO_4 units ultimately results in a broadening of the Q^4 signal.

Figure 3.9 shows the silicon-29 MAS NMR for the reaction products of $SiCl_4$ with $Si_8O_{20}(SnMe_3)_8$ in hexane at 50°C where the initial amount of tetrachlorosilane was varied in a manner similar to that in the higher temperature studies where toluene was used as the solvent. As in the high temperature studies, the degree of cross-linking increases as the concentration of $SiCl_4$ decreases. However, when the same initial stoichiometries are compared at different temperatures, it appears that at high temperatures in toluene the development of linking groups connecting two, three, and four building blocks are favored as opposed to a lower degree of cross-linking observed when lower

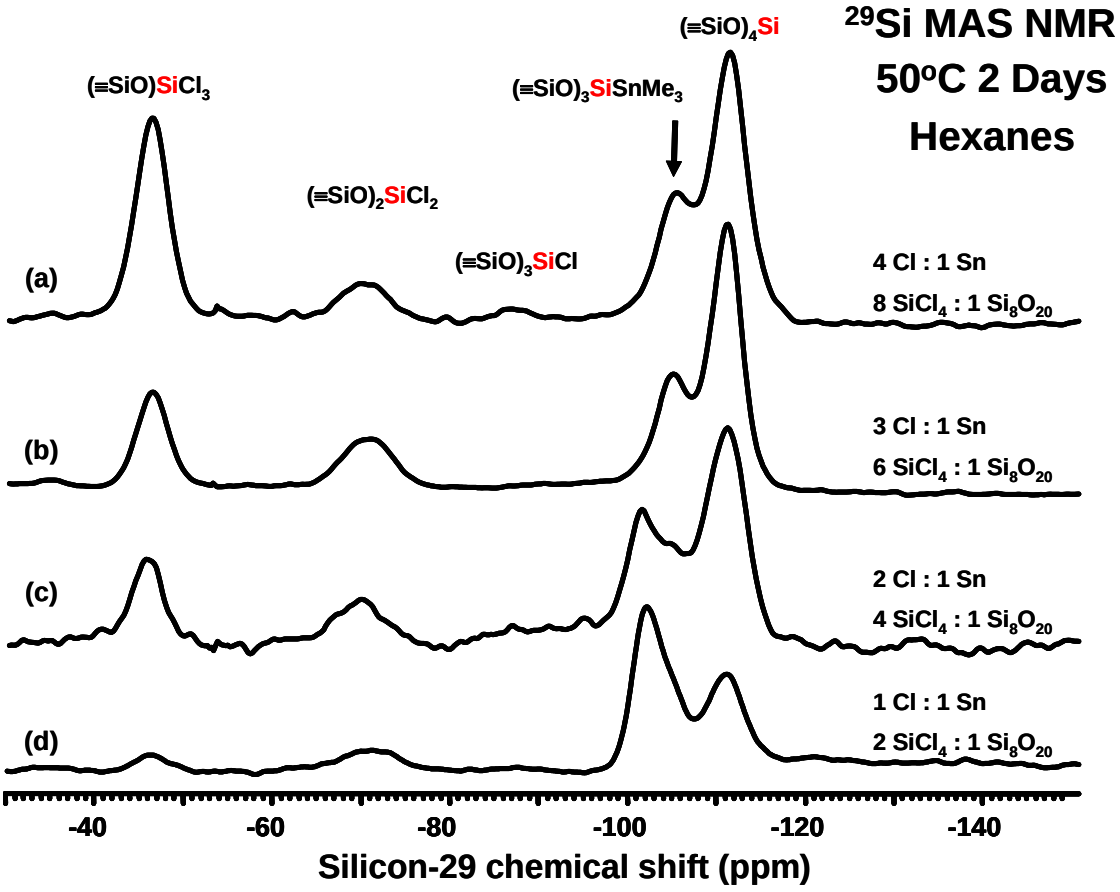

Figure 3. 9 Silicon-29 MAS NMR spectra of materials cross-linked at 50°C in hexanes using tetrachlorosilane.

temperature and hexane is used as a solvent. Also, in the lower temperature/hexane reactions, residual mixed tin-silicon ether groups are present in all instances. These observations suggest that the reaction rates of silylchloride groups present on a single linking unit decreases after each group subsequently reacts. These rates of reaction for the subsequent Si-Cl groups could be influenced by steric and/or electronic factors associated with cross-linking building units.

The chemical shift of the signal of silicon in Si_8O_{20} bearing a trimethyltin group has an observed range of -99 to -104 ppm in silicon-29 NMR. This range represents the limiting chemical shift values observed for amorphous anhydrous $Si_8O_{20}(SnMe_3)_8$ in the solid state which was discussed in chapter 2 of this thesis. In all of these samples, a large increase in relative intensity of this signal was observed when silicon-29 cross-polarization MAS experiments were conducted which is consistent with this signal assignment.

Exposure to trace amounts of water would produce silanol groups which would give rise to silicon-29 chemical shifts also in this range. In addition, silanol groups would also show a signal enhancement in CPMAS experiments. In order to verify that the signals observed were not due to the presence of such silanol groups, IR analysis of these samples was carried out. IR spectra showed no signals in the range 3400-3200 cm^{-1} indicating no hydroxyl groups were present. Finally, tin-119 signals were observed in solid state MAS experiments consistent with the presence of trimethyltin groups. Based on these data, we assigned these signals solely to residual trimethyltin groups remaining on the material.

When BET surface area measurements were compared for the products of the samples described above, the low temperature/hexane samples had significantly smaller overall surface areas (Table 3.3). The smaller observed surface areas were interpreted as resulting from the formation of small oligomeric species made up of only a few cross-linked Si_8O_{20} building block units that formed during the reaction. In contrast, the high temperature reaction products all had much higher high surface areas. These higher surface area measurements were interpreted as resulting from the formation of extended cross-linked silicate matrix with open pores primarily in the mesoporous range as opposed to small oligomeric, molecular species. Spectroscopic evidence that supports this interpretation will be discussed momentarily.

The second silylchloride cross-linking reagent studied was $HSiCl_3$. This linking unit can connect a maximum of three building blocks. Figure 3.10 shows the silicon-29 MAS solid state NMR of the products from these reactions carried out in toluene at 80-90^oC. The amount of $HSiCl_3$ was varied in the same manner as in the experiments using $SiCl_4$. As was seen in the reactions with $SiCl_4$, a decrease in the initial amount of $HSICl_3$ resulted in an increase in the degree of cross-linking. In the reactions where an excess of silylchloride linking unit is present, hydridosilyl linking groups are present connecting two (-60 ppm) and three (-80 ppm) building blocks as well as capping dichlorohydridosilyl groups (-35 ppm). Also, all trimethyltin groups reacted in these samples (Figure 3.10 a-c). In the reaction where a stoichiometric amount of silylchloride to trimethyltin was used (Si-Cl : Me_3Sn, 1 : 1), only hydridosilyl linking species connecting two and

Table 3. 3 Table listing surface area and pore properties for cross-linked samples.

Sample	Silane	Conditions	Cl:Sn	Surface Area (m^2/g)	Total Pore Volume (cc/g)	Average Pore Diameter (Å)
041130	$SiCl_4$	Toluene, 80-90ºC, 2 days	4:1	203	0.165	34
041117	$SiCl_4$	Toluene, 80-90ºC, 2 days	3:1	258	0.180	28
041129	$SiCl_4$	Toluene, 80-90ºC, 2 days	2:1	570	0.385	26
041208	$SiCl_4$	Toluene, 80-90ºC, 2 days	1:1	590	0.423	28
040506	$SiCl_4$	Hexanes, 50ºC, overnight	4:1	low	low	low
040504	$SiCl_4$	Hexanes, 50ºC, overnight	3:1	low	low	low
040422	$SiCl_4$	Hexanes, 50ºC, overnight	2:1	low	low	low
040421	$SiCl_4$	Hexanes, 50ºC, overnight	1:1	low	low	low
041217	$HSiCl_3$	Toluene, 80-90ºC, 2 days	4:1	low	low	low
041212	$HSiCl_3$	Toluene, 80-90ºC, 2 days	3:1	558	400	28
041213	$HSiCl_3$	Toluene, 80-90ºC, 2 days	2:1	660	513	32
041209	$HSiCl_3$	Toluene, 80-90ºC, 2 days	1:1	672	539	32
040223	$HSiCl_3$	Hexanes, 50ºC, overnight	4:1	336	243	28
040218	$HSiCl_3$	Hexanes, 50ºC, overnight	3:1	324	254	32
040217	$HSiCl_3$	Hexanes, 50ºC, overnight	2:1	401	295	30
040216	$HSiCl_3$	Hexanes, 50ºC, overnight	1:1	58	46	32
050106	Me_2SiCl_2	Toluene, 80-90ºC, 2 days	4:1	low	low	low
041221	Me_2SiCl_2	Toluene, 80-90ºC, 2 days	3:1	low	low	low
041220	Me_2SiCl_2	Toluene, 80-90ºC, 2 days	2:1	172	.150	34
041218	Me_2SiCl_2	Toluene, 80-90ºC, 2 days	1:1	669	.496	30
040305	Me_2SiCl_2	Hexanes, 50ºC, overnight	4:1	13	.015	48
040302	Me_2SiCl_2	Hexanes, 50ºC, overnight	3:1	29	.171	26
040225	Me_2SiCl_2	Hexanes, 50ºC, overnight	2:1	12	.010	38
040224	Me_2SiCl_2	Hexanes, 50ºC, overnight	1:1	14	.021	60

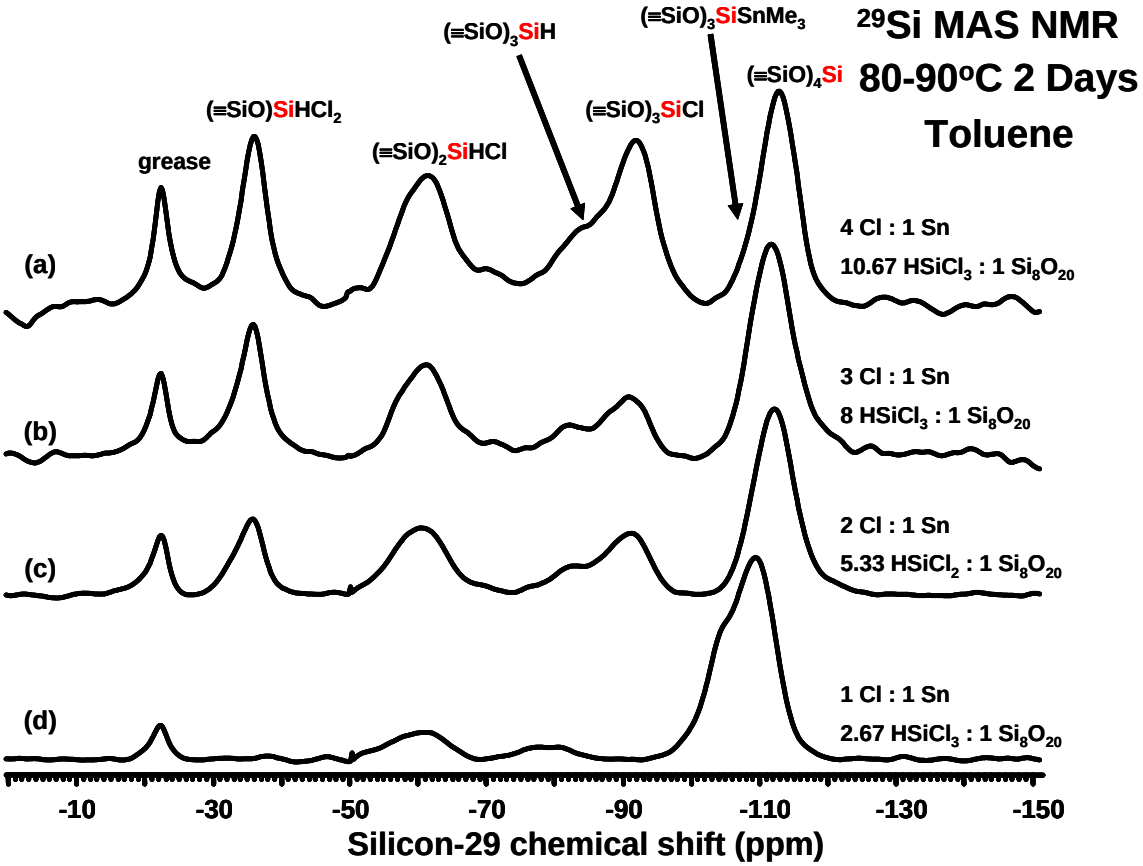

Figure 3. 10 Silicon-29 MAS NMR spectra of materials cross-linked at 80-90°C in toluene using trichlorosilane.

three building blocks were observed along with unreacted trimethyltin groups on the building blocks (Figure 3.10 d). This presence of residual trimethyltin groups was verified using both tin-119 MAS and silicon-29 CPMAS NMR.

It is also noteworthy that in all cases where an excess of silylchloride is used, a signal is seen centered at -90 ppm (Figure 3.10 a-c). This signal was assigned to a chlorosilyl group having three siloxane groups [$(\equiv SiO)_3SiCl$] based on its chemical shift value. This assignment is supported by observations made from the CPMAS experiments. In this experiment, the signal at -90 ppm showed no enhancement consistent with a silicon nucleus having no hydrogen atoms in close proximity. *One explanation for the presence of this group is that Si-O-Si bonds making up Si_8O_{20} are attacked during the reaction.* As shown in Figure 11, the intensity of this signal appears to decrease as the initial amount of $HSiCl_3$ decreases. Thus large excesses of hydridosilylchloride groups at high temperatures in toluene appear to cause a loss of structural integrity of the building block.

Disruption of Si_8O_{20} building blocks is not seen, however, when milder conditions are used (Figure 3.11 a-d). No signal is observed at -90 ppm in these spectra where the same initial stoichiometries were used but the reaction was run at a lower temperature. Using these milder reaction conditions (50^oC overnight, hexanes), hydridosilyl groups linking three Si_8O_{20} building blocks are only seen when a stoichiometric amount of silylchloride is used per mixed tin-silicon ether group. Also, residual mixed tin-silicon ether groups are present in all samples. Despite a lower amount of observed cross-linking for samples

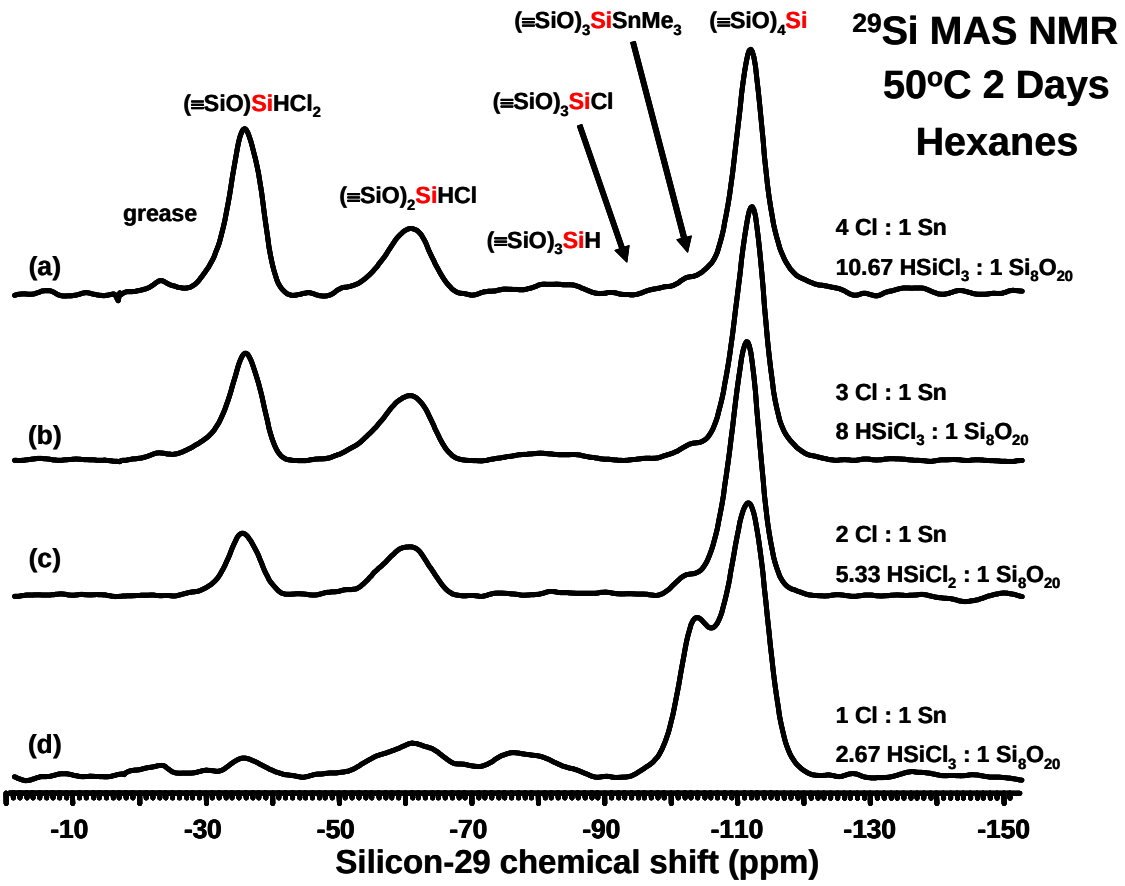

Figure 3. 11 Silicon-29 MAS NMR spectra of materials cross-linked at 50°C in hexanes using trichlorosilane.

synthesized using milder conditions, all samples have reasonably high surface areas (Table 3.3). The high surface areas are also observed in the high temperature samples except when the largest excess of silylchloride is used (Table 3.3).

The final silylchloride linking group studied was dichlorodimethylsilane. This linking moiety can connect a maximum of two Si_8O_{20} building blocks. Figure 3.12 shows the silicon-29 MAS NMR of the products from these reactions in toluene at 80-90^{o}C. These reactions again illustrate the trend of increasing cross-linking as the initial ratio of silylchloride to mixed tin-silicon ether group decreases. In reactions where an excess of the silylchloride was used, all trimethyltin groups reacted forming capping chlorodimethylsilyl groups (10 ppm) and dimethylsilyl groups linking two building blocks (-15 ppm). Only in reactions having a stoichiometric amount of reactive groups were residual trimethyltin groups observed in the reaction products. The higher degree of cross-linking in the samples having lower chloride-to-tin ratios also has significant effects on the surface areas of these reaction products (Table 3.3). When an excess of silylchloride was used or a stoichiometric amount of silylchloride per mixed tin-silicon ether was used, the surface areas of the resulting solids were too low to be measured accurately via adsorption isotherm experiments. We interpret these low surface area measurements to indicate the formation of small oligomeric species where only a few Si_8O_{20} building blocks are linked. It was found that the integrated intensities of the signal assigned to surface bound chlorodimethylsilyl *capping* group is approximately five times greater than the

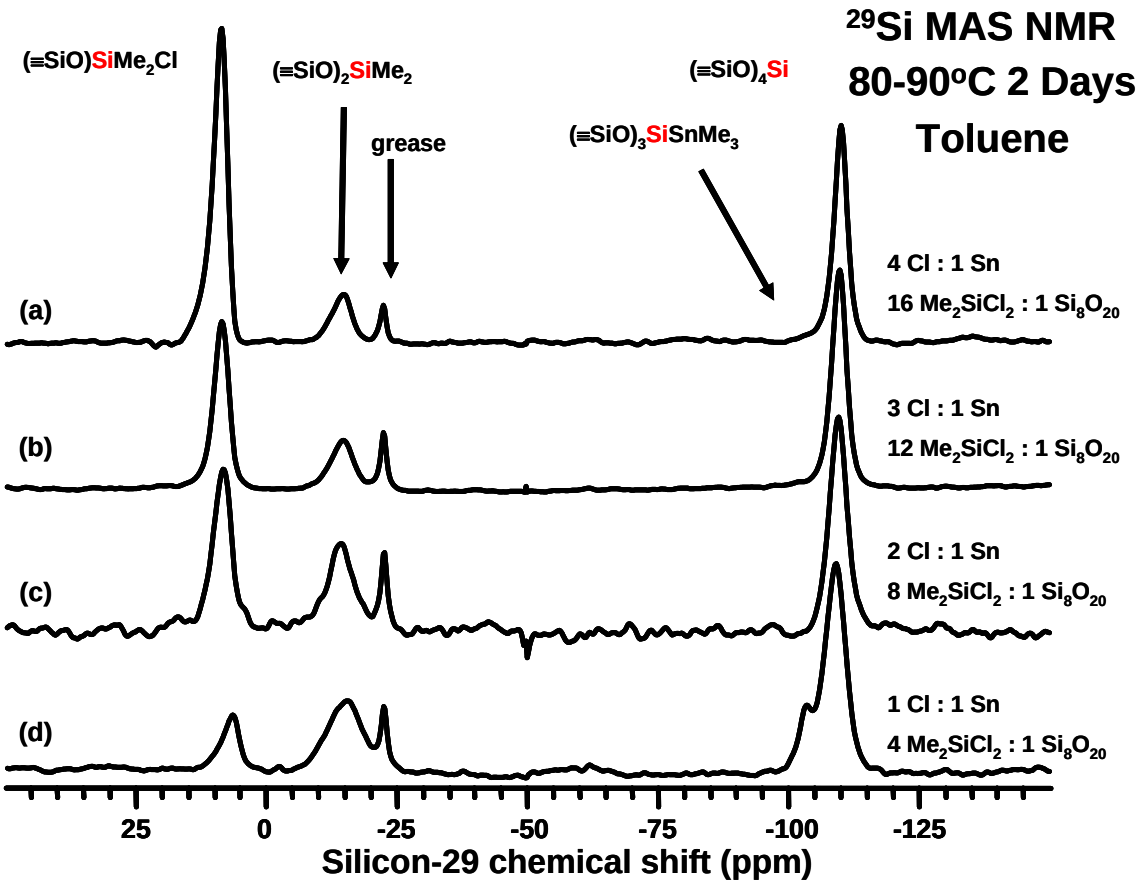

Figure 3. 12 Silicon-29 MAS NMR spectra of materials cross-linked at 80-90°C in toluene using dichlorodimethylsilane.

signal assigned to dimethylsilyl *linking* groups in the silicon-29 MAS NMR of the sample having the largest excess of silylchloride present in the reaction of Me_2SiCl_2 with $Si_8O_{20}(SnMe_3)_8$. In this case NMR signal intensities may be more reliable for these two signals due to the relaxation properties associated with the linking atoms having the two methyl groups present. However, these numbers should be considered as an upper bound to the ratio of capping groups to to linking groups. This evidence supports the notion that a majority of the corners of Si_8O_{20} units present in the sample where excess linking reagents is used are capping chlorodimethylsilyl groups. Due to this, very few linkages occur between building blocks, consistent with our interpretation of the BET surface area data.

Figure 3.13 shows the silicon-29 MAS NMR of the products from the reactions of Me_2SiCl_2 with $Si_8O_{20}(SnMe_3)_8$ in hexanes at 50^oC. In this case, the reaction which had a stoichiometric amount of silylchloride has only linking units that connect two building blocks along with residual trimethyltin groups. Despite the increase in cross-linking, the surface areas for all reaction stoichiometries investigated are less than 30 m^2/g (Table 3.3). Unlike higher temperature reactions, residual mixed tin-silicon ether groups are present in all cases. As was observed in the cases with the other silyl chlorides at both high and low temperature, the amount of residual trimethyltin groups present increases as the chlorine-to-tin ratio decreases.

The overall goal of this portion of the study was to investigate how the distribution of linking groups would be influenced by stoichiometry and reaction conditions (time, solvent, temperature) when forming Si_8O_{20} building block

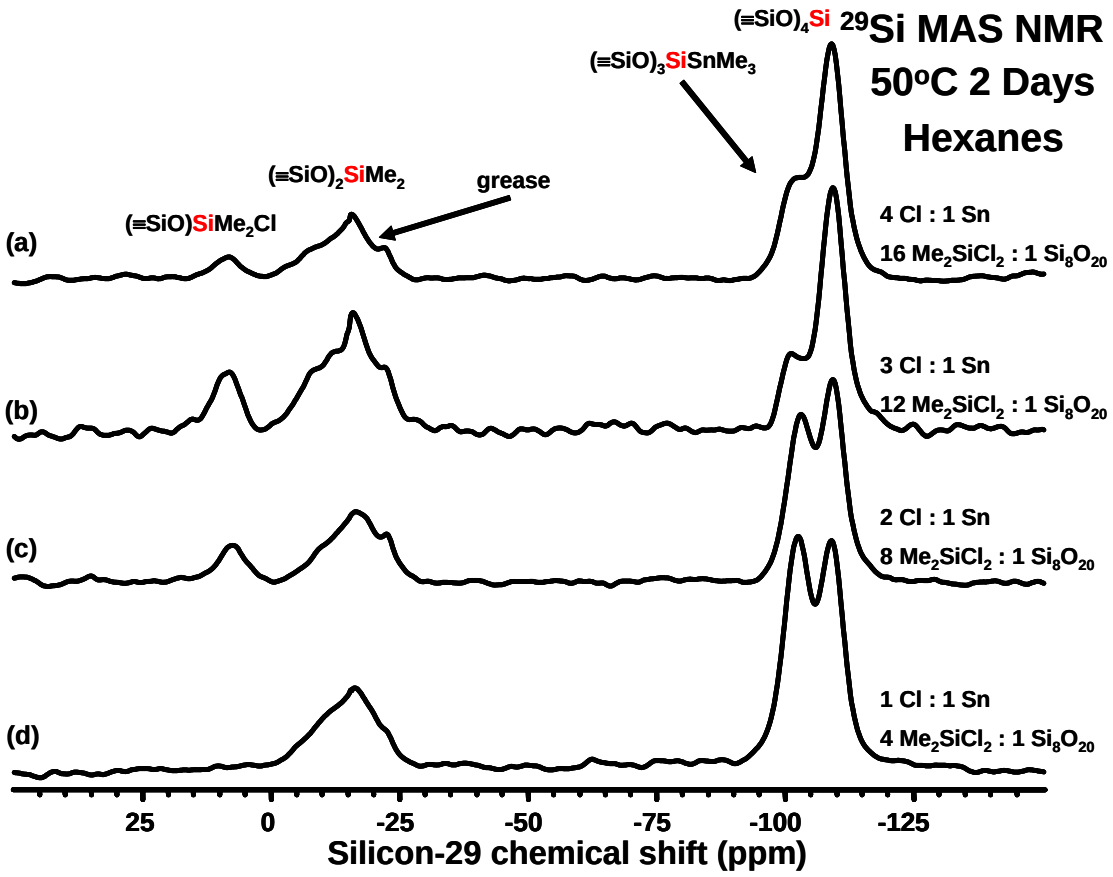

Figure 3. 13 Silicon-29 MAS NMR spectra of materials cross-linked at 50°C in hexanes using dichlorodimethylsilane.

materials using a single linking silylchloride. We found that as the initial stoichiometry of silyl chloride to trimethyltin group decreases, the degree of cross-linking increases. The degree of cross-linking also increases as the raction temperature increases. In the case where trichlorosilane is used as a linking unit, high temperature should be avoided in order to insure that the SI_8O_{20} is not attacked during the synthesis. A second goal was to use the information about cross-linking kinetics to develop a methodology by which tailored silicate materials may be prepared by design.

Tailoring in this context refers to preparing cross-linked building block matrices containing specific, unique types of linking groups throughout. For example, we would like to be able to prepare a sample that contains only embedded dimethylsilyl linking groups connecting two building blocks. Also, methods to obtain exclusively surface bound capping dichlorohydridosilyl and chlorodimethylsilyl species were desired. The next section describes our studies at extending this methodology toward preparing nanostructured solids.

3.3.5 Tailored Solids

Tailored solid materials were produced using trichlorosilane and dichlorodimethylsilane in limiting amounts in combination with different addition methods. These materials were cross-linked using tetrachlorosilane. Because a linking unit is comprised of not only the linking silyl group and associated nanometer sized Si_8O_{20} building blocks, this methodology may also be described as an approach to producing nanostructured silicate solids. These methods

simulate more closely how single-site, metal oxide-silicate based materials can be synthesized using methods where nanostructuring linking unit environment is desired.

A matrix having silyl linkers surrounded by three Si_8O_{20} building units was prepared using trichlorosilane. This was achieved using a limiting amount of trichlorosilane in the presence of $Si_8O_{20}(SnMe_3)_8$ and heating to 80-90^oC for two days in toluene. Under these conditions, all silylchloride groups react to form soluble oligomeric species made up of three connected Si_8O_{20} units and with many unreacted trimethyltin groups on the corners of building blocks. Based on the studies described in section 3.2.4, no disruption of Si_8O_{20} cages should occur. These oligomers, when reacted further with $SiCl_4$ formed a cross-linked, porous high surface area material. Removing any remaining trimethyltin groups that were present in the material was accomplished by drying the gel under vacuum for several hours at room temperature and exposing the resulting powder to excess $SiCl_4$ without a solvent.

Figure 3.14 shows the silicon-29 MAS and CPMAS of the reaction product. In the MAS spectrum, signals were present that were consistent with a distribution of linking groups associated with $SiCl_4$. A small signal observed at –80 ppm was assigned to hydridosilyl groups connecting three Si_8O_{20} units. No signals were observed at –35 ppm or -60 ppm indicating that dichlorohydridosilyl capping groups or chlorohydridosilyl groups linking two building blocks, respectively, were not present in the matrix.

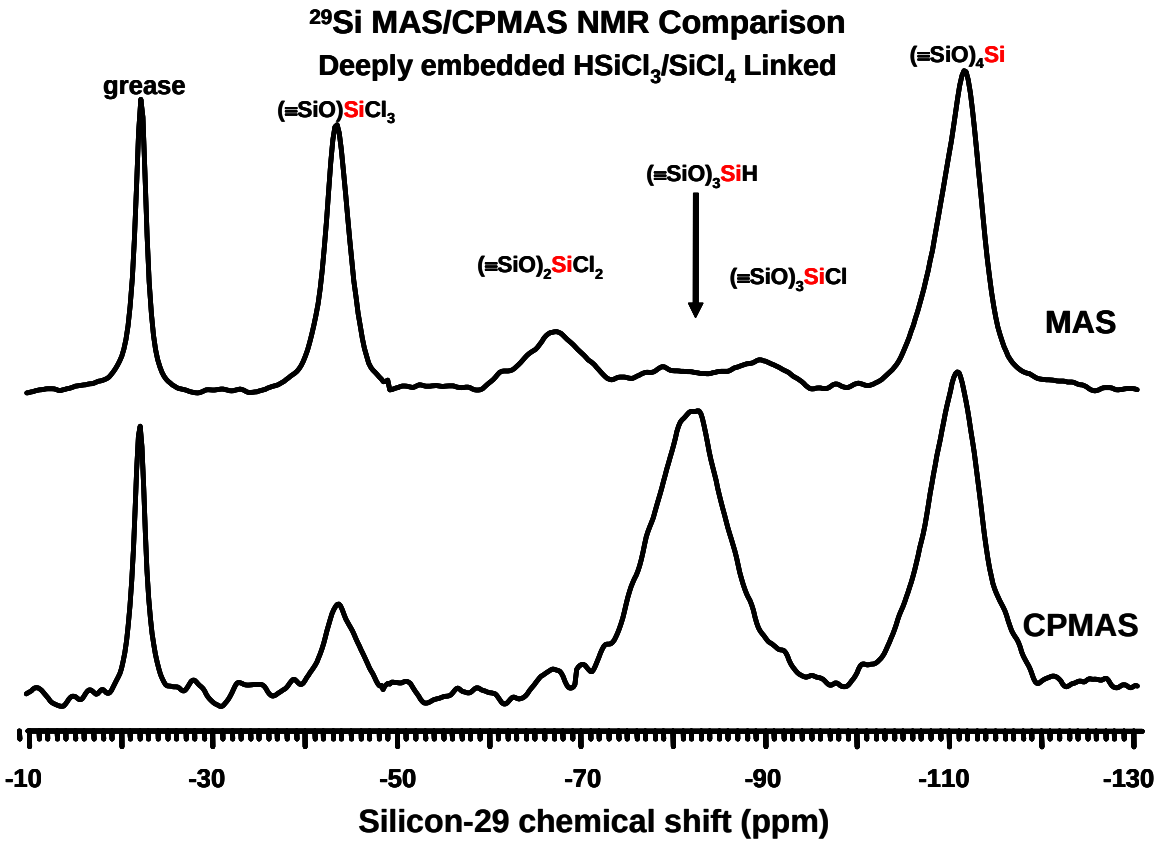

Figure 3. 14 Silicon-29 MAS and CPMAS spectra of deeply embedded hydridosilyl linking group.

Due to the low concentration of linking hydridosilyl groups and problems with resolution, a silicon-29 CPMAS experiment was conducted to enhance all signals present that correspond to hydridosilyl containing species. As illustrated in Figure 3.14, the signal at -80 ppm is greatly enhanced and no signals are observed at -35 or -60 ppm. Based on these NMR data, the sample contains only one type of hydridosilyl linking group and a distribution of chlorosilyl linking and capping groups derived from tetrachlorosilane.

Using dichlorodimethylsilane and the same procedure just described for trichlorosilane, a sample was synthesized that contained dimethylsilyl linking units connecting two building blocks only. Figure 3.15 shows the silicon-29 MAS and CPMAS NMR for this material. As was previously seen in Figure 3.14, a distribution of linking and capping chlorosilyl groups are present from the cross-linking and vapor phase exposure to tetrachlorosilane. The only signal that can be assigned to dimethylsilyl linking groups has a chemical shift of -11 ppm. No signal is seen in the MAS or CPMAS spectra at 10 ppm corresponding to a capping chlorodimethylsilyl group.

A variation of this general approach was used to prepare building block silicate platforms where only capping groups were present. This material was prepared using methods previously described to cross-link Si_8O_{20} building blocks with tetrachlorosilane at initial reactant stoichiometries (Si-Cl : Me_3Sn, 2 : 1) that yield a product having a distribution of linking and capping groups as well as residual mixed tin-silicon ether groups (Figure 3.8 c). The resulting powder was then exposed to either trichlorosilane or dichlorodimethylsilane in the gas phase

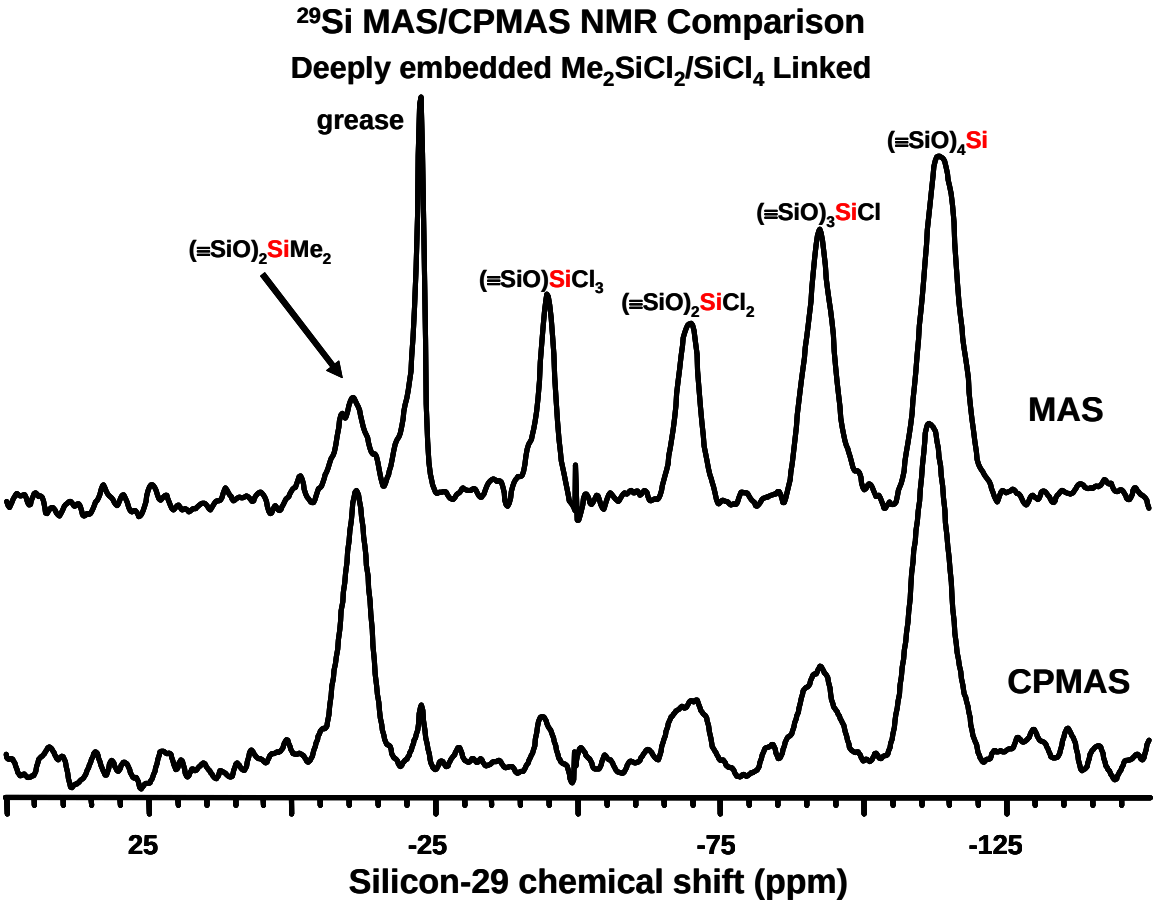

Figure 3. 15 Silicon-29 MAS and CPMAS spectra of deeply embedded dimethylsilyl linking groups.

and allowed to react overnight. Because the rigid three-dimensional matrix of cross-linked cubes has mixed tin-silicon ether groups fixed in space, no further cross-linking was expected from this dose of chlorosilanes.

Figures 3.16 – 3.17 show silicon-29 MAS and CPMAS NMR spectra for the products from these two reactions. As indicated by the MAS spectra, both have signals that indicate a distribution of linking and capping groups derived from initial cross-linking reactions with tetrachlorosilane. The corresponding CPMAS spectra shows that in both cases *only* capping dichlorohydridosilyl or chlorodimethylsilyl groups are present in these materials. Furthermore, little to no residual trimethyltin groups are observed. In all cases, nitrogen adsorption-desorption surface area analyses indicate that all of these materials have a high surface area with a broad distribution of pore diameters in the mesoporous region (Table 3.4).

3.4 Summary and Conclusions

Next generation catalysts will require novel design principles to optimize their performance. Single site, supported metal oxide materials can offer the advantages observed in homogeneous catalysts in terms of activity and selectivity.[106] In this study a methodology is defined where cubic, Si_8O_{20} spherosilicate building blocks are cross-linked with various silylchlorides and the distribution of types of linking silyl groups are influenced by design. The parameters that were studied to achieve this were solvent, temperature, and use of a variety of linking silylchlorides. The materials produced using the methods

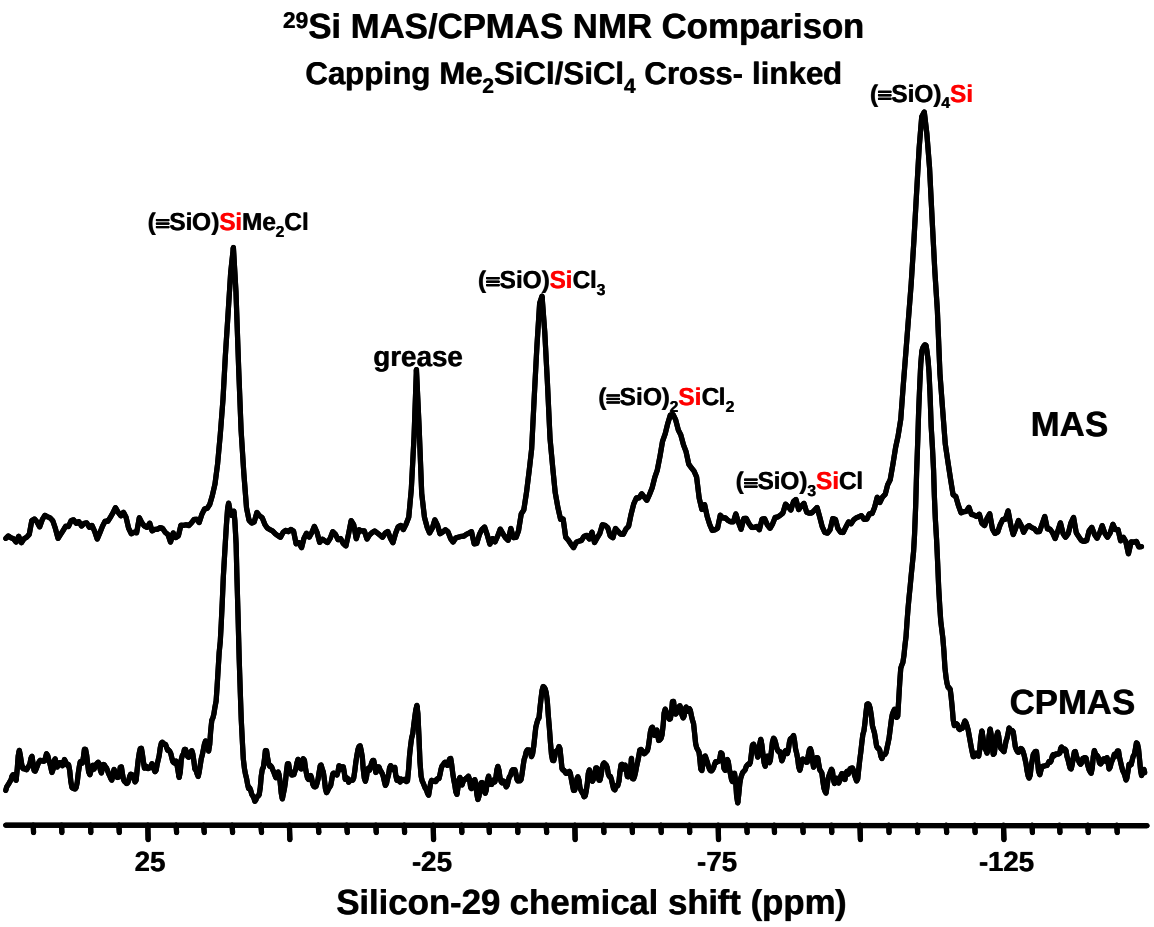

Figure 3. 16 Silicon-29 MAS and CPMAS spectra of "capping" chlorodimethylsilyl groups.

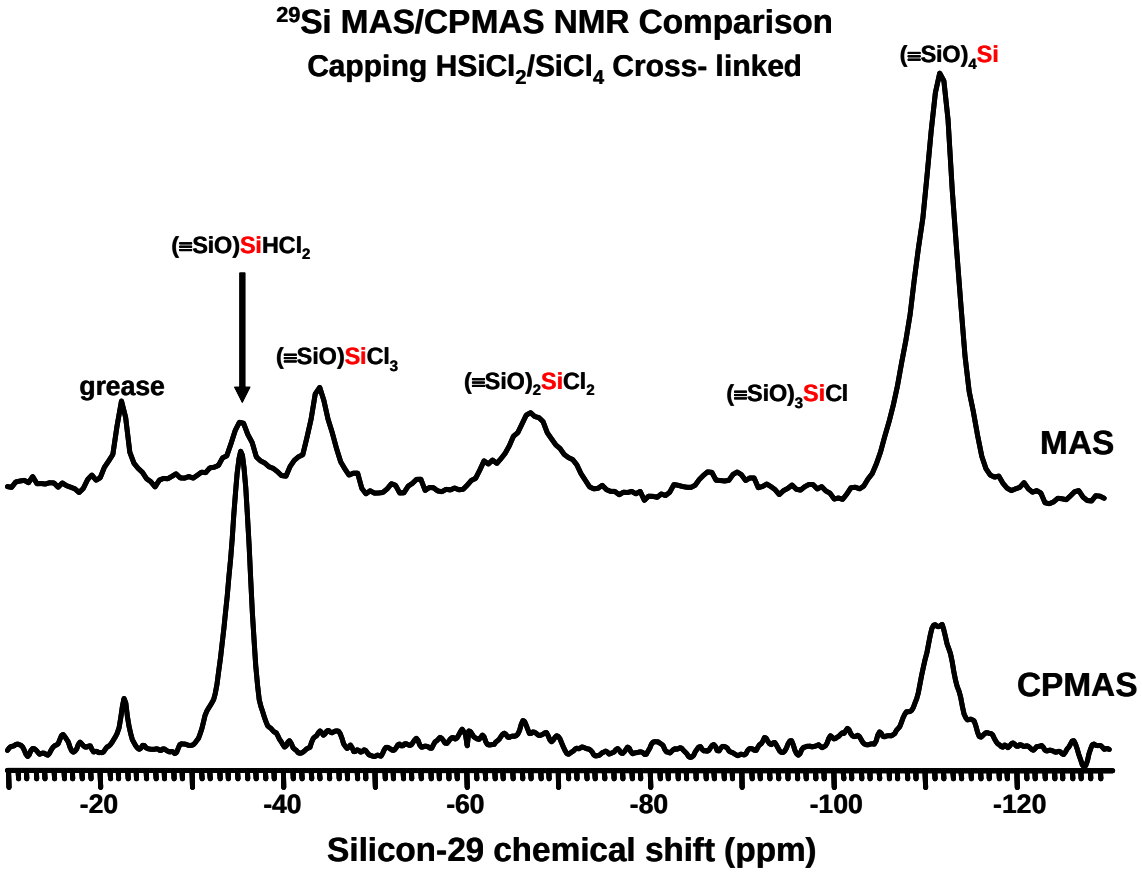

Figure 3. 17 Silicon-29 MAS and CPMAS spectra of "capping" dichlorohydridosilyl groups.

Table 3. 4 Table listing surface area and pore properties of nanostructured building block materials.

Sample	Silane Linker	Linking	Surface Area (m^2/g)	Total Pore Volume (cc/g)	Average Pore Diameter (Å)
050311	Me_2SiCl_2	Capping	607	0.380	24
050310	$HSiCl_3$	Capping	619	0.396	26
050107	Me_2SiCl_2	Dilink	739	0.891	48
050110	$HSiCl_3$	Trilink	513	0.386	30

described herein were analyzed using silicon-29 MAS and CPMAS solid-state NMR to probe the immediate environment of the linking species based on chemical shift values and cross-polarization behavior.

The information gained from the single silane cross-linking part of this investigation was then applied to materials having mixed silyl linking moieties. These materials had loadings of site isolated silyl groups linking spherosilicates in concentrations that resemble amounts used in real heterogeneous catalysts. Additionally, the silyl linkers present in limiting amounts had uniform local environments throughout the entire sample. This type of control over the local environment of atomic centers is exactly what is needed to prepare next generation heterogeneous catalysts. These next generation heterogeneous catalysts will provide deeper understanding of the relationship between the immediate environment of the catalytic site and activity and selectivity.

A fundamental difference between this approach of preparing nanostructured catalysts and previous approaches is the involvement of the catalytic site in the development of the support. This involvement is what allows control over the local environment of the sites because the support itself is synthesized by linking together preformed molecular precursors with, in this case, silyl linking species as opposed to grafting sites onto an existing support. This method can easily be extended to a wide variety of metal chlorides where the resulting siloxy linkages are replaced with metal oxide linkages by using metal chlorides as opposed to silylchlorides.[28,29]

This approach to synthesizing nanostructured building block materials where linking groups present in limiting amounts have uniform local environments throughout the material was achieved by using dosing techniques and different silylchlorides. These samples have silyl linkages connecting either two or three Si_8O_{20} building blocks exclusively. By utilizing a different addition procedure, materials can be synthesized where only capping silyl groups are present. These procedures demonstrate a new approach to designing nanostructured building block matrices. This is of obvious interest in the area of heterogeneous catalysts because this type of control could lead to novel heterogeneous catalysts having many of the advantages observed in homogeneous catalysis.

One critical factor that must be mentioned in this context is the synthetic control illustrated here will be successful only if the building block remains intact during cross-linking reactions. Disruption of the Si_8O_{20} building block was observed *only* in the case of high temperature reactions of trichlorosilane and $Si_8O_{20}(SnMe_3)_8$ where an excess of silylchloride was used. Evidence for this disruption was identified by the silicon-29 solid state MAS NMR signal at -90 ppm assigned to chlorosilyl groups. However, no dichlorosilyl groups (-65 ppm) were observed in the NMR in these cases. Also, chlorosilyl groups were not observed in the high temperature reactions involving dichlorodimethylsilane where the same excess of silylchloride groups per mixed tin-silicon ether groups was used as in the case where cage disruption was observed (Figures 3.8 a-c, 3.10 a-c, 3.12 a-c). In similar reactions involving tetrachlorosilane at both high and low

temperatures, the silicon-29 MAS NMR displays little if any signal that can be assigned to a chlorosilyl group. This is consistent with Si_8O_{20} building block units remaining intact in reactions involving tetrachlorosilane and dichlorodimethylsilane as well as trichlorosilane under milder conditions. Furthermore, no spectroscopic evidence was found that suggest the building block is attacked during cross-linking reactions involving vanadium and titanium in other ongoing investigations. Thus, it appears that the disruption of the building block observed with trichlorosilane only occurs with this linker at high silylchloride concentrations and high temperatures.

The methodologies described here are important because they can be applied to a wide variety of metal and main group chlorides that may have catalytic properties but can not be probed very easily using spectroscopic means. Also when Si_8O_{20} building blocks are linked together using catalytically active metals, generally low ratios of metal-to-building block are used. These metals can be incorporated into building block solids so that they have one unique environment throughout the sample. For embedded samples, they should initially form oligomeric species. These species of linked spherosilicates must then be further cross-linked together using an inert linking unit. Silylchlorides should provide robust siloxy linkages between these oligomers. By using different silylchlorides and different stoichiometries, the cross-linking properties of these materials can be influenced. In addition to control over such properties, the polarity of the material can be changed by using different silylchloride linkers.

Adjusting the polarity of the surfaces of the support has been shown to have an effect on the activity in heterogeneous catalysts.[26]

Chapter 4: Synthesis of Aluminum and Titanium Based Solid Catalysts for the Transesterification of Triacetin using Building Block Methods

4.1 Introduction

Biodiesel refers to non-petroleum-based fuels that are commonly used in fuel blends.[110] The production of biodiesel in the United States is currently at a level of 20 – 25 million gallons/year.[111] The high production levels of these fuels occur because they are non-toxic, superior in terms of sulfur content and aromatic content, and they are more biodegradable.[112] In addition, since these fuels are derived from biofeedstocks, they represent a recycling of carbon dioxide and do not contribute to global warming.[111] Because current levels of production of biodiesel are likely to increase due to incentives from federal and state governments, more effective production methods are needed to make biodiesel fuels more economically competitive with petroleum based fuels.[111]

The use of vegetable oils directly as a fuel source for combustion engines has been explored but is problematic because their viscosities are generally too high. Despite attempts to overcome the problems associated with high viscosities, the direct use of the vegetable oil as an engine fuel is not probable.[112] Therefore, vegetable oils need to be chemically modified to become a suitable source of fuel. One approach to this problem is to obtain acid esters from these feedstocks. Fatty acid esters can be derived from vegetable oils using acid or base catalysts. They exhibit properties much more conducive to their use as fuels for combustion engines. Thus there is considerable interest in developing

economical and efficient methods of obtaining these fatty acid esters from vegetable oil feedstocks.

Transesterification of vegetable oils with alcohols produce long chain esters. This can be achieved using several different approaches including using excess alcohol to push the equilibrium reaction towards the formation of esters, using supercritical conditions with alcohols, or using acidic or basic catalysts (Scheme 4.1).[112] Transesterification reactions catalyzed by either strong acids or strong bases are currently being utilized industrially. Strong basic homogeneous catalysts such as sodium hydroxide, potassium hydroxide, and sodium methoxide are used most frequently because they are much faster than acid catalysts and operate at more moderate conditions.[113,114] Despite the high activity of the basic catalysts in the transesterification of vegetable oils, some drawbacks exist that makes research and development of new catalysts attractive. One drawback involves the content of the feedstock. The total free fatty acid content of a feedstock must be less than 0.5 wt % or soap formation occurs when basic catalysts are used. This in turn causes gel formation, higher viscosities, and difficulties with the separation of products.[110] The system must also be anhydrous in nature because water may cause hydrolysis of the alkyl esters which would also lead to soap formation.[110] To overcome this issue, pretreatment of the feedstocks must be performed which increase production costs.[110]

(a) Acid catalyzed transesterification with alcohol reaction

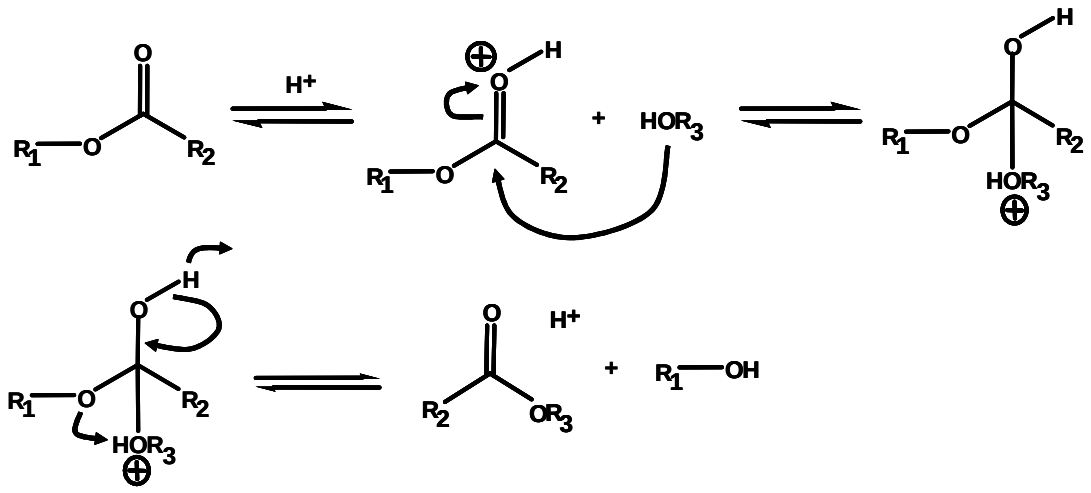

(b) Base catalyzed transesterification with alcohol reaction

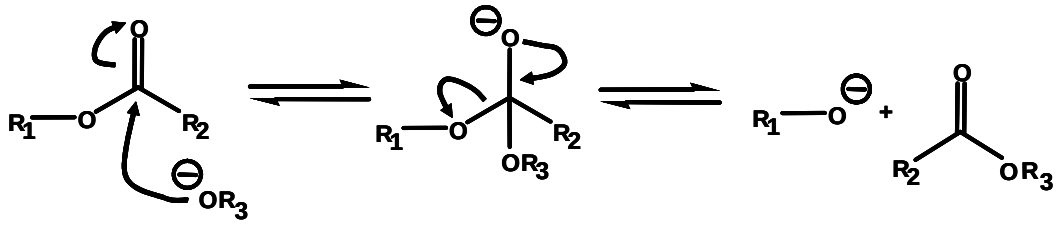

Scheme 4. 1 Mechanism for the transesterification reaction with alcohol using either (a) an acidic catalyst, or (b) a basic catalyst.

Not only does the pretreatment of the feedstock affect the cost of production of biodiesel, but the source of the raw material must also be considered. In the United States, soybean oil is the predominant source used for biodiesel production.[115] Since soybean oil is a food source, the cost of biodiesel produced from this oil is expensive.[115] Other sources of raw materials such as animal fats, and used cooking grease can be less expensive sources for the feedstock for biodiesel. However, as was discussed above, the base catalyzed transesterification of these materials requires pretreatments that increase the price.[113] One possible solution to this problem is the use of acid catalysts because they are capable of converting free fatty acids to esters as well as catalyzing transesterification reactions. Although acid catalysts are typically slower when compared to basic catalysts, by avoiding the pretreatment of the feedstock, it may be possible to produce biodiesel at a lower cost overall with acid catalysts.

One final consideration that must be taken into account to make biodiesel economically comparable to petroleum based fuels is post reaction processing. Current technologies rely on the use of soluble bases as catalysts. Although these catalysts are effective, they do require additional steps for processing the final material. The separation of the catalyst from the final product most certainly adds extra costs to the final biodiesel.[116]

When considering new catalysts for transesterification with alcohol for the production of biodiesels, sensitivity of the catalyst, expense of the feedstock, and post processing costs need to be addressed. Having a strong solid acid catalyst

would address all of these issues because acids are not sensitive to free fatty acids and thus feedstocks other than highly refined vegetables oils can be used as raw materials. Also, the post processing of heterogeneous catalysts is much simpler than with homogeneous versions.

Zeolites are crystalline, microporous aluminosilicates having both Bronsted and Lewis acid sites.[117] These materials are very acidic and capable of catalyzing many reactions including acid catalyzed transesterification.[116,118,119] However, the small size of the micropores in these materials inhibit larger substrate molecules such as those involved in the transesterification of triglycerides with methanol from accessing the acid sites in zeolites.[26,110] Thus, new mesoporous materials having high concentrations of strong acid sites would be ideal candidates to catalyze reactions that produce biodiesel fuels.

Reports of titanosilicate and aluminosilicate based materials that are active as catalysts for transesterification of several reactions have appeared in the literature.[120-122] Mesoporous metallosilicate materials have been produced using building block methods.[29] These building block materials can be synthesized having a variety of different main group and transition metal sites were the metal groups present are monodispersed and site isolated.[28,29] Furthermore, these materials can be synthesized so that control over the local environment of the metal is realized.[29] Such species have the potential to be used as heterogeneous catalysts where the control over the local environment can be exploited to tailor their activity. For solid acids, this tailoring could result in a change in the acid strength of the catalytic centers.

Building block methods were used to prepare aluminosilicate and titanosilicate based materials. These materials were developed using strategies outlined in chapter 3 of this thesis to yield highly embedded uniform centers throughout the material. The catalytic properties of the aluminum and titanium building block based materials were studied for activity in transesterification of triacetin with methanol reactions which serve as a model reaction for the production of biodiesel fuels (Scheme 4.2).

4.2 Experimental

This research project was a collaborative effort between the research groups of Dr Craig E. Barnes in the Department of Chemistry at the University of Tennessee - Knoxville and Dr James G. Goodwin, Jr. in Department of Chemical and Biomolecular Engineering at Clemson University. Jason C. Clark (UTK) performed all of the synthesis and characterization studies of the aluminosilicate and titanosilicate solid acid catalysts. These samples were sent to Dora E. López from Dr Goodwin's group were she investigated the activity and deactivation properties of these catalysts for the transesterification of triacetin with methanol.

4.2.2 Catalyst Preparation and Characterization

This portion of the study was carried out by Jason C. Clark from the University of Tennessee – Knoxville.

Reaction Scheme: Transesterification of Triacetin

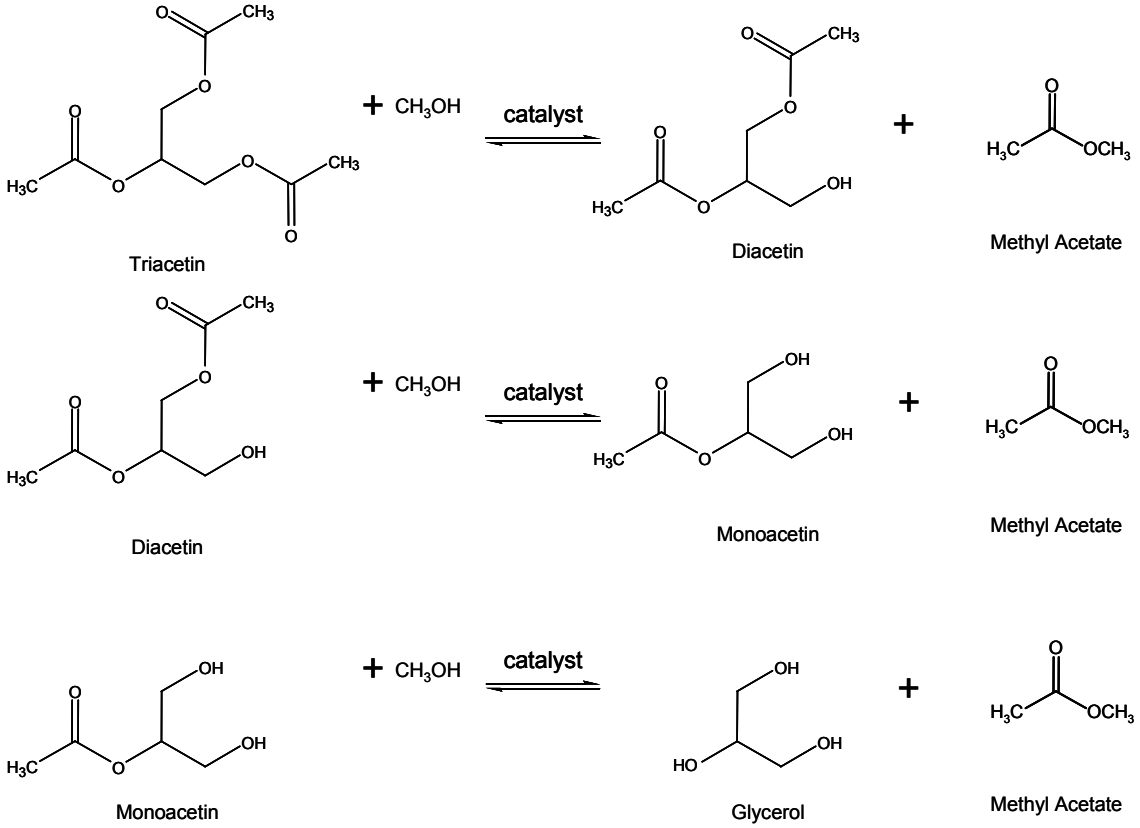

Scheme 4. 2 The transesterification of triacetin with methanol reaction.

4.2.2.1 General Preparation

Standard Schlenk techniques were employed for all described syntheses. All glassware was pretreated with chlorotrimethylsilane in order to passivate the surface. Toluene was distilled and dried using sodium potassium alloy. Methanol was dried with sodium metal and distilled. $Si_8O_{20}(SnMe_3)_8$ was prepared according to previously described methods and was heated to 100^oC overnight under vacuum to remove any residual water prior to use.[57]

4.2.2.2 Synthesis of Embedded Aluminum samples

Four aluminosilicate samples were made and were assigned the following numbers which link them to specific pages in my research notebook II: 041005, 041006, 041019, and 041020. These codes are the dates that the experiments began where the first two digits in the code are the year, the second two digits the month, and the final two digits the day. The experimental details are written down chronologically in notebook II. The samples were prepared by placing approximately 2.5 g $Si_8O_{20}(SnMe_3)_8$ and various amounts of anhydrous aluminum trichloride powder (Aldrich 99.999%, used as received) in a Schlenk tube in a N_2 dry box. Table 4.1 gives the specific initial stoichiometries used for these reactions. Using vapor transfer techniques, 25-30 ml of toluene was transferred into the reaction Schlenk. The reaction was allowed to stir for 2 days at 85-90^oC for samples 041005, 041006, and 041019. Sample 041020 was allowed to stir for 2 days at 50^oC. In all cases, the aluminum trichloride powder did not immediately dissolve in the toluene and appeared as a dense white

Table 4. 1 Table outlining the initial stoichiometries used for preparing aluminosilicate and titanosilicate building block catalysts.

Catalyst Identification Code	Metal Chloride (grams)	$Si_8O_{20}(SnMe_3)_8$ (grams)	$Si_8O_{20}:MCl_x$ X=3,4	Temperature (^oC)
041006	0.0437 ($AlCl_3$)	2.480	4:1	85-90
041005	0.0570 ($AlCl_3$)	2.530	3:1	85-90
041020	0.0608 ($AlCl_3$)	2.496	3:1	45-50
041019	0.0898 ($AlCl_3$)	2.499	2:1	85-90
041012	0.065 ($TiCl_4$)	2.514	4:1	85-90
041013	0.144 ($TiCl_4$)	2.513	2:1	85-90
050613	0.214 ($TiCl_4$)	2.752	1:1	85-90

powder in solution for all reactions. Some flocculate white precipitate in a cloudy solution could be observed after several hours. This precipitate had a different appearance from the aluminum trichloride powder. After one day, more of this flocculate precipitate was observed and no signs of aluminum trichloride were present. After two days, no further changes were observed.

After two days, a dose of tetrachlorosilane was added using vapor transfer techniques to the reaction to further cross-link the solid. The amount of cross-linking silylchloride used must be in a specific range to insure adequate cross-linking occurs. A more detailed description of this process has already been presented in chapter 3 of this thesis. The cross-linking reaction was allowed to react overnight at 85-90^{o}C. In all cases, the volume of tetrachlorosilane added was such that the total Me_3Sn : MCl (M = Al + Si) ratio was 1 : 2. In all cases, a white cloudy gel was observed. All volatiles were removed, and a white powder was obtained. A final dose of tetrachlorosilane was added to the powder in the gas phase to react with any residual trimethyltin groups. The amount of tetrachlorosilane added here was such that the total Me_3Sn:MCl (M = Al, Si) ratio was 1 : 4. The reaction was run overnight at room temperature. All volatiles were removed and the remaining white powder was dried at 100^{o}C for several hours. The resulting white powder was then treated with methanol by vapor transferring 25-30 ml of toluene into the reaction Schlenk vessel followed by vapor transferring an excess of methanol into this vessel and stirring under vacuum at 50^{o}C for 2 hours. All volatiles were then removed and the product was heated overnight at 100^{o}C under vacuum.

4.2.2.3 Synthesis of Embedded Titanium samples

Titanium containing samples were synthesized using procedures similar to those described above for the embedded aluminum samples with the following changes. To a Schlenk flask, approximately 2.5 g of $Si_8O_{20}(SnMe_3)_8$ was added and 25-30 ml of toluene was vapor transferred into the reaction vessel. An appropriate amount of $TiCl_4$ was vapor transferred into the reaction and allowed to stir for 2 days at 85-90^oC (Table 4.1). These samples were also assigned numerical identification tags which link them to my research notebook II. Table 4.1 should be used as a cross-reference these samples.

Upon the addition of titanium tetrachloride, a cloudy yellow/green flocculate precipitate formed. After stirring for 2 days, tetrachlorosilane was added to cross-link the product as described previously and a yellow/green gel formed. This was allowed to stir overnight at 85-90^oC under vacuum. All volatiles were removed and a white powder was observed. A volatile yellow material was removed during this step. It was determined by control experiments that this material was residual titanium tetrachloride complexed to trimethyltin chloride in the reaction mixture.

An off-white powder remained after volatiles were removed. This product was then exposed to a final gas phase dose of tetrachlorosilane to react with any remaining trimethyltin groups on the material overnight at room temperature. The samples were then treated with excess methanol in toluene in the same manner as described for the preparation of the aluminosilicate samples.

For the titanosilicate sample that contained the highest metal loading (050613), a slightly different procedure was used in an attempt to assess the average degree of connectivity of the titanium centers. Before the reaction, the mass of the Schlenk containing $Si_8O_{20}(SnMe_3)_8$ was evacuated and the mass determined. After the addition of the solvent and titanium tetrachloride, the reaction stirred for 2 days at 85-90^oC under vacuum. All volatiles were removed and a white powder was observed. The powder was heated at 100^oC under vacuum and periodically weighed until a stable mass was obtained. This was done to monitor the weight change of the reaction in order to determine the amount of trimethyltin chloride that was removed from the reaction.

4.2.3. Catalyst Characterization

The following techniques were used to characterize the samples prepared in this investigation: nitrogen adsorption-desorption surface area analysis, multinuclear solid-state NMR, thermal gravimetric analysis (TGA), atomic emission (AE) spectroscopy, and infrared (IR) spectroscopy.

BET nitrogen adsorption-desorption surface area analyses were performed using a Quanta Chrome Nova 1000 instrument.

Multinuclear solid-state MAS NMR data was acquired using a broadband Inova Varian NMR. Silicon-29 spectra were acquired at 79.43 MHz at spin rates of 3.5 kHz – 5.5 kHz and aluminum-27 spectra were recorded at 104.192 MHz at spin rates of 4.5 kHz – 7.5 kHz. Samples were placed in 5 mm pencil rotors and sealed with paraffin wax.

Infrared spectra were obtained using a Bio-Rad FTS-60A spectrometer. Samples were prepared for IR analysis by mixing an appropriate amount in potassium bromide and making pellets.

Thermal gravimetric analyses (TGA) were performed on a TA Instruments Q50 TGA equipped with platinum pans. Experiments were run in air.

Flame atomic emission (AE) analysis was performed using an air-acetylene flame on a Perkin-Elmer AAnalyst 100 spectrometer. Titanosilicate samples were analyzed for weight percent titanium using AE spectroscopy. Samples were prepared for AE analysis by digestion of approximately 100 mg of sample in a solution of 1.5 g nitric acid; 1.5 g hydrofluoric acid and 20 g of deionized water in plastic bottles overnight. Standard solutions were prepared by serial dilution of a titanium atomic absorption standard solution (Aldridge, 991 μg/mL of Ti in H_2O). Sample matrix components nitric acid and hydrofluoric acid were added to each standard in appropriate concentrations before diluting to the proper volume. Standard calibration curves were made by obtaining measurements at 399.9 nm for the standards. These curves were used to determine the total titanium content in each sample. A sample of “used” titanosilicate catalyst 050613 (initial loading of approximately 5 weight % titanium) was also analyzed by AE to determine the extent of leaching from the material during reactions.

4.2.4 Catalyst Test Protocol

This portion of the study was carried out by Dora E. López at Clemson University.

4.2.4.1 Materials

For the catalysis studies, a mixture of reactant/products (4 wt% glycerol, 26 wt% monoacetin, 45 %wt diacetin, and 25 wt% triacetin), glycerol (99 wt%), methyl acetate (99 wt%), triacetin (99 wt%) and anhydrous methanol (99 wt%) were used. These reagents were purchased from Fisher Scientific and used for GC/FID calibration and reaction experiments. Toluene and ethanol were purchased from Fisher Scientific and used as an internal standard and a solvent (for GC analysis), respectively. Reactants and standards were high purity (anhydrous) chemicals and used as received.

4.2.4.2 Catalyst Pretreatment

Prior to catalytic reactions, samples were calcined at 350 °C under flowing UHP air for 3 h.

4.2.4.3 Transesterification Studies

All transesterification with alcohol (Scheme 4.2) experiments used a mixture consisting of anhydrous methanol and triacetin in a 6 : 1 (methanol : triacetin) initial molar ratio (2-fold excess stoichiometry for complete conversion) which is the suggested proportion for homogeneous base catalysts.[123] Prior to

reaction, a sample of the reactant mixture was analyzed by GC in order to verify initial concentrations. Catalyst loading (wt cat/wt reaction mixture) was 2 wt%. Reactions were carried out in 50 ml flasks in a Innova Reactor Shaker System (model 4080) with constant temperature bath. General catalyst activity studies were carried out in an Innova Reactor Shaker System at a shake rate of 120 rpm at 60 °C.

Two replicates samples of metallosilicates were tested for each reaction. To carry out the reactions, 0.04 g of catalyst was quickly added to 1.96 g of a liquid mixture of methanol/triacetin with an initial molar ratio 6 : 1. A sample was shaken for 8 hours and analyzed of reaction for reactant and product concentrations. To separate the catalysts from the reactant mixture, the sample was centrifuged prior to analysis.

4.2.4.4 Catalyst Deactivation Studies

For the catalyst deactivation studies, reactions were started as previously described above in section 4.2.4.3. After 4 h of reaction, the reaction mixture was centrifuged, the catalyst recovered, and the reaction mixture analyzed. A new reaction solution was mixed with the recovered catalyst, and a new reaction cycle was started. This process was repeated several times, and the catalytic activity for each cycle was recorded.

4.2.4.5 Method of Analysis

The reaction products were diluted with ethanol using 1 : 10 v/v (reaction mixture/ethanol) and a toluene internal standard using 1 : 20 v/v (toluene/ethanol). Samples were analyzed using HP 6890 gas chromatograph system combined with a HP 5973 mass selective detector. The collection and analysis of data was carried out using HP Chemstation software. An Altech Econo-Cap EC-WAX fused silica capillary column (30 m x 0.25 mm x 25 μm) was used for analyte separation. One microliter of this mixture was injected into the column using the splitless mode option. The injector and detector temperatures were set to 255°C and 280°C, respectively. The oven temperature program was held at 45 °C for 3 min, then ramped up at a rate of 90°C/min to 180°C and held there for 6 min.

4.3 Results and Discussion

4.3.1 Preparation and Characterization of Single-Site, Site Isolated Solid Acid Catalysts

Metallosilicate based solid acid catalysts having mesoporous properties capable of catalyzing the transesterification of triglycerides with alcohols were prepared. These catalysts should have well dispersed, deeply embedded atomic centers of titanium or aluminum throughout a silicate support based on the preparative methods utilized in the synthesis of these materials.[29] Well separated sites are generally thought to be crucial to producing strong acid sites

in silicate matrices. The methods utilized to synthesize the materials described in this chapter that should have well dispersed sites were first presented in chapter 3 of this thesis where silylchlorides were used as model metal centers because the environment of these sites could easily be probed using solid state NMR. Since routine spectroscopic evidence for probing the immediate environment of titanium and aluminum in these materials is challenging, we must make assumptions as to what occurs during the synthesis of these catalysts based on the studies described in chapter 2 as well as studies previously present in the literature.[18,29]

In addition to being well dispersed, the active sites in these samples should also be deeply embedded in the silicate matrix. In the context of building block solids, deeply embedded centers refer to multiple connections to building blocks. A high degree of connectivity of the metal centers to the silicate support was desirable in these samples in order to address the issue of leaching. Leaching is a problem which is frequently encountered in heterogeneous catalysts and can result in deactivation of the catalyst. We feel that by placing atomic centers into a silicate support through multiple robust metal oxide bonds, this issue will not be as problematic.

A speculative discussion of what potentially occurs during the synthetic steps to produce deeply embedded, site isolated titanosilicate and aluminosilicate materials follows in the next two sections. Again, since we do not have any direct spectroscopic evidence that describes the immediate environment of the metal centers in these materials, we must rely on the model

study and previous work using vanadyl chloride to predict the structure of the active site.[29]

4.3.1.1 Aluminosilicate Samples: The Nature of the Acid Site

In the aluminosilicate samples that were heated to 80-90°C, we hypothesize that small oligomeric species consisting of a single aluminum atom connected to three Si_8O_{20} building units form initially due to the presence of an excess of trimethyltin groups on the building blocks with respect to the number of aluminum chloride groups in the reaction along with the forcing reaction conditions (Figure 4.1). Three coordinate aluminum species would be Lewis acidic centers. Although rare due to valence electron issues, this type of coordination around aluminum has been observed in the solid state when sterically demanding ligands are utilized.[124,125] Structural details of Si_8O_{20} previously described in chapter 2 of this thesis suggests that the Si_8O_{20} building block will behave as a sterically demanding ligand in this situation.

A second factor to be considered in this context is charge balance. Four-coordinate aluminum centers carry a formal negative charge. The conditions of the reaction used (nonpolar, aprotic solvent) to synthesize these materials are not conducive to the formation of charged species. The positive charge to balance a four-coordinate aluminum species would have to result from chemistry that was not anticipated based on previous analogous reactions. However, the possibility of these four-coordinate species can not be excluded due to the propensity of aluminum to form such moieties. Figure 4.2 illustrates some

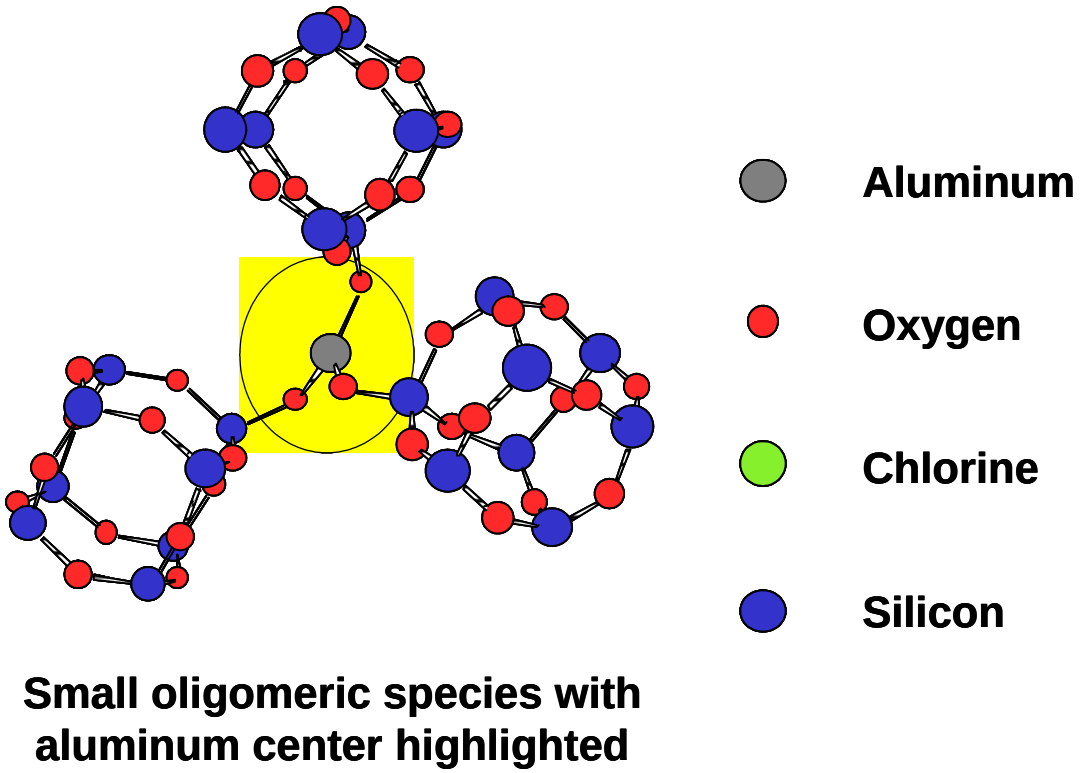

Figure 4. 1 Molecular model of predicted three-coordinate aluminum species that forms from the initial reaction of aluminum trichloride with three spherosilicate building blocks.

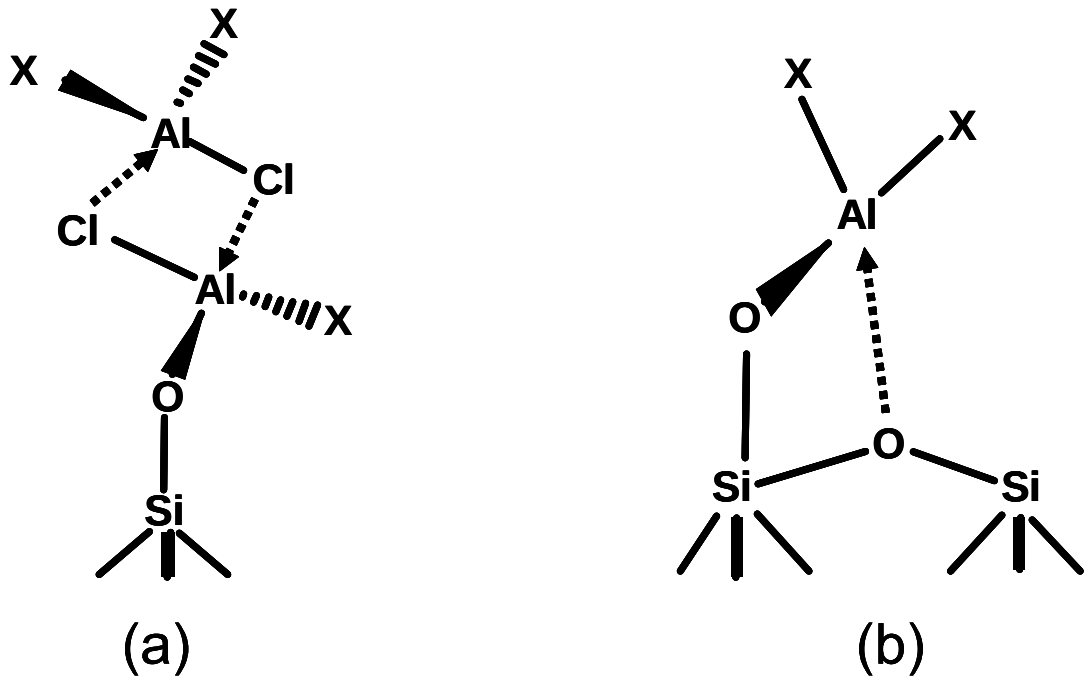

X = Cl, O

Possible aluminum environments leading to a coordination number of four around the metal

Figure 4. 2 Illustration of possible four-coordinate aluminum species.

possibilities of aluminum having a coordination number of four in these materials. In (a) of this figure, the Al_2Cl_6 dimer that exists in the solid state does not dissociate and one aluminum chloride group reacts with a trimethyltin groups of a building block. The bonding in this dimer can be described as a three center two electron bond where a lone electron pair on a chlorine atom forms a dative bond with the Lewis acidic aluminum center. These dative bonds are illustrated as dotted arrow in the figure. In (b) of the same figure, a similar type of dative bonding occurs from the lone electron pair on the oxygen atom present on a neighboring Si-O-Si edge of a Si_8O_{20} building block to a Lewis acidic aluminum in a three coordinate environment.

Assuming that the aluminum centers in these oligomeric species are three coordinate based on the steric and charge-balance arguments, they would be Lewis acidic in nature and potential solid acid catalysts. Thus cross-linking these oligomeric species would result in a high surface area porous material. To achieve this, a cross-linking dose of tetrachlorosilane was added to the reaction mixture resulting in an aluminosilicate matrix containing various amounts of monodispersed aluminum atoms linking spherosilicate building blocks (Figure 4.3).

The aluminosilicate sample (041020) that was prepared using lower temperatures (45-50^oC) could possibly only be bound to two Si_8O_{20} units and still contain one aluminum chloride group based on a previous study. [29] If only two building block units are bound to the aluminum then the acid strength of the aluminum centers is expected to be different than the aluminum centers

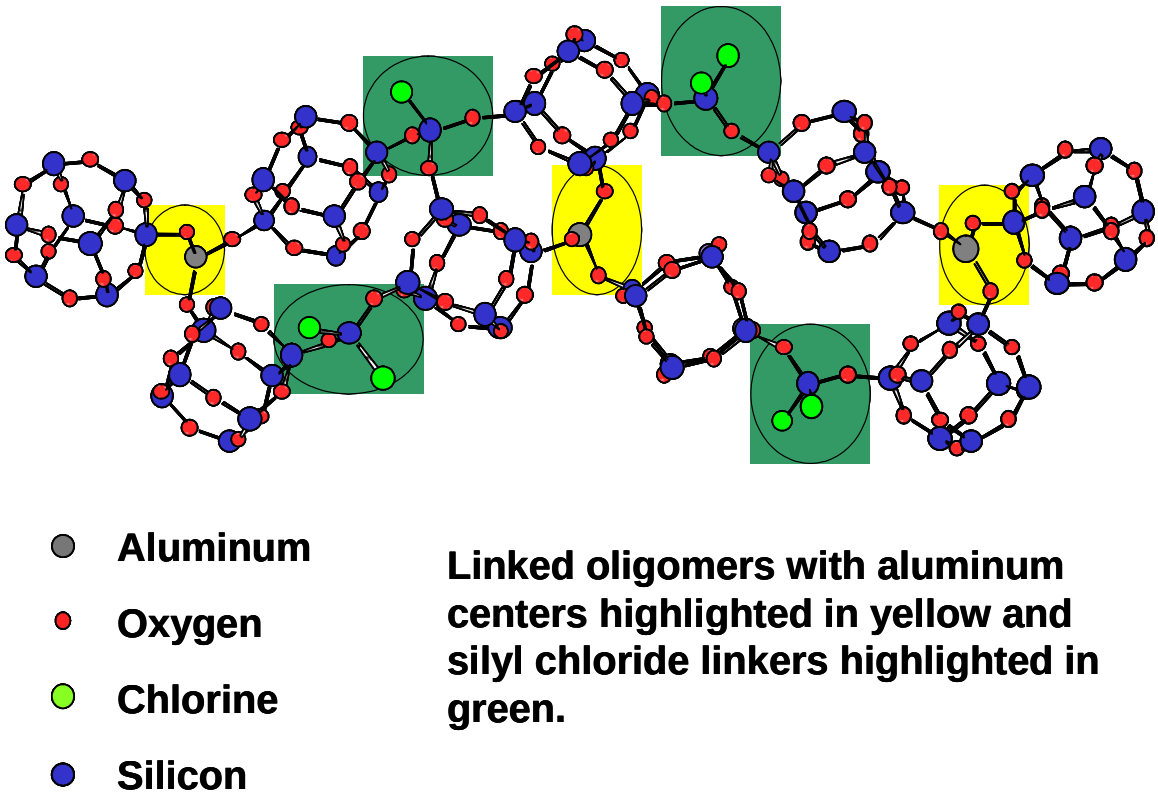

Figure 4. 3 Molecular model of cross-linked oligomeric three-coordinate aluminum based oligomeric species.

surrounded by three building units. Unfortunately, aluminum-27 MAS NMR shows little difference between this sample and the three other high temperature samples (Figure 4.4). In all samples, three broad signals are observed at 4 ppm, 35 ppm, and 80 ppm that were assigned as octahedral, pentagonal, and tetrahedral aluminum coordination respectively. [126,127] Controversy over these assignments exist in the literature. Most agree that signals close to 0 ppm and signal around 80 – 100 ppm correspond to octahedral and tetrahedral aluminum centers respectively. However, signals between these to values have been assigned to five coordinate centers as well as distorted tetrahedral centers.[126,127]

In these samples octahedral aluminum centers were not expected and believed to have formed during the methanol treatment. Reports in the literature of sample prepared from Al_2Cl_6 supported on silica also exhibit signals in aluminum-27 solid-state NMR consistent with octahedral aluminum centers where only tetrahedral centers are expected.[24]

4.3.1.2 Titanosilicate Samples: The Nature of the Acid Site

The titanosilicate catalysts should be very similar to the aluminosilicate catalysts in that the limiting amount of titanium used in the synthesis should lead to deeply embedded, monodispersed titanium atoms linking multiple Si_8O_{20} building blocks. They should only differ in that the titanium center can link up to four Si_8O_{20} building blocks to form oligomeric species that will then be cross-linked with a silyl chloride (Figure 4.5 – 4.6).

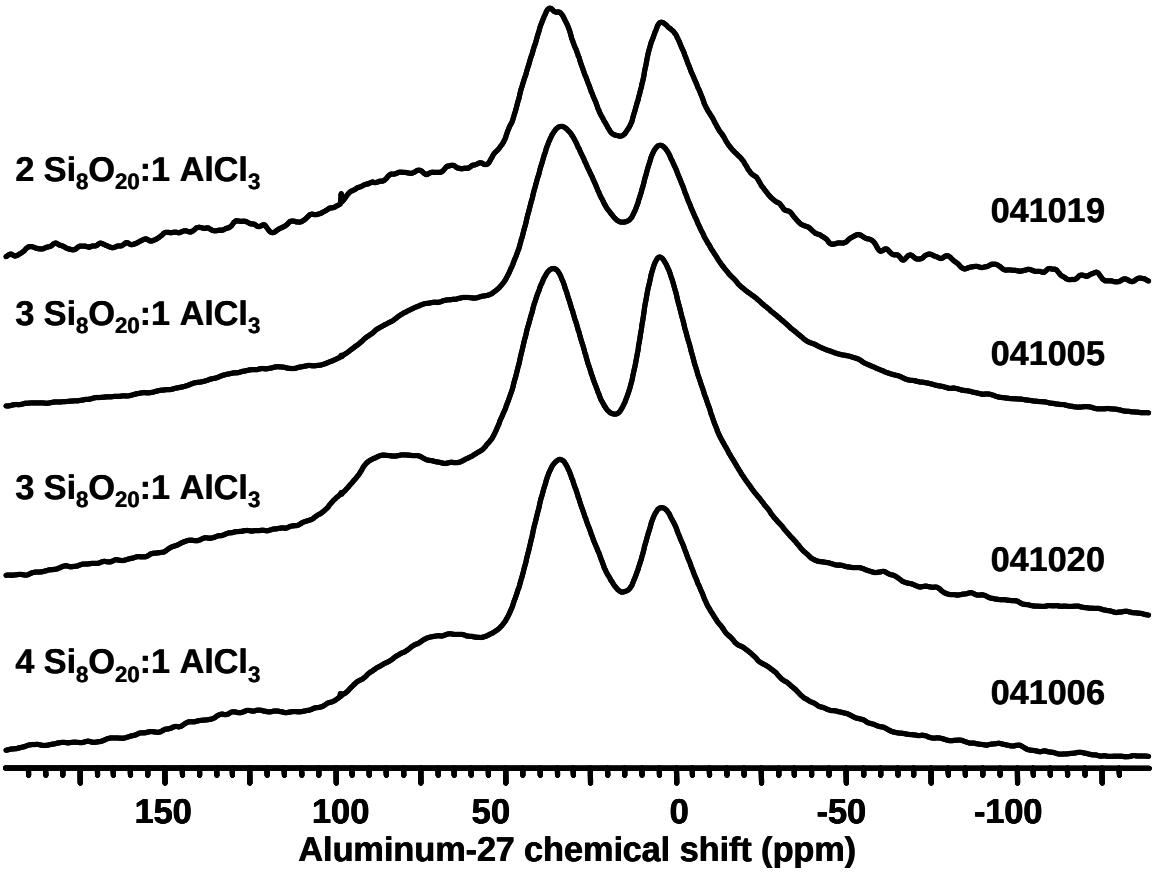

Figure 4. 4 Aluminum-27 MAS solid-state NMR of aluminosilicate catalysts.

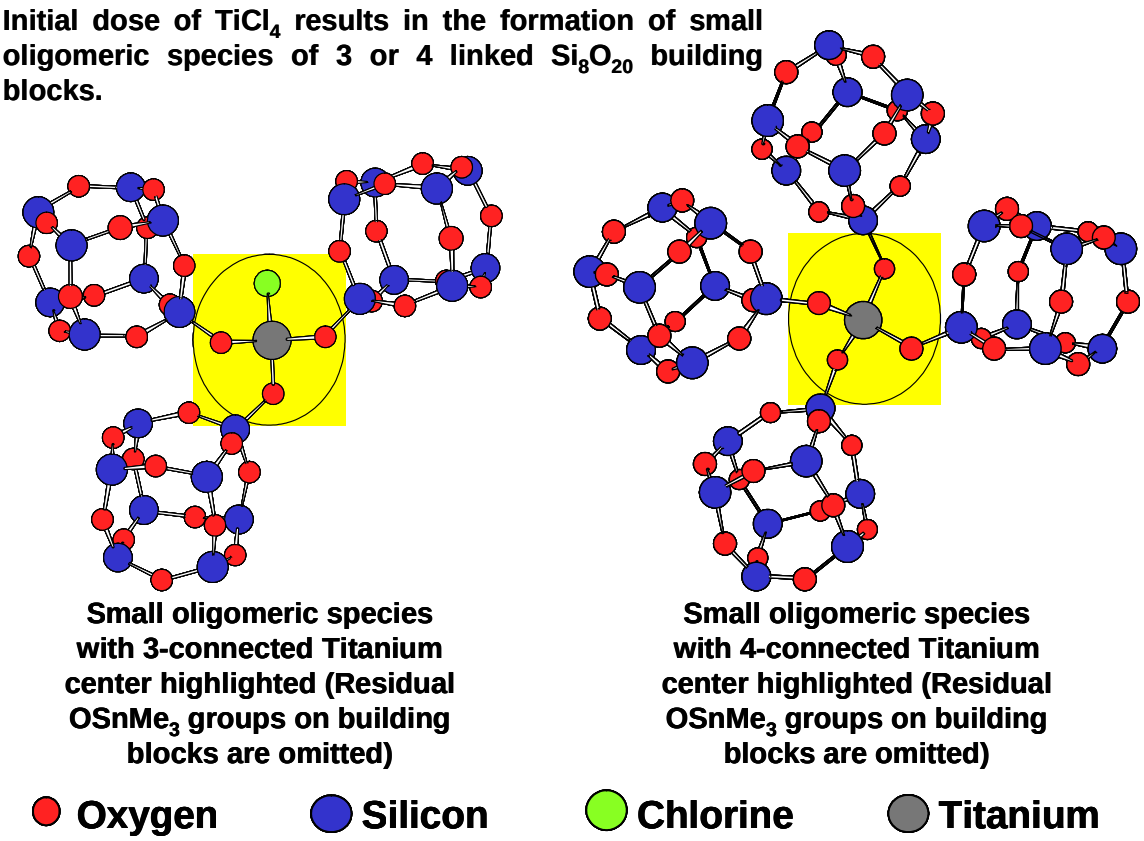

Figure 4. 5 Molecular model of proposed oligomeric species that form when a titanium links three or four spherosilicate building blocks.

A dose of $SiCl_4$ cross-links "oligomeric" species resulting in a silicate matrix having embedded titanium centers

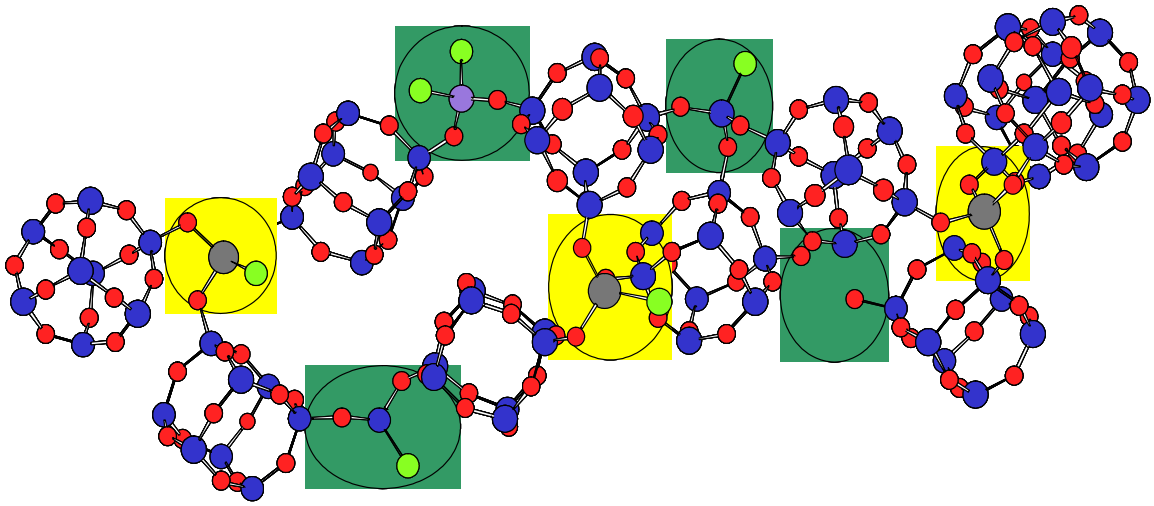

Silane linked oligomers with titanium centers highlighted in yellow and silyl chloride linkers highlighted in green. Residual metal-chloride groups remain present in the material.

Figure 4. 6 Molecular model of cross-linked titanium based oligomeric species that were illustrated in Figure 4.5.

Routine spectroscopic tools for probing the local environment of the titanium centers are not available. Thus gravimetric analysis was used to monitor the weight change in the reaction due to liberated trimethyltin chloride for sample 050613. The weight change for this sample indicates that the coordination lies in between linking two and three Si_8O_{20} building blockls and has an average coordination of $TiO_{2.52}Cl_{1.48}$. This analysis was not carried out for the other two titanosilicate samples. Since sample 050613 had the highest initial loading of titanium, the other two samples 050412 and 050413 will most likely have a similar immediate environment or lie even closer to having only four-connected Si_8O_{20} building blocks because a larger excess of trimethyltin groups were present in the reaction relative to titanium chloride groups and the same conditions were used in these reactions. Unfortunately, as was stated earlier, some titanium tetrachloride was removed from the reaction as a titanium tetrachloride/trimethyltin chloride complex. As a result, the average coordination number can not reliably be predicted using this method. Future work will be needed to quantify the amount of titanium tetrachloride that is lost due to this process. However, AE analysis indicates that only a small amount of titanium is lost. This will be discussed in a future section of this chapter.

4.3.2 Passivation of the Catalysts

The chlorinated species are extremely moisture sensitive and susceptible to hydrolysis and thus extremely difficult to handle. To address this problem, samples were treated with methanol in order to passivate the material (Figure

4.7). This treatment will affect the titanium and aluminum centers as well as the cross-linking silicon groups. Any residual titanium chloride groups will react and form titanium methoxide groups. This treatment could lead to the formation of Bronsted acid sites in the material as illustrated in Figure 4.8. The same will reaction of residual chloride groups described for the titanium centers will also occur for any aluminum chloride groups as well as with all silylchloride groups. The aluminum centers at this point could become four coordinate after the methanol treatment. Any creation of charge on the aluminum and titanium centers must be balanced by a proton from the methanol groups. Despite the changes to any terminal chloride ligands on aluminum or titanium linking groups, their bonding to silicate cubes should remain unchanged and these centers should remain monodispersed and single site in nature.

The effect of the methanol treatment on the silylchloride linking groups in these matrices was examined using solid state NMR. Figure 4.9 shows the silicon-29 MAS solid-state NMR spectra of a chlorinated building block material before and after methanol treatment. This sample illustrates the changes that occur when a chlorinated silicate platform synthesized using building block methods is treated with methanol. In this figure, capping trichlorosilyl groups (-44 ppm), dichlorodisiloxysilyl linking groups (-68 ppm), and chlorotrisiloxysilyl linking groups (-92 ppm) are converted to trimethoxysiloxysilyl capping groups (-84 ppm), dimethoxydisilxysilyl linking groups (-92 ppm), and methoxytrisiloxysilyl linking groups (-102 ppm) respectively when treated with methanol.

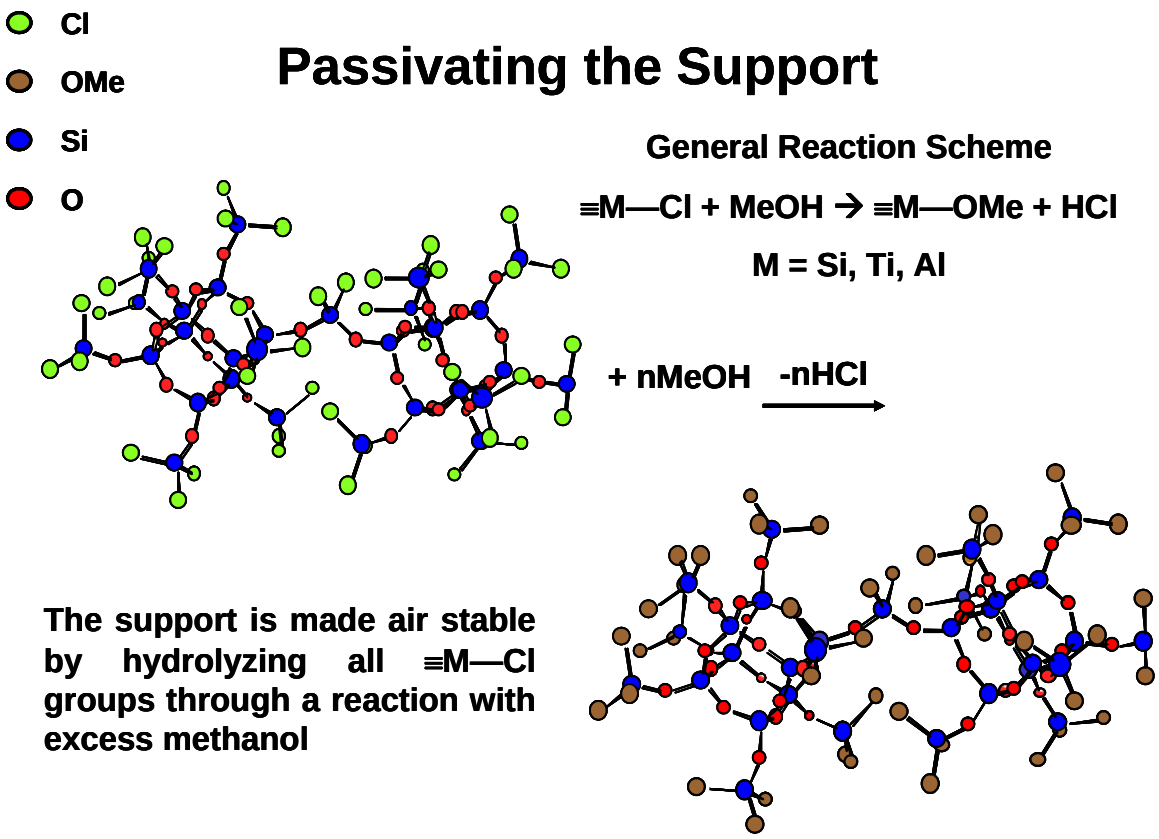

Figure 4. 7 Illustration of the reaction of metal chloride groups with methanol that is utilized to passivate the catalyst.

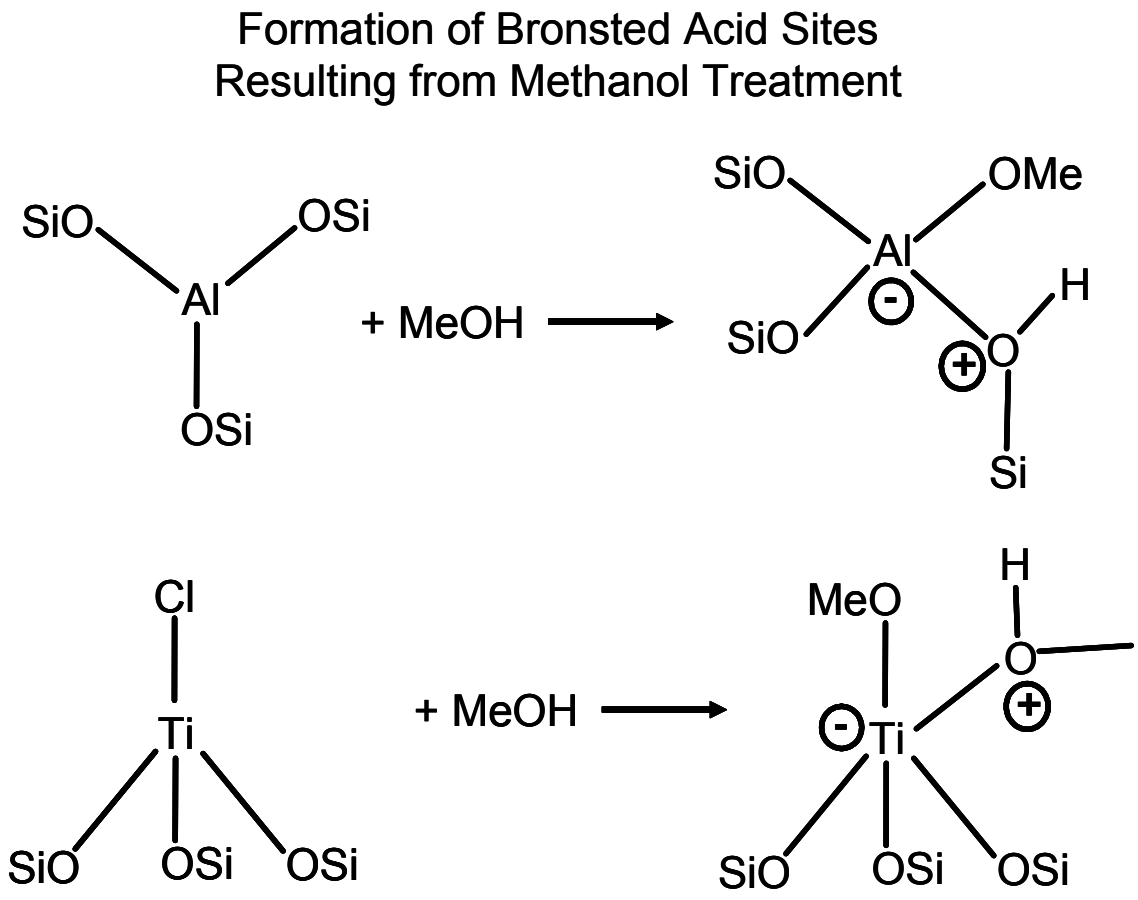

Figure 4. 8 Proposed Bronsted acid sites that results from the methanol treatment of the catalysts.

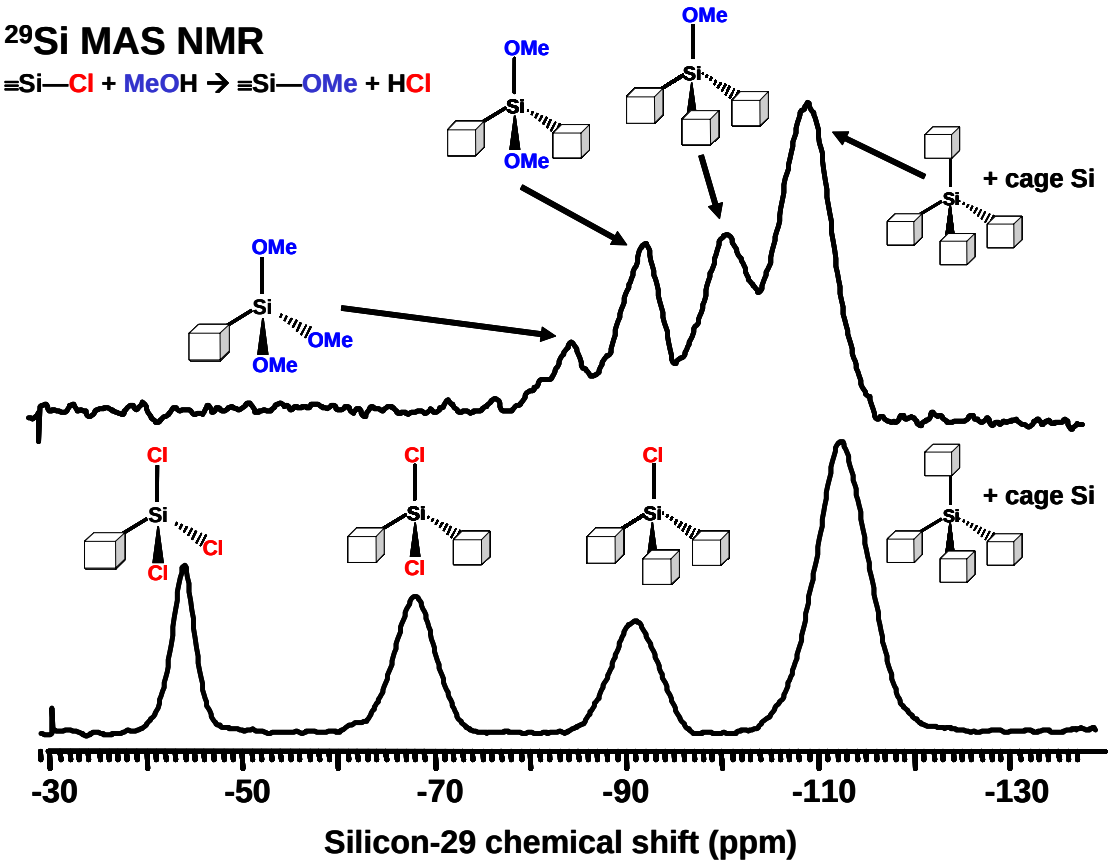

Figure 4. 9 Silicon-29 MAS solid-state NMR of silicate platform before and after methanol treatment.

Despite having different metals as linking units, the overall silicate matrix of the aluminosilicate and the titanosilicate should be similar due the low concentration of these metals in these materials. Silicon-29 MAS NMR of these samples shows little difference in the silicate matrix regardless of the presence of these metal centers, loading level, or reaction temperature (Figure 4.10). In all the metallosilicate samples described in this chapter, four signals are present which have been assigned to trimethoxysiloxysilyl capping groups (-86 ppm), dimethoxydisilxysilyl linking groups (-94 ppm), methoxytrisiloxysilyl linking groups (-102 ppm) and Q^4 tetrasiloxysilyl groups (-109 ppm). The similarities in the silicate matrices are also evident from the BET surface area measurements. All samples (including the aluminosilicate samples) have surface areas between 299 - 543 m^2/g (Table 4.2).

4.3.3 Calcination of the Catalyst

Several samples were calcined in order to further passivate the samples. The effects of calcination on these samples were studied using a variety of characterization techniques. TGA analysis showed that a significant weight loss occurs in all samples at between 250 - 300^oC. A major component of this weight loss is assumed to be due to the combustion of methoxy groups based on the spectroscopic findings of these samples before and after calcination. The samples did not contain any organic functional groups after calcination as indicated by monitoring the C-H stretching modes in the IR spectra. This was also verified using silicon-29 MAS and CPMAS solid-state NMR before and after

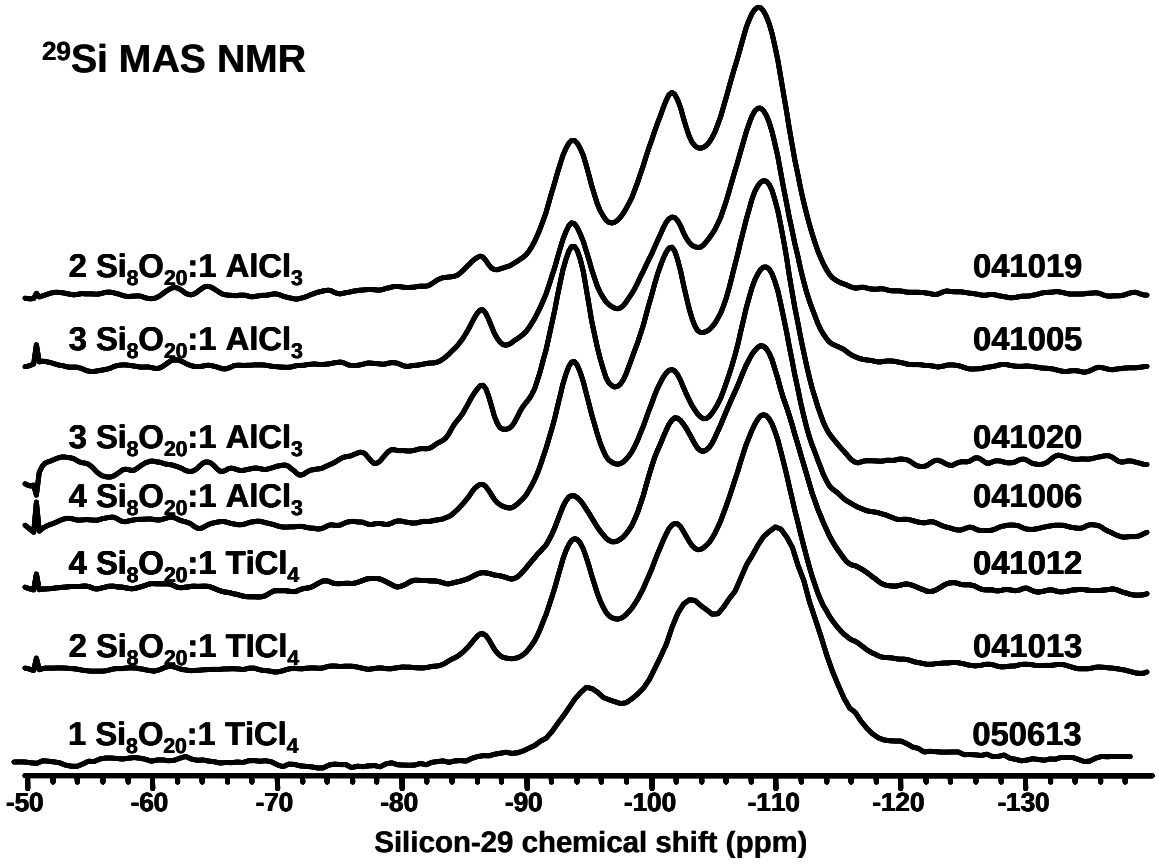

Figure 4. 10 Silicon-29 MAS solid-state NMR of metallosilicate catalysts.

Table 4. 2 Table listing surface area values for metallosilicate catalysts.

Sample ID	Metal present	Treatment	Reaction Temperature (ºC)	Si_8O_{20}:M	Surface Area (m^2/g)
041019	Aluminum	Methanol	80-90	2 : 1	457
041005	Aluminum	Methanol	80-90	3 : 1	354
041005cal	Aluminum	Calcined 350 ºC	80-90	3 : 1	410
041020	Aluminum	Methanol	45-50	3 : 1	479
041006	Aluminum	Methanol	80-90	4 : 1	514
041006cal	Aluminum	Calcined 350 ºC	80-90	4 : 1	516
050613	Titanium	Methanol	80-90	1 : 1	299
041013	Titanium	Methanol	80-90	2 : 1	543
041013cal	Titanium	Calcined 350 ºC	80-90	2 : 1	473
041012	Titanium	Methanol	80-90	4 : 1	473
041012cal	Titanium	Calcined 350 ºC	80-90	4 : 1	459

calcination. No signals were present in the NMR that were consistent with silicon methoxide groups after calcination. Due to these findings, samples were calcined at 350^{o}C before catalytic testing was performed.

The silicon-29 MAS NMR spectra of the calcined aluminosilicate samples (041005 and 041006) is very similar and displays typical patterns of incompletely resolved Q^2, Q^3, and Q^4 signals associated with silicates. This observation is consistent with the methoxy groups being replaced by hydroxyl groups (Figure 4.11).[109] The aluminum-27 MAS NMR spectra of these samples display observable differences when compared to the uncalcined samples (Figure 4.12). The octahedral signal in the uncalcined samples located at 4 ppm is shifted to –4 ppm after calcination in samples with different aluminum loadings. These signals also appear to broaden which might indicate a more distorted octahedral environment. The relative intensity of the signal assigned to octahedral aluminum appears to increase with respect to the signal assigned to aluminum in a tetrahedral environment in both samples. The signal assigned to pentagonal aluminum sites at 35 ppm does not appear to change significantly after calcinations. However, the tetrahedral signal shifted from a broad signal at 80 ppm to a narrower signal at 65 ppm. This could also be attributed to aluminum centers having a less distorted tetrahedral environment.

Calcination of these samples at 350^{o}C has an affect on surface bound groups present in of these samples, but it did not cause dramatic effects to the overall surface area of the samples (Table 4.2). When the BJH pore size distribution plots of the calcined materials are compared to the uncalcined

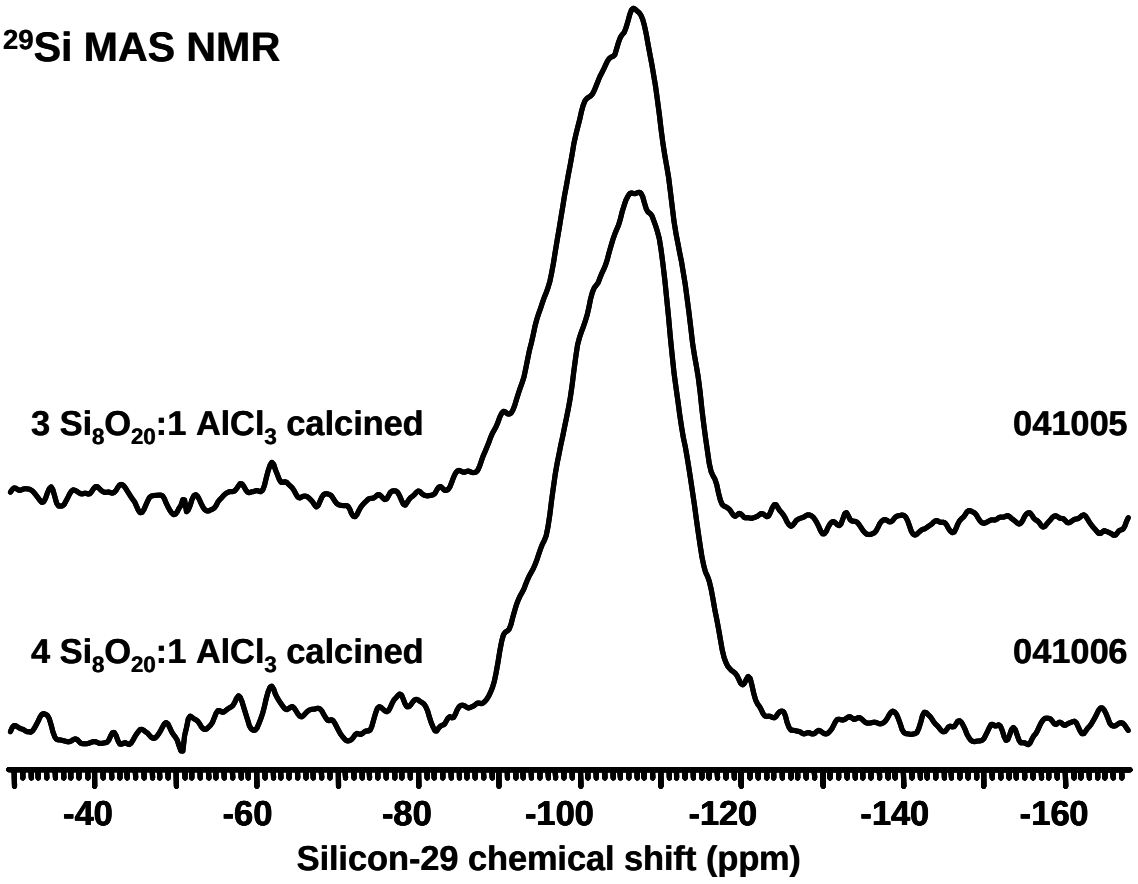

Figure 4. 11 Silicon-29 MAS solid-state NMR of calcined aluminosilicate catalysts.

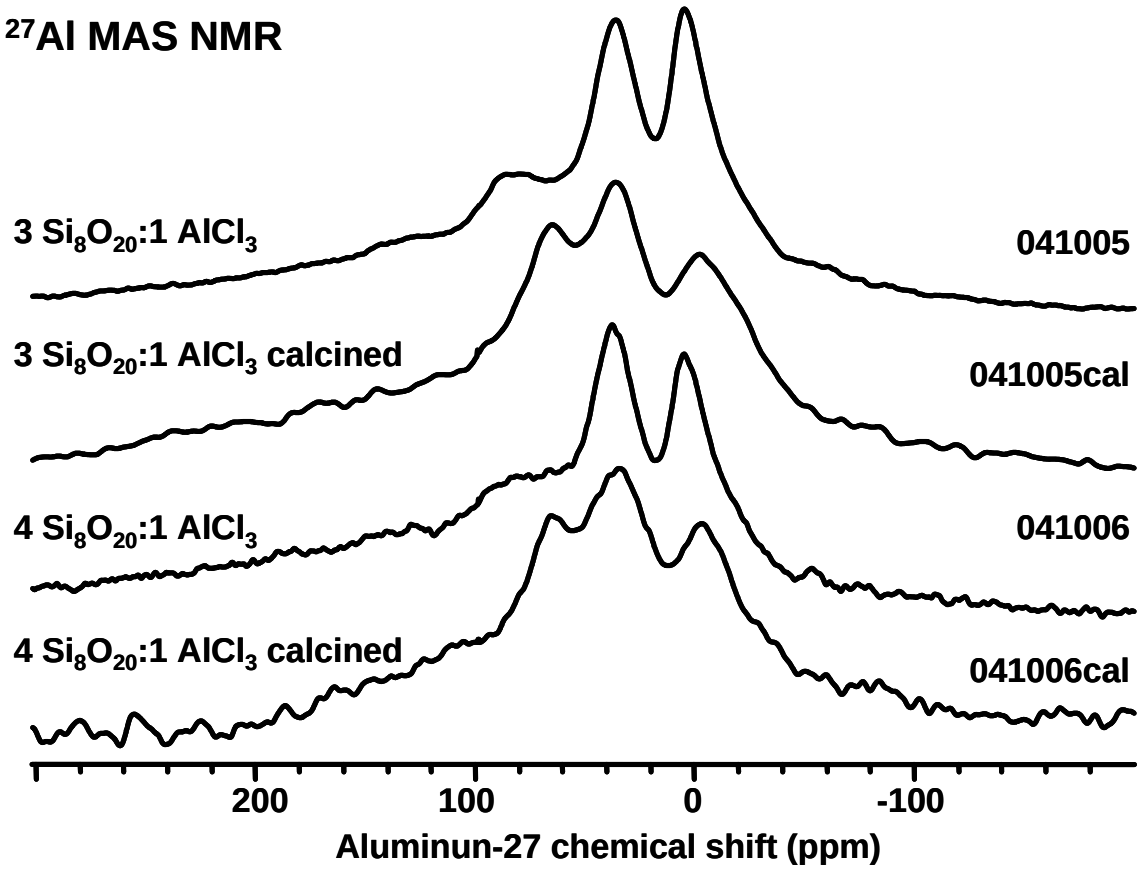

Figure 4. 12 Aluminum-27 MAS solid-state NMR of calcined and uncalcined aluminosiicate catalysts.

samples, observable changes can be seen (Figure 4.13 – 4.16). In all cases the contribution to the overall surface area from mesoporosity and macroporosity is lower in the calcined samples. IR and NMR spectroscopic experiments suggest that after calcination the methoxy groups are lost and the surface becomes functionalized with hydroxyl groups. These silanol groups can condense to form siloxy groups which would result in further cross-linking. Change in the functional groups present on the surface as well as changes in the overall cross-linking of the matrix due to condensation of silanol groups are possible explanations for the differences observed in the surface area properties of these materials after calcinations. Thus, surface area analysis is consistent with other spectroscopic finding in that calcination does cause some changes to the surface of these materials. However these changes do not cause the matrix to collapse to form dense SiO_2 glassy materials under these conditions since the calcined samples retain a high surface area.

4.3.4 Concentration of Titanium in the Catalysts

AE analysis of the titanosilicate samples yielded the weight % titanium per sample. This analysis was conducted for all three titanosilicate samples (040412, 040413, 050613). This analysis was also conducted for sample 050613 after an 8 hour transesterification of triacetin with methanol reaction. Table 4.3 summarizes the results of these reactions.

Most of the titanium that was dosed into this reaction was incorporated into the material. The target initial loading of 1.4%, 2.9%, and 4.7% were very

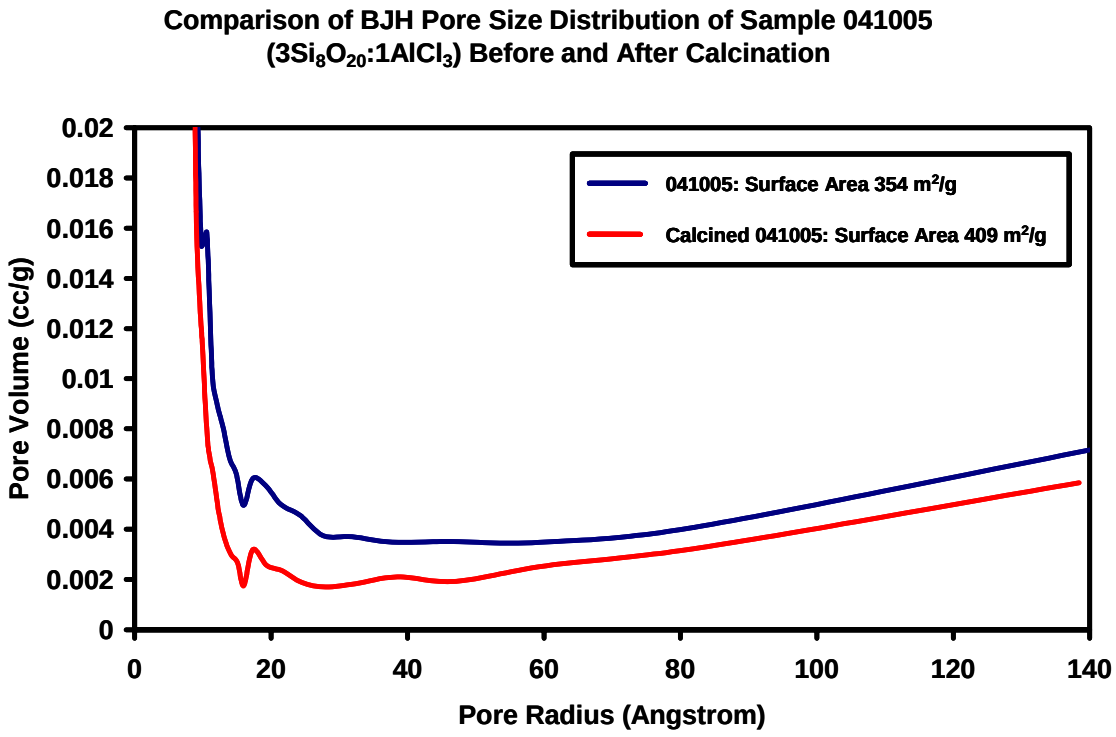

Figure 4. 13 BJH pore size distribution of aluminosilicate catalyst 041005 before and after calcination.

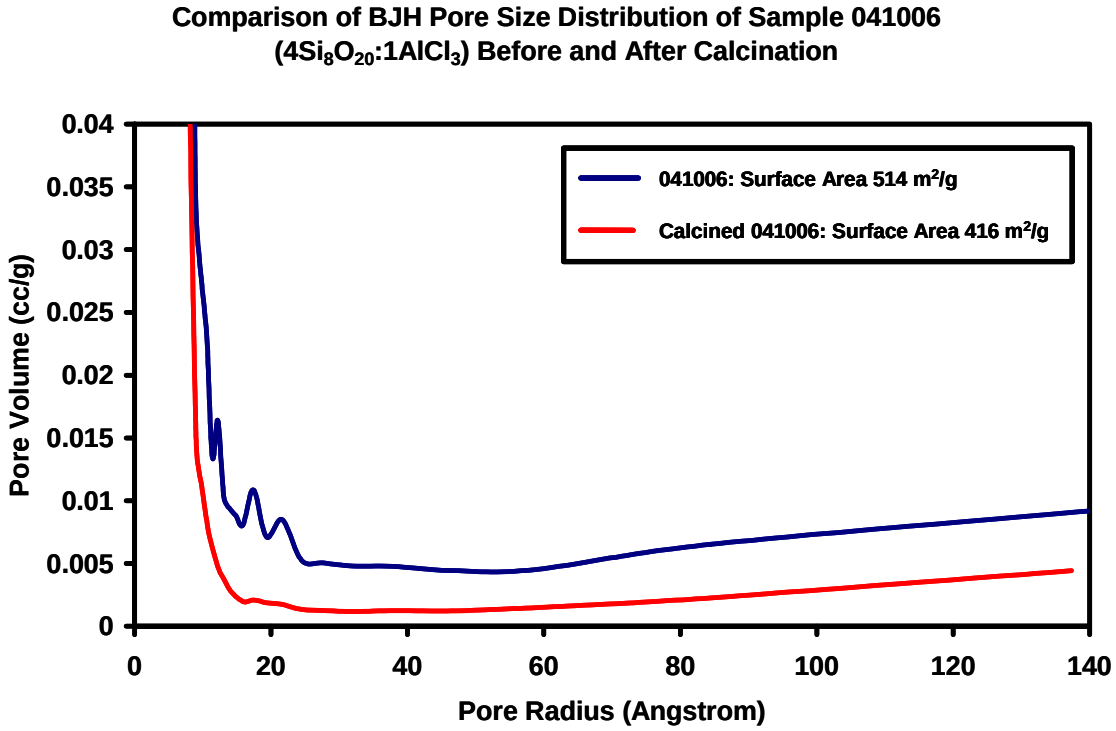

Figure 4. 14 BJH pore size distribution of aluminosilicate catalyst 041006 before and after calcination.

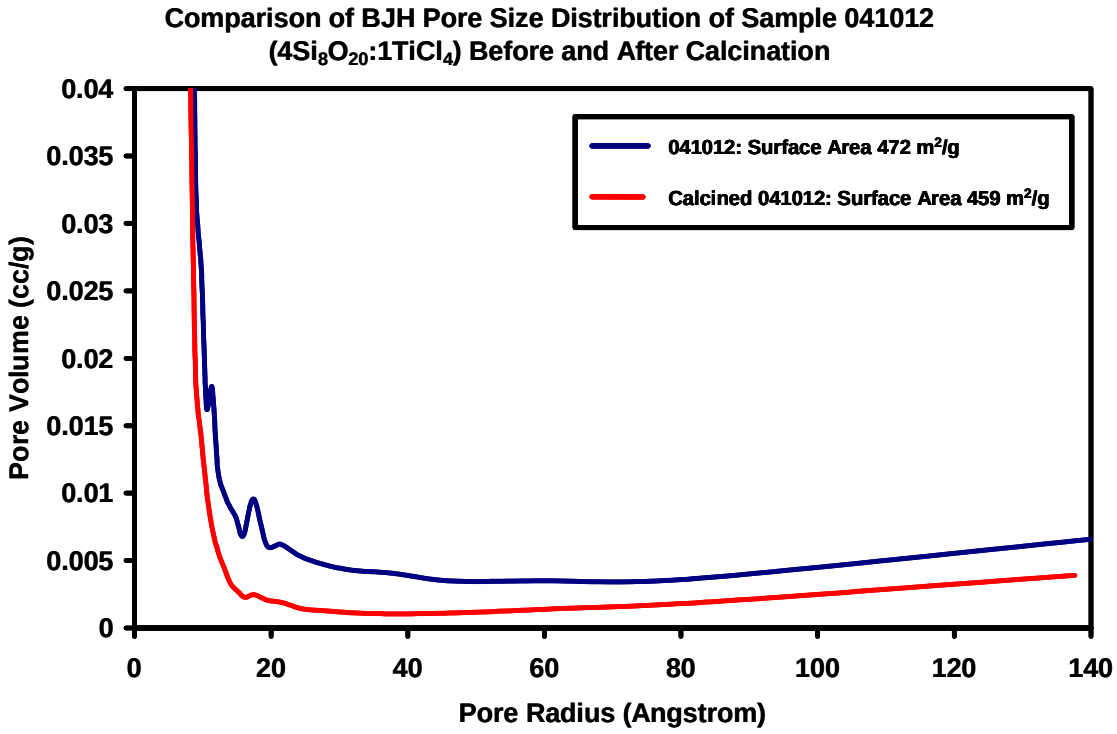

Figure 4. 15 BJH pore size distribution of titanosilicate catalyst 041012 before and after calcination.

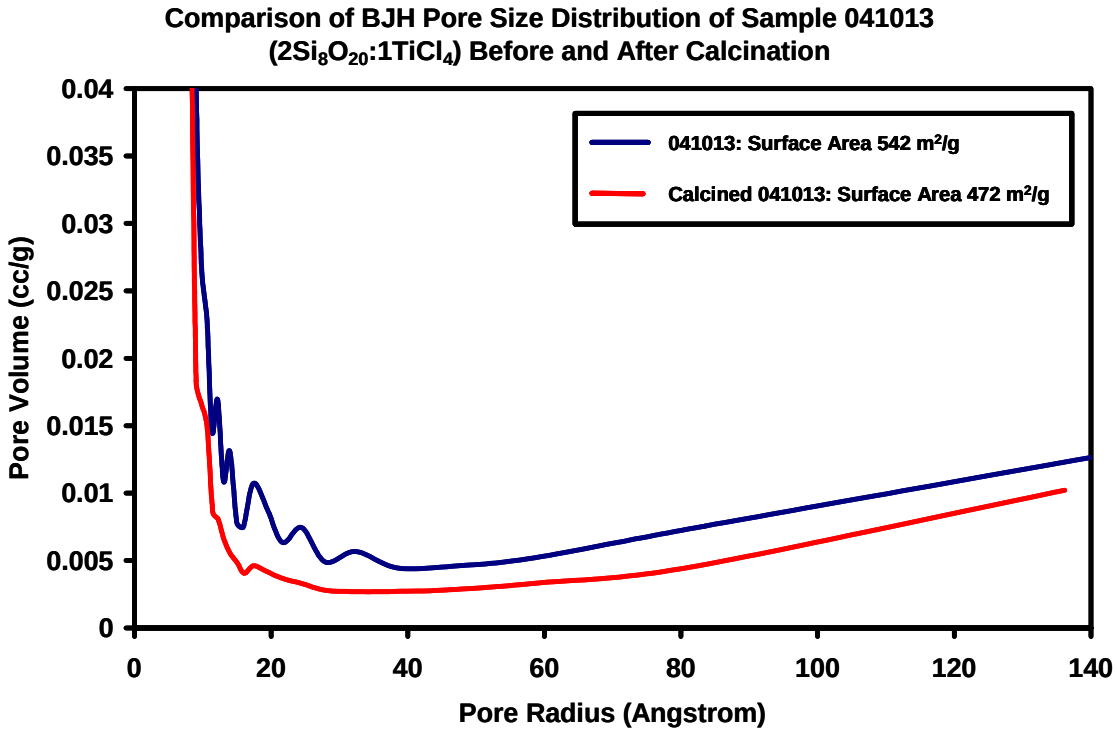

Figure 4. 16 BJH pore size distribution of titanosilicate catalyst 041013 before and after calcination.

Table 4. 3 Atomic emission results for titanosilicate catalysts.

Sample	Theoretical wt % titanium	Determined wt % titanium	Difference	% Error
041012	1.40	1.10	0.30	21.7
041013	2.88	2.23	0.65	19.2
050613	4.69	4.24	0.45	9.41
Used 050613	4.69	3.55	n/a	n/a

nearly achieved because metal loadings of 1.1%, 2.3%, and 4.2% respectively were found. The discrepancy between the initial amount and the amount that actually linked building blocks could be due to the removal of some unreacted titanium tetrachloride. Unreacted titanium tetrachloride presumable occurs due to the interactions of titanium tetrachloride and trimethyltin chloride. This complex was observed as a yellow volatile material that was removed during the workup of the reaction.

4.3.5 Characterization of Catalytic Activity: Transesterification Studies with Triacetin

As described earlier, samples were sent to Clemson University for analysis of activity for the transesterification of triacetin with methanol by Dora E. López. We focused on first determining the samples were active as catalysts and if the activity scaled with metal loading. We also studied the effects of calcination on the activity. We then compared the observed activity with that of commercially available catalysts tested at Clemson University. Finally, we examined the deactivation properties of the most active catalysts.

All aluminosilicate and titanosilicate samples displayed some activity for the transesterification of triacetin with methanol under the conditions studied (Table 4.4). Activities of 3 – 76% conversion were observed and titanosilicate samples displayed activities that were similar to those of the aluminosilicate samples with comparable loading. The observed activity of the samples also appears to scale with initial loading indicating that the metal centers are at least

Table 4. 4 Triacetin conversion (%) for aluminosilicate and titanosilicate catalysts.

Catalyst Identification Code	Metal Loading	$Si_8O_{20}:MCl_x$ X=3,4	% Triacetin Conversion (8 hours)
041006	50Si:Al (±11)	4:1	6 ± 2
041006 calcined	50Si:Al (±11)	4:1	3 ± 1
041005	37Si:Al (±8)	3:1	11 ± 5
041005 calcined	37Si:Al (±8)	3:1	6 ± 1
041020	37SI:Al (±8)	3:1	42
041019	25Si:Al (±5)	2:1	33
041012	50Si:Ti (±11)	4:1	17
041012 calcined	50Si:Ti (±11)	4:1	<1
041013	24Si:Ti (±5)	2:1	30
041013 calcined	24Si:Ti (±5)	2:1	7
050613	11Si:Ti (±1)	1:1	76

in part, responsible for the observed activity. For example aluminosilicate samples 041006. 041005, and 041019 had initial metal to building block rations that range from 4 : 1 – 2 : 1. In these samples, the activity increases as the aluminum loading increases. For the titanium sample, the % triacetin conversion was examined as a function of weight % titanium in the samples determined by AE analysis and a linear correlation was observed (Figure 4.17). The implications of this correlation will be discussed in a future section of this chapter.

The samples having highest loadings of each metal had activities that were comparable to that of observed for other commercially available catalysts tested at Clemson University (Table 4.5). Based on these findings, the most active samples were tested for deactivation. These samples included the aluminosilicate samples 041019 and 041020 and the titanosilicates 041013 and 050613. These results of the deactivation studies will be discussed in a later section.

Calcination of the catalysts caused significant loss of activity in all cases studied. One possible reason for this deactivation could be due to the changes previously described to the groups covering the surfaces of the catalysts that occur during calcination. By changing these methoxy groups to hydroxyl groups, the hydrophobic nature of the surface changes dramatically. This has been shown to greatly effect the activity solid acid of catalysts.[26] This change from a hydrophobic surface to a hydrophilic surface could explain why the catalysts deactivate because characterization of the calcined samples did not indicate major changes occurred to the material other than changing the surface groups.

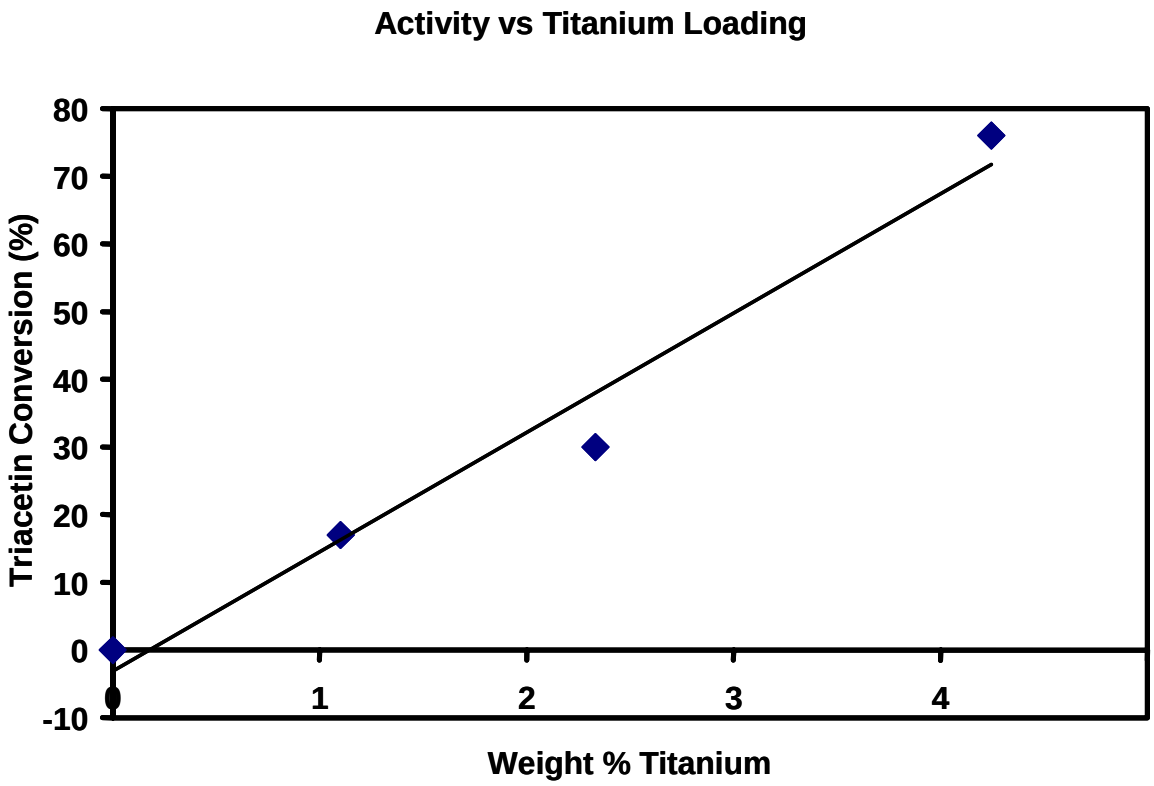

Figure 4. 17 Triacetin conversion (%) as a function of titanium loading. The Line represents the LS fit to the points in the figure.

Table 4. 5 Triacetin conversion (%) for several commercially available catalysts.

Catalyst	Catalyst Phase	% Triacetin Conversion (8 hours)
No catalyst	N/A	0
ETS-10 (Na)	Solid	92
Amberlyst-15	Solid	81
SZ (Sulfonated Zirconia)	Solid	54
WZ (Tungstated Zirconia)	Solid	20
MgO	Solid	14
Supported Phosphoric Acid	Solid	<1
ETS-10 (H)	Solid	<1
Zeolite Hβ	Solid	<1
H_2SO_4	Liquid	93
NaOH	Liquid	92

4.3.6 Recycling the Catalysts: Effects Upon Activity

The two most active aluminosilicate (041019 and 041020) and titanosilicate (041013 and 050613) samples were tested for deactivation by stopping the transesterification reaction after 4 hours and adding fresh solution until the catalysts deactivated or a constant activity was observed. Figures 4.18–4.21 show the results from these studies. Both of the aluminosilicate samples exhibited reasonable activities when compared to commercially available catalysts. However, deactivation of these catalysts was substantial after 4 hours. Both of the most active titanosilicate samples also had good activity relative to other catalysts. However, titanosilicate sample 041013 (which was the second most active titanium containing sample), deactivated appreciably after four hours. The most active titanosilicate catalyst (050613) had good initial activity (76% conversion), and despite significant deactivation after 4 hours, the activity became stable after a fourth cycle.

This sample (050613) was tested for changes in weight % titanium after one eight hour run using AE analysis. The results indicated a loss of 0.69% titanium after the reaction which represents just over 16% of the titanium contained in this catalyst (050613) (Table 4.3). Part of the loss in activity for this is probably due to the leaching of titanium from the support. This type of post reaction characterization of the catalyst was only conducted for this one sample. However, it should become routine analysis for all catalysts so that this issue can be addressed and any observed deactivation better understood.

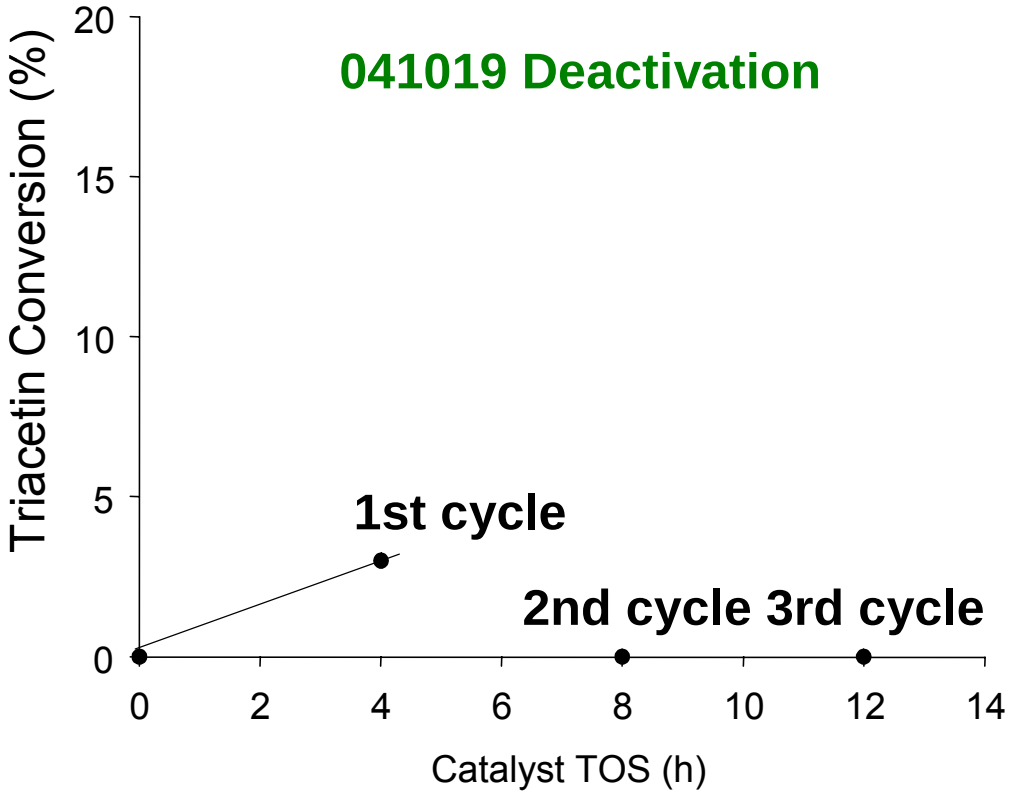

Figure 4. 18 Catalysts recycling investigations for aluminosilicate catalyst 041019.

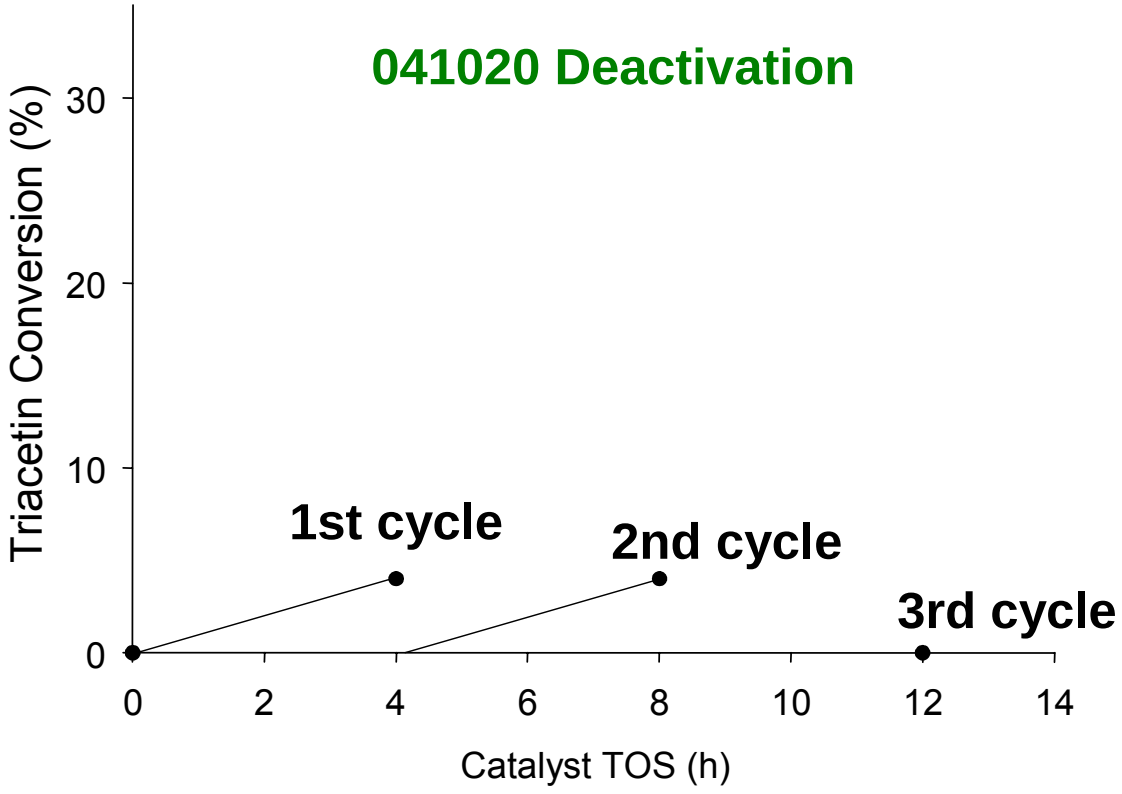

Figure 4. 19 Catalysts recycling investigations for aluminosilicate catalyst 041020.

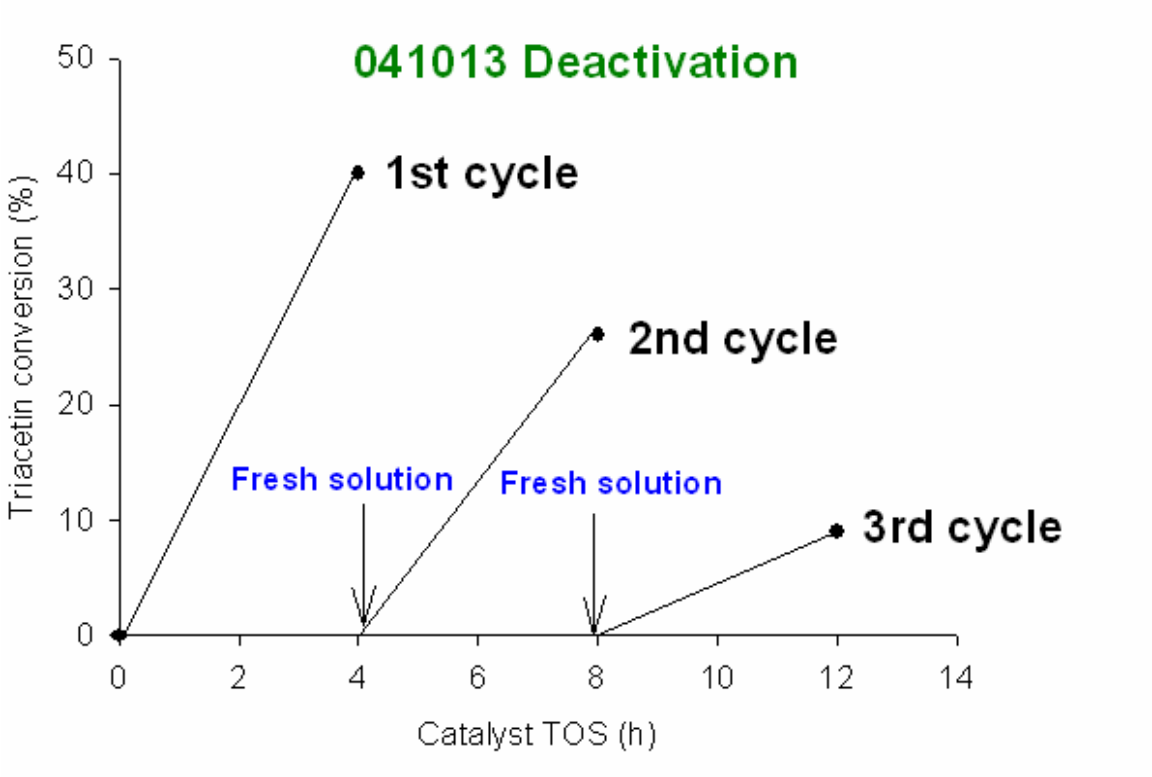

Figure 4. 20 Catalysts recycling investigations for titanosilicate catalyst 041013.

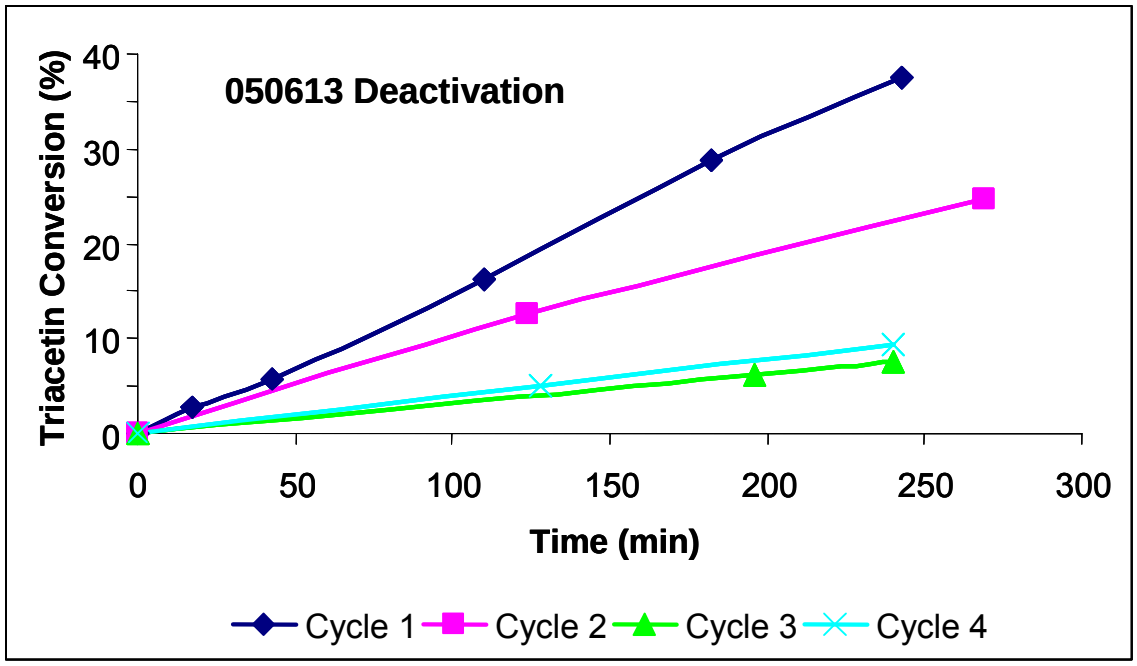

Figure 4. 21 Catalysts recycling investigations for titanosilicate catalyst 050613.

Based on these studies, the titanosilicate samples perform better than the aluminosilicate samples for the transesterification of triacetin with methanol in terms of catalyst lifetime. This is significant because these samples represent only initial efforts in designing catalysts that are active for the transesterification of triacetin with methanol. Since these materials have an open framework, they could be good catalysts for transesterification of triglycerides containing long chain alkyl groups with alcohols for the production of biodiesel.

4.3.7 Control Samples

Since the aluminosilicate samples deactivated appreciably, control studies were conducted with silicate samples that contained no metal centers. A sample (050329) was synthesized by linking only with tetrachlorosilane using methods described previously in this thesis where a distribution of silylchloride linking groups was present. The activity of this sample was tested fresh with no pretreatment. A second sample (050203) was synthesized using identical conditions and stoichiometric ratios followed by treatment with methanol as described previously for the aluminosilicate and titanosilicate samples. The results for these reactions are given in Figure 4.22.

The purpose of the control sample 050329 was to examine the activity that would result from the generation of hydrochloric acid from the reaction of silylchloride groups with methanol used in the transesterification reaction (Figure 4.7). This catalyst was very active for the first 8 hours and remained active for a second run of 10 hours. However, deactivation was appreciable during the third

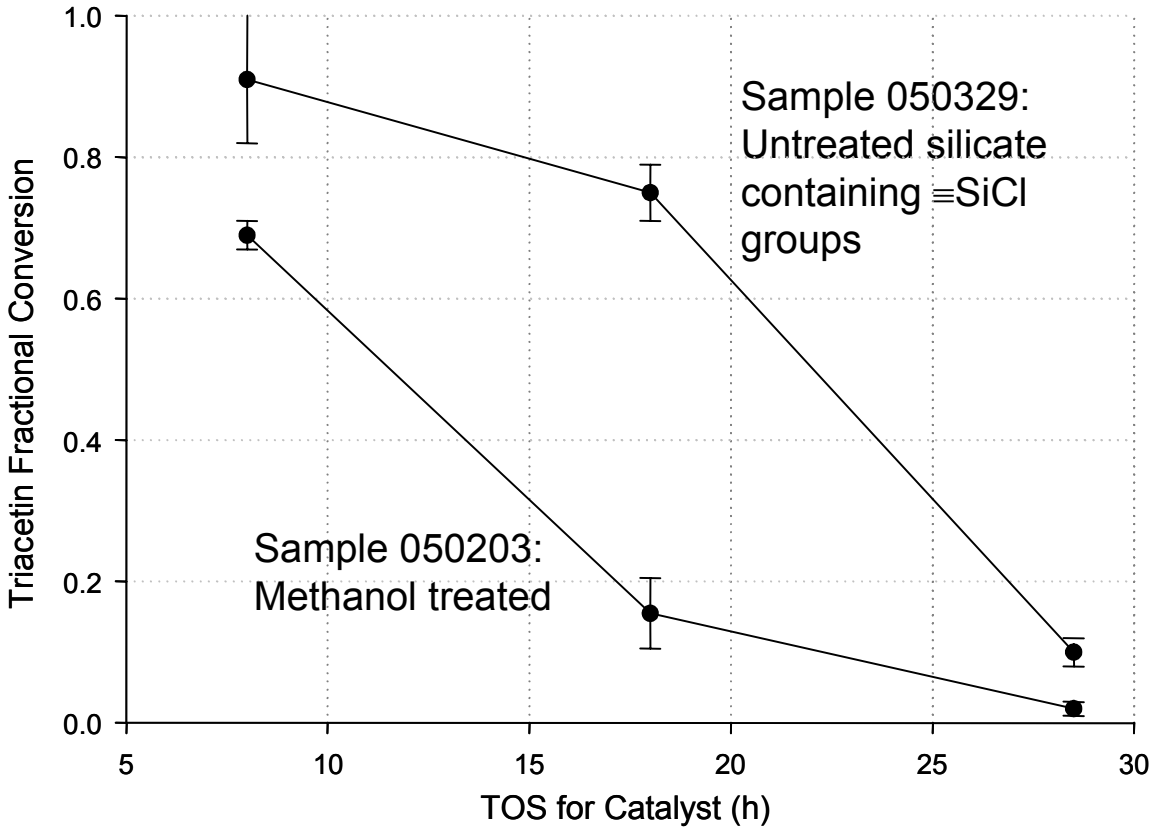

Figure 4. 22 Reactivity studies for control silicate samples.

run of 10.5 hours. Since the catalyst was not washed between runs, the continued activity presumably occurred due to residual hydrochloric acid.

Sample 050203 was investigated to determine activity that could come from possible residual hydrochloric acid after methanol treatment or from other sources from the silicate platform. This sample displayed good activity during the first 8 hour run, but quickly deactivated. The initial activity could be due to residual HCl or other processes not yet determined.

These studies show that at least some activity in these samples is due to processes that do not involve the metals that were present in the aluminosilicate and titanosilicate samples. The reason for this activity is presumable due to the presence of HCl. However, since only a small amount of metal chloride was used in these samples relative to the amount of tetrachlorosilane, and identical conditions were used for methanol treatments, all sample should have comparable levels of residual HCl. In the methanol treated control sample, the initial activity approached 70% triacetin conversion which is greater than all but one metallosilicate sample (Table 4.4). Thus it is not entirely clear why this sample has high activity. Further studies needs to be conducted to determine what is responsible for these studies.

4.3.8 Source of Catalytic Activity

The metal centers in the metallosilicate samples appear to be responsible for the observed activity for the transesterification of triacetin with methanol. As was previously described, the activity correlates with the metal loading for both

aluminosilicate and titanosilicate samples. Although we have not quantitatively measured the amount of residual HCl in the samples, we feel that the concentrations should be very similar in all samples for the following reasons. The only source of HCl in these reactions is from the reaction of metal chloride groups on the platform with methanol during the treatment designed to passivate the support. The initial metal loading in all of these samples is relatively small compared to the amount of tetrachlorosilane added to cross-link the material. Therefore the main source of metal chloride groups in the samples before the methanol treatment should originate from the distribution of linking silylchloride groups which should be fairly consistent in all samples since identical conditions were used for cross-linking reactions and the subsequent reaction workup step involving heating the isolated powders to 100^{o}C under vacuum overnight. Thus the amount of residual HCl should be very similar in all cases. The scaling of activity with loading previously discussed suggests that the metal centers are at least in part responsible for the activity.

Further evidence that the activity is due mostly to the metal centers is seen in the case of the titanosilicate catalysts. When the activity is examined as a function of weight percent titanium, a linear correlation was observed (Figure 4.22). Extrapolation of this correlation shows that as the loading approaches 0 weight % titanium, the activity also approaches 0 % triacetin conversion. If residual HCl were responsible for a significant portion of the activity, the extrapolated data should approach some value greater than 0 % conversion.

This trend strongly suggests that the titanium centers are mostly responsible for the activity.

The initial loss in activity in the titanosilicate samples could be due to leaching of some of the titanium from the support. The titanosilicate sample 050613 had an initial triacetin conversion rate of 76% and lost approximately 16% titanium during the reaction. The correlation of a loss in activity with a loss of titanium from the support also indicates that the titanium is responsible for the activity.

The one piece of evidence that we have obtained that suggest that HCl is responsible for activity is the control sample that was treated with methanol. However, in this sample, an initial activity of nearly 70% triacetin conversion was observed. As previously mentioned, this rate approaches that of the most active titanium sample and is greater than all other metallosilicate samples investigated. If HCl were the source of the activity, then this near 70% conversion should be a "baseline" for the activity for all samples since it was prepared using identical conditions as the metallosilicate samples excluding the initial dose of metal chloride. Again, the reason for the high initial activity for this sample is not known.

4.4 Summary and Conclusions

An initial, small subset of nanostructured, mesoporous metallosilicate samples have been synthesized and tested as catalysts for the transesterification of triacetin with methanol. This work represents initial investigations in

developing novel solid acid catalysts using building block methods. Using the methods presented in chapter 3 of this thesis, catalysts were designed to have site isolated, atomic aluminum or titanium centers that are deeply embedded in silicate matrices. The catalysts were synthesized and characterized at the University of Tennessee and tested for their activity for the transesterification reaction as prepared and selected samples were tested for activity after calcination at Clemson University. Deactivation studies were undertaken for the most active aluminosilicate and titanosilicate samples at Clemson University.

Investigations of these “first generation” building block solid acid catalysts indicate that they have the potential to be useful solid acid catalysts for the transesterification of triglycerides with alcohols. Conversion rates of 3-76% were observed for the building block catalysts which is comparable to the range of activity (>1 – 92%) observed in commercially available catalysts using the same conditions. Among the building block catalysts, the sample with the highest titanium loading exhibited 76% conversion to product(s) after one 8 hour reaction while the sample with the highest aluminum loading exhibited 33% conversion to product(s) using the same conditions (Table 4.4). Both of the conversion rates observed in these building block catalysts are greater than the activity observed for commercially available tungstated zirconia catalyst using the same conditions. These two building block catalysts fall third overall on the list of the tested commercial heterogeneous catalysts (Table 4.5).

Regardless the metal used, metal loadings affect the activity. As the loading increases, the activity also increases (Table 4.4). Furthermore, a linear

relationship exists between loading and activity for the titanosilicate catalysts based on three catalysts indicating that the activity observed is due to the mostly due to metal centers (Figure 4.17). *This finding is important since the possibility of residual HCl being physisorbed on these materials exists which could play a role in the catalysis.*

The catalysts that showed the least activity were those that had been calcined. Both the aluminum and titanium based catalysts suffered substantial losses in activity after calcination. TGA, silicon-29 MAS and CPMAS NMR, and IR analysis indicates that heating these samples to 350^{o}C in air burns off all methoxy groups. Surface area analyses indicate that little change occurs to the silicate matrices during this process. This suggests that either the methoxy groups play a role in the activity of these catalysts or that the hydrophilic nature of the support after calcination inhibits substrates from getting to catalytic sites in the mesopores of these materials.[26]

All samples deactivated appreciably after one 4 hour reaction. The titanosilicate catalysts exhibited activities that were are large as the activity observed for aluminosilicate samples, but did not deactivate as readily. Initial AE analysis of the titanosilicate sample with the largest metal loading before and after an 8 hour reaction indicates that some of the metal leached from the support during the reaction. This could explain some of the loss in activity for these samples. Despite this loss in activity, the catalysts reach a stable activity after three 4 hour runs.

These initial studies form the basis for future studies using building block methods to produce tailored solid acid catalysts. In the next chapter, suggestions for the direction of this project will be given.

Chapter 5: Conclusion and Future Work

5.1 Conclusion and Future Work

Designing heterogeneous catalysts that have highly dispersed single-site active centers represents one of the major challenges in catalysis sciences. This is absolutely necessary in order to identify a correlation between the activity and selectivity observed in a particular reaction with the structure of the active site. The design of heterogeneous catalysts using building block techniques was employed to make single site metal oxide/silicate based materials where control over the structure of the active site was achieved in model studies.

The building block utilized in this study was the octameric spherosilicate, $Si_8O_{20}(SnMe_3)_8$.[57] This building block was chosen because it is chemically robust and should maintain its structural integrity not only during conditions utilized to synthesize the catalysts, but also during catalysis testing. The mixed tin-silicon ether functionality present on the building block allows for reactions with metal chlorides giving trimethyltin chloride as a by product.[28,37] This reaction can be utilized to produce molecular species or cross-linked materials.[28,37]

This building block has a core silicate cage structure that is seen in many silicates and zeolites as well as in silsesquioxanes. Structural studies of the stannalyated octameric spherosilicate reveal that the cage structure is composed of eight rigid SiO_4 tetrahedron connected by a corner shared bridging oxygen. Comparison of the angles present in the siloxy bridge reveals the “soft” nature of this bond.[50] Observed angles of greater than 172^o were observed in

$Si_8O_{20}(SnMe_3)_8 \cdot 4H_2O$. This value represents the largest reported angle for structures containing the Si_8O_{12} cage that has been reported in the Cambridge Structural Database.

Future work in this area could include further comparison of the Si_8O_{12} cage unit for “all capping” species that are being prepared my Ming-Yung Lee in Dr Craig E. Barnes research group. The structural information described in this chapter could also be used to aid in the data work-up and interpretation of neutron and high energy X-ray scattering experiments for building block materials. This method of comparing structural features of analogous building blocks outlined in this chapter could be used as a basis for looking at other potential building blocks that are yet to be utilized for designing building block materials.

Si_8O_{12} building block has been used in the design of materials for many different applications.[28,29,37,38,44,45,51,53,56,82] In this thesis, the goal was to develop methods for designing next generation heterogeneous catalysts by cross-linking this spherosilicate building block using three different silylchlorides. The cross-linking properties of the resulting materials were controlled by changing the initial stoichiometry. By linking $Si_8O_{20}(SnMe_3)_8$ with a limiting amount of a silyl chloride and cross-linking with tetrachlorosilane, materials were prepared having silicon based linking units embedded in a cross-linked silicate matrix. These embedded linking units had unique local environments blocks throughout the entire material. Samples were also made where a limiting amount of a silylchloride was attached to the surface of the material through a single siloxy linkage. This was achieved

by first cross-linking the building blocks using tetrachlorosilane and isolating a free flowing powder. This powder was then exposed to silylchloride in the gas phase which reacted with residual mixed tin-silicon ether groups. The procedures outlined here are the basis for using building block methods to design heterogeneous catalysts having a unique environment throughout the entire material. These tailored solids made by design address one of the fundamental challenges in catalysis sciences. These types of breakthroughs in developing new methods are required to advancing the field of heterogeneous catalysis such that the reactive properties of the catalysts equal that of their homogeneous counterparts.

Future studies involving the cross-linking of spherosilicates with silyl chlorides should involve applying the methods presented in chapter 3 to $Si_8O_{20}(Sn^nBu_3)_8$. The use of the tri-*n*-butyl analogue would be advantageous for two reasons. The reaction by-products are much less toxic than are the trimethyl version. It is also considerably less expensive to synthesize the tri-*n*-butyltin octafunctional spherosilicate in terms of chemical costs and time. Methodologies using this analogue need to be developed as was with the case with $Si_8O_{20}(SnMe_3)_8$.

The methods developed to produce embedded silylchlorides in a cross-linked silicate matrix were employed to produce aluminosilicate and titanosilicate samples. These samples were tested as catalysts for the transesterification of triacetin with methanol. This reaction is a good model reaction for the transesterification of triglycerides with alcohols which is employed in making

biodiesel fuel with strong liquid acids. These samples had conversion rates up to 76%. In both cases, the conversion rates scaled with initial metal loading. The titanosilicate samples had the highest conversion rate of 76%. The two most active aluminosilicate and titanosilicate samples (four in total) were tested for deactivation. All samples deactivated appreciably after one four hour reaction. However, a stable rate was observed in the most active titanosilicate sample after three four hour cycles.

The study presented in chapter 4 represents the first successful attempt at synthesizing building block heterogeneous materials that were active as catalysts. Further studies that utilize these materials as acid catalysts should be fruitful based on preliminary results. These studies should include quantitative analysis for HCl content on the methanol treated samples to provide additional evidence that the metal centers are actually the active species in the materials.

It would also be interesting to probe these samples for their acid characteristics. Temperature programmed desorption methods could be used for this to determine the number and types of acid sites presents. Pyridine adsorption studies using IR could also be done on these samples to distinguish Bronsted and Lewis acid sites. It would be interesting to look at aluminum samples before and after methanol treatment using these methods to monitor changes in the nature of the acid centers. Of course these techniques could be used for titanosilicate samples as well.

Building block methods offer one approach to designing metal oxide/silicate based materials. These materials have metal centers which are

single site in nature. The amount of loading of the metal can be varied and mixed metal systems are also possible. These systems ultimately may allow for a correlation to be developed between activity and selectivity with structural properties of the active centers. Determining and understanding this relationship will lead to the development of next generation heterogeneous catalysts that have reactive properties that approach 100% selectivity.

References

(1) Armor, J. N. *www.nacatsoc.org/who.asp* 2001.

(2) Hegedus, L. L.; Editor *Catalyst Design: Progress and Perspectives*, 1987.

(3) Imelik, B.; Vedrine, J. C.; Editors *Catalyst Characterization: Physical Techniques for Solid Material*, 1994.

(4) Neurock, M. *Journal of Catalysis* **2003**, *216*, 73-88.

(5) Somorjai, G. A.; McCrea, K. R.; Zhu, J. *Topics in Catalysis* **2002**, *18*, 157-166.

(6) Wight, A. P.; Davis, M. E. *Chemical Reviews (Washington, DC, United States)* **2002**, *102*, 3589-3613.

(7) Barteau, M. A.; Lyons, J. E.; Song, I. K. *Journal of Catalysis* **2003**, *216*, 236-245.

(8) Kung, H. H.; Kung, M. C. *Topics in Catalysis* **2005**, *34*, 77-83.

(9) Haruta, M. *Cattech* **2002**, *6*, 102-115.

(10) Pugin, B. *Journal of Molecular Catalysis A: Chemical* **1996**, *107*, 273-279.

(11) Lu, Z.-l.; Lindner, E.; Mayer, H. A. *Chemical Reviews (Washington, DC, United States)* **2002**, *102*, 3543-3577.

(12) Zaera, F. *Journal of Physics: Condensed Matter* **2004**, *16*, S2299-S2310.

(13) Trifiro, F. *Catalysis Today* **1998**, *41*, 21-35.

(14) Sadykov, V. A.; Tikhov, S. F.; Tsybulya, S. V.; Kryukova, G. N.; Veniaminov, S. A.; Kolomiichuk, V. N.; Bulgakov, N. N.; Paukshtis, E. A.; Ivanov, V. P.; Koshcheev, S. V.; Zaikovskii, V. I.; Isupova, L. A.; Burgina, L. B. *Journal of Molecular Catalysis A: Chemical* **2000**, *158*, 361-365.

(15) Weiss, W.; Schlogl, R. *Topics in Catalysis* **2000**, *13*, 75-90.

(16) Okuhara, T. *Chemical Reviews (Washington, DC, United States)* **2002**, *102*, 3641-3665.

(17) Clark, J. H. *Accounts of Chemical Research* **2002**, *35*, 791-797.

(18) Corma, A. *Current Opinion in Solid State & Materials Science* **1997**, *2*, 63-75.

(19) Mizuno, N.; Misono, M. *Chemical Reviews (Washington, D. C.)* **1998**, *98*, 199-217.

(20) Yang, H.; Lu, R.; Zhao, J.; Yang, X.; Shen, L.; Wang, Z. *Materials Chemistry and Physics* **2003**, *80*, 68-72.

(21) Venkatesh, K. R.; Hu, J.; Dogan, C.; Tierney, J. W.; Wender, I. *Energy & Fuels* **1995**, *9*, 888-893.

(22) Drago, R. S.; Getty, E. E. *Journal of the American Chemical Society* **1988**, *110*, 3311-3312.

(23) Drago, R. S.; Petrosius, S. C.; Kaufman, P. B. *Journal of Molecular Catalysis* **1994**, *89*, 317-328.

(24) Drago, R. S.; Petrosius, S. C.; Chronister, C. W. *Inorganic Chemistry* **1994**, *33*, 367-372.

(25) Corma, A. *Journal of Catalysis* **2003**, *216*, 298-312.

(26) Corma, A. *Chemical Reviews (Washington, D. C.)* **1997**, *97*, 2373-2419.

(27) De Vos, D. E.; Dams, M.; Sels, B. F.; Jacobs, P. A. *Chemical Reviews (Washington, DC, United States)* **2002**, *102*, 3615-3640.

(28) Feher, F. J.; Weller, K. J. *Chemistry of Materials* **1994**, *6*, 7-9.

(29) Ghosh, N. N.; Clark, J. C.; Eldridge, G. T.; Barnes, C. E. *Chemical Communications (Cambridge, United Kingdom)* **2004**, 856-857.

(30) Thomas, J. M.; Lambert, R. M.; Editors *Characterization of Catalysts*, 1980.

(31) Kruk, M.; Jaroniec, M. *Chemistry of Materials* **2000**, *12*, 222-230.

(32) Kruk, M.; Jaroniec, M.; Sayari, A. *Chemistry of Materials* **1999**, *11*, 492-500.

(33) Kruk, M.; Jaroniec, M. *Chemistry of Materials* **2001**, *13*, 3169-3183.

(34) Barrett, E. P.; Joyner, L. G.; Halenda, P. P. *Journal of the American Chemical Society* **1951**, *73*, 373-380.

(35) Akitt, J. W.; Mann, B. E. *NMR and Chemistry: An Introduction to Modern NMR Spectroscopy*; 4th ed., 2000.

(36) Kolodziejski, W.; Klinowski, J. *Chemical Reviews (Washington, D. C.)* **2002**, *102*, 613-628.

(37) Saengkerdsub, S. In *Department of Chemistry*; University of Tennessee - Knoxville: Knoxville, 2002, p 159.

(38) Harrison, P. G. *Journal of Organometallic Chemistry* **1997**, *542*, 141-183.

(39) Hoebbel, D.; Wieker, W.; Franke, P.; Otto, A. *Zeitschrift fuer Anorganische und Allgemeine Chemie* **1975**, *418*, 35-44.

(40) Hoebbel, D.; Garzo, G.; Engelhardt, G.; Ebert, R.; Lippmaa, E.; Alla, M. *Zeitschrift fuer Anorganische und Allgemeine Chemie* **1980**, *465*, 15-33.

(41) Auner, N.; Ziemer, B.; Herrschaft, B.; Ziche, W.; John, P.; Weis, J. *European Journal of Inorganic Chemistry* **1999**, 1087-1094.

(42) Paech, M.; Stoesser, R. *Journal of Physical Chemistry A* **1997**, *101*, 8360-8365.

(43) Hayashino, Y.; Isobe, T.; Matsuda, Y. *ChemPhysChem* **2001**, *2*, 748-750.

(44) Hong, B.; Thoms, T. P. S.; Murfee, H. J.; Lebrun, M. J. *Inorganic Chemistry* **1997**, *36*, 6146-6147.

(45) Provatas, A.; Luft, M.; Mu, J. C.; White, A. H.; Matisons, J. G. *Journal of Organometallic Chemistry* **1998**, *565*, 159-164.

(46) Buergi, H. B.; Toernroos, K. W.; Calzaferri, G.; Buergy, H. *Inorganic Chemistry* **1993**, *32*, 4914-4919.

(47) Baertsch, M.; Bornhauser, P.; Calzaferri, G.; Imhof, R. *Vibrational Spectroscopy* **1995**, *8*, 305-308.

(48) Huang, Y.; Xu, Z.; Havenga, E. A.; Butler, I. S. *Vibrational Spectroscopy* **2000**, *22*, 175-180.

(49) Marcolli, C.; Laine, P.; Buehler, R.; Calzaferri, G.; Tomkinson, J. *Journal of Physical Chemistry B* **1997**, *101*, 1171-1179.

(50) Bieniok, A. M.; Buergi, H.-B. *Journal of Physical Chemistry* **1994**, *98*, 10735-10741.

(51) Barton, T. J.; Bull, L. M.; Klemperer, W. G.; Loy, D. A.; McEnaney, B.; Misono, M.; Monson, P. A.; Pez, G.; Scherer, G. W.; Vartuli, J. C.; Yaghi, O. M. *Chemistry of Materials* **1999**, *11*, 2633-2656.

(52) Brevett, C. S.; Cagle, P. C.; Klemperer, W. G.; Millar, D. M.; Ruben, G. C. *Journal of Inorganic and Organometallic Polymers* **1991**, *1*, 335-342.

(53) Hasegawa, I.; Hibino, K.; Takei, K. *Applied Organometallic Chemistry* **1999**, *13*, 549-554.

(54) Zhang, C.; Babonneau, F.; Bonhomme, C.; Laine, R. M.; Soles, C. L.; Hristov, H. A.; Yee, A. F. *Journal of the American Chemical Society* **1998**, *120*, 8380-8391.

(55) Soles, C. L.; Lin, E. K.; Wu, W.-L.; Zhang, C.; Laine, R. M. *Materials Research Society Symposium Proceedings* **2001**, *628*, CC4.2.1-CC4.2.6.

(56) Lamm, M. H.; Chen, T.; Glotzer, S. C. *Nano Letters* **2003**, *3*, 989-994.

(57) Feher, F. J.; Weller, K. J. *Inorganic Chemistry* **1991**, *30*, 880-882.

(58) Sheldrick, G. M. *A Program for the Refinement of Crystal Structures* **1997**, *University of Gottingen*, Gottingen, Germany.

(59) Sheldrick, G. M. *University of Gottingen, Gottingen, Germany* **1996**.

(60) Kennard, O.; Allen, F. H.; Brice, M. D.; Hummelink, T. W. A.; Motherwell, W. D. S.; Rodgers, J. R.; Watson, D. G. *Pure and Applied Chemistry* **1977**, *49*, 1807-1816.

(61) Podberezskaya, N. V.; Baidina, I. A.; Alekseev, V. I.; Borisov, S. V.; Martynova, T. N. *Zhurnal Strukturnoi Khimii* **1981**, *22*, 116-119.

(62) Smolin, Y. I.; Shepelev, Y. F.; Pomes, R.; Hoebbel, D.; Wieker, W. *Kristallografiya* **1975**, *20*, 917-924.

(63) Day, V. W.; Klemperer, W. G.; Mainz, V. V.; Millar, D. M. *Journal of the American Chemical Society* **1985**, *107*, 8262-8264.

(64) Smolin, Y. I.; Shepelev, Y. F.; Butikova, I. K. *Kristallografiya* **1972**, *17*, 15-21.

(65) Said, M. A.; Roesky, H. W.; Rennekamp, C.; Andruh, M.; Schmidt, H.-G.; Noltemeyer, M. *Angewandte Chemie, International Edition* **1999**, *38*, 661-664.

(66) Shepelev, Y. F.; Smolin, Y. I.; Ershov, A. S.; Rademacher, O.; Sheller, G. *Kristallografiya* **1987**, *32*, 1399-1403.

(67) Wiebcke, M.; Koller, H. *Acta Crystallographica, Section B: Structural Science* **1992**, *B48*, 449-458.

(68) Rattay, M.; Fenske, D.; Jutzi, P. *Organometallics* **1998**, *17*, 2930-2932.

(69) Tacke, R.; Lopez-Mras, A.; Sheldrick, W. S.; Sebald, A. *Zeitschrift fuer Anorganische und Allgemeine Chemie* **1993**, *619*, 347-358.

(70) Duchateau, R.; Van Santen, R. A.; Yap, G. P. A. *Organometallics* **2000**, *19*, 809-816.

(71) Calzaferri, G.; Imhof, R.; Tornroos, K. W. *Journal of the Chemical Society, Dalton Transactions: Inorganic Chemistry* **1994**, 3123-3128.

(72) Smolin, Y. I.; Shepelev, Y. F.; Pomes, R. *Khimiya Silikatov i Oksidov* **1982**, 68-85.

(73) Auner, N.; Bats, J. W.; Katsoulis, D. E.; Suto, M.; Tecklenburg, R. E.; Zank, G. A. *Chemistry of Materials* **2000**, *12*, 3402-3418.

(74) Ropartz, L.; Foster, D. F.; Morris, R. E.; Slawin, A. M. Z.; Cole-Hamilton, D. J. *Journal of the Chemical Society, Dalton Transactions* **2002**, 1997-2008.

(75) Larsson, K. *Arkiv foer Kemi* **1960**, *16*, 203-208.

(76) Koellner, G.; Mueller, U. *Acta Crystallographica, Section C: Crystal Structure Communications* **1989**, *C45*, 1106-1107.

(77) Shklover, V. E.; Struchkov, Y. T.; Makarova, N. N.; Andrianov, K. A. *Zhurnal Strukturnoi Khimii* **1978**, *19*, 1107-1119.

(78) Hossain, M. A.; Hursthouse, M. B.; Malik, K. M. A. *Acta Crystallographica, Section B: Structural Crystallography and Crystal Chemistry* **1979**, *B35*, 2258-2260.

(79) Calzaferri, G.; Imhof, R.; Toernroos, K. W. *Journal of the Chemical Society, Dalton Transactions: Inorganic Chemistry (1972-1999)* **1993**, 3741-3748.

(80) Wiebcke, M.; Emmer, J.; Felsche, J.; Hoebbel, D.; Engelhardt, G. *Zeitschrift fuer Anorganische und Allgemeine Chemie* **1994**, *620*, 757-765.

(81) Emmer, J.; Wiebcke, M. *Journal of the Chemical Society, Chemical Communications* **1994**, 2079-2080.

(82) Jaffres, P.-A.; Morris, R. E. *Journal of the Chemical Society, Dalton Transactions: Inorganic Chemistry* **1998**, 2767-2770.

(83) Nowotny, M.; Maschmeyer, T.; Johnson, B. F. G.; Lahuerta, P.; Thomas, J. M.; Davies, J. E. *Angewandte Chemie, International Edition* **2001**, *40*, 955-958.

(84) Lucke, S.; Stoppek-Langner, K.; Krebs, B.; Lage, M. *Zeitschrift fuer Anorganische und Allgemeine Chemie* **1997**, *623*, 1243-1246.

(85) Calzaferri, G.; Marcolli, C.; Imhof, R.; Toernroos, K. W. *Journal of the Chemical Society, Dalton Transactions: Inorganic Chemistry* **1996**, 3313-3322.

(86) Harris, R. K.; Naumov, D. Y.; Samadi-Maybodi, A. *Journal of the Chemical Society, Dalton Transactions: Inorganic Chemistry* **1996**, 3349-3355.

(87) Feher, F. J.; Budzichowski, T. A. *Journal of Organometallic Chemistry* **1989**, *373*, 153-163.

(88) Wiebcke, M.; Hoebbel, D. *Journal of the Chemical Society, Dalton Transactions: Inorganic Chemistry (1972-1999)* **1992**, 2451-2455.

(89) Wiebcke, M.; Grube, M.; Koller, H.; Engelhardt, G.; Felsche, J. *Microporous Materials* **1993**, *2*, 55-63.

(90) Dittmar, U.; Hendan, B. J.; Floerke, U.; Marsmann, H. C. *Journal of Organometallic Chemistry* **1995**, *489*, 185-194.

(91) Harris, R. K.; Howard, J. A. K.; Samadi-Maybodi, A.; Yao, J. W.; Smith, W. *Journal of Solid State Chemistry* **1995**, *120*, 231-237.

(92) Podberezskaya, N. V.; Magarill, S. A.; Baidina, I. A.; Borisov, S. V.; Gorsh, L. E.; Kanev, A. N.; Martynova, T. N. *Zhurnal Strukturnoi Khimii* **1982**, *23*, 120-129.

(93) Baidina, I. A.; Podberezskaya, N. V.; Borisov, S. V.; Alekseev, V. I.; Martynova, T. N.; Kanev, A. N. *Zhurnal Strukturnoi Khimii* **1980**, *21*, 125-129.

(94) Agaskar, P. A. *Inorganic Chemistry* **1991**, *30*, 2707-2708.

(95) Armitage, D. A.; Robinson, R. N.; Abel, E. W. *Inorg. Synth.* **1977**, *17*, 181-183.

(96) Barnes, C. E.

(97) Blaschette, A.; Schomburg, D.; Wieland, E. *Zeitschrift fuer Anorganische und Allgemeine Chemie* **1989**, *571*, 75-81.

(98) Poll, E.-M.; Samba, S.; Fischer, R. D.; Olbrich, F.; Davies, N. A.; Avalle, P.; Apperley, D. C.; Harris, R. K. *Journal of Solid State Chemistry* **2000**, *152*, 286-301.

(99) Hanika-Heidl, H. *Thesis* **2002**.

(100) Lange, I.; Henschel, D.; Wirth, A.; Krahl, J.; Blaschette, A.; Jones, P. G. *Journal of Organometallic Chemistry* **1995**, *503*, 155-170.

(101) Molloy, K. C.; Quill, K.; Cunningham, D.; McArdle, P.; Higgins, T. *Journal of the Chemical Society, Dalton Transactions: Inorganic Chemistry (1972-1999)* **1989**, 267-273.

(102) Jaeger, L.; Freude, B.; Krug, A.; Hartung, H. *Journal of Organometallic Chemistry* **1994**, *476*, 163-171.

(103) Parvez, M.; Ali, S.; Mazhar, M.; Bhatti, M. H.; Khokhar, M. N. *Acta Crystallographica, Section C: Crystal Structure Communications* **1999**, *C55*, 1280-1282.

(104) Eckhardt, R.; Hanika-Heidl, H.; Fischer, R. D. *Chemistry--A European Journal* **2003**, *9*, 1795-1804.

(105) Ovsetsina, T. I.; Furmanova, N. G.; Chuprunova, E. V.; Sheherbakov, V. I. *Kristallografiya* **1993**, *38*, 71-76.

(106) Hartley, F. R. *Supported Metal Complexes*; 1st ed.; D. Reidel Publishing Company: Boston, 1985.

(107) Yermakov, Y. I.; Kuznetsov, B. N.; Zakharov, V. A. *Catalysis by Supported Complexes*; elsevier Scientific Publishing Company: New York, 1981; Vol. 8.

(108) Stiles, A. B. *Catalyst Supports and Supported Catalysts Theoretical and Applied Concepts*; Butterworth Publishers: Boston, 1987.

(109) Engelhardt, G.; Michel, D. *High-resolution solid-state NMR of silicates and zeolites*; Wiley: New York, 1987; Vol. xiv.

(110) Lotero, E.; Liu, Y.; Lopez, D. E.; Suwannakarn, K.; Bruce, D. A.; Goodwin, J. G., Jr. *Industrial & Engineering Chemistry Research* **2005**, *44*, 5353-5363.

(111) Van Gerpen, J. *Fuel Processing Technology* **2005**, *86*, 1097-1107.

(112) Demirbas, A. *Energy Conversion and Management* **2003**, *44*, 2093-2109.

(113) Vicente, G.; Martinez, M.; Aracil, J. *Bioresource Technology* **2004**, *92*, 297-305.

(114) Furuta, S.; Matsuhashi, H.; Arata, K. *Catalysis Communications* **2004**, *5*, 721-723.

(115) Haas, M. J. *Fuel Processing Technology* **2005**, *86*, 1087-1096.

(116) Suppes, G. J.; Dasari, M. A.; Doskocil, E. J.; Mankidy, P. J.; Goff, M. J. *Applied Catalysis, A: General* **2004**, *257*, 213-223.

(117) Van Bokhoven, J. A.; Van der Eerden, A. M. J.; Koningsberger, D. C. *Journal of the American Chemical Society* **2003**, *125*, 7435-7442.

(118) Busco, C.; Barbaglia, A.; Broyer, M.; Bolis, V.; Foddanu, G. M.; Ugliengo, P. *Thermochimica Acta* **2004**, *418*, 3-9.

(119) Platon, A.; Thomson, W. J. *Applied Catalysis, A: General* **2005**, *282*, 93-100.

(120) Rios, L. A.; Weckes, P.; Schuster, H.; Hoelderich, W. F. *Journal of Catalysis* **2005**, *232*, 19-26.

(121) Sasidharan, M.; Kumar, R. *Journal of Molecular Catalysis A: Chemical* **2004**, *210*, 93-98.

(122) Srinivas, D.; Srivastava, R.; Ratnasamy, P. *Catalysis Today* **2004**, *96*, 127-133.

(123) Ma, F.; Hanna, M. A. *Bioresource Technology* **1999**, *70*, 1-15.

(124) Radzewich, C. E.; Guzei, I. A.; Jordan, R. F. *Journal of the American Chemical Society* **1999**, *121*, 8673-8674.

(125) Healy, M. D.; Power, M. B.; Barron, A. R. *Coordination Chemistry Reviews* **1994**, *130*, 63-135.

(126) Fyfe, C. A.; Bretherton, J. L.; Lam, L. Y. *Chemical Communications (Cambridge)* **2000**, 1575-1576.

(127) Fyfe, C. A.; Bretherton, J. L.; Lam, L. Y. *Journal of the American Chemical Society* **2001**, *123*, 5285-5291.

Appendices

Appendix A

X-ray Tables for $Si_8O_{20}(SnMe_3)_8$ (I)

Crystal data and structure refinement for $Si_8O_{20}(SnMe_3)_8$.

Identification code	**I (CSD – 279729)**	
Empirical formula	C24 H72 O20 Si8 Sn8	
Formula weight	1855.06	
Temperature	173(2) K	
Wavelength	0.71073 Å	
Crystal system	Triclinic	
Space group	P-1	
Unit cell dimensions	a = 11.339(3) Å	α= 68.973(4)°.
	b = 11.569(3) Å	β= 76.426(4)°.
	c = 13.258(3) Å	γ = 71.264(4)°.
Volume	1523.2(7) $Å^3$	
Z	1	
Density (calculated)	2.022 Mg/m^3	
Absorption coefficient	3.436 mm^{-1}	
F(000)	888	
Crystal size	0.5 x 0.5 x 0.5 mm^3	
Theta range for data collection	1.91 to 23.32°.	
Index ranges	-12<=h<=12, -12<=k<=12, -14<=l<=14	
Reflections collected	11644	
Independent reflections	4387 [R(int) = 0.0182]	
Completeness to theta = 23.32°	99.4 %	
Refinement method	Full-matrix least-squares on F^2	
Data / restraints / parameters	4387 / 0 / 283	
Goodness-of-fit on F^2	1.026	
Final R indices [I>2sigma(I)]	R1 = 0.0261, wR2 = 0.0733	
R indices (all data)	R1 = 0.0292, wR2 = 0.0760	
Largest diff. peak and hole	2.059 and -0.411 $e.Å^{-3}$	

Atomic coordinates (x 10^4) and equivalent isotropic displacement parameters ($Å^2$x 10^3) for **I**. U(eq) is defined as one third of the trace of the orthogonalized U^{ij} tensor.

	x	y	z	U(eq)
C(1)	6027(6)	11773(7)	3460(6)	61(2)
C(2)	8043(8)	8886(7)	4856(7)	80(2)
C(3)	8164(9)	11834(11)	5082(7)	93(3)
C(4)	14394(6)	5151(6)	3837(5)	50(2)
C(5)	11355(7)	4964(8)	3880(6)	65(2)
C(6)	13740(6)	4771(7)	1504(6)	58(2)
C(7)	10771(5)	3406(5)	2018(5)	40(1)
C(8)	7697(5)	4445(6)	1066(5)	42(1)
C(9)	8102(6)	5500(7)	3084(5)	58(2)
C(10)	5420(5)	7736(5)	1080(5)	39(1)
C(11)	5347(6)	8344(7)	3578(5)	53(2)
C(12)	3190(5)	10517(6)	1829(5)	44(1)
O(1)	9090(3)	11158(4)	2866(3)	34(1)
O(2)	12474(3)	7334(3)	2281(3)	32(1)
O(3)	9494(3)	6293(3)	612(3)	34(1)
O(4)	6130(3)	10163(3)	1226(3)	33(1)
O(5)	10509(3)	9318(3)	2054(3)	30(1)
O(6)	10689(3)	7490(3)	1228(3)	29(1)
O(7)	8331(3)	8558(3)	872(3)	30(1)
O(8)	8169(3)	10386(3)	1668(3)	31(1)
O(9)	10115(3)	8317(3)	-767(3)	31(1)
O(10)	7828(3)	10960(3)	-361(3)	31(1)
Si(1)	9419(1)	10643(1)	1843(1)	22(1)
Si(2)	11473(1)	8282(1)	1484(1)	23(1)
Si(3)	9651(1)	7647(1)	490(1)	22(1)
Si(4)	7592(1)	10018(1)	855(1)	22(1)
Sn(1)	7744(1)	10903(1)	4136(1)	40(1)
Sn(2)	13006(1)	5441(1)	2876(1)	30(1)

Sn(3)	9021(1)	4779(1)	1753(1)	29(1)
Sn(4)	4928(1)	9088(1)	1944(1)	31(1)

Bond lengths [Å] and angles [°] for **I**.

C(1)-Sn(1)	2.127(7)	O(9)-Si(3)	1.606(3)
C(2)-Sn(1)	2.125(7)	O(9)-Si(1)#1	1.608(3)
C(3)-Sn(1)	2.131(7)	O(10)-Si(2)#1	1.603(3)
C(4)-Sn(2)	2.124(6)	O(10)-Si(4)	1.607(3)
C(5)-Sn(2)	2.133(6)	Si(1)-O(9)#1	1.608(3)
C(6)-Sn(2)	2.119(6)	Si(2)-O(10)#1	1.603(3)
C(7)-Sn(3)	2.119(5)	Si(1)-O(1)-Sn(1)	129.1(2)
C(8)-Sn(3)	2.121(5)	Si(2)-O(2)-Sn(2)	132.4(2)
C(9)-Sn(3)	2.129(6)	Si(3)-O(3)-Sn(3)	140.2(2)
C(10)-Sn(4)	2.120(5)	Si(4)-O(4)-Sn(4)	140.1(2)
C(11)-Sn(4)	2.131(6)	Si(1)-O(5)-Si(2)	144.1(2)
C(12)-Sn(4)	2.123(6)	Si(2)-O(6)-Si(3)	142.8(2)
O(1)-Si(1)	1.591(4)	Si(4)-O(7)-Si(3)	144.4(2)
O(1)-Sn(1)	1.994(3)	Si(4)-O(8)-Si(1)	143.5(2)
O(2)-Si(2)	1.594(3)	Si(3)-O(9)-Si(1)#1	159.8(2)
O(2)-Sn(2)	1.979(3)	Si(2)#1-O(10)-Si(4)	161.2(2)
O(3)-Si(3)	1.580(3)	O(1)-Si(1)-O(5)	110.4(2)
O(3)-Sn(3)	1.991(3)	O(1)-Si(1)-O(9)#1	110.18(19)
O(4)-Si(4)	1.587(3)	O(5)-Si(1)-O(9)#1	109.05(19)
O(4)-Sn(4)	1.985(3)	O(1)-Si(1)-O(8)	108.62(18)
O(5)-Si(1)	1.611(4)	O(5)-Si(1)-O(8)	108.90(19)
O(5)-Si(2)	1.619(4)	O(9)#1-Si(1)-O(8)	109.67(19)
O(6)-Si(2)	1.624(4)	O(2)-Si(2)-O(10)#1	110.11(19)
O(6)-Si(3)	1.628(3)	O(2)-Si(2)-O(5)	109.18(19)
O(7)-Si(4)	1.620(4)	O(10)#1-Si(2)-O(5)	108.52(19)
O(7)-Si(3)	1.620(4)	O(2)-Si(2)-O(6)	110.54(19)
O(8)-Si(4)	1.617(4)	O(10)#1-Si(2)-O(6)	109.17(19)
O(8)-Si(1)	1.620(3)	O(5)-Si(2)-O(6)	109.29(19)
		O(3)-Si(3)-O(9)	108.72(19)
		O(3)-Si(3)-O(7)	110.86(19)

O(9)-Si(3)-O(7)	109.05(19)	C(6)-Sn(2)-C(5)	118.9(3)
O(3)-Si(3)-O(6)	110.64(19)	C(4)-Sn(2)-C(5)	111.0(3)
O(9)-Si(3)-O(6)	108.94(18)	O(3)-Sn(3)-C(7)	103.5(2)
O(7)-Si(3)-O(6)	108.59(19)	O(3)-Sn(3)-C(9)	103.1(2)
O(4)-Si(4)-O(10)	109.89(19)	C(7)-Sn(3)-C(9)	114.6(2)
O(4)-Si(4)-O(8)	109.96(19)	O(3)-Sn(3)-C(8)	103.1(2)
O(10)-Si(4)-O(8)	108.78(19)	C(7)-Sn(3)-C(8)	120.0(2)
O(4)-Si(4)-O(7)	111.13(18)	C(9)-Sn(3)-C(8)	110.1(3)
O(10)-Si(4)-O(7)	108.75(19)	O(4)-Sn(4)-C(10)	104.09(18)
O(8)-Si(4)-O(7)	108.29(19)	O(4)-Sn(4)-C(11)	101.2(2)
O(1)-Sn(1)-C(1)	105.2(2)	C(10)-Sn(4)-C(11)	115.9(2)
O(1)-Sn(1)-C(2)	106.1(3)	O(4)-Sn(4)-C(12)	100.75(19)
C(1)-Sn(1)-C(2)	112.2(3)	C(10)-Sn(4)-C(12)	120.8(2)
O(1)-Sn(1)-C(3)	100.2(2)	C(11)-Sn(4)-C(12)	110.4(3)
C(1)-Sn(1)-C(3)	117.0(4)		
C(2)-Sn(1)-C(3)	114.4(4)		
O(2)-Sn(2)-C(6)	105.7(2)		
O(2)-Sn(2)-C(4)	102.26(19)		
C(6)-Sn(2)-C(4)	113.4(3)		
O(2)-Sn(2)-C(5)	103.4(2)		

Symmetry transformations used to generate equivalent atoms:
#1 -x+2,-y+2,-z

Anisotropic displacement parameters ($Å^2 x\ 10^3$) for **I**. The anisotropic displacement factor exponent takes the form: $-2\pi^2[\ h^2\ a^{*2}U^{11} + ...\ + 2\ h\ k\ a^*\ b^*\ U^{12}\ ]$

	U^{11}	U^{22}	U^{33}	U^{23}	U^{13}	U^{12}
C(1)	39(4)	64(5)	67(5)	-25(4)	4(3)	2(3)
C(2)	91(6)	49(4)	77(5)	20(4)	-21(5)	-26(4)
C(3)	106(7)	153(9)	62(5)	-71(6)	27(5)	-74(7)
C(4)	60(4)	37(3)	52(4)	-6(3)	-36(3)	-2(3)
C(5)	68(5)	84(5)	46(4)	-4(4)	-2(3)	-46(4)
C(6)	53(4)	68(5)	63(4)	-41(4)	-19(3)	-1(3)
C(7)	38(3)	33(3)	56(4)	-16(3)	-19(3)	-5(2)

C(8)	33(3)	37(3)	60(4)	-15(3)	-14(3)	-8(2)
C(9)	48(4)	80(5)	41(4)	-22(3)	-2(3)	-9(4)
C(10)	30(3)	40(3)	48(3)	-20(3)	0(2)	-7(2)
C(11)	66(4)	59(4)	30(3)	-12(3)	-2(3)	-18(3)
C(12)	24(3)	48(4)	61(4)	-24(3)	3(3)	-8(3)
O(1)	34(2)	44(2)	28(2)	-19(2)	4(2)	-13(2)
O(2)	31(2)	26(2)	31(2)	-1(2)	-14(2)	0(2)
O(3)	39(2)	25(2)	39(2)	-11(2)	3(2)	-14(2)
O(4)	21(2)	33(2)	40(2)	-10(2)	3(2)	-9(2)
O(5)	29(2)	28(2)	28(2)	-7(2)	-3(1)	-2(2)
O(6)	29(2)	23(2)	32(2)	-4(2)	-9(2)	-5(1)
O(7)	23(2)	27(2)	36(2)	-9(2)	0(1)	-6(2)
O(8)	23(2)	41(2)	29(2)	-14(2)	0(1)	-9(2)
O(9)	38(2)	26(2)	26(2)	-6(2)	0(2)	-11(2)
O(10)	28(2)	36(2)	25(2)	-4(2)	-3(1)	-10(2)
Si(1)	22(1)	25(1)	19(1)	-8(1)	0(1)	-5(1)
Si(2)	20(1)	23(1)	20(1)	-2(1)	-5(1)	-2(1)
Si(3)	23(1)	18(1)	24(1)	-5(1)	-1(1)	-6(1)
Si(4)	17(1)	25(1)	21(1)	-7(1)	1(1)	-5(1)
Sn(1)	45(1)	45(1)	27(1)	-11(1)	6(1)	-16(1)
Sn(2)	34(1)	28(1)	28(1)	-5(1)	-15(1)	-5(1)
Sn(3)	27(1)	28(1)	29(1)	-3(1)	-5(1)	-11(1)
Sn(4)	22(1)	34(1)	33(1)	-10(1)	3(1)	-7(1)

Hydrogen coordinates (x 10^4) and isotropic displacement parameters ($Å^2$x 10^3) for **I**.

	x	y	z	U(eq)
H(1A)	5873	12709	3224	91
H(1B)	5336	11520	4012	91
H(1C)	6081	11492	2832	91
H(2A)	8507	8457	4310	120
H(2B)	7230	8679	5127	120

H(2C)	8529	8593	5464	120
H(3A)	8571	12505	4599	139
H(3B)	8730	11205	5600	139
H(3C)	7384	12221	5483	139
H(4A)	15086	5501	3369	74
H(4B)	14715	4230	4193	74
H(4C)	14021	5587	4394	74
H(5A)	11138	5329	4483	97
H(5B)	11509	4029	4174	97
H(5C)	10658	5316	3446	97
H(6A)	13173	5225	948	87
H(6B)	13818	3848	1726	87
H(6C)	14570	4931	1203	87
H(7A)	11152	3157	1357	60
H(7B)	10641	2647	2625	60
H(7C)	11332	3777	2195	60
H(8A)	6859	4986	1232	63
H(8B)	7689	3541	1376	63
H(8C)	7931	4656	274	63
H(9A)	8522	6103	3116	87
H(9B)	8138	4787	3766	87
H(9C)	7222	5943	2984	87
H(10A)	5011	8116	419	58
H(10B)	5143	6969	1543	58
H(10C)	6334	7499	878	58
H(11A)	6239	7885	3585	79
H(11B)	4832	7754	4022	79
H(11C)	5163	9053	3879	79
H(12A)	3238	11215	2059	67
H(12B)	2516	10141	2302	67
H(12C)	3015	10856	1072	67

Appendix B

X-ray Tables for $Si_8O_{20}(SnMe_3)_8 \cdot 4H_2O$ (I•4H$_2$O)

Crystal data and structure refinement for **I•4H$_2$O**.

Identification code	**I•4H$_2$O (CSD – 279730)**	
Empirical formula	C24 H80 O24 Si8 Sn8	
Formula weight	1927.12	
Temperature	293(2) K	
Wavelength	0.71073 Å	
Crystal system	Triclinic	
Space group	P-1	
Unit cell dimensions	a = 11.2046(6) Å	α= 86.6650(10)°.
	b = 12.0644(6) Å	β= 81.8930(10)°.
	c = 12.3545(6) Å	γ = 85.4890(10)°.
Volume	1646.35(14) Å^3	
Z	1	
Density (calculated)	1.944 Mg/m^3	
Absorption coefficient	3.187 mm^{-1}	
F(000)	928	
Crystal size	0.5 x 0.4 x 0.4 mm^3	
Theta range for data collection	1.67 to 28.28°.	
Index ranges	-14<=h<=14, -15<=k<=16, -15<=l<=16	
Reflections collected	17832	
Independent reflections	7705 [R(int) = 0.0240]	
Completeness to theta = 28.28°	94.4 %	
Refinement method	Full-matrix least-squares on F^2	
Data / restraints / parameters	7705 / 5 / 317	
Goodness-of-fit on F^2	1.135	
Final R indices [I>2sigma(I)]	R1 = 0.0243, wR2 = 0.0634	
R indices (all data)	R1 = 0.0267, wR2 = 0.0647	
Largest diff. peak and hole	0.363 and -1.802 e.Å^{-3}	

Atomic coordinates (x 10^4) and equivalent isotropic displacement parameters (Å^{2}x 10^3) for **I•4H$_2$O**. U(eq) is defined as one third of the trace of the orthogonalized U^{ij} tensor.

	x	y	z	U(eq)
Sn(1)	414(1)	7301(1)	1781(1)	41(1)
Sn(2)	6883(1)	3219(1)	3852(1)	39(1)
Sn(3)	5723(1)	8900(1)	2196(1)	35(1)
Sn(4)	1666(1)	2275(1)	2783(1)	44(1)
Si(4)	2974(1)	5841(1)	1149(1)	27(1)
Si(2)	3756(1)	3377(1)	1037(1)	27(1)
Si(1)	6461(1)	3878(1)	1309(1)	26(1)
Si(3)	5673(1)	6353(1)	1422(1)	27(1)
O(9)	6380(2)	5161(1)	1654(1)	34(1)
O(10)	7051(2)	3076(1)	2187(1)	36(1)
O(5)	1970(2)	6450(2)	2005(1)	37(1)
O(4)	2768(1)	6228(1)	-96(1)	34(1)
O(6)	3253(2)	2363(1)	1817(1)	37(1)
O(1)	5764(2)	7184(1)	2352(1)	37(1)
O(2)	6240(2)	6874(1)	238(1)	34(1)
O(7)	2906(1)	4505(1)	1307(1)	35(1)
O(3)	4287(1)	6138(1)	1362(1)	36(1)
O(8)	5113(1)	3544(1)	1237(1)	35(1)
C(1)	7420(3)	9114(3)	1260(4)	70(1)
C(2)	4168(3)	9177(3)	1389(4)	70(1)
C(3)	5588(5)	9098(3)	3889(3)	88(1)
C(6)	4980(3)	3489(3)	4183(3)	63(1)
C(5)	7771(3)	1646(3)	4192(3)	68(1)
C(12)	944(3)	8679(3)	748(3)	67(1)
C(4)	7884(4)	4608(4)	3957(3)	74(1)
C(7)	1456(4)	3704(4)	3730(3)	85(1)
C(10)	-545(4)	6104(4)	1149(4)	84(1)
C(9)	1955(5)	783(4)	3712(4)	106(2)

C(8)	421(4)	2221(6)	1653(4)	118(2)
C(11)	-252(5)	7704(5)	3418(4)	111(2)
O(11)	6597(3)	3196(3)	6141(2)	86(1)
O(12)	5562(3)	1101(2)	2147(3)	82(1)

Bond lengths [Å] and angles [°] for **I•4H_2O**.

Sn(1)-O(5)	1.9978(15)	Si(1)-O(8)	1.6095(16)
Sn(1)-C(12)	2.108(3)	Si(1)-O(9)	1.6211(16)
Sn(1)-C(10)	2.112(4)	Si(1)-O(4)#1	1.6277(17)
Sn(1)-C(11)	2.125(4)	Si(3)-O(1)	1.5872(16)
Sn(2)-O(10)	2.0549(16)	Si(3)-O(3)	1.6066(17)
Sn(2)-C(4)	2.108(4)	Si(3)-O(9)	1.6176(16)
Sn(2)-C(6)	2.117(3)	Si(3)-O(2)	1.6216(17)
Sn(2)-C(5)	2.120(3)	O(4)-Si(1)#1	1.6277(17)
Sn(3)-O(1)	2.0648(16)	O(2)-Si(2)#1	1.6211(16)
Sn(3)-C(3)	2.102(3)	O(5)-Sn(1)-C(12)	104.17(11)
Sn(3)-C(1)	2.108(3)	O(5)-Sn(1)-C(10)	102.72(13)
Sn(3)-C(2)	2.122(3)	C(12)-Sn(1)-C(10)	118.00(17)
Sn(4)-O(6)	2.0032(16)	O(5)-Sn(1)-C(11)	100.29(15)
Sn(4)-C(9)	2.107(4)	C(12)-Sn(1)-C(11)	114.1(2)
Sn(4)-C(8)	2.115(4)	C(10)-Sn(1)-C(11)	114.4(2)
Sn(4)-C(7)	2.118(4)	O(10)-Sn(2)-C(4)	101.42(12)
Si(4)-O(5)	1.5966(16)	O(10)-Sn(2)-C(6)	98.94(10)
Si(4)-O(3)	1.6015(17)	C(4)-Sn(2)-C(6)	116.28(17)
Si(4)-O(7)	1.6194(17)	O(10)-Sn(2)-C(5)	95.87(11)
Si(4)-O(4)	1.6241(16)	C(4)-Sn(2)-C(5)	115.67(17)
Si(2)-O(6)	1.6001(16)	C(6)-Sn(2)-C(5)	121.29(16)
Si(2)-O(8)	1.6040(16)	O(1)-Sn(3)-C(3)	94.15(12)
Si(2)-O(7)	1.6204(16)	O(1)-Sn(3)-C(1)	100.48(11)
Si(2)-O(2)#1	1.6210(16)	C(3)-Sn(3)-C(1)	117.00(19)
Si(1)-O(10)	1.5902(15)	O(1)-Sn(3)-C(2)	98.00(11)
		C(3)-Sn(3)-C(2)	120.2(2)
		C(1)-Sn(3)-C(2)	117.72(17)
		O(6)-Sn(4)-C(9)	101.88(15)

O(6)-Sn(4)-C(8)	103.11(15)	O(9)-Si(1)-O(4)#1	109.33(9)
C(9)-Sn(4)-C(8)	115.1(3)	O(1)-Si(3)-O(3)	110.75(10)
O(6)-Sn(4)-C(7)	106.05(13)	O(1)-Si(3)-O(9)	111.20(9)
C(9)-Sn(4)-C(7)	113.1(2)	O(3)-Si(3)-O(9)	107.61(9)
C(8)-Sn(4)-C(7)	115.6(2)	O(1)-Si(3)-O(2)	110.27(9)
O(5)-Si(4)-O(3)	109.43(10)	O(3)-Si(3)-O(2)	107.83(9)
O(5)-Si(4)-O(7)	110.08(9)	O(9)-Si(3)-O(2)	109.07(9)
O(3)-Si(4)-O(7)	108.17(9)	Si(3)-O(9)-Si(1)	140.94(11)
O(5)-Si(4)-O(4)	110.45(9)	Si(1)-O(10)-Sn(2)	128.23(10)
O(3)-Si(4)-O(4)	109.87(9)	Si(4)-O(5)-Sn(1)	130.40(10)
O(7)-Si(4)-O(4)	108.80(9)	Si(4)-O(4)-Si(1)#1	136.35(10)
O(6)-Si(2)-O(8)	109.07(9)	Si(2)-O(6)-Sn(4)	129.26(10)
O(6)-Si(2)-O(7)	109.82(9)	Si(3)-O(1)-Sn(3)	127.15(9)
O(8)-Si(2)-O(7)	109.85(9)	Si(2)#1-O(2)-Si(3)	137.21(11)
O(6)-Si(2)-O(2)#1	110.70(9)	Si(4)-O(7)-Si(2)	139.28(11)
O(8)-Si(2)-O(2)#1	108.78(9)	Si(4)-O(3)-Si(3)	172.13(12)
O(7)-Si(2)-O(2)#1	108.60(9)	Si(2)-O(8)-Si(1)	171.10(12)
O(10)-Si(1)-O(8)	109.90(9)		
O(10)-Si(1)-O(9)	110.64(9)		
O(8)-Si(1)-O(9)	108.17(9)		
O(10)-Si(1)-O(4)#1	111.19(9)		
O(8)-Si(1)-O(4)#1	107.51(9)		

Symmetry transformations used to generate equivalent atoms:
#1 -x+1,-y+1,-z

Anisotropic displacement parameters ($Å^2 x\ 10^3$) for **I•4H$_2$O**. The anisotropic displacement factor exponent takes the form: $-2\pi^2[\ h^2\ a^{*2}U^{11} + ...\ + 2\ h\ k\ a^*\ b^*\ U^{12}\ ]$

	U^{11}	U^{22}	U^{33}	U^{23}	U^{13}	U^{12}
Sn(1)	30(1)	44(1)	45(1)	0(1)	0(1)	8(1)
Sn(2)	41(1)	45(1)	32(1)	1(1)	-10(1)	1(1)
Sn(3)	39(1)	31(1)	36(1)	-6(1)	-6(1)	-3(1)
Sn(4)	41(1)	52(1)	36(1)	6(1)	3(1)	-10(1)
Si(4)	24(1)	28(1)	26(1)	-1(1)	-1(1)	4(1)

Si(2)	28(1)	25(1)	27(1)	2(1)	-2(1)	-3(1)
Si(1)	27(1)	26(1)	25(1)	1(1)	-6(1)	2(1)
Si(3)	30(1)	25(1)	26(1)	-4(1)	-6(1)	-1(1)
O(9)	37(1)	29(1)	39(1)	-5(1)	-12(1)	2(1)
O(10)	42(1)	35(1)	30(1)	2(1)	-11(1)	10(1)
O(5)	34(1)	45(1)	30(1)	-3(1)	1(1)	12(1)
O(4)	32(1)	41(1)	27(1)	1(1)	-3(1)	5(1)
O(6)	38(1)	30(1)	39(1)	6(1)	4(1)	-5(1)
O(1)	53(1)	30(1)	30(1)	-7(1)	-10(1)	-3(1)
O(2)	38(1)	36(1)	29(1)	-2(1)	-4(1)	-8(1)
O(7)	33(1)	29(1)	39(1)	0(1)	1(1)	-1(1)
O(3)	30(1)	39(1)	40(1)	-4(1)	-7(1)	-2(1)
O(8)	30(1)	39(1)	36(1)	2(1)	-6(1)	-6(1)
C(1)	50(2)	58(2)	99(3)	2(2)	8(2)	-8(2)
C(2)	56(2)	53(2)	108(3)	-6(2)	-39(2)	7(2)
C(3)	162(5)	63(2)	41(2)	-16(2)	-3(2)	-35(3)
C(6)	47(2)	89(3)	49(2)	-1(2)	2(1)	7(2)
C(5)	82(2)	66(2)	53(2)	16(2)	-18(2)	18(2)
C(12)	60(2)	53(2)	88(3)	22(2)	-21(2)	-4(2)
C(4)	85(3)	88(3)	57(2)	-11(2)	-14(2)	-36(2)
C(7)	93(3)	87(3)	67(2)	-23(2)	26(2)	-4(2)
C(10)	71(2)	73(3)	114(4)	9(2)	-31(2)	-27(2)
C(9)	138(4)	73(3)	89(3)	41(2)	26(3)	0(3)
C(8)	62(3)	223(7)	77(3)	-23(4)	-20(2)	-28(3)
C(11)	99(3)	152(5)	66(3)	-28(3)	22(2)	47(3)
O(11)	85(2)	140(3)	33(1)	-14(1)	0(1)	-19(2)
O(12)	78(2)	30(1)	142(3)	4(1)	-34(2)	2(1)

Hydrogen coordinates (x 10^4) and isotropic displacement parameters ($Å^2$x 10^3) for **I•4H_2O**.

	x	y	z	U(eq)
H(1A)	7844	8399	1136	105
H(1B)	7883	9553	1648	105
H(1C)	7307	9487	570	105
H(2A)	4371	8982	639	105
H(2B)	3884	9948	1416	105
H(2C)	3546	8726	1746	105
H(3A)	4808	8898	4238	131
H(3B)	5686	9860	4018	131
H(3C)	6206	8627	4184	131
H(6A)	4725	4170	3813	95
H(6B)	4742	3539	4957	95
H(6C)	4609	2881	3928	95
H(5A)	8185	1355	3523	102
H(5B)	7186	1143	4521	102
H(5C)	8344	1727	4686	102
H(12A)	1474	9093	1090	101
H(12B)	242	9150	618	101
H(12C)	1358	8424	64	101
H(4A)	8671	4491	3541	111
H(4B)	7965	4702	4708	111
H(4C)	7471	5263	3668	111
H(7A)	2179	3767	4050	128
H(7B)	785	3636	4300	128
H(7C)	1309	4355	3269	128
H(10A)	-166	5936	426	126
H(10B)	-1363	6394	1121	126
H(10C)	-542	5438	1614	126
H(9A)	2676	378	3387	159
H(9B)	1278	339	3726	159

H(9C)	2042	951	4446	159
H(8A)	806	2415	930	177
H(8B)	-260	2740	1846	177
H(8C)	152	1484	1670	177
H(11A)	218	7279	3910	167
H(11B)	-1082	7532	3585	167
H(11C)	-193	8484	3499	167
H(1)	5930(20)	3150(40)	6560(30)	97(16)
H(2)	7010(40)	3240(40)	6670(30)	107(17)
H(4)	4910(30)	1510(40)	2270(50)	160(30)
H(3)	6030(30)	1610(30)	2110(40)	97(16)

Appendix C

X-ray Tables for $Si_{10}O_{25}(SnMe_3)_{10}•4H_2O$ (II)

Crystal data and structure refinement for $Si_{10}O_{25}(SnMe_3)_{10}•4H_2O$ (**II**)

Identification code	**II (CSD – 279728)**	
Empirical formula	C30 H98 O24 Si10 Sn10	
Formula weight	2390.88	
Temperature	173(2) K	
Wavelength	0.71073 Å	
Crystal system	Orthorhombic	
Space group	P b c a	
Unit cell dimensions	a = 21.834(5) Å	α= 90°.
	b = 26.567(7) Å	β= 90°.
	c = 28.037(7) Å	γ = 90°.
Volume	16264(7) $Å^3$	
Z	8	
Density (calculated)	1.953 Mg/m^3	
Absorption coefficient	3.224 mm^{-1}	
F(000)	9200	
Crystal size	0.20 x 0.15 x 0.10 mm^3	
Theta range for data collection	1.41 to 23.27°.	
Index ranges	-23<=h<=24, -29<=k<=29, -31<=l<=31	
Reflections collected	120540	
Independent reflections	11673 [R(int) = 0.0641]	
Completeness to theta = 23.27°	99.7 %	
Absorption correction	Semi-empirical from equivalents	
Max. and min. transmission	0.7244 and 0.5246	
Refinement method	Full-matrix least-squares on F^2	
Data / restraints / parameters	11673 / 16 / 806	
Goodness-of-fit on F^2	1.216	
Final R indices [I>2sigma(I)]	R1 = 0.0323, wR2 = 0.0790	
R indices (all data)	R1 = 0.0637, wR2 = 0.1137	
Largest diff. peak and hole	2.547 and -0.888 $e.Å^{-3}$	

Atomic coordinates (x 10^4) and equivalent isotropic displacement parameters ($Å^2$x 10^3) for **II**. U(eq) is defined as one third of the trace of the orthogonalized U^{ij} tensor.

	x	y	z	U(eq)
C(27)	-2250(6)	1008(4)	-254(4)	64(3)
Sn(9)	-2266(1)	1758(1)	48(2)	39(1)
C(33)	-2449(8)	1746(7)	807(7)	75(6)
C(35)	-2671(7)	2331(6)	-368(7)	70(6)
Sn(12)	-2194(2)	1765(1)	-218(4)	34(2)
C(34)	-2700(30)	2000(30)	388(18)	150(30)
C(36)	-2100(20)	2092(15)	-919(15)	94(19)
C(25)	-586(5)	4067(4)	2791(3)	54(3)
Sn(10)	-1119(2)	4109(3)	2178(1)	38(1)
C(32)	-1709(19)	3490(16)	2021(15)	108(14)
C(30)	-1540(20)	4804(11)	2010(15)	103(13)
Sn(11)	-929(2)	4380(2)	2147(1)	42(1)
C(29)	-707(17)	5148(7)	2058(7)	124(13)
C(31)	-1840(9)	4235(18)	1943(8)	170(20)
Sn(7)	-1175(1)	712(1)	1587(1)	42(1)
C(18)	-1252(7)	564(5)	847(4)	69(4)
C(21)	-2005(6)	701(6)	1966(5)	87(5)
C(22)	-491(8)	318(6)	1969(6)	97(5)
Sn(14)	-1633(6)	1036(5)	1461(5)	37(4)
C(1)	841(5)	4710(3)	125(3)	39(2)
C(2)	-71(5)	4348(4)	-935(4)	52(3)
C(3)	1587(4)	4368(4)	-998(3)	46(3)
C(4)	831(5)	2891(4)	3227(3)	46(3)
C(5)	2799(5)	4340(4)	1769(4)	58(3)
C(6)	1541(6)	3814(5)	2388(4)	67(3)
C(7)	2766(6)	1574(5)	1760(5)	79(4)
C(8)	2331(5)	385(5)	914(5)	75(4)
C(9)	793(6)	-24(5)	979(5)	84(4)

C(10)	1394(7)	691(5)	1932(4)	83(4)
C(11)	-509(5)	1531(4)	-989(4)	45(2)
C(12)	84(6)	786(4)	-42(4)	68(4)
C(13)	947(6)	889(4)	-1108(4)	62(3)
C(14)	688(5)	1572(4)	2855(4)	58(3)
C(15)	-419(5)	2080(4)	3650(3)	47(3)
C(16)	-2409(5)	3242(4)	808(5)	68(3)
C(17)	-2285(4)	4513(4)	418(4)	52(3)
C(23)	2469(7)	2147(7)	2905(4)	112(7)
C(24)	3258(7)	2856(6)	2028(10)	184(13)
C(26)	-1904(6)	3523(5)	-436(4)	71(4)
C(28)	1302(6)	4883(5)	1651(5)	76(4)
O(1)	740(2)	2544(2)	2043(2)	30(1)
O(2)	162(3)	1515(2)	1194(2)	32(1)
O(3)	561(3)	3699(2)	1367(2)	36(2)
O(4)	-220(2)	2111(2)	76(2)	31(1)
O(5)	-96(3)	3440(2)	187(2)	32(1)
O(6)	-992(3)	2800(2)	379(2)	31(1)
O(7)	817(2)	1996(2)	541(2)	28(1)
O(8)	-826(2)	1979(2)	876(2)	31(1)
O(9)	-318(3)	2271(2)	1670(2)	32(1)
O(10)	1226(3)	1930(2)	1421(2)	32(1)
O(11)	1224(3)	2885(2)	1251(2)	36(2)
O(12)	-158(3)	3195(2)	1962(2)	30(1)
O(13)	1035(3)	3468(2)	521(2)	34(1)
O(14)	-460(3)	3296(2)	1063(2)	32(1)
O(15)	1733(3)	3798(2)	1214(2)	36(2)
O(16)	-465(3)	4089(2)	1637(2)	35(2)
O(17)	830(3)	3645(2)	-390(2)	27(1)
O(18)	-1176(3)	3781(2)	460(2)	32(1)
O(19)	-1381(3)	1925(2)	43(2)	35(1)
O(20)	756(3)	1819(2)	-389(2)	32(1)
O(21)	-896(3)	1417(2)	1646(2)	36(2)
O(22)	1195(3)	1134(2)	858(2)	34(1)

O(23)	-223(2)	2463(2)	2595(2)	31(1)
O(24)	701(3)	2742(2)	-61(2)	29(1)
O(25)	1934(3)	2524(3)	1946(2)	46(2)
O(26)	999(4)	2021(3)	3887(3)	65(2)
O(27)	3750(3)	1877(3)	2467(3)	51(2)
O(28)	6764(3)	3728(3)	10041(3)	49(2)
O(30)	4287(3)	4668(3)	4183(2)	48(2)
Si(11)	616(1)	3335(1)	64(1)	23(1)
Si(12)	849(1)	1645(1)	1006(1)	26(1)
Si(13)	-133(1)	3570(1)	1505(1)	23(1)
Si(14)	511(1)	2171(1)	42(1)	21(1)
Si(15)	1152(1)	3460(1)	1088(1)	26(1)
Si(16)	-689(1)	3338(1)	517(1)	24(1)
Si(17)	-869(1)	2203(1)	343(1)	24(1)
Si(18)	9(1)	2614(1)	2078(1)	25(1)
Si(19)	-471(1)	1797(1)	1346(1)	25(1)
Si(20)	1305(1)	2475(1)	1674(1)	27(1)
Sn(1)	781(1)	4403(1)	-573(1)	27(1)
Sn(2)	1836(1)	4230(1)	1780(1)	39(1)
Sn(3)	311(1)	2224(1)	3174(1)	28(1)
Sn(4)	1444(1)	512(1)	1201(1)	35(1)
Sn(5)	2733(1)	2231(1)	2187(1)	37(1)
Sn(6)	-2092(1)	3744(1)	273(1)	32(1)
Sn(8)	281(1)	1230(1)	-655(1)	39(1)

Bond lengths [Å] and angles [°] for **II**.

O(27)-H(27D)	0.84(2)	C(1)-H(1A)	0.9800
O(27)-H(27E)	0.84(2)	C(1)-H(1B)	0.9800
Sn(14)-O(21)	1.971(15)	C(1)-H(1C)	0.9800
C(1)-Sn(1)	2.126(9)	C(2)-Sn(1)	2.125(9)
		C(2)-H(2A)	0.9800
		C(2)-H(2B)	0.9800
		C(2)-H(2C)	0.9800

C(3)-Sn(1)	2.127(9)	C(11)-H(11B)	0.9800
C(3)-H(3A)	0.9800	C(11)-H(11C)	0.9800
C(3)-H(3B)	0.9800	C(12)-Sn(8)	2.130(10)
C(3)-H(3C)	0.9800	C(12)-H(12A)	0.9800
C(4)-Sn(3)	2.110(9)	C(12)-H(12B)	0.9800
C(4)-H(4A)	0.9800	C(12)-H(12C)	0.9800
C(4)-H(4B)	0.9800	C(13)-Sn(8)	2.134(11)
C(4)-H(4C)	0.9800	C(13)-H(13A)	0.9800
C(5)-Sn(2)	2.123(10)	C(13)-H(13B)	0.9800
C(5)-H(5A)	0.9800	C(13)-H(13C)	0.9800
C(5)-H(5B)	0.9800	C(14)-Sn(3)	2.116(10)
C(5)-H(5C)	0.9800	C(14)-H(14A)	0.9800
C(6)-Sn(2)	2.130(10)	C(14)-H(14B)	0.9800
C(6)-H(6A)	0.9800	C(14)-H(14C)	0.9800
C(6)-H(6B)	0.9800	C(15)-Sn(3)	2.114(9)
C(6)-H(6C)	0.9800	C(15)-H(15A)	0.9800
C(7)-Sn(5)	2.118(11)	C(15)-H(15B)	0.9800
C(7)-H(7A)	0.9800	C(15)-H(15C)	0.9800
C(7)-H(7B)	0.9800	C(16)-Sn(6)	2.123(11)
C(7)-H(7C)	0.9800	C(16)-H(16A)	0.9800
C(8)-Sn(4)	2.125(11)	C(16)-H(16B)	0.9800
C(8)-H(8A)	0.9800	C(16)-H(16C)	0.9800
C(8)-H(8B)	0.9800	C(17)-Sn(6)	2.125(9)
C(8)-H(8C)	0.9800	C(17)-H(17A)	0.9800
C(9)-Sn(4)	2.105(12)	C(17)-H(17B)	0.9800
C(9)-H(9A)	0.9800	C(17)-H(17C)	0.9800
C(9)-H(9B)	0.9800	C(18)-Sn(7)	2.120(11)
C(9)-H(9C)	0.9800	C(18)-H(18A)	0.9800
C(10)-Sn(4)	2.107(11)	C(18)-H(18B)	0.9800
C(10)-H(10A)	0.9800	C(18)-H(18C)	0.9800
C(10)-H(10B)	0.9800	C(21)-Sn(7)	2.099(12)
C(10)-H(10C)	0.9800	C(21)-H(21A)	0.9800
C(11)-Sn(8)	2.120(10)	C(21)-H(21B)	0.9800
C(11)-H(11A)	0.9800	C(21)-H(21C)	0.9800

C(22)-Sn(7)	2.114(14)	C(31)-H(31B)	0.9800
C(22)-H(22A)	0.9800	C(31)-H(31C)	0.9800
C(22)-H(22B)	0.9800	C(32)-Sn(10)	2.13(4)
C(22)-H(22C)	0.9800	C(32)-H(32A)	0.9800
C(23)-Sn(5)	2.105(11)	C(32)-H(32B)	0.9800
C(23)-H(23A)	0.9800	C(32)-H(32C)	0.9800
C(23)-H(23B)	0.9800	C(33)-Sn(9)	2.167(18)
C(23)-H(23C)	0.9800	C(33)-H(33A)	0.9800
C(24)-Sn(5)	2.067(15)	C(33)-H(33B)	0.9800
C(24)-H(24A)	0.9800	C(33)-H(33C)	0.9800
C(24)-H(24B)	0.9800	C(35)-Sn(9)	2.111(16)
C(24)-H(24C)	0.9800	C(35)-H(35A)	0.9800
C(25)-Sn(10)	2.079(10)	C(35)-H(35B)	0.9800
C(25)-H(25A)	0.9800	C(35)-H(35C)	0.9800
C(25)-H(25B)	0.9800	C(36)-Sn(12)	2.16(4)
C(25)-H(25C)	0.9800	C(36)-H(36A)	0.9800
C(26)-Sn(6)	2.111(11)	C(36)-H(36B)	0.9800
C(26)-H(26A)	0.9800	C(36)-H(36C)	0.9800
C(26)-H(26B)	0.9800	O(1)-Si(18)	1.610(6)
C(26)-H(26C)	0.9800	O(1)-Si(20)	1.620(6)
C(27)-Sn(9)	2.165(11)	O(2)-Si(12)	1.627(6)
C(27)-H(27A)	0.9800	O(2)-Si(19)	1.629(6)
C(27)-H(27B)	0.9800	O(3)-Si(13)	1.603(6)
C(27)-H(27C)	0.9800	O(3)-Si(15)	1.636(6)
C(28)-Sn(2)	2.122(12)	O(4)-Si(14)	1.608(6)
C(28)-H(28A)	0.9800	O(4)-Si(17)	1.619(6)
C(28)-H(28B)	0.9800	O(5)-Si(16)	1.614(6)
C(28)-H(28C)	0.9800	O(5)-Si(11)	1.617(6)
C(29)-Sn(11)	2.11(2)	O(6)-Si(17)	1.612(6)
C(29)-H(29A)	0.9800	O(6)-Si(16)	1.622(6)
C(29)-H(29B)	0.9800	O(7)-Si(12)	1.604(6)
C(29)-H(29C)	0.9800	O(7)-Si(14)	1.619(6)
C(31)-Sn(11)	2.11(2)	O(8)-Si(19)	1.604(6)
C(31)-H(31A)	0.9800	O(8)-Si(17)	1.611(6)

O(9)-Si(19)	1.588(6)	O(25)-Si(20)	1.576(6)
O(9)-Si(18)	1.627(6)	O(25)-Sn(5)	2.026(6)
O(10)-Si(12)	1.616(6)	O(26)-H(26D)	0.84(2)
O(10)-Si(20)	1.622(6)	O(26)-H(26E)	0.85(2)
O(11)-Si(15)	1.602(6)	Sn(10)-C(30)	2.118(18)
O(11)-Si(20)	1.621(6)	Sn(12)-C(34)	2.12(2)
O(12)-Si(18)	1.619(6)	O(28)-H(28D)	0.83(2)
O(12)-Si(13)	1.623(6)	O(28)-H(28E)	0.83(2)
O(13)-Si(15)	1.610(6)	O(30)-H(30A)	0.84(2)
O(13)-Si(11)	1.616(6)	O(30)-H(30B)	0.84(2)
O(14)-Si(13)	1.607(6)	C(30)-H(30C)	0.9800
O(14)-Si(16)	1.611(6)	C(30)-H(30D)	0.9800
O(15)-Si(15)	1.594(6)	C(30)-H(30E)	0.9800
O(15)-Sn(2)	1.973(6)	C(34)-H(34A)	0.9800
O(16)-Si(13)	1.600(6)	C(34)-H(34B)	0.9800
O(16)-Sn(11)	1.914(6)	C(34)-H(34C)	0.9800
O(16)-Sn(10)	2.082(7)	H(27D)-O(27)-H(27E)	92(5)
O(17)-Si(11)	1.587(5)	Si(18)-O(1)-Si(20)	143.7(4)
O(17)-Sn(1)	2.081(5)	Si(12)-O(2)-Si(19)	140.3(4)
O(18)-Si(16)	1.595(6)	Si(13)-O(3)-Si(15)	141.1(4)
O(18)-Sn(6)	2.070(5)	Si(14)-O(4)-Si(17)	151.8(4)
O(19)-Si(17)	1.582(6)	Si(16)-O(5)-Si(11)	149.8(4)
O(19)-Sn(12)	1.966(6)	Si(17)-O(6)-Si(16)	144.5(4)
O(19)-Sn(9)	1.984(6)	Si(12)-O(7)-Si(14)	152.5(4)
O(20)-Si(14)	1.618(6)	Si(19)-O(8)-Si(17)	154.4(4)
O(20)-Sn(8)	2.018(6)	Si(19)-O(9)-Si(18)	159.7(4)
O(21)-Si(19)	1.608(6)	Si(12)-O(10)-Si(20)	142.0(4)
O(21)-Sn(7)	1.976(6)	Si(15)-O(11)-Si(20)	149.3(4)
O(22)-Si(12)	1.608(6)	Si(18)-O(12)-Si(13)	137.4(4)
O(22)-Sn(4)	1.989(5)	Si(15)-O(13)-Si(11)	150.6(4)
O(23)-Si(18)	1.587(5)	Si(13)-O(14)-Si(16)	147.1(4)
O(23)-Sn(3)	2.096(5)	Si(15)-O(15)-Sn(2)	126.6(3)
O(24)-Si(14)	1.599(6)	Si(13)-O(16)-Sn(11)	139.4(4)
O(24)-Si(11)	1.623(6)	Si(13)-O(16)-Sn(10)	120.0(4)

Sn(11)-O(16)-Sn(10)	23.63(10)	O(24)-Si(14)-O(20)	109.2(3)
Si(11)-O(17)-Sn(1)	133.3(3)	O(4)-Si(14)-O(20)	108.4(3)
Si(16)-O(18)-Sn(6)	129.4(3)	O(24)-Si(14)-O(7)	108.6(3)
Si(17)-O(19)-Sn(12)	159.5(4)	O(4)-Si(14)-O(7)	109.2(3)
Si(17)-O(19)-Sn(9)	142.2(4)	O(20)-Si(14)-O(7)	110.1(3)
Sn(12)-O(19)-Sn(9)	22.24(19)	O(15)-Si(15)-O(11)	113.3(3)
Si(14)-O(20)-Sn(8)	123.6(3)	O(15)-Si(15)-O(13)	109.6(3)
Si(19)-O(21)-Sn(14)	131.1(5)	O(11)-Si(15)-O(13)	108.0(3)
Si(19)-O(21)-Sn(7)	136.8(4)	O(15)-Si(15)-O(3)	107.6(3)
Sn(14)-O(21)-Sn(7)	40.5(4)	O(11)-Si(15)-O(3)	108.3(3)
Si(12)-O(22)-Sn(4)	134.9(4)	O(13)-Si(15)-O(3)	110.0(3)
Si(18)-O(23)-Sn(3)	127.4(3)	O(18)-Si(16)-O(14)	110.6(3)
Si(14)-O(24)-Si(11)	148.4(4)	O(18)-Si(16)-O(5)	110.7(3)
Si(20)-O(25)-Sn(5)	151.6(4)	O(14)-Si(16)-O(5)	107.9(3)
H(26D)-O(26)-H(26E)	91(5)	O(18)-Si(16)-O(6)	110.7(3)
O(17)-Si(11)-O(13)	110.8(3)	O(14)-Si(16)-O(6)	107.0(3)
O(17)-Si(11)-O(5)	111.4(3)	O(5)-Si(16)-O(6)	109.8(3)
O(13)-Si(11)-O(5)	109.7(3)	O(19)-Si(17)-O(8)	111.2(3)
O(17)-Si(11)-O(24)	107.3(3)	O(19)-Si(17)-O(6)	112.0(3)
O(13)-Si(11)-O(24)	108.5(3)	O(8)-Si(17)-O(6)	108.4(3)
O(5)-Si(11)-O(24)	109.0(3)	O(19)-Si(17)-O(4)	107.6(3)
O(7)-Si(12)-O(22)	107.7(3)	O(8)-Si(17)-O(4)	108.8(3)
O(7)-Si(12)-O(10)	109.6(3)	O(6)-Si(17)-O(4)	108.8(3)
O(22)-Si(12)-O(10)	109.9(3)	O(23)-Si(18)-O(1)	110.0(3)
O(7)-Si(12)-O(2)	110.3(3)	O(23)-Si(18)-O(12)	110.7(3)
O(22)-Si(12)-O(2)	109.7(3)	O(1)-Si(18)-O(12)	108.8(3)
O(10)-Si(12)-O(2)	109.6(3)	O(23)-Si(18)-O(9)	111.1(3)
O(16)-Si(13)-O(3)	107.5(3)	O(1)-Si(18)-O(9)	109.1(3)
O(16)-Si(13)-O(14)	111.6(3)	O(12)-Si(18)-O(9)	107.1(3)
O(3)-Si(13)-O(14)	109.2(3)	O(9)-Si(19)-O(8)	109.4(3)
O(16)-Si(13)-O(12)	109.4(3)	O(9)-Si(19)-O(21)	108.7(3)
O(3)-Si(13)-O(12)	110.7(3)	O(8)-Si(19)-O(21)	109.8(3)
O(14)-Si(13)-O(12)	108.5(3)	O(9)-Si(19)-O(2)	109.7(3)
O(24)-Si(14)-O(4)	111.2(3)	O(8)-Si(19)-O(2)	109.4(3)

O(21)-Si(19)-O(2)	109.8(3)	O(25)-Sn(5)-C(7)	99.1(4)
O(25)-Si(20)-O(1)	110.2(3)	C(24)-Sn(5)-C(7)	121.5(9)
O(25)-Si(20)-O(11)	113.2(4)	C(23)-Sn(5)-C(7)	117.5(7)
O(1)-Si(20)-O(11)	108.1(3)	O(18)-Sn(6)-C(26)	93.7(4)
O(25)-Si(20)-O(10)	112.2(3)	O(18)-Sn(6)-C(16)	99.5(4)
O(1)-Si(20)-O(10)	107.4(3)	C(26)-Sn(6)-C(16)	123.6(5)
O(11)-Si(20)-O(10)	105.5(3)	O(18)-Sn(6)-C(17)	95.6(3)
O(17)-Sn(1)-C(2)	95.5(3)	C(26)-Sn(6)-C(17)	119.1(5)
O(17)-Sn(1)-C(1)	98.1(3)	C(16)-Sn(6)-C(17)	113.8(5)
C(2)-Sn(1)-C(1)	121.4(4)	O(21)-Sn(7)-C(21)	103.7(4)
O(17)-Sn(1)-C(3)	93.0(3)	O(21)-Sn(7)-C(22)	102.1(5)
C(2)-Sn(1)-C(3)	117.0(4)	C(21)-Sn(7)-C(22)	110.3(6)
C(1)-Sn(1)-C(3)	118.8(4)	O(21)-Sn(7)-C(18)	106.3(4)
O(15)-Sn(2)-C(28)	106.0(4)	C(21)-Sn(7)-C(18)	115.1(6)
O(15)-Sn(2)-C(5)	100.4(4)	C(22)-Sn(7)-C(18)	117.4(6)
C(28)-Sn(2)-C(5)	115.4(5)	O(20)-Sn(8)-C(11)	106.8(3)
O(15)-Sn(2)-C(6)	107.9(3)	O(20)-Sn(8)-C(12)	103.6(3)
C(28)-Sn(2)-C(6)	113.3(5)	C(11)-Sn(8)-C(12)	113.7(5)
C(5)-Sn(2)-C(6)	112.6(4)	O(20)-Sn(8)-C(13)	101.5(4)
O(23)-Sn(3)-C(4)	95.7(3)	C(11)-Sn(8)-C(13)	116.9(4)
O(23)-Sn(3)-C(15)	97.2(3)	C(12)-Sn(8)-C(13)	112.5(5)
C(4)-Sn(3)-C(15)	120.9(4)	O(19)-Sn(9)-C(35)	104.0(5)
O(23)-Sn(3)-C(14)	97.9(4)	O(19)-Sn(9)-C(27)	100.8(4)
C(4)-Sn(3)-C(14)	120.6(4)	C(35)-Sn(9)-C(27)	117.1(6)
C(15)-Sn(3)-C(14)	114.3(4)	O(19)-Sn(9)-C(33)	100.9(5)
O(22)-Sn(4)-C(9)	103.6(4)	C(35)-Sn(9)-C(33)	118.4(8)
O(22)-Sn(4)-C(10)	105.6(4)	C(27)-Sn(9)-C(33)	111.9(6)
C(9)-Sn(4)-C(10)	114.0(6)	C(25)-Sn(10)-O(16)	102.6(4)
O(22)-Sn(4)-C(8)	101.3(4)	C(25)-Sn(10)-C(30)	118.3(13)
C(9)-Sn(4)-C(8)	113.4(6)	O(16)-Sn(10)-C(30)	99.2(12)
C(10)-Sn(4)-C(8)	116.8(6)	C(25)-Sn(10)-C(32)	117.9(12)
O(25)-Sn(5)-C(24)	95.5(5)	O(16)-Sn(10)-C(32)	104.1(12)
O(25)-Sn(5)-C(23)	97.1(4)	C(30)-Sn(10)-C(32)	111.2(17)
C(24)-Sn(5)-C(23)	116.3(10)	O(16)-Sn(11)-C(31)	102.8(9)

O(16)-Sn(11)-C(29)	100.4(8)	H(28D)-O(28)-H(28E)	94(5)
C(31)-Sn(11)-C(29)	111.1(15)	H(30A)-O(30)-H(30B)	92(5)
O(19)-Sn(12)-C(34)	96(2)		
O(19)-Sn(12)-C(36)	99.3(13)	Symmetry transformations used to	
C(34)-Sn(12)-C(36)	131(3)	generate equivalent atoms:	

Anisotropic displacement parameters ($Å^2 x\ 10^3$) for **II**. The anisotropic displacement factor exponent takes the form: $-2\pi^2[\ h^2\ a^{*2}U^{11} + ... + 2\ h\ k\ a^*\ b^*\ U^{12}\ ]$

	U^{11}	U^{22}	U^{33}	U^{23}	U^{13}	U^{12}
O(27)	31(4)	68(5)	55(4)	10(4)	-16(3)	-7(3)
C(1)	52(6)	27(5)	37(5)	1(4)	-4(5)	-7(5)
C(2)	49(6)	40(6)	66(7)	-12(5)	-23(5)	13(5)
C(3)	49(6)	43(6)	46(6)	6(5)	21(5)	-10(5)
C(4)	54(6)	45(6)	38(5)	1(5)	-5(5)	-15(5)
C(5)	51(7)	56(7)	67(7)	21(6)	-27(6)	-26(6)
C(6)	85(9)	78(9)	37(6)	-2(6)	1(6)	-29(7)
C(7)	62(8)	92(10)	83(9)	-38(8)	-38(7)	22(7)
C(8)	72(9)	63(8)	89(9)	23(7)	20(7)	25(7)
C(9)	94(10)	53(8)	106(11)	21(8)	-19(9)	-11(7)
C(10)	128(13)	80(9)	40(7)	9(6)	11(7)	26(9)
C(11)	48(6)	37(6)	51(6)	-7(5)	-6(5)	-9(5)
C(12)	103(10)	42(7)	58(7)	9(6)	-6(7)	-28(7)
C(13)	90(9)	35(6)	62(7)	-19(5)	0(7)	10(6)
C(14)	71(8)	42(6)	63(7)	11(5)	12(6)	15(6)
C(15)	45(6)	57(7)	39(6)	5(5)	13(5)	-8(5)
C(16)	54(7)	59(8)	90(9)	20(7)	-6(7)	-5(6)
C(17)	32(6)	33(6)	92(8)	-10(6)	-16(5)	3(5)
C(18)	100(11)	60(8)	48(7)	-8(6)	-9(7)	-19(7)
C(21)	76(10)	94(11)	90(10)	-9(9)	33(8)	-41(9)
C(22)	114(13)	72(10)	104(12)	19(9)	-9(10)	29(9)

C(23)	82(10)	220(20)	36(7)	8(9)	8(7)	67(12)
C(24)	55(10)	67(11)	430(40)	90(17)	-26(16)	12(8)
C(25)	67(7)	73(8)	22(5)	9(5)	1(5)	-4(6)
C(26)	62(8)	93(10)	57(7)	-27(7)	-18(6)	25(7)
C(27)	73(8)	40(6)	79(8)	-12(6)	-35(7)	-7(6)
C(28)	78(9)	59(8)	90(10)	1(7)	-5(8)	7(7)
C(29)	290(40)	41(13)	43(12)	-15(10)	-20(18)	36(18)
C(31)	24(12)	420(70)	55(14)	40(20)	0(10)	-10(20)
C(33)	62(12)	75(13)	86(13)	-10(11)	37(10)	-33(10)
C(35)	37(9)	39(9)	134(17)	-4(10)	-42(10)	-2(7)
C(36)	150(50)	50(30)	80(30)	60(20)	-70(30)	-50(30)
O(1)	30(3)	36(3)	24(3)	9(3)	1(3)	3(3)
O(2)	28(3)	30(3)	38(3)	5(3)	2(3)	7(3)
O(3)	31(3)	36(4)	42(4)	-7(3)	2(3)	-5(3)
O(4)	26(3)	30(3)	36(3)	-6(3)	-1(3)	0(3)
O(5)	31(3)	34(3)	30(3)	2(3)	0(3)	5(3)
O(6)	28(3)	29(3)	35(3)	-6(3)	-7(3)	7(3)
O(7)	30(3)	21(3)	32(3)	2(2)	-1(3)	0(3)
O(8)	27(3)	33(3)	35(3)	3(3)	-3(3)	-4(3)
O(9)	40(4)	24(3)	31(3)	2(3)	-5(3)	5(3)
O(10)	31(3)	30(3)	35(3)	4(3)	-7(3)	8(3)
O(11)	45(4)	35(4)	28(3)	7(3)	8(3)	-4(3)
O(12)	41(4)	24(3)	26(3)	1(2)	0(3)	0(3)
O(13)	37(4)	34(4)	32(3)	3(3)	-4(3)	-8(3)
O(14)	32(3)	36(4)	27(3)	5(3)	-4(3)	4(3)
O(15)	28(3)	45(4)	35(3)	-3(3)	3(3)	-13(3)
O(16)	52(4)	22(3)	29(3)	5(3)	6(3)	10(3)
O(17)	38(3)	17(3)	25(3)	3(2)	4(3)	-1(3)
O(18)	29(3)	22(3)	45(3)	-6(3)	-13(3)	6(3)
O(19)	23(3)	41(4)	42(4)	-9(3)	-3(3)	-6(3)
O(20)	32(3)	30(3)	33(3)	-4(3)	4(3)	1(3)
O(21)	43(4)	28(3)	36(3)	4(3)	13(3)	-7(3)
O(22)	35(3)	22(3)	44(4)	7(3)	2(3)	11(3)
O(23)	31(3)	38(3)	25(3)	12(3)	5(3)	-3(3)

O(24)	34(3)	21(3)	33(3)	1(3)	5(3)	0(3)
O(25)	26(3)	59(4)	53(4)	-11(3)	-16(3)	6(3)
O(26)	60(5)	92(6)	44(4)	40(4)	-4(4)	-11(5)
Si(11)	28(1)	20(1)	22(1)	1(1)	2(1)	-1(1)
Si(12)	25(1)	21(1)	31(1)	5(1)	-1(1)	6(1)
Si(13)	26(1)	22(1)	22(1)	1(1)	2(1)	4(1)
Si(14)	22(1)	17(1)	24(1)	1(1)	2(1)	1(1)
Si(15)	24(1)	29(1)	24(1)	1(1)	-1(1)	-6(1)
Si(16)	25(1)	21(1)	26(1)	0(1)	-3(1)	6(1)
Si(17)	18(1)	24(1)	30(1)	-3(1)	-5(1)	-2(1)
Si(18)	27(1)	23(1)	24(1)	4(1)	0(1)	0(1)
Si(19)	24(1)	23(1)	29(1)	3(1)	1(1)	-3(1)
Si(20)	21(1)	33(1)	28(1)	3(1)	-3(1)	3(1)
Sn(1)	32(1)	22(1)	26(1)	2(1)	1(1)	1(1)
Sn(2)	45(1)	39(1)	33(1)	1(1)	-8(1)	-14(1)
Sn(3)	33(1)	28(1)	24(1)	5(1)	3(1)	1(1)
Sn(4)	44(1)	25(1)	37(1)	5(1)	0(1)	11(1)
Sn(5)	24(1)	47(1)	42(1)	-3(1)	-9(1)	0(1)
Sn(6)	29(1)	25(1)	43(1)	-6(1)	-11(1)	5(1)
Sn(7)	49(1)	31(1)	47(1)	6(1)	2(1)	-12(1)
Sn(8)	56(1)	25(1)	35(1)	-5(1)	-3(1)	-4(1)
Sn(9)	25(1)	31(1)	60(2)	-6(1)	-8(1)	-7(1)
Sn(10)	38(2)	50(3)	24(1)	4(1)	7(1)	15(2)
Sn(11)	50(1)	49(2)	27(1)	-2(1)	8(1)	18(1)
Sn(12)	26(1)	32(1)	43(4)	-4(2)	-11(2)	-4(1)

Hydrogen coordinates (x 10^4) and isotropic displacement parameters ($Å^2$x 10^3) for **II**.

	x	y	z	U(eq)
H(27A)	-1854	949	-408	97
H(27B)	-2579	975	-490	97
H(27C)	-2310	759	1	97
H(33A)	-2259	1447	949	112
H(33B)	-2892	1736	861	112
H(33C)	-2278	2050	955	112
H(35A)	-2582	2659	-225	105
H(35B)	-3115	2279	-381	105
H(35C)	-2502	2319	-692	105
H(34A)	-2994	2261	293	228
H(34B)	-2420	2135	628	228
H(34C)	-2923	1712	521	228
H(36A)	-2174	1834	-1162	141
H(36B)	-1678	2222	-957	141
H(36C)	-2389	2368	-957	141
H(25A)	-561	3717	2897	80
H(25B)	-773	4273	3043	80
H(25C)	-174	4193	2722	80
H(32A)	-1464	3201	1919	162
H(32B)	-1992	3585	1765	162
H(32C)	-1943	3401	2307	162
H(30C)	-1834	4755	1748	154
H(30D)	-1230	5048	1914	154
H(30E)	-1760	4931	2291	154
H(29A)	-331	5225	2234	187
H(29B)	-1043	5356	2181	187
H(29C)	-646	5219	1719	187
H(31A)	-1974	3914	2079	251

H(31B)	-1866	4219	1594	251
H(31C)	-2105	4506	2060	251
H(18A)	-1335	879	677	104
H(18B)	-1588	327	792	104
H(18C)	-868	418	730	104
H(21A)	-1934	814	2294	130
H(21B)	-2169	358	1969	130
H(21C)	-2299	927	1811	130
H(22A)	-147	244	1756	145
H(22B)	-662	2	2092	145
H(22C)	-349	525	2236	145
H(1A)	482	4608	311	58
H(1B)	857	5079	106	58
H(1C)	1213	4586	282	58
H(2A)	-360	4155	-740	78
H(2B)	-11	4177	-1241	78
H(2C)	-235	4686	-991	78
H(3A)	1943	4310	-792	69
H(3B)	1639	4686	-1169	69
H(3C)	1550	4092	-1228	69
H(4A)	1186	2870	3014	68
H(4B)	971	2935	3557	68
H(4C)	577	3180	3135	68
H(5A)	3001	4059	1932	87
H(5B)	2900	4656	1931	87
H(5C)	2940	4356	1437	87
H(6A)	1120	3696	2337	100
H(6B)	1555	4030	2671	100
H(6C)	1812	3524	2435	100
H(7A)	2371	1528	1599	118
H(7B)	2850	1281	1963	118
H(7C)	3091	1608	1522	118
H(8A)	2447	671	712	112
H(8B)	2328	77	723	112

H(8C)	2627	350	1175	112
H(9A)	385	130	976	126
H(9B)	795	-310	1200	126
H(9C)	895	-141	657	126
H(10A)	1149	997	1974	124
H(10B)	1808	747	2057	124
H(10C)	1202	412	2105	124
H(11A)	-753	1716	-753	68
H(11B)	-755	1257	-1122	68
H(11C)	-385	1760	-1245	68
H(12A)	454	754	154	101
H(12B)	-52	450	-142	101
H(12C)	-240	948	145	101
H(13A)	1087	1135	-1345	94
H(13B)	764	600	-1272	94
H(13C)	1297	776	-917	94
H(14A)	388	1425	2635	87
H(14B)	790	1327	3103	87
H(14C)	1059	1663	2678	87
H(15A)	-268	2094	3979	71
H(15B)	-589	1745	3586	71
H(15C)	-739	2334	3606	71
H(16A)	-2071	3024	910	102
H(16B)	-2741	3035	678	102
H(16C)	-2560	3435	1081	102
H(17A)	-2201	4585	754	78
H(17B)	-2717	4582	349	78
H(17C)	-2026	4727	217	78
H(23A)	2332	2472	3031	168
H(23B)	2819	2027	3092	168
H(23C)	2134	1903	2926	168
H(24A)	3187	2955	1696	276
H(24B)	3692	2776	2073	276
H(24C)	3143	3134	2240	276

H(26A)	-1680	3793	-599	106
H(26B)	-2290	3458	-603	106
H(26C)	-1655	3216	-434	106
H(28A)	1379	5004	1326	114
H(28B)	1415	5146	1880	114
H(28C)	867	4801	1687	114
H(26D)	960(60)	1780(20)	4080(30)	78
H(26E)	1030(60)	1820(30)	3650(20)	78
H(27D)	3820(50)	1720(40)	2720(20)	78
H(27E)	4090(30)	2030(40)	2480(40)	78
H(28D)	6640(40)	3990(20)	10180(30)	59
H(28E)	6730(50)	3850(30)	9771(14)	59
H(30A)	4020(30)	4690(40)	3970(20)	58
H(30B)	4050(30)	4500(30)	4360(30)	58

Appendix D

X-ray Tables for $Si_8O_{20}(Cp_2TiCl)_8 \cdot 3CH_2Cl_2$ (III)

Crystal data and structure refinement for $Si_8O_{20}(Cp_2TiCl)_8 \cdot 3CH_2Cl_2$

Identification code	**III (CSD – 279731)**	
Empirical formula	C83 H86 Cl14 O20 Si8 Ti8	
Formula weight	2507.74	
Temperature	198(2) K	
Wavelength	0.71073 A	
Crystal system	Triclinic	
space group	P-1	
Unit cell dimensions	a = 13.6919(5) A	α = 101.9820(10) deg.
	b = 14.1160(5) A	β = 99.8590(10) deg.
	c = 14.2380(5) A	γ = 107.7540(10) deg.
Volume	2481.12(15) A^3	
Z	1	
Calculated density	1.678 Mg/m^3	
Absorption coefficient	1.149 mm^-1	
F(000)	1270	
Crystal size	0.2 x 0.2 x 0.05 mm	
Theta range for data collection	1.51 to 27.65 deg.	
Limiting indices	-17<=h<=17, -18<=k<=18, -18<=l<=18	
Reflections collected / unique	27306 / 27306 [R(int) = 0.0000]	
Completeness to theta = 22.50	99.7 %	
Refinement method	Full-matrix least-squares on F^2	
Data / restraints / parameters	27306 / 3712 / 1022	
Goodness-of-fit on F^2	1.031	
Final R indices [I>2sigma(I)]	R1 = 0.0670, wR2 = 0.1698	
R indices (all data)	R1 = 0.0884, wR2 = 0.1862	
Largest diff. peak and hole	0.877 and -0.947 e.A^-3	

Atomic coordinates (x 10^4) and equivalent isotropic displacement parameters (A^2 x 10^3) for **III**. U(eq) is defined as one third of the trace of the orthogonalized Uij tensor.

	x	y	z	U(eq)
Si(1)	3957(1)	3905(1)	6076(1)	25(1)
Si(2)	3365(1)	3367(1)	3801(1)	25(1)
Si(3)	3683(1)	5670(1)	3916(1)	28(1)
Si(4)	4280(1)	6209(1)	6199(1)	27(1)
O(1)	3334(2)	3377(2)	4927(2)	34(1)
O(2)	3298(2)	4427(2)	3607(2)	38(1)
O(3)	3708(2)	6079(2)	5067(2)	35(1)
O(4)	4027(2)	5092(2)	6392(2)	38(1)
O(5)	4864(2)	6118(2)	3778(2)	36(1)
O(6)	5534(2)	6733(2)	6364(2)	38(1)
O(7)	3338(2)	3270(2)	6719(2)	39(1)
O(8)	2390(2)	2411(2)	3073(2)	36(1)
O(9)	2912(2)	6038(2)	3242(2)	49(1)
O(10)	3900(2)	6910(2)	6964(2)	46(1)
Ti(1)	3191(1)	2763(1)	7812(1)	32(1)
Cl(1)	1519(1)	2833(1)	7865(1)	93(1)
C(1)	3718(12)	4589(8)	8633(10)	110(4)
C(2)	3334(12)	4065(11)	9295(10)	121(5)
C(3)	3952(12)	3513(12)	9529(10)	93(4)
C(4)	4783(8)	3693(10)	9058(7)	78(3)
C(5)	4637(10)	4409(10)	8541(8)	77(4)
C(1')	4271(13)	4370(10)	8813(11)	85(4)

C(2')	3729(13)	3842(11)	9410(11)	78(3)
C(3')	4076(9)	3041(11)	9455(9)	57(3)
C(4')	4831(8)	3072(13)	8916(8)	63(3)
C(5')	4970(8)	3903(12)	8527(8)	72(4)
C(6)	2157(11)	980(11)	7060(10)	70(3)
C(7)	2548(12)	1134(10)	8069(10)	84(3)
C(8)	3618(11)	1479(11)	8312(11)	109(4)
C(9)	3940(11)	1578(12)	7449(13)	98(4)
C(10)	3024(14)	1218(14)	6684(10)	81(3)
C(6')	1916(10)	1088(12)	6721(11)	63(4)
C(7')	2233(10)	963(10)	7638(12)	62(4)
C(8')	3269(10)	1086(9)	7878(11)	76(3)
C(9')	3679(10)	1332(9)	7066(10)	61(3)
C(10')	2791(12)	1242(14)	6351(10)	66(4)
Ti(2)	1747(1)	1272(1)	1968(1)	29(1)
Cl(2)	53(3)	1384(4)	1610(5)	61(1)
Cl(2')	49(9)	1449(12)	1988(18)	71(3)
C(11)	699(8)	-391(9)	2020(9)	67(2)
C(12)	1009(7)	219(7)	2969(8)	54(2)
C(13)	2081(7)	532(8)	3306(7)	62(2)
C(14)	2461(8)	112(8)	2519(9)	65(2)
C(15)	1575(10)	-494(8)	1740(8)	74(2)
C(11')	700(20)	-520(30)	1960(30)	65(6)
C(12')	1190(20)	-20(30)	2940(30)	60(6)
C(13')	2270(20)	310(20)	3060(20)	57(5)
C(14')	2460(20)	10(20)	2120(20)	61(5)
C(15')	1480(30)	-500(30)	1460(20)	70(5)
C(16)	2687(8)	2551(5)	1215(6)	56(2)
C(17)	1751(8)	1913(6)	525(6)	68(2)
C(18)	1766(7)	910(6)	258(6)	68(2)

C(19)	2742(6)	938(6)	790(5)	55(2)
C(20)	3276(5)	1921(5)	1376(5)	47(2)
C(16')	2220(30)	2702(17)	1254(17)	69(6)
C(17')	1300(20)	1990(20)	602(18)	79(7)
C(18')	1480(20)	1100(20)	250(20)	74(5)
C(19')	2540(20)	1240(20)	670(20)	71(5)
C(20')	2980(20)	2240(20)	1285(19)	62(5)
Ti(3)	1781(1)	5957(1)	2270(1)	31(1)
Cl(3)	2375(2)	5128(2)	985(1)	71(1)
C(21)	2752(6)	7438(6)	1794(8)	88(2)
C(22)	1727(7)	7092(5)	1255(5)	72(2)
C(23)	1108(5)	7213(5)	1880(7)	81(2)
C(24)	1757(9)	7622(5)	2826(7)	101(2)
C(25)	2741(8)	7757(5)	2758(7)	109(3)
C(26)	909(4)	4290(4)	2489(5)	58(2)
C(27)	385(5)	4275(5)	1572(5)	69(2)
C(28)	-57(5)	5023(6)	1688(6)	77(2)
C(29)	145(6)	5479(6)	2671(7)	84(2)
C(30)	756(5)	5038(5)	3180(5)	72(2)
Ti(3')	3178(2)	7377(2)	7816(2)	29(1)
Cl(3')	4382(4)	7259(3)	9105(3)	71(1)
C(21')	4390(9)	9143(8)	8279(12)	72(3)
C(22')	3679(11)	9084(9)	8866(9)	74(3)
C(23')	2711(9)	8869(9)	8268(11)	79(3)
C(24')	2778(12)	8746(10)	7280(11)	84(3)
C(25')	3811(12)	8902(9)	7305(11)	82(3)
C(26')	2180(8)	5574(8)	7482(9)	55(2)
C(27')	2151(10)	6049(9)	8410(9)	65(3)
C(28')	1657(10)	6749(9)	8354(10)	73(3)
C(29')	1347(9)	6698(9)	7361(11)	71(3)

C(30')	1647(9)	5963(9)	6826(8)	61(3)
Ti(4)	3286(1)	7796(1)	7534(1)	29(1)
Cl(4)	4718(1)	9336(1)	7703(1)	56(1)
C(31)	2636(4)	7672(4)	5815(4)	45(1)
C(32)	2533(5)	8545(4)	6374(4)	50(1)
C(33)	1810(5)	8233(5)	6931(4)	56(1)
C(34)	1476(4)	7170(5)	6717(5)	56(1)
C(35)	1970(4)	6817(4)	6025(4)	50(1)
C(36)	2668(5)	6896(5)	8661(4)	53(1)
C(37)	2415(5)	7796(6)	8857(5)	64(2)
C(38)	3342(6)	8628(5)	9209(5)	69(2)
C(39)	4204(5)	8265(5)	9279(4)	62(2)
C(40)	3730(5)	7216(5)	8977(5)	57(2)
Ti(4')	2053(2)	6554(2)	2579(1)	31(1)
Cl(4')	3422(3)	7975(2)	2437(3)	56(1)
C(31')	2301(8)	7382(8)	4280(7)	47(2)
C(32')	1977(8)	7983(8)	3746(8)	52(2)
C(33')	951(8)	7407(9)	3160(9)	61(2)
C(34')	646(8)	6432(10)	3353(10)	70(3)
C(35')	1481(9)	6437(9)	4054(9)	60(3)
C(36')	824(10)	5016(9)	1378(10)	74(3)
C(37')	488(9)	5816(11)	1237(9)	75(3)
C(38')	1252(11)	6464(11)	905(9)	76(3)
C(39')	2040(9)	6035(11)	832(9)	78(3)
C(40')	1749(10)	5126(10)	1069(10)	75(3)
C(41)	-930(20)	7430(20)	4960(50)	76(2)
Cl(5)	168(11)	8351(9)	4851(10)	94(1)
Cl(6)	-772(6)	6391(6)	5316(6)	92(1)
C(41')	-946(11)	7558(10)	5010(30)	76(2)
Cl(5')	181(5)	8604(4)	5123(5)	94(1)

Cl(6')	-853(3)	6337(3)	4785(3)	92(1)
C(42)	4840(50)	10150(30)	5500(30)	106(6)
Cl(7)	5190(20)	9200(20)	4878(17)	120(2)
Cl(8)	4763(15)	10997(15)	4803(14)	67(1)
C(42')	4362(12)	10125(12)	4940(20)	106(6)
Cl(7')	5242(6)	9638(6)	5400(6)	120(2)
Cl(8')	4844(4)	11388(4)	4991(5)	67(1)

Bond lengths [A] and angles [deg] for **III**.

Si(1)-O(7)	1.582(2)	O(5)-Si(1)#1	1.603(2)
Si(1)-O(5)#1	1.603(2)	O(6)-Si(2)#1	1.608(2)
Si(1)-O(1)	1.609(2)	O(7)-Ti(1)	1.859(2)
Si(1)-O(4)	1.610(2)	O(8)-Ti(2)	1.856(2)
Si(2)-O(8)	1.589(2)	O(9)-Ti(4')	1.798(3)
Si(2)-O(2)	1.604(2)	O(9)-Ti(3)	1.849(2)
Si(2)-O(1)	1.608(2)	O(10)-Ti(3')	1.833(3)
Si(2)-O(6)#1	1.608(2)	O(10)-Ti(4)	1.839(2)
Si(3)-O(9)	1.581(2)	Ti(1)-C(9)	2.232(13)
Si(3)-O(2)	1.607(2)	Ti(1)-C(8)	2.274(11)
Si(3)-O(5)	1.609(2)	Ti(1)-C(1')	2.293(14)
Si(3)-O(3)	1.612(2)	Ti(1)-C(2')	2.312(15)
Si(4)-O(10)	1.579(2)	Ti(1)-C(7)	2.327(11)
Si(4)-O(4)	1.601(2)	Ti(1)-C(3')	2.335(11)
Si(4)-O(6)	1.602(2)	Ti(1)-Cl(1)	2.3356(12)
Si(4)-O(3)	1.612(2)	Ti(1)-C(10)	2.346(18)
		Ti(1)-C(3)	2.359(14)
		Ti(1)-C(4)	2.363(9)
		Ti(1)-C(4')	2.369(10)
		C(1)-C(5)	1.380(11)

C(1)-C(2)	1.391(11)	C(11)-C(12)	1.358(8)
C(2)-C(3)	1.360(11)	C(11)-C(15)	1.365(8)
C(3)-C(4)	1.401(11)	C(12)-C(13)	1.362(8)
C(4)-C(5)	1.408(10)	C(13)-C(14)	1.410(8)
C(1')-C(5')	1.388(12)	C(14)-C(15)	1.395(8)
C(1')-C(2')	1.403(12)	C(11')-C(12')	1.373(13)
C(2')-C(3')	1.362(11)	C(11')-C(15')	1.375(13)
C(3')-C(4')	1.384(10)	C(12')-C(13')	1.379(13)
C(4')-C(5')	1.374(11)	C(13')-C(14')	1.402(13)
C(6)-C(10)	1.363(11)	C(14')-C(15')	1.375(13)
C(6)-C(7)	1.391(11)	C(16)-C(17)	1.384(8)
C(7)-C(8)	1.350(11)	C(16)-C(20)	1.399(7)
C(8)-C(9)	1.394(11)	C(17)-C(18)	1.395(8)
C(9)-C(10)	1.389(11)	C(18)-C(19)	1.404(8)
C(6')-C(10')	1.367(11)	C(19)-C(20)	1.360(7)
C(6')-C(7')	1.368(11)	C(16')-C(17')	1.374(13)
C(7')-C(8')	1.348(11)	C(16')-C(20')	1.382(13)
C(8')-C(9')	1.429(11)	C(17')-C(18')	1.370(13)
C(9')-C(10')	1.400(11)	C(18')-C(19')	1.402(13)
Ti(2)-C(19')	2.29(3)	C(19')-C(20')	1.387(13)
Ti(2)-C(14')	2.30(3)	Ti(3)-C(24)	2.331(6)
Ti(2)-C(20')	2.32(3)	Ti(3)-C(29)	2.340(6)
Ti(2)-C(14)	2.345(8)	Ti(3)-C(23)	2.351(6)
Ti(2)-C(15')	2.35(4)	Ti(3)-C(30)	2.353(6)
Ti(2)-Cl(2)	2.350(4)	Ti(3)-C(28)	2.359(6)
Ti(2)-C(18')	2.36(3)	Ti(3)-Cl(3)	2.3622(19)
Ti(2)-C(11)	2.372(12)	Ti(3)-C(25)	2.363(7)
Ti(2)-C(15)	2.378(11)	Ti(3)-C(22)	2.379(6)
Ti(2)-C(20)	2.384(5)	Ti(3)-C(26)	2.404(5)
Ti(2)-C(18)	2.389(8)	Ti(3)-C(21)	2.409(6)

Ti(3)-C(27)	2.425(6)	C(28')-C(29')	1.386(12)
C(21)-C(25)	1.357(10)	C(29')-C(30')	1.366(11)
C(21)-C(22)	1.362(9)	Ti(4)-C(34)	2.351(6)
C(22)-C(23)	1.350(8)	Ti(4)-C(36)	2.359(5)
C(23)-C(24)	1.374(9)	Ti(4)-C(33)	2.364(6)
C(24)-C(25)	1.325(10)	Ti(4)-Cl(4)	2.3768(17)
C(26)-C(27)	1.371(8)	Ti(4)-C(35)	2.387(6)
C(26)-C(30)	1.379(8)	Ti(4)-C(32)	2.391(6)
C(27)-C(28)	1.363(8)	Ti(4)-C(37)	2.396(5)
C(28)-C(29)	1.355(9)	Ti(4)-C(38)	2.407(6)
C(29)-C(30)	1.381(8)	Ti(4)-C(31)	2.408(5)
Ti(3')-C(29')	2.312(12)	Ti(4)-C(40)	2.414(6)
Ti(3')-Cl(3')	2.318(5)	Ti(4)-C(39)	2.436(6)
Ti(3')-C(28')	2.327(11)	C(31)-C(32)	1.381(7)
Ti(3')-C(30')	2.373(11)	C(31)-C(35)	1.396(7)
Ti(3')-C(25')	2.376(12)	C(32)-C(33)	1.397(7)
Ti(3')-C(22')	2.379(12)	C(33)-C(34)	1.378(7)
Ti(3')-C(23')	2.379(11)	C(34)-C(35)	1.381(7)
Ti(3')-C(27')	2.381(11)	C(36)-C(40)	1.346(7)
Ti(3')-C(26')	2.393(10)	C(36)-C(37)	1.403(8)
Ti(3')-C(24')	2.395(12)	C(37)-C(38)	1.367(8)
Ti(3')-C(21')	2.413(11)	C(38)-C(39)	1.420(8)
C(21')-C(22')	1.382(12)	C(39)-C(40)	1.361(8)
C(21')-C(25')	1.390(12)	Ti(4')-C(33')	2.353(11)
C(22')-C(23')	1.354(12)	Ti(4')-C(34')	2.358(11)
C(23')-C(24')	1.404(12)	Ti(4')-Cl(4')	2.362(3)
C(24')-C(25')	1.357(12)	Ti(4')-C(32')	2.374(10)
C(26')-C(27')	1.364(11)	Ti(4')-C(31')	2.376(10)
C(26')-C(30')	1.389(11)	Ti(4')-C(35')	2.383(11)
C(27')-C(28')	1.365(11)	Ti(4')-C(36')	2.391(12)

Ti(4')-C(37')	2.396(11)	O(2)-Si(2)-O(1)	109.78(12)
Ti(4')-C(38')	2.407(12)	O(8)-Si(2)-O(6)#1	110.56(12)
Ti(4')-C(39')	2.438(12)	O(2)-Si(2)-O(6)#1	109.09(13)
Ti(4')-C(40')	2.499(13)	O(1)-Si(2)-O(6)#1	108.48(12)
C(31')-C(32')	1.369(10)	O(9)-Si(3)-O(2)	110.31(13)
C(31')-C(35')	1.389(11)	O(9)-Si(3)-O(5)	109.90(12)
C(32')-C(33')	1.397(11)	O(2)-Si(3)-O(5)	108.51(13)
C(33')-C(34')	1.411(11)	O(9)-Si(3)-O(3)	110.37(13)
C(34')-C(35')	1.381(11)	O(2)-Si(3)-O(3)	108.90(12)
C(36')-C(37')	1.380(12)	O(5)-Si(3)-O(3)	108.80(12)
C(36')-C(40')	1.386(12)	O(10)-Si(4)-O(4)	109.35(13)
C(37')-C(38')	1.386(12)	O(10)-Si(4)-O(6)	108.89(13)
C(38')-C(39')	1.397(12)	O(4)-Si(4)-O(6)	108.75(13)
C(39')-C(40')	1.354(12)	O(10)-Si(4)-O(3)	111.89(13)
C(41)-Cl(6)	1.714(14)	O(4)-Si(4)-O(3)	109.28(12)
C(41)-Cl(5)	1.720(13)	O(6)-Si(4)-O(3)	108.63(12)
C(41')-Cl(6')	1.735(11)	Si(2)-O(1)-Si(1)	145.36(14)
C(41')-Cl(5')	1.735(9)	Si(2)-O(2)-Si(3)	151.21(16)
C(42)-Cl(7)	1.700(15)	Si(4)-O(3)-Si(3)	145.85(14)
C(42)-Cl(8)	1.716(15)	Si(4)-O(4)-Si(1)	151.05(16)
C(42')-Cl(7')	1.665(12)	Si(1)#1-O(5)-Si(3)	149.40(15)
C(42')-Cl(8')	1.683(13)	Si(4)-O(6)-Si(2)#1	149.27(15)
O(7)-Si(1)-O(5)#1	110.61(12)	Si(1)-O(7)-Ti(1)	155.66(15)
O(7)-Si(1)-O(1)	108.31(12)	Si(2)-O(8)-Ti(2)	154.22(14)
O(5)#1-Si(1)-O(1)	108.80(12)	Si(3)-O(9)-Ti(4')	174.6(2)
O(7)-Si(1)-O(4)	110.60(13)	Si(3)-O(9)-Ti(3)	159.22(17)
O(5)#1-Si(1)-O(4)	108.72(12)	Ti(4')-O(9)-Ti(3)	25.33(7)
O(1)-Si(1)-O(4)	109.77(12)	Si(4)-O(10)-Ti(3')	164.05(17)
O(8)-Si(2)-O(2)	110.02(13)	Si(4)-O(10)-Ti(4)	163.77(19)
O(8)-Si(2)-O(1)	108.88(11)	Ti(3')-O(10)-Ti(4)	24.31(6)

O(7)-Ti(1)-C(9)	96.6(5)	C(8)-Ti(1)-C(10)	57.8(4)
O(7)-Ti(1)-C(8)	132.7(4)	C(1')-Ti(1)-C(10)	148.2(6)
C(9)-Ti(1)-C(8)	36.0(3)	C(2')-Ti(1)-C(10)	150.5(5)
O(7)-Ti(1)-C(1')	88.6(3)	C(7)-Ti(1)-C(10)	56.0(4)
C(9)-Ti(1)-C(1')	117.4(5)	C(3')-Ti(1)-C(10)	116.5(4)
C(8)-Ti(1)-C(1')	111.9(4)	Cl(1)-Ti(1)-C(10)	110.2(4)
O(7)-Ti(1)-C(2')	122.1(3)	O(7)-Ti(1)-C(3)	132.4(3)
C(9)-Ti(1)-C(2')	118.4(5)	C(9)-Ti(1)-C(3)	102.6(5)
C(8)-Ti(1)-C(2')	92.9(4)	C(8)-Ti(1)-C(3)	77.0(5)
C(1')-Ti(1)-C(2')	35.5(3)	C(1')-Ti(1)-C(3)	43.9(4)
O(7)-Ti(1)-C(7)	135.8(4)	C(2')-Ti(1)-C(3)	16.3(4)
C(9)-Ti(1)-C(7)	57.9(4)	C(7)-Ti(1)-C(3)	90.6(4)
C(8)-Ti(1)-C(7)	34.1(3)	C(3')-Ti(1)-C(3)	17.8(4)
C(1')-Ti(1)-C(7)	134.2(4)	Cl(1)-Ti(1)-C(3)	95.3(4)
C(2')-Ti(1)-C(7)	102.1(5)	C(10)-Ti(1)-C(3)	134.3(5)
O(7)-Ti(1)-C(3')	141.2(3)	O(7)-Ti(1)-C(4)	106.6(3)
C(9)-Ti(1)-C(3')	85.4(5)	C(9)-Ti(1)-C(4)	85.0(4)
C(8)-Ti(1)-C(3')	59.4(4)	C(8)-Ti(1)-C(4)	77.6(4)
C(1')-Ti(1)-C(3')	57.2(4)	C(1')-Ti(1)-C(4)	35.2(4)
C(2')-Ti(1)-C(3')	34.1(3)	C(2')-Ti(1)-C(4)	41.7(4)
C(7)-Ti(1)-C(3')	77.2(4)	C(7)-Ti(1)-C(4)	106.2(4)
O(7)-Ti(1)-Cl(1)	98.01(8)	C(3')-Ti(1)-C(4)	34.7(4)
C(9)-Ti(1)-Cl(1)	138.9(4)	Cl(1)-Ti(1)-C(4)	126.3(4)
C(8)-Ti(1)-Cl(1)	117.6(4)	C(10)-Ti(1)-C(4)	119.9(5)
C(1')-Ti(1)-Cl(1)	101.2(4)	C(3)-Ti(1)-C(4)	34.5(3)
C(2')-Ti(1)-Cl(1)	84.8(4)	O(7)-Ti(1)-C(4')	113.4(3)
C(7)-Ti(1)-Cl(1)	85.5(4)	C(9)-Ti(1)-C(4')	64.5(5)
C(3')-Ti(1)-Cl(1)	105.7(3)	C(8)-Ti(1)-C(4')	57.5(4)
O(7)-Ti(1)-C(10)	82.0(4)	C(1')-Ti(1)-C(4')	56.7(4)
C(9)-Ti(1)-C(10)	35.2(3)	C(2')-Ti(1)-C(4')	57.1(4)

C(7)-Ti(1)-C(4')	89.0(4)	C(5')-C(4')-C(3')	108.9(9)
C(3')-Ti(1)-C(4')	34.2(3)	C(5')-C(4')-Ti(1)	73.4(6)
Cl(1)-Ti(1)-C(4')	139.3(3)	C(3')-C(4')-Ti(1)	71.6(6)
C(10)-Ti(1)-C(4')	99.7(5)	C(4')-C(5')-C(1')	106.5(9)
C(3)-Ti(1)-C(4')	44.4(5)	C(4')-C(5')-Ti(1)	72.9(6)
C(4)-Ti(1)-C(4')	21.5(3)	C(1')-C(5')-Ti(1)	69.5(7)
C(5)-C(1)-C(2)	106.3(9)	C(10)-C(6)-C(7)	105.6(9)
C(5)-C(1)-Ti(1)	73.6(6)	C(10)-C(6)-Ti(1)	71.8(9)
C(2)-C(1)-Ti(1)	73.7(6)	C(7)-C(6)-Ti(1)	70.7(7)
C(3)-C(2)-C(1)	108.7(10)	C(8)-C(7)-C(6)	110.6(9)
C(3)-C(2)-Ti(1)	70.6(7)	C(8)-C(7)-Ti(1)	70.8(6)
C(1)-C(2)-Ti(1)	73.0(5)	C(6)-C(7)-Ti(1)	75.0(7)
C(2)-C(3)-C(4)	110.1(9)	C(7)-C(8)-C(9)	107.2(8)
C(2)-C(3)-Ti(1)	76.4(7)	C(7)-C(8)-Ti(1)	75.1(6)
C(4)-C(3)-Ti(1)	72.9(6)	C(9)-C(8)-Ti(1)	70.3(6)
C(3)-C(4)-C(5)	104.3(9)	C(10)-C(9)-C(8)	106.7(9)
C(3)-C(4)-Ti(1)	72.6(7)	C(10)-C(9)-Ti(1)	76.9(8)
C(5)-C(4)-Ti(1)	75.4(6)	C(8)-C(9)-Ti(1)	73.6(6)
C(1)-C(5)-C(4)	110.2(8)	C(6)-C(10)-C(9)	109.7(9)
C(1)-C(5)-Ti(1)	73.3(6)	C(6)-C(10)-Ti(1)	74.7(9)
C(4)-C(5)-Ti(1)	70.5(5)	C(9)-C(10)-Ti(1)	67.9(8)
C(5')-C(1')-C(2')	109.0(9)	C(10')-C(6')-C(7')	104.8(9)
C(5')-C(1')-Ti(1)	75.9(7)	C(10')-C(6')-Ti(1)	75.6(8)
C(2')-C(1')-Ti(1)	73.0(8)	C(7')-C(6')-Ti(1)	71.7(7)
C(3')-C(2')-C(1')	106.5(9)	C(8')-C(7')-C(6')	112.5(9)
C(3')-C(2')-Ti(1)	73.9(6)	C(8')-C(7')-Ti(1)	74.1(6)
C(1')-C(2')-Ti(1)	71.5(7)	C(6')-C(7')-Ti(1)	75.8(8)
C(2')-C(3')-C(4')	109.0(9)	C(7')-C(8')-C(9')	106.5(9)
C(2')-C(3')-Ti(1)	72.0(6)	C(7')-C(8')-Ti(1)	73.5(6)
C(4')-C(3')-Ti(1)	74.2(6)	C(9')-C(8')-Ti(1)	72.5(6)

C(10')-C(9')-C(8')	104.5(9)	C(20')-Ti(2)-C(18')	56.6(6)
C(10')-C(9')-Ti(1)	77.0(8)	C(14)-Ti(2)-C(18')	114.7(8)
C(8')-C(9')-Ti(1)	73.1(6)	C(15')-Ti(2)-C(18')	82.6(9)
C(6')-C(10')-C(9')	111.1(9)	Cl(2)-Ti(2)-C(18')	80.3(8)
C(6')-C(10')-Ti(1)	72.5(8)	O(8)-Ti(2)-C(11)	124.2(3)
C(9')-C(10')-Ti(1)	70.0(7)	C(19')-Ti(2)-C(11)	113.7(8)
O(8)-Ti(2)-C(19')	116.9(7)	C(14')-Ti(2)-C(11)	58.1(9)
O(8)-Ti(2)-C(14')	109.9(8)	C(20')-Ti(2)-C(11)	147.9(9)
C(19')-Ti(2)-C(14')	79.8(8)	C(14)-Ti(2)-C(11)	56.5(3)
O(8)-Ti(2)-C(20')	82.8(6)	C(15')-Ti(2)-C(11)	36.2(12)
C(19')-Ti(2)-C(20')	35.0(4)	Cl(2)-Ti(2)-C(11)	79.8(3)
C(14')-Ti(2)-C(20')	98.9(9)	C(18')-Ti(2)-C(11)	102.8(7)
O(8)-Ti(2)-C(14)	99.1(3)	O(8)-Ti(2)-C(15)	131.2(3)
C(19')-Ti(2)-C(14)	92.2(8)	C(19')-Ti(2)-C(15)	86.7(8)
C(14')-Ti(2)-C(14)	13.7(7)	C(14')-Ti(2)-C(15)	28.7(10)
C(20')-Ti(2)-C(14)	106.6(9)	C(20')-Ti(2)-C(15)	116.8(9)
O(8)-Ti(2)-C(15')	140.6(8)	C(14)-Ti(2)-C(15)	34.4(2)
C(19')-Ti(2)-C(15')	79.9(10)	C(15')-Ti(2)-C(15)	9.6(9)
C(14')-Ti(2)-C(15')	34.4(5)	Cl(2)-Ti(2)-C(15)	109.2(3)
C(20')-Ti(2)-C(15')	112.1(12)	C(18')-Ti(2)-C(15)	92.1(7)
C(14)-Ti(2)-C(15')	42.4(9)	C(11)-Ti(2)-C(15)	33.4(2)
O(8)-Ti(2)-Cl(2)	98.88(16)	O(8)-Ti(2)-C(20)	86.60(16)
C(19')-Ti(2)-Cl(2)	114.7(8)	C(19')-Ti(2)-C(20)	31.4(7)
C(14')-Ti(2)-Cl(2)	137.3(7)	C(14')-Ti(2)-C(20)	81.6(7)
C(20')-Ti(2)-Cl(2)	115.8(8)	C(20')-Ti(2)-C(20)	17.5(8)
C(14)-Ti(2)-Cl(2)	135.6(3)	C(14)-Ti(2)-C(20)	89.2(3)
C(15')-Ti(2)-Cl(2)	105.7(9)	C(15')-Ti(2)-C(20)	98.5(10)
O(8)-Ti(2)-C(18')	132.4(7)	Cl(2)-Ti(2)-C(20)	132.20(19)
C(19')-Ti(2)-C(18')	35.1(5)	C(18')-Ti(2)-C(20)	62.6(7)
C(14')-Ti(2)-C(18')	101.0(9)	C(11)-Ti(2)-C(20)	134.6(4)

C(15)-Ti(2)-C(20)	101.6(3)	C(11')-C(12')-C(13')	108.3(13)
O(8)-Ti(2)-C(18)	135.5(2)	C(11')-C(12')-Ti(2)	72.7(15)
C(19')-Ti(2)-C(18)	25.3(7)	C(13')-C(12')-Ti(2)	69.7(13)
C(14')-Ti(2)-C(18)	88.9(8)	C(12')-C(13')-C(14')	107.9(12)
C(20')-Ti(2)-C(18)	53.9(6)	C(12')-C(13')-Ti(2)	77.9(14)
C(14)-Ti(2)-C(18)	102.6(3)	C(14')-C(13')-Ti(2)	68.2(15)
C(15')-Ti(2)-C(18)	74.4(9)	C(15')-C(14')-C(13')	106.8(12)
Cl(2)-Ti(2)-C(18)	92.04(19)	C(15')-C(14')-Ti(2)	74.8(17)
C(18')-Ti(2)-C(18)	12.8(8)	C(13')-C(14')-Ti(2)	77.4(15)
C(11)-Ti(2)-C(18)	100.1(4)	C(14')-C(15')-C(11')	109.1(13)
C(15)-Ti(2)-C(18)	83.4(3)	C(14')-C(15')-Ti(2)	70.9(16)
C(20)-Ti(2)-C(18)	55.7(2)	C(11')-C(15')-Ti(2)	79.0(18)
C(12)-C(11)-C(15)	108.5(7)	C(17)-C(16)-C(20)	106.1(5)
C(12)-C(11)-Ti(2)	74.2(5)	C(17)-C(16)-Ti(2)	72.5(4)
C(15)-C(11)-Ti(2)	73.5(6)	C(20)-C(16)-Ti(2)	71.2(4)
C(11)-C(12)-C(13)	109.8(6)	C(16)-C(17)-C(18)	109.2(6)
C(11)-C(12)-Ti(2)	72.7(5)	C(16)-C(17)-Ti(2)	74.3(4)
C(13)-C(12)-Ti(2)	73.7(4)	C(18)-C(17)-Ti(2)	72.2(4)
C(12)-C(13)-C(14)	107.0(6)	C(17)-C(18)-C(19)	106.9(5)
C(12)-C(13)-Ti(2)	73.2(4)	C(17)-C(18)-Ti(2)	74.0(4)
C(14)-C(13)-Ti(2)	70.7(4)	C(19)-C(18)-Ti(2)	73.2(4)
C(15)-C(14)-C(13)	106.7(6)	C(20)-C(19)-C(18)	107.7(5)
C(15)-C(14)-Ti(2)	74.1(5)	C(20)-C(19)-Ti(2)	73.0(3)
C(13)-C(14)-Ti(2)	74.7(4)	C(18)-C(19)-Ti(2)	72.7(4)
C(11)-C(15)-C(14)	108.0(7)	C(19)-C(20)-C(16)	110.0(5)
C(11)-C(15)-Ti(2)	73.1(6)	C(19)-C(20)-Ti(2)	73.9(3)
C(14)-C(15)-Ti(2)	71.5(5)	C(16)-C(20)-Ti(2)	75.1(4)
C(12')-C(11')-C(15')	108.0(13)	C(17')-C(16')-C(20')	107.4(13)
C(12')-C(11')-Ti(2)	75.5(14)	C(17')-C(16')-Ti(2)	75.0(11)
C(15')-C(11')-Ti(2)	68.1(18)	C(20')-C(16')-Ti(2)	69.3(13)

C(18')-C(17')-C(16')	108.3(13)	C(23)-Ti(3)-Cl(3)	113.9(2)
C(18')-C(17')-Ti(2)	69.9(12)	C(30)-Ti(3)-Cl(3)	122.31(19)
C(16')-C(17')-Ti(2)	72.1(10)	C(28)-Ti(3)-Cl(3)	99.6(2)
C(17')-C(18')-C(19')	109.2(13)	O(9)-Ti(3)-C(25)	79.4(2)
C(17')-C(18')-Ti(2)	77.1(11)	C(24)-Ti(3)-C(25)	32.8(2)
C(19')-C(18')-Ti(2)	70.0(13)	C(29)-Ti(3)-C(25)	114.8(4)
C(20')-C(19')-C(18')	105.4(12)	C(23)-Ti(3)-C(25)	55.1(3)
C(20')-C(19')-Ti(2)	73.4(14)	C(30)-Ti(3)-C(25)	125.8(3)
C(18')-C(19')-Ti(2)	74.9(14)	C(28)-Ti(3)-C(25)	130.8(3)
C(16')-C(20')-C(19')	109.7(13)	Cl(3)-Ti(3)-C(25)	109.8(3)
C(16')-C(20')-Ti(2)	76.7(13)	O(9)-Ti(3)-C(22)	128.0(2)
C(19')-C(20')-Ti(2)	71.6(14)	C(24)-Ti(3)-C(22)	55.5(2)
O(9)-Ti(3)-C(24)	99.2(3)	C(29)-Ti(3)-C(22)	106.7(3)
O(9)-Ti(3)-C(29)	114.6(2)	C(23)-Ti(3)-C(22)	33.2(2)
C(24)-Ti(3)-C(29)	82.9(3)	C(30)-Ti(3)-C(22)	140.8(3)
O(9)-Ti(3)-C(23)	132.3(2)	C(28)-Ti(3)-C(22)	92.9(3)
C(24)-Ti(3)-C(23)	34.1(2)	Cl(3)-Ti(3)-C(22)	82.7(2)
C(29)-Ti(3)-C(23)	77.8(2)	C(25)-Ti(3)-C(22)	54.7(3)
O(9)-Ti(3)-C(30)	83.9(2)	O(9)-Ti(3)-C(26)	85.68(16)
C(24)-Ti(3)-C(30)	102.7(3)	C(24)-Ti(3)-C(26)	135.8(3)
C(29)-Ti(3)-C(30)	34.2(2)	C(29)-Ti(3)-C(26)	56.0(2)
C(23)-Ti(3)-C(30)	109.9(3)	C(23)-Ti(3)-C(26)	131.0(2)
O(9)-Ti(3)-C(28)	138.56(19)	C(30)-Ti(3)-C(26)	33.68(19)
C(24)-Ti(3)-C(28)	99.7(4)	C(28)-Ti(3)-C(26)	55.6(2)
C(29)-Ti(3)-C(28)	33.5(2)	Cl(3)-Ti(3)-C(26)	88.65(17)
C(23)-Ti(3)-C(28)	77.3(2)	C(25)-Ti(3)-C(26)	156.7(3)
C(30)-Ti(3)-C(28)	56.1(2)	C(22)-Ti(3)-C(26)	145.3(2)
O(9)-Ti(3)-Cl(3)	92.77(11)	O(9)-Ti(3)-C(21)	95.1(2)
C(24)-Ti(3)-Cl(3)	134.4(2)	C(24)-Ti(3)-C(21)	55.2(3)
C(29)-Ti(3)-Cl(3)	130.8(2)	C(29)-Ti(3)-C(21)	132.5(2)

C(23)-Ti(3)-C(21)	55.1(2)	C(24)-C(25)-C(21)	109.9(7)
C(30)-Ti(3)-C(21)	157.5(3)	C(24)-C(25)-Ti(3)	72.3(4)
C(28)-Ti(3)-C(21)	125.9(3)	C(21)-C(25)-Ti(3)	75.3(4)
Cl(3)-Ti(3)-C(21)	80.2(2)	C(27)-C(26)-C(30)	107.2(6)
C(25)-Ti(3)-C(21)	33.0(3)	C(27)-C(26)-Ti(3)	74.3(3)
C(22)-Ti(3)-C(21)	33.0(2)	C(30)-C(26)-Ti(3)	71.1(3)
C(26)-Ti(3)-C(21)	168.8(3)	C(28)-C(27)-C(26)	108.6(6)
O(9)-Ti(3)-C(27)	116.46(18)	C(28)-C(27)-Ti(3)	70.8(4)
C(24)-Ti(3)-C(27)	132.6(3)	C(26)-C(27)-Ti(3)	72.7(3)
C(29)-Ti(3)-C(27)	55.1(2)	C(29)-C(28)-C(27)	108.3(6)
C(23)-Ti(3)-C(27)	108.1(2)	C(29)-C(28)-Ti(3)	72.5(4)
C(30)-Ti(3)-C(27)	55.2(2)	C(27)-C(28)-Ti(3)	76.1(4)
C(28)-Ti(3)-C(27)	33.1(2)	C(28)-C(29)-C(30)	108.1(6)
Cl(3)-Ti(3)-C(27)	76.43(18)	C(28)-C(29)-Ti(3)	74.0(4)
C(25)-Ti(3)-C(27)	163.2(3)	C(30)-C(29)-Ti(3)	73.4(4)
C(22)-Ti(3)-C(27)	112.6(3)	C(26)-C(30)-C(29)	107.6(6)
C(26)-Ti(3)-C(27)	32.98(18)	C(26)-C(30)-Ti(3)	75.2(3)
C(21)-Ti(3)-C(27)	141.2(3)	C(29)-C(30)-Ti(3)	72.4(3)
C(25)-C(21)-C(22)	106.5(7)	O(10)-Ti(3')-C(29')	118.4(4)
C(25)-C(21)-Ti(3)	71.6(4)	O(10)-Ti(3')-Cl(3')	88.19(15)
C(22)-C(21)-Ti(3)	72.3(3)	C(29')-Ti(3')-Cl(3')	130.7(4)
C(23)-C(22)-C(21)	108.7(7)	O(10)-Ti(3')-C(28')	139.4(3)
C(23)-C(22)-Ti(3)	72.3(3)	C(29')-Ti(3')-C(28')	34.8(3)
C(21)-C(22)-Ti(3)	74.7(4)	Cl(3')-Ti(3')-C(28')	97.8(4)
C(22)-C(23)-C(24)	107.3(6)	O(10)-Ti(3')-C(30')	86.8(3)
C(22)-C(23)-Ti(3)	74.5(3)	C(29')-Ti(3')-C(30')	33.9(3)
C(24)-C(23)-Ti(3)	72.1(4)	Cl(3')-Ti(3')-C(30')	123.6(3)
C(25)-C(24)-C(23)	107.7(7)	C(28')-Ti(3')-C(30')	56.4(4)
C(25)-C(24)-Ti(3)	75.0(4)	O(10)-Ti(3')-C(25')	82.2(3)
C(23)-C(24)-Ti(3)	73.7(4)	C(29')-Ti(3')-C(25')	110.6(5)

Cl(3')-Ti(3')-C(25')	113.7(4)	C(22')-Ti(3')-C(26')	147.7(4)
C(28')-Ti(3')-C(25')	129.5(5)	C(23')-Ti(3')-C(26')	131.4(4)
C(30')-Ti(3')-C(25')	121.1(5)	C(27')-Ti(3')-C(26')	33.2(3)
O(10)-Ti(3')-C(22')	126.8(4)	O(10)-Ti(3')-C(24')	105.7(4)
C(29')-Ti(3')-C(22')	107.1(5)	C(29')-Ti(3')-C(24')	79.0(5)
Cl(3')-Ti(3')-C(22')	81.7(4)	Cl(3')-Ti(3')-C(24')	136.1(4)
C(28')-Ti(3')-C(22')	93.8(4)	C(28')-Ti(3')-C(24')	97.5(5)
C(30')-Ti(3')-C(22')	140.7(5)	C(30')-Ti(3')-C(24')	99.0(5)
C(25')-Ti(3')-C(22')	55.9(4)	C(25')-Ti(3')-C(24')	33.0(3)
O(10)-Ti(3')-C(23')	137.0(4)	C(22')-Ti(3')-C(24')	56.4(4)
C(29')-Ti(3')-C(23')	77.3(4)	C(23')-Ti(3')-C(24')	34.2(3)
Cl(3')-Ti(3')-C(23')	112.1(4)	C(27')-Ti(3')-C(24')	130.8(5)
C(28')-Ti(3')-C(23')	77.3(4)	C(26')-Ti(3')-C(24')	132.4(4)
C(30')-Ti(3')-C(23')	109.2(4)	O(10)-Ti(3')-C(21')	93.5(3)
C(25')-Ti(3')-C(23')	55.1(4)	C(29')-Ti(3')-C(21')	130.9(4)
C(22')-Ti(3')-C(23')	33.1(3)	Cl(3')-Ti(3')-C(21')	82.5(4)
O(10)-Ti(3')-C(27')	112.8(3)	C(28')-Ti(3')-C(21')	127.1(4)
C(29')-Ti(3')-C(27')	56.3(4)	C(30')-Ti(3')-C(21')	153.9(5)
Cl(3')-Ti(3')-C(27')	75.7(3)	C(25')-Ti(3')-C(21')	33.7(3)
C(28')-Ti(3')-C(27')	33.7(3)	C(22')-Ti(3')-C(21')	33.5(3)
C(30')-Ti(3')-C(27')	55.4(4)	C(23')-Ti(3')-C(21')	54.9(3)
C(25')-Ti(3')-C(27')	163.2(5)	C(27')-Ti(3')-C(21')	144.8(5)
C(22')-Ti(3')-C(27')	114.8(5)	C(26')-Ti(3')-C(21')	171.8(4)
C(23')-Ti(3')-C(27')	109.0(4)	C(24')-Ti(3')-C(21')	55.7(4)
O(10)-Ti(3')-C(26')	83.7(3)	C(22')-C(21')-C(25')	107.0(10)
C(29')-Ti(3')-C(26')	56.7(4)	C(22')-C(21')-Ti(3')	71.9(6)
Cl(3')-Ti(3')-C(26')	89.7(3)	C(25')-C(21')-Ti(3')	71.7(7)
C(28')-Ti(3')-C(26')	56.4(3)	C(23')-C(22')-C(21')	107.6(10)
C(30')-Ti(3')-C(26')	33.9(3)	C(23')-C(22')-Ti(3')	73.5(6)
C(25')-Ti(3')-C(26')	152.1(5)	C(21')-C(22')-Ti(3')	74.6(6)

C(22')-C(23')-C(24')	109.8(10)	O(10)-Ti(4)-Cl(4)	95.36(9)
C(22')-C(23')-Ti(3')	73.5(6)	C(34)-Ti(4)-Cl(4)	133.21(17)
C(24')-C(23')-Ti(3')	73.5(7)	C(36)-Ti(4)-Cl(4)	133.81(16)
C(25')-C(24')-C(23')	105.7(10)	C(33)-Ti(4)-Cl(4)	101.57(17)
C(25')-C(24')-Ti(3')	72.7(7)	O(10)-Ti(4)-C(35)	78.29(16)
C(23')-C(24')-Ti(3')	72.3(7)	C(34)-Ti(4)-C(35)	33.88(17)
C(24')-C(25')-C(21')	109.8(10)	C(36)-Ti(4)-C(35)	101.7(2)
C(24')-C(25')-Ti(3')	74.3(7)	C(33)-Ti(4)-C(35)	56.1(2)
C(21')-C(25')-Ti(3')	74.6(7)	Cl(4)-Ti(4)-C(35)	124.30(16)
C(27')-C(26')-C(30')	106.7(9)	O(10)-Ti(4)-C(32)	112.30(16)
C(27')-C(26')-Ti(3')	72.9(6)	C(34)-Ti(4)-C(32)	56.4(2)
C(30')-C(26')-Ti(3')	72.3(6)	C(36)-Ti(4)-C(32)	135.1(2)
C(26')-C(27')-C(28')	109.7(10)	C(33)-Ti(4)-C(32)	34.16(18)
C(26')-C(27')-Ti(3')	73.9(6)	Cl(4)-Ti(4)-C(32)	77.57(15)
C(28')-C(27')-Ti(3')	71.0(6)	C(35)-Ti(4)-C(32)	55.85(19)
C(27')-C(28')-C(29')	107.3(10)	O(10)-Ti(4)-C(37)	131.79(19)
C(27')-C(28')-Ti(3')	75.3(6)	C(34)-Ti(4)-C(37)	76.1(2)
C(29')-C(28')-Ti(3')	72.0(7)	C(36)-Ti(4)-C(37)	34.31(19)
C(30')-C(29')-C(28')	107.8(10)	C(33)-Ti(4)-C(37)	77.2(2)
C(30')-C(29')-Ti(3')	75.5(7)	Cl(4)-Ti(4)-C(37)	116.35(19)
C(28')-C(29')-Ti(3')	73.2(7)	C(35)-Ti(4)-C(37)	107.5(2)
C(29')-C(30')-C(26')	108.5(9)	C(32)-Ti(4)-C(37)	109.5(2)
C(29')-C(30')-Ti(3')	70.6(7)	O(10)-Ti(4)-C(38)	135.0(2)
C(26')-C(30')-Ti(3')	73.8(6)	C(34)-Ti(4)-C(38)	103.7(2)
O(10)-Ti(4)-C(34)	108.64(18)	C(36)-Ti(4)-C(38)	56.1(2)
O(10)-Ti(4)-C(36)	97.55(18)	C(33)-Ti(4)-C(38)	90.3(2)
C(34)-Ti(4)-C(36)	83.1(2)	Cl(4)-Ti(4)-C(38)	84.15(19)
O(10)-Ti(4)-C(33)	133.24(17)	C(35)-Ti(4)-C(38)	137.5(2)
C(34)-Ti(4)-C(33)	33.97(19)	C(32)-Ti(4)-C(38)	111.5(2)
C(36)-Ti(4)-C(33)	101.1(2)	C(37)-Ti(4)-C(38)	33.1(2)

O(10)-Ti(4)-C(31)	80.57(15)	C(32)-C(31)-C(35)	107.3(5)
C(34)-Ti(4)-C(31)	56.4(2)	C(32)-C(31)-Ti(4)	72.6(3)
C(36)-Ti(4)-C(31)	135.4(2)	C(35)-C(31)-Ti(4)	72.3(3)
C(33)-Ti(4)-C(31)	56.29(18)	C(31)-C(32)-C(33)	108.3(5)
Cl(4)-Ti(4)-C(31)	90.46(15)	C(31)-C(32)-Ti(4)	73.9(3)
C(35)-Ti(4)-C(31)	33.86(17)	C(33)-C(32)-Ti(4)	71.9(3)
C(32)-Ti(4)-C(31)	33.46(16)	C(34)-C(33)-C(32)	107.8(5)
C(37)-Ti(4)-C(31)	130.6(2)	C(34)-C(33)-Ti(4)	72.5(3)
C(38)-Ti(4)-C(31)	144.3(2)	C(32)-C(33)-Ti(4)	74.0(3)
O(10)-Ti(4)-C(40)	83.66(16)	C(33)-C(34)-C(35)	108.3(5)
C(34)-Ti(4)-C(40)	115.6(2)	C(33)-C(34)-Ti(4)	73.5(3)
C(36)-Ti(4)-C(40)	32.72(18)	C(35)-C(34)-Ti(4)	74.5(3)
C(33)-Ti(4)-C(40)	130.7(2)	C(34)-C(35)-C(31)	108.3(5)
Cl(4)-Ti(4)-C(40)	106.29(17)	C(34)-C(35)-Ti(4)	71.6(3)
C(35)-Ti(4)-C(40)	127.3(2)	C(31)-C(35)-Ti(4)	73.9(3)
C(32)-Ti(4)-C(40)	163.43(19)	C(40)-C(36)-C(37)	105.6(6)
C(37)-Ti(4)-C(40)	54.14(19)	C(40)-C(36)-Ti(4)	75.9(3)
C(38)-Ti(4)-C(40)	54.0(2)	C(37)-C(36)-Ti(4)	74.3(3)
C(31)-Ti(4)-C(40)	158.0(2)	C(38)-C(37)-C(36)	108.0(5)
O(10)-Ti(4)-C(39)	101.67(19)	C(38)-C(37)-Ti(4)	73.9(3)
C(34)-Ti(4)-C(39)	132.0(2)	C(36)-C(37)-Ti(4)	71.4(3)
C(36)-Ti(4)-C(39)	56.3(2)	C(37)-C(38)-C(39)	108.9(6)
C(33)-Ti(4)-C(39)	124.3(2)	C(37)-C(38)-Ti(4)	73.0(3)
Cl(4)-Ti(4)-C(39)	77.73(16)	C(39)-C(38)-Ti(4)	74.1(3)
C(35)-Ti(4)-C(39)	158.0(2)	C(40)-C(39)-C(38)	103.8(6)
C(32)-Ti(4)-C(39)	139.4(2)	C(40)-C(39)-Ti(4)	72.8(4)
C(37)-Ti(4)-C(39)	56.0(2)	C(38)-C(39)-Ti(4)	71.8(3)
C(38)-Ti(4)-C(39)	34.1(2)	C(36)-C(40)-C(39)	113.4(6)
C(31)-Ti(4)-C(39)	168.1(2)	C(36)-C(40)-Ti(4)	71.4(4)
C(40)-Ti(4)-C(39)	32.58(19)	C(39)-C(40)-Ti(4)	74.6(4)

O(9)-Ti(4')-C(33')	129.2(3)	C(34')-Ti(4')-C(37')	75.4(4)
O(9)-Ti(4')-C(34')	106.1(3)	Cl(4')-Ti(4')-C(37')	116.5(4)
C(33')-Ti(4')-C(34')	34.8(3)	C(32')-Ti(4')-C(37')	110.9(4)
O(9)-Ti(4')-Cl(4')	95.92(14)	C(31')-Ti(4')-C(37')	130.7(4)
C(33')-Ti(4')-Cl(4')	99.9(3)	C(35')-Ti(4')-C(37')	106.5(4)
C(34')-Ti(4')-Cl(4')	132.8(3)	C(36')-Ti(4')-C(37')	33.5(3)
O(9)-Ti(4')-C(32')	106.8(3)	O(9)-Ti(4')-C(38')	140.2(4)
C(33')-Ti(4')-C(32')	34.4(3)	C(33')-Ti(4')-C(38')	89.7(4)
C(34')-Ti(4')-C(32')	57.2(4)	C(34')-Ti(4')-C(38')	102.8(5)
Cl(4')-Ti(4')-C(32')	76.8(3)	Cl(4')-Ti(4')-C(38')	83.6(3)
O(9)-Ti(4')-C(31')	75.3(2)	C(32')-Ti(4')-C(38')	111.8(4)
C(33')-Ti(4')-C(31')	56.5(3)	C(31')-Ti(4')-C(38')	144.4(4)
C(34')-Ti(4')-C(31')	56.8(4)	C(35')-Ti(4')-C(38')	136.5(5)
Cl(4')-Ti(4')-C(31')	91.1(3)	C(36')-Ti(4')-C(38')	55.2(4)
C(32')-Ti(4')-C(31')	33.5(3)	C(37')-Ti(4')-C(38')	33.5(3)
O(9)-Ti(4')-C(35')	74.8(3)	O(9)-Ti(4')-C(39')	107.3(4)
C(33')-Ti(4')-C(35')	56.6(4)	C(33')-Ti(4')-C(39')	123.1(4)
C(34')-Ti(4')-C(35')	33.9(3)	C(34')-Ti(4')-C(39')	130.7(4)
Cl(4')-Ti(4')-C(35')	125.0(3)	Cl(4')-Ti(4')-C(39')	77.6(3)
C(32')-Ti(4')-C(35')	56.2(3)	C(32')-Ti(4')-C(39')	138.9(4)
C(31')-Ti(4')-C(35')	33.9(3)	C(31')-Ti(4')-C(39')	168.6(4)
O(9)-Ti(4')-C(36')	101.1(3)	C(35')-Ti(4')-C(39')	157.2(4)
C(33')-Ti(4')-C(36')	103.1(5)	C(36')-Ti(4')-C(39')	54.5(4)
C(34')-Ti(4')-C(36')	84.3(5)	C(37')-Ti(4')-C(39')	55.3(4)
Cl(4')-Ti(4')-C(36')	132.0(3)	C(38')-Ti(4')-C(39')	33.5(3)
C(32')-Ti(4')-C(36')	137.2(4)	O(9)-Ti(4')-C(40')	88.1(3)
C(31')-Ti(4')-C(36')	136.5(4)	C(33')-Ti(4')-C(40')	132.4(4)
C(35')-Ti(4')-C(36')	102.7(4)	C(34')-Ti(4')-C(40')	117.0(5)
O(9)-Ti(4')-C(37')	134.6(4)	Cl(4')-Ti(4')-C(40')	104.7(4)
C(33')-Ti(4')-C(37')	78.0(4)	C(32')-Ti(4')-C(40')	164.9(4)

C(31')-Ti(4')-C(40')	158.3(4)	C(37')-C(36')-Ti(4')	73.4(6)
C(35')-Ti(4')-C(40')	128.3(5)	C(40')-C(36')-Ti(4')	77.9(7)
C(36')-Ti(4')-C(40')	32.8(3)	C(36')-C(37')-C(38')	107.1(10)
C(37')-Ti(4')-C(40')	54.6(4)	C(36')-C(37')-Ti(4')	73.1(6)
C(38')-Ti(4')-C(40')	54.2(4)	C(38')-C(37')-Ti(4')	73.7(6)
C(39')-Ti(4')-C(40')	31.8(3)	C(37')-C(38')-C(39')	107.5(10)
C(32')-C(31')-C(35')	108.5(8)	C(37')-C(38')-Ti(4')	72.8(6)
C(32')-C(31')-Ti(4')	73.1(6)	C(39')-C(38')-Ti(4')	74.5(7)
C(35')-C(31')-Ti(4')	73.3(6)	C(40')-C(39')-C(38')	108.7(10)
C(31')-C(32')-C(33')	108.1(9)	C(40')-C(39')-Ti(4')	76.6(8)
C(31')-C(32')-Ti(4')	73.3(6)	C(38')-C(39')-Ti(4')	72.0(7)
C(33')-C(32')-Ti(4')	72.0(6)	C(39')-C(40')-C(36')	107.7(10)
C(32')-C(33')-C(34')	107.7(9)	C(39')-C(40')-Ti(4')	71.6(7)
C(32')-C(33')-Ti(4')	73.6(6)	C(36')-C(40')-Ti(4')	69.3(7)
C(34')-C(33')-Ti(4')	72.8(6)	Cl(6)-C(41)-Cl(5)	117.7(14)
C(35')-C(34')-C(33')	107.0(9)	Cl(6')-C(41')-Cl(5')	117.9(8)
C(35')-C(34')-Ti(4')	74.1(6)	Cl(7)-C(42)-Cl(8)	109.8(16)
C(33')-C(34')-Ti(4')	72.4(6)	Cl(7')-C(42')-Cl(8')	115.8(10)
C(34')-C(35')-C(31')	108.6(9)		
C(34')-C(35')-Ti(4')	72.1(6)		
C(31')-C(35')-Ti(4')	72.7(6)		
C(37')-C(36')-C(40')	108.8(10)		

Symmetry transformations used to generate equivalent atoms:

#1 -x+1,-y+1,-z+1

Anisotropic displacement parameters (A^2 x 10^3) for **III**. The anisotropic displacement factor exponent takes the form: -2 pi^2 [h^2 a*^2 U11 + ... + 2 h k a* b* U12]

	U11	U22	U33	U23	U13	U12
Si(1)	27(1)	24(1)	23(1)	12(1)	10(1)	4(1)
Si(2)	25(1)	21(1)	22(1)	2(1)	7(1)	2(1)
Si(3)	28(1)	29(1)	29(1)	15(1)	7(1)	10(1)
Si(4)	29(1)	21(1)	30(1)	1(1)	14(1)	7(1)
O(1)	34(1)	35(1)	25(1)	8(1)	9(1)	3(1)
O(2)	43(1)	29(1)	36(1)	10(1)	1(1)	7(1)
O(3)	36(1)	38(1)	36(1)	9(1)	12(1)	16(1)
O(4)	51(1)	25(1)	41(1)	10(1)	23(1)	11(1)
O(5)	30(1)	46(1)	39(1)	22(1)	14(1)	12(1)
O(6)	29(1)	34(1)	40(1)	-3(1)	13(1)	2(1)
O(7)	32(1)	48(1)	35(1)	25(1)	11(1)	0(1)
O(8)	28(1)	32(1)	32(1)	-4(1)	11(1)	-5(1)
O(9)	42(1)	51(2)	60(2)	35(1)	5(1)	18(1)
O(10)	48(1)	37(1)	51(2)	-5(1)	25(1)	16(1)
Ti(1)	32(1)	35(1)	28(1)	16(1)	13(1)	5(1)
Cl(1)	67(1)	111(1)	153(1)	73(1)	72(1)	55(1)
C(1)	154(10)	38(4)	95(8)	-29(4)	-4(7)	22(6)
C(2)	130(9)	115(7)	69(7)	-51(5)	39(7)	20(6)
C(3)	106(7)	93(7)	26(4)	11(4)	17(4)	-36(6)
C(4)	66(4)	94(6)	37(4)	17(5)	-6(3)	-11(4)
C(5)	85(7)	57(5)	34(5)	8(4)	-4(5)	-39(5)
C(1')	119(8)	40(5)	56(7)	-1(4)	-19(6)	2(5)
C(2')	108(7)	83(8)	38(5)	-10(5)	20(5)	44(6)
C(3')	49(5)	93(8)	34(4)	34(6)	13(3)	21(6)

C(4')	40(4)	107(9)	48(6)	32(6)	12(4)	28(6)
C(5')	49(5)	107(10)	23(5)	26(6)	-8(4)	-19(5)
C(6)	72(6)	33(5)	78(9)	-6(7)	0(5)	8(4)
C(7)	128(8)	47(4)	83(8)	46(5)	36(6)	16(5)
C(8)	138(8)	72(6)	101(8)	40(6)	-39(6)	42(6)
C(9)	71(6)	66(6)	167(10)	21(6)	29(6)	46(5)
C(10)	126(9)	40(4)	68(6)	2(5)	31(6)	21(6)
C(6')	54(6)	29(6)	74(9)	1(6)	0(5)	-11(5)
C(7')	71(7)	34(5)	76(10)	13(8)	34(7)	3(5)
C(8')	88(8)	33(5)	109(9)	40(6)	10(6)	20(5)
C(9')	52(6)	29(5)	88(9)	-12(6)	24(6)	9(5)
C(10')	87(8)	39(6)	51(7)	-14(6)	20(6)	10(6)
Ti(2)	29(1)	23(1)	28(1)	2(1)	5(1)	4(1)
Cl(2)	39(1)	59(1)	68(2)	-8(1)	-2(1)	20(1)
Cl(2')	23(3)	84(5)	83(9)	-22(6)	-2(4)	28(3)
C(11)	64(4)	28(3)	89(5)	9(3)	21(4)	-6(3)
C(12)	62(4)	40(4)	73(4)	34(3)	32(3)	16(3)
C(13)	74(5)	54(5)	64(4)	38(3)	15(3)	19(4)
C(14)	67(4)	57(5)	102(7)	51(5)	38(4)	38(3)
C(15)	108(6)	25(3)	93(5)	18(4)	43(5)	18(3)
C(11')	52(8)	39(10)	97(11)	29(9)	13(8)	5(8)
C(12')	62(10)	57(14)	83(9)	42(9)	37(8)	27(9)
C(13')	60(9)	54(11)	71(9)	28(8)	9(8)	39(8)
C(14')	56(7)	35(7)	103(13)	16(8)	34(9)	28(6)
C(15')	88(10)	31(5)	80(10)	-5(6)	20(9)	21(7)
C(16)	91(6)	43(3)	49(4)	21(3)	41(4)	24(3)
C(17)	81(5)	97(5)	45(3)	42(3)	22(3)	42(4)
C(18)	71(4)	80(4)	25(3)	-5(3)	7(3)	4(3)
C(19)	72(4)	53(3)	46(3)	8(3)	35(3)	24(3)
C(20)	49(3)	58(3)	35(3)	12(2)	25(2)	13(2)

C(16')	102(14)	58(8)	52(11)	39(7)	16(10)	21(8)
C(17')	87(13)	108(12)	43(11)	39(9)	3(11)	31(10)
C(18')	79(10)	90(10)	30(5)	12(6)	14(6)	-1(9)
C(19')	79(9)	82(10)	51(8)	8(7)	41(7)	19(8)
C(20')	60(8)	72(10)	42(8)	21(7)	23(8)	0(8)
Ti(3)	36(1)	30(1)	30(1)	12(1)	9(1)	14(1)
Cl(3)	94(1)	71(1)	57(1)	12(1)	36(1)	35(1)
C(21)	59(4)	71(4)	179(7)	86(5)	62(5)	31(3)
C(22)	109(5)	62(4)	60(4)	44(3)	19(3)	34(4)
C(23)	53(3)	54(4)	171(7)	66(4)	45(4)	35(3)
C(24)	216(7)	39(3)	95(5)	38(3)	88(5)	71(4)
C(25)	119(5)	27(3)	126(6)	30(4)	-52(5)	-8(3)
C(26)	50(3)	35(3)	80(4)	29(3)	6(3)	2(2)
C(27)	62(4)	48(3)	70(4)	9(3)	-1(3)	-3(2)
C(28)	38(3)	83(4)	111(5)	52(4)	12(3)	12(3)
C(29)	80(4)	68(4)	138(6)	46(4)	81(5)	32(3)
C(30)	81(4)	59(4)	58(4)	24(3)	32(3)	-13(3)
Ti(3')	34(1)	27(1)	31(1)	6(1)	14(1)	14(1)
Cl(3')	94(1)	71(1)	57(1)	12(1)	36(1)	35(1)
C(21')	54(5)	23(4)	136(10)	1(5)	41(5)	15(3)
C(22')	85(7)	41(4)	76(6)	-18(5)	22(5)	15(5)
C(23')	58(5)	42(4)	138(9)	0(6)	47(6)	25(4)
C(24')	107(8)	33(5)	106(8)	17(6)	1(6)	33(5)
C(25')	127(9)	23(5)	112(8)	23(6)	74(7)	21(5)
C(26')	55(6)	33(3)	85(7)	19(4)	40(5)	14(3)
C(27')	75(7)	57(6)	64(6)	27(5)	32(5)	11(5)
C(28')	64(6)	64(6)	94(7)	10(6)	56(6)	17(5)
C(29')	38(4)	56(5)	116(8)	27(6)	16(5)	13(4)
C(30')	57(6)	46(5)	60(6)	9(4)	13(4)	-7(4)
Ti(4)	34(1)	27(1)	31(1)	6(1)	14(1)	14(1)

Cl(4)	50(1)	38(1)	84(1)	21(1)	25(1)	12(1)
C(31)	52(3)	57(3)	35(2)	9(2)	11(2)	31(3)
C(32)	67(4)	45(3)	52(3)	20(3)	19(3)	32(3)
C(33)	63(4)	75(4)	50(3)	18(3)	20(3)	48(3)
C(34)	36(3)	76(4)	55(3)	22(3)	13(2)	18(3)
C(35)	45(3)	49(3)	48(3)	0(2)	-4(2)	22(2)
C(36)	53(3)	62(3)	46(3)	25(3)	27(3)	10(3)
C(37)	62(3)	112(5)	53(3)	38(3)	41(3)	55(3)
C(38)	108(5)	62(4)	42(3)	-2(3)	38(3)	37(3)
C(39)	63(3)	67(4)	31(3)	-4(3)	3(2)	4(3)
C(40)	63(3)	88(4)	61(3)	39(3)	45(3)	53(3)
Ti(4')	36(1)	30(1)	30(1)	12(1)	9(1)	14(1)
Cl(4')	50(1)	38(1)	84(1)	21(1)	25(1)	12(1)
C(31')	42(5)	75(6)	36(3)	13(4)	13(4)	36(4)
C(32')	59(5)	55(5)	58(6)	15(3)	24(4)	38(4)
C(33')	52(5)	94(7)	60(6)	26(5)	17(4)	51(5)
C(34')	34(4)	96(7)	77(6)	24(6)	27(4)	13(5)
C(35')	70(7)	78(7)	60(5)	42(5)	40(5)	35(5)
C(36')	68(6)	58(5)	61(6)	9(4)	-9(5)	-6(4)
C(37')	36(5)	104(8)	64(5)	3(5)	-9(4)	23(5)
C(38')	91(8)	83(8)	44(4)	27(5)	-10(5)	25(5)
C(39')	60(6)	110(8)	34(4)	-2(5)	9(5)	4(6)
C(40')	57(7)	75(6)	62(6)	-24(5)	-26(5)	31(6)
C(41)	52(3)	73(4)	92(4)	17(5)	22(3)	8(3)
Cl(5)	58(1)	76(3)	112(4)	-11(2)	30(2)	-5(2)
Cl(6)	92(1)	91(1)	97(3)	26(2)	22(2)	41(1)
C(41')	52(3)	73(4)	92(4)	17(5)	22(3)	8(3)
Cl(5')	58(1)	76(3)	112(4)	-11(2)	30(2)	-5(2)
Cl(6')	92(1)	91(1)	97(3)	26(2)	22(2)	41(1)
C(42)	92(12)	92(8)	164(18)	74(11)	66(12)	31(9)

Cl(7)	155(5)	101(5)	90(5)	37(4)	-3(4)	39(4)
Cl(8)	63(2)	49(3)	76(3)	10(3)	22(2)	6(2)
C(42')	92(12)	92(8)	164(18)	74(11)	66(12)	31(9)
Cl(7')	155(5)	101(5)	90(5)	37(4)	-3(4)	39(4)
Cl(8')	63(2)	49(3)	76(3)	10(3)	22(2)	6(2)

Vita

Jason Curtis Clark was born in Spartanburg, SC on June 21, 1973. He grew up in Spartanburg and graduated from Spartanburg High School in June of 1991. He then enrolled at the University of South Carolina – Spartanburg and obtained a Bachelors of Science in chemistry and a Bachelors of Science in biology in May 2000 (this University has since changed its name to the University of South Carolina – Upstate). During his tenure at USCS, Jason conducted research under the guidance of Professors Jack Turner and Christopher Bender from the Department of Natural Sciences and Engineering investigating the creek waters at Cowpens National Battlefield for chemical and biological contaminants.

In August 2000, he enrolled at the University of Tennessee – Knoxville in the Department of Chemistry where he began his pursuit of a doctoral degree in inorganic chemistry under the supervision of Dr. Craig E. Barnes. His research involved the synthesis and characterizing of novel heterogeneous catalysts. Jason held the position of student operator for the Bruker Avance 400 MHz NMR and the Varian Inova 400 MHz solid state NMR from the spring 2001 semester until he completed his degree requirements. His graduate studies were partially supported by the Joint Institute for Neutron Science from Fall 2003 semester until he completed his degree requirements as a recipient of the UT Neutron Sciences Fellowship. He was also awarded the Eugene John Barber Fellowship in Chemistry in May 2003 and April 2004 for his research efforts. He completed the requirements for his Doctor of Philosophy in chemistry in October of 2005.